論文 / 著書情報
Article / Book Information

題目(和文)	
Title(English)	A Study of the Slot Design for Radial Line Slot Antennas
著者(和文)	高田潤一
Author(English)	Jun-ichi Takada
出典(和文)	学位:博士(工学), 学位授与機関:東京工業大学, 報告番号:甲第2451号, 授与年月日:1992年3月26日, 学位の種別:課程博士, 審査員:
Citation(English)	Degree:Doctor of Engineering, Conferring organization: , Report number:甲第2451号, Conferred date:1992/3/26, Degree Type:Course doctor, Examiner:
学位種別(和文)	博士論文
Type(English)	Doctoral Thesis

A STUDY OF THE SLOT DESIGN FOR RADIAL LINE SLOT ANTENNAS

December 1991

Under the Supervision of

Associate Professor MAKOTO ANDO

Presented by

JUN-ICHI TAKADA

Department of Electrical and Electronic Engineering

Tokyo Insititute of Technology

CONTENTS

CHAPTER 1. INTRODUCTION

1-1. Background and Historical Notes

- BS and CS System for Subscribers -

1-1-1. Broadcasting Satellite (BS)

The direct broadcasting from satellites (DBS) has been widely spread in Japan.

The brief history of Japanese DBS system is summarized in Table 1-1 [1][2]. Since the operational service has begun, the number of subscribers are continuously increasing and over 35 million in March 1991, which is about 10% of the number of the households in Japan.

The channel plan of Japan is shown in Fig. 1-1 [3]. 8 channels in 300MHz bandwidth between 11.7GHz and 12.0GHz are allocated to Japan. For the effective use of frequency, the adjacent channels overlap. Right-hand circular polarization (RH-CP) is used for odd channels, which is therefore allotted to Japan, while left-hand circular polarization (LH-CP) is used for even channels.

The satellite is located on the stationary orbit 35,780km above the equator and longitude 110° east. The azimuth and the elevation angle of the satellite from Tokyo is 224.43° and 38.01° respectively.

1-1-2. Communication Satellite (CS)

After the liberalization of common career, several companies have launched their own communication satellites for the commercial use. The advantages of satellite communication comparing with the wired one are

i) the cost of communication is independent of the distance, and

ii) the same information can be sent to more than one subscribers all at once.

Especially, the system is suitable for one-way transmission system like the relay of lectures in preparatory schools or the CATV program supply. Therefore, the use of CS for the broadcasting has been technically possible, but the definitions of broadcast and communication in law have prohibited to realize the subscriber service [4].

In May 1991, the Ministry of Posts and Telecommunications announced the sanction for broadcasting use of CS. The service with six TV channels and four PCM channels will start from April 1992.

At present, there are two satellites to be used for the broadcast, JC-SAT 2 and SUPERBIRD B. The channel plans for both satellites are shown in Fig. 1-2. Both satellites use 12GHz band, the same as BS, while they use linear polarization. The location of the satellites are long. 154° E. and 162° E., respectively.

1-1-3. System Requirement for Subscriber Antenna

Figure 1-3 shows the receiving system of BS [5]. The outdoor module consists of antenna and LNB (Low Noise Brockdown converter). The 12GHz signal received by the antenna is converted into 1GHz IF to reduce the transmission loss of the cable.

In DBS system, frequency modulation (FM) is used to improve the S/N (signal vs. noise) ratio. In the FM transmission, the relation between S/N and C/N (career vs. noise) is given as [1]

$$\frac{C}{N}=\frac{S}{N}-24 \ [dB] \qquad (1-1).$$

To obtain the good quality of picture, S/N of more than 38dB, i.e. C/N>14dB, is required. The received career power C is given as [5]

$$C=P_o\cdot\frac{G_t\cdot G_r}{L_t\cdot L_r\cdot L}\cdot\left(\frac{\lambda}{4\pi d}\right)^2 \qquad (1-2),$$

where

P_o: transmission power,

G_t: gain of transmission antenna,

L_t: loss of transmission circuit,

G_r: gain of receiving antenna,

L_r: loss of receiving circuit,

L : loss of propagation (rain attenuation),

λ : wavelength,

d : distance between satellite and receiver.

On the other hand, the noise power N is given as [5]

$$N=N_e+N_a+N_l$$
$$=k\cdot B\cdot\{(NF-1)\cdot T_o+Ta+Tl) \qquad (1-3),$$

where

N_e: noise power at LNB,

N_a: noise power at antenna,

N_l: noise power at transmission line between LNB and antenna,

k : Boltzmann's constant (1.38×10^{-23} [J/K]),

NF: noise figure of LNB,

T_o: standard temperature (290 [K]).

T_a: noise temperature of antenna,

T_l: noise temperature of transmission line.

Substituting the parameters for BS-3 system listed in Table 1-2, the relation between the receiving antenna gain and the NF of LNB is given as

$$G[dB]=33.8+10\log_{10}(NF-0.431) \qquad (1-4).$$

At the beginning stage, the C/N of LNB was about 5dB, where the gain of 37.5dBi (750ϕ; 65%) was required. After the technological improvement, the C/N of LNB is reduced to about 1.5dB. The antenna gain of 33.7dBi (450ϕ; 80%) is sufficient, which is still the ultra high gain, comparing to the other subscriber antennas, e.g. Yagi-Uda antenna for V/UHF.

The required C/N depends on the style of service. For HDTV,

C/N=14dB is the lower limit and C/N=18dB is necessary for the noise suppression [8], while C/N=10dB is enough for PCM sound [8] or normal TV for LCD portable display [1].

As for the CS, the standard values of EIRP ($=P_o \cdot G_t \cdot L_t$) are 51dBw and 52dBw for JC-SAT 2 and SUPERBIRD B, respectively [9][10]. They are smaller comparing to 58dBw of BS and 800mmϕ antenna (40dBi; NF=1.0dB) is required for C/N=14dB.

1-2. Planar Antennas

1-2-1. Reflector Antennas and Their Disadvantages

For the high gain use of more than 30dBi, the reflector antennas have been popularly used. As it can be easily designed by the simple optics free from frequency characteristic. In the early stage of DBS, center feed parabola with axial symmetrical surface was used (Fig. 1-4(a)). However, the feed horn and the arm hide the aperture (blocking) and the efficiency is degraded to about 60%. To improve the efficiency, the offset parabola have been widely used (Fig. 1-4(b)). The surface of the reflector does not include the symmetrical axis to avoid the blocking. Moreover, feed horn and LNB are directly connected to reduce the transmission loss. The offset parabola has, however, still some defects:

i) The curvature of the reflector suffers much from snow and wind.

ii) It occupies a large volume by the feed horn and its arm.

iii) The antenna efficiency cannot be improved to more than 80% due to the directivity of the feed horn.

1-2-2. Planar Antennas

As an alternative of reflectors, various kinds of planar array antennas have been studied to solve the problems i)~iii) [11]. At the viewpoint of feed circuit, they are classified into three

groups.

a) Microstrip line (Fig. 1-4(c), (d)) [12][13].

b) Triplate and suspended line (Fig. 1-4(e), (f)) [11][14].

c) Waveguide (Fig. 1-4(g)~(j)) [15]-[18].

In the design of high gain planar arrays, the loss in feeding lines determines the antenna efficiency while the choice of radiating elements affects the manufacturing cost. Table 1-3 summarizes the loss of the feeding line [19]. The loss in the microstrip is the largest, which is due to the transmission loss and radiation loss. The triplate line is applied to suppress the radiation loss, but the transmission loss is still considerable. On the other hand, the loss is negligible for the waveguide owing to it closed structure and the thickness of the guide.

A radial line slot antenna (RLSA) was proposed in this context [20]. Figure 1-5 summarizes the state of the art of commercial antennas for DBS reception. The efficiencies of the arrays using microstrip, triplate and suspended lines are degraded as the antenna gain increases. Two kinds of RLSAs are included in the figure, as well. RLSAs with uniform slots on a double-layered waveguide (●) were developed first and single-layered RLSAs with non-uniform slots (○) dispensed with the complicated structure and were commercialized later. In contrast with other planar arrays, the efficiency of RLSAs remains high enough and is comparable with that of reflector antennas. The highest efficiency of 85% at 36.8dB is about twice as high as that for conventional planar arrays.

Not only the antenna performance, but also the cost performance of RLSA exceeds the other planar antennas, due to the simple structure comparing with other waveguide-fed antennas.

1-3. History of Radial Line Slot Antenna

As mentioned in 1-2, radial line slot antenna (RLSA) is proposed by Goto in 1980 [20]. Figure 1-6 shows the configuration of RLSA. A notable features of RLSA are

i) The power is fed at one point for the excitation of thousands of slots.

ii) It utilize the oversized radial waveguide.

iii) The waveguide and the radiation slots are not separated. The slot plate acts as the waveguide wall.

iv) The elements are excited by the traveling wave.

i) and iii) are the reasons of the simple structure. However, ii) and iii) indicate the difficulty of stable antenna operation with the suppression of higher order modes.

The original one presented in [20] is in the single-layered structure for circular polarization. The operation is expressed as follows:

[Single-layered structure]

Two conductor discs form a radial waveguide. The power is fed at the coaxial cable connected at the center. The power is transferred into rotationally symmetrical outward propagating wave by coaxial-to-radial adaptor. On the upper plate, a lot of slots are arranged to radiate the desired polarization. While propagating outward, the power is gradually radiated from these slots. The residual power is absorbed by the absorber set at the outermost part.

[Circularly-polarized slot arrangement]

Two slots form a slot pair as a unit radiator of polarization. To excite the circular polarization, (1) two slots are arranged perpendicular to each other, (2) they are excited with equal amplitude and (3) relative phase shift of 90°. To satisfy these three conditions, they are separated $\lambda_g/4$ in ρ direction with the coupling angle of 45° and 135°. To excite all the pairs in phase,

they are arranged spirally with the pitch of λ_g.

At the first experiments with eight pairs, the circular polarization is observed. In 1981, the theoretical radiation pattern was calculated, where large grating lobes appeared in the end-fire direction [21]. To suppress the grating lobes, the slot wave circuit is inserted in the waveguide.

The defect of single-layered structure is that the inner field attenuation due to the radiation accelerate the $1/\sqrt{\rho}$ taper of cylindrical wave, to degrade the antenna efficiency. To compensate this, a double-layered structure is presented in 1982 [22]:

[Double-layered structure]

Three conductor discs form a two-fold radial waveguide. The power is fed at the coaxial cable connected at the center of lower waveguide. The power fed at the center propagates in the rotationally symmetrical outward propagating wave. At the outermost part, it is transferred into the inward traveling wave in the upper guide by 180° E-bend. The slots are arranged on the top plate and while propagating inward the power is gradually radiated by these slots. In this design, the inner field attenuation due to the radiation is cancelled by the $1/\sqrt{\rho}$ taper of cylindrical wave and uniform aperture illumination can be realized.

By the use of double-layered structure, the first normal operation was realized in 1985 by a 600mmϕ model antenna, where the gain of 35.0dBi and the antenna efficiency of 57% was measured [23]. The simplified antenna gain calculation method was presented at the same time [24].

The main reason of the efficiency degradation was then the return loss characteristics at the feed point. The coaxial-to-radial adaptor and the 180° E-bend had been numerically optimized during 1985~1987 [25][26]. On the other hand, the theoretical study of

frequency characteristics of the slot coupling started by the use of surface impedance model in 1986 [27]. As the result of these discussions, the predicted antenna operation, the gain of 36.3dBi and the efficiency of 75% for 600mmϕ model antenna, was finally realized in 1988 [28].

As for the linear polarization, the design concept was presented by Ando in 1987 [29][30].

[Linealy-polarized slot arrangement] (see 7-2 in detail)

Two slots form a slot pair as a unit radiator of polarization. Under the assumption that the coupling amplitude of a slot is proportional to $sin\theta$, where θ is the angle between the slot longitudinal direction and the current flow direction. To excite the linear polarization, (1) two slots are excited in alternating phase and (2) set perpendicular to each other, where the angle of each slot is determined by the relation between the current flow direction and the polarization. To satisfy (1), they are separated $\lambda_g/2$ in ρ direction. The coupling angle is given as a function of ϕ. To excite all the pairs in phase, they are arranged annularly with the spacing of λ_g.

Though radiation of linear polarization was confirmed, the annular arrangement spacing $\lambda_g/2$ resulted in the serious return loss degradation. To reduce the return loss, the beam-tilt design was presented [31]. The return loss improvement was observed but the rotational symmetry was degraded due to the local reflection. To cancel the reflection locally, the reflection canceling slot sets as unit radiators of linear polarization were presented [32][33], but the predicted operation was not realized, since they were only conceptual and the slot length and the spacing were not optimized. The accurate prediction of slot coupling was highly required.

The rigorous analysis of slot coupling had been studied using a

variety of analysis models since 1988 [34]-[36], and finally the periodic boundary model gave the high accuracy of the analysis for CP-RLSA [37], though it took a large CPU time.

1-4. Summary of This Study

The aim of this study is to establish and to generalize the slot design of RLSA for high efficiency. Following the historical background, this dissertation discusses

i) the basic discussion about the analytical techniques and the equivalent circuit of a slot as the background of the antenna design,

ii) the aperture illumination design, which is common among all kinds of RLSA, and

iii) the suppression of reflection from slots in linearly-polarized RLSA (LP-RLSA).

The remaining chapters are divided into three parts, which correspond to what listed above.

In part 1, the basic background for the antenna design is discussed. The analytical techniques commonly used for RLSA are summarized in chapter 2, which includes the new analysis of equivalent circuit technique. Before the discussion of antenna design, basic characteristics of coupling for a slot are discussed in chapter 3.

Part 2 includes the aperture illumination design of RLSA in the traveling wave operation. Under the assumption of traveling wave operation, the design is much simplified. Furthermore, since the radial waveguide is the oversized one, the reflection perturbs the rotational symmetry of inner field. Chapter 4 gives an equivalent S-matrix circuit of a slot set, a unit radiator of polarization. It is necessary for the stable operation to suppress the reflection from

each slot set. Moreover, the illumination design parameters are related to the S-matrix element. Using this analysis, chapter 5 discusses the conventional structure of double-layered one with a variety of design parameters. The tendency of the results can be applied to the single-layered one which is discussed in chapter 6. The coupling control on the aperture is necessary for single-layered RLSA, where the weakly coupled slots and the strongly coupled slots are arranged at the inner and the outer part, respectively. The design is confirmed by a variety of model antennas, where antenna efficiencies of 75~85% are obtained.

The design of LP-RLSA is much more difficult than that of CP-RLSA, because of the serious reflection and the variation of the slot set configuration along ϕ direction. Part 3 discusses the problems and the solutions of LP-RLSA. Chapter 7 discusses about the slot set with the reflection canceling additional slots. The parameters are numerically optimized to suppress the reflection. The experiments with the model antennas show the good antenna performance of more than 65%. An alternative slot set using parallel slot pairs are presented in chapter 8. The parallel slot pair is a new radiation device with small reflection. It is also applied to various traveling wave antennas as well. The slot sets for LP-RLSA are constructed by the use of parallel slot pairs. The experiments confirm the radiation of desired polarization.

Chapter 9 summarizes the results of this study, together with the future problems.

References

[1] K. Itoh, "The Perspective and Future Trend of DBS Receiving Antennas," IEICE Technical Report, AP90-S1 (Jan. 1991).

[2] M. Hashimoto (ed.), "Multi Channel Service by BS-3 - New Era of

DBS -," Electronics Life, no. 701, pp. 11-74 (Jan. 1991).

[3] Y. Imabori, "New Media - All about DBS -," pt. 1, Dempa Kagaku, no. 615, pp. 121-127 (Nov. 1983).

[4] S. Fujiwara, "Realization of Broadcasting Service by Communications Satellites," J. IEICE, vol. 72, no. 11, pp. 1256-1259 (Nov. 1989).

[5] Nippon Hoso Kyokai (ed.), "DBS Reception and Instruments," Electronics Life, no. 669, pp. 11-84 (May 1988).

[6] N. Toyama and T. Akanuma, "Current Status and Future Prospects of Satellite Broadcasting in Japan - Subjects Suggested to Receiving Antenna Designers -," IEICE Technical Report, AP90-S6 (Jan. 1991).

[7] K. Konno, "New Media - All about DBS -," pt. 3, Denpa Kagaku, no. 617, pp. 91-96 (Jan. 1984).

[8] Y. Iwadate, T. Susaki, H. Tanabe, Y. Takeuchi and T. Mituhasi, "The Relationship between C/N and Signal Quality for HDTV Satellite Broadcasting," ITEJ Technical Report, RE88-32 (Sep. 1988).

[9] Y. Nagai, "Satellite Communications using JC-SAT," J. IEICE, vol. 72, no. 11, pp. 1243-1250 (Nov. 1989).

[10] M. Ogata, "Satellite Communications Services via SUPERBIRD," J. IEICE, vol. 72, no. 11, pp. 1250-1255 (Nov. 1989).

[11] K. Ito, K. Ohmaru and Y. Konishi, "Planar Antennas for Satellite Reception," IEEE Trans. Broadcasting, vol. 34, no. 4, pp. 457-464 (Dec. 1988).

[12] S. Nishimura, A. Nishigaki, Y. Sugio and T. Makimoto, "Microstrip Line Planar Antenna," ITEJ Technical Report, RE87-3 (Jan. 1987).

[13] K. Ito, "Circularly Polarized Printed Array Antenna Composed of End-Fed Strip Dipoles and Slots," Trans. IECEJ, vol. J-67B,

no. 3, pp. 289-296, (Mar. 1984).

[14] M. Haneishi, S. Saito, K. Yahagi and A. Kaise, "A Consideration on Beamtilt-Type Planar DBS antenna," ITEJ Technical Report, RE88-31 (Sep. 1988).

[15] M. Takahashi, J. Takada, M. Ando and N. Goto, "A Slot Design for Uniform Aperture Field Distribution in Single-Layered Radial Line Slot Antennas," IEEE Trans. Antennas and Propag., vol. AP-39, no. 7, pp. 954-959 (July 1991).

[16] H. Nakano, H. Takeda, H. Mimaki and J. Yamauchi, "A High-Efficiency, Extremely Low-Profile Helical Array Antenna," 1989 IEICE Natl. Conv. Rec., B-29 (Oct. 1989).

[17] S. Saito and M. Haneishi, "Microstrip Patch Array Fed by Radial Line," IEICE Technical Report, AP91-37 (May 1991).

[18] Y. Furukawa, N. Goto and K. Maehara, "A Beam-Tilt Planar Waveguide Slot Antenna of Single Layer Structure for Satellite TV," IEICE Technical Report, AP88-40 (July 1988).

[19] S. Tshurumaru, "The Development and the Technological Trend of Circularly-Polarized Planar Array Antennas," Newest Antenna Technologies and Their Applications, Techno System Seminar Record (Jan. 1988).

[20] N. Goto and M. Yamamoto, "Circularly Polarized Radial-Line Slot Antennas," IECEJ Technical Report, AP80-57 (Aug. 1980).

[21] N. Goto, N. Miyahara and K. Arimura, "Radiation Pattern of a Radial Line Slot Antenna," IECEJ Technical Report, AP81-90 (Oct. 1981).

[22] M. Suzuki and N. Goto, "A Matched Load of Radial Line Slot Antenna," IECEJ Technical Report, AP82-100 (Nov. 1982).

[23] T. Shirai, M. Ando, K. Sakurai, N. Goto, K. Arimura and A. Ishii, "Gain of a Radial Line Slot Antenna," 1985 IECEJ Natl. Conv. Rec., 746 (Mar. 1985).

[24] T. Nagatsuka, M. Ando and N. Goto, "A Calculation of the Directive Gain of a Radial Line Slot Antenna," 1985 IECEJ Natl. Conv. Rec., 747 (Mar. 1985).

[25] M. Ando, S. Ito, H. Kawasaki and N. Goto, "A Design of a Radial Line Slot Antenna with Improved Input VSWR," Trans. IEICE, vol. J70-B, no. 4, pp. 495-504 (Apr. 1987).

[26] S. Nishikata, K. Sakurai, M. Ando and N. Goto, "Suppression of Reflection from the Feeding Structure in a Radial Line Slot Antenna," IECEJ Technical Report, AP86-106 (Nov. 1986).

[27] H. Sasazawa, Y. Oshima, K. Sakurai, M. Ando and N. Goto, "Slot Coupling in a Radial Line Slot Antenna for 12GHz Band Satellite TV Reception," IEEE Trans. Antennas and Propag., vol. AP-36, no. 9, pp. 1221-1226 (Sep. 1988).

[28] M. Ando, H. Sasazawa, S. Nishikata and N. Goto, "A Slot Design of Radial Line Slot Antennas," Trans. IEICE, vol. J71-B, no. 11, pp. 1345-1351 (Nov. 1988).

[29] M. Ando, T. Numata and N. Goto, "A Linearly-Polarized Radial Line Slot Antenna," IEICE Technical Report, AP87-87 (Oct. 1987).

[30] M. Ando, T. Numata, J. Takada and N. Goto, "A Linearly-Polarized Radial Line Slot Antenna," IEEE Trans. Antennas and Propag., vol. AP-36, no. 12, pp. 1675-1680 (Dec. 1988).

[31] J. Takada, M. Ando and N. Goto, "A Beam-Tilted Linearly-Polarized Radial Line Slot Antenna," Trans. IEICE, vol. J71-B, no. 11, pp. 1352-1357 (Nov. 1988).

[32] M. Ando, J. Takada and N. Goto, "A High Efficiency Radial Line Slot Antenna," ITEJ Technical Report, RE88-30 (Sep. 1988).

[33] T. Ikeda, J. Takada, M. Ando and N. Goto, "Slots Reflection Suppression of Linearly-Polarized Radial Line Slot Antenna," 1989 IEICE Autumn Natl. Conv. Rec., B-42 (Sep. 1989).

[34] J. Hirokawa, M. Ando and N. Goto, "An Analysis of Slot Coupling

in a Radial Line Slot Antenna," 1988 IEICE Autumn Natl. Conv. Rec., B-51 (Sep. 1988).

[35] J. Hirokawa, M. Ando and N. Goto, "An Analysis of Slot Coupling on a Radial Waveguide," IEICE Technical Report, AP88-76 (Oct. 1988).

[36] J. Hirokawa, M. Ando and N. Goto, "An Analysis of Slot Radiation on the Waveguide with a Magnetic Wall for a RLSA," 1989 IEICE Spring Natl. Conv. Rec., B-67 (Mar. 1989).

[37] J. Hirokawa, M. Ando and N. Goto, "Analysis of Slot Coupling in a Radial Line Slot Antenna for DBS Reception," IEE Proc., vol. 137, pt. H, no. 5, pp. 249-254 (Oct. 1990).

[38] K. Konno, "New Media - All about DBS -," pt. 4, Denpa Kagaku, no. 618, pp. 81-87 (Jan. 1984).

[39] "The Catalogue of Flat Antennas for DBS Reception", Matsushita Electric Works, Ltd., (1990).

Table 1-1. History of 12GHz DBS service in Japan.

Apr. 1978	BS-E launched
Jul. 1978	broadcasting test (100w, 1ch)
Jan. 1984	BS-2a launched
May 1984	pre-operational broadcasting service (100w, 1ch)
Feb. 1986	BS-2b launched
Dec. 1986	two channel service started by BS-2b (100w/ch, NHK BS-1(15ch) and BS-2 (11ch))
Jul. 1987	24hours service started (NHK BS-1)
Apr. 1989	BS-2a orbit end
Jun. 1989	24hours operational service (NHK BS-1 and BS-2)
Jun. 1989	HDTV experimental broadcasting start (NHK BS-2)
Aug. 1989	commercial service (NHK)
Feb. 1990	BS-2X launch in failure
Aut. 1990	BS-3a launched
Nov. 1990	three channel service started by BS-3a (120w/ch, NHK BS-1(7ch), BS-2(11ch) & JSB(3ch))
Apr. 1991	BS-3H launch in failure
Aug. 1991	BS-3b launched
Nov. 1991	four channel service started by BS-3a & BS-3b (120w/ch, NHK BS-1(7ch), BS-2(11ch), JSB(5ch) & HDTV(9ch))

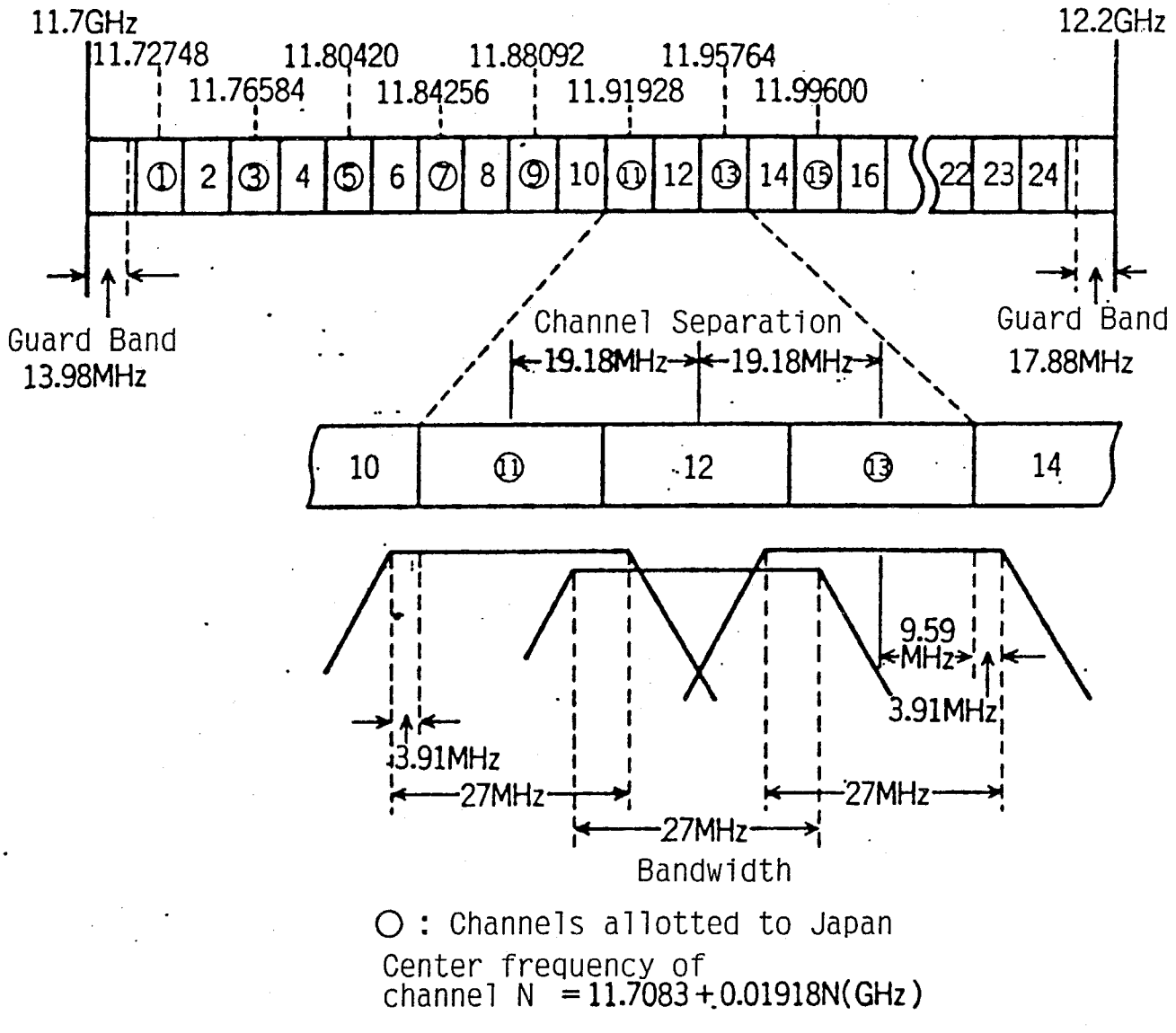

Fig. 1-1. Channel plan of DBS in Japan (from Imabori [3]).

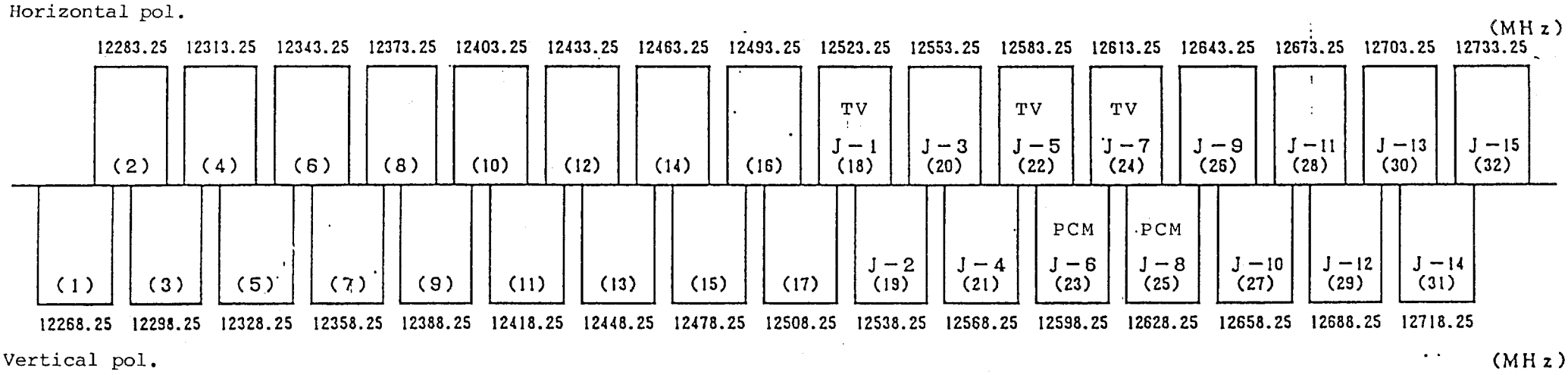

(a) JC-SAT 2.

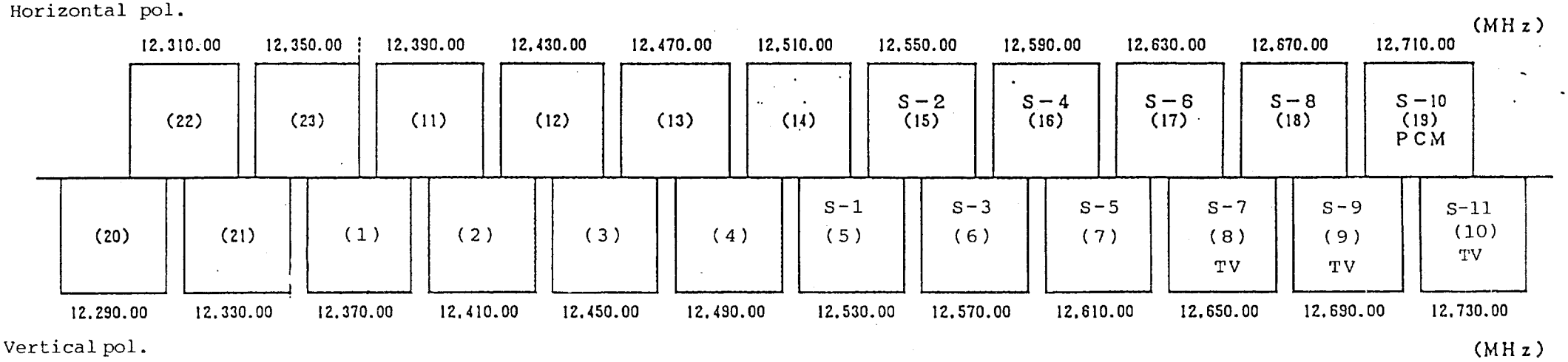

(b) SUPERBIRD B.

Fig. 1-2. Channel plan of CS in Japan.

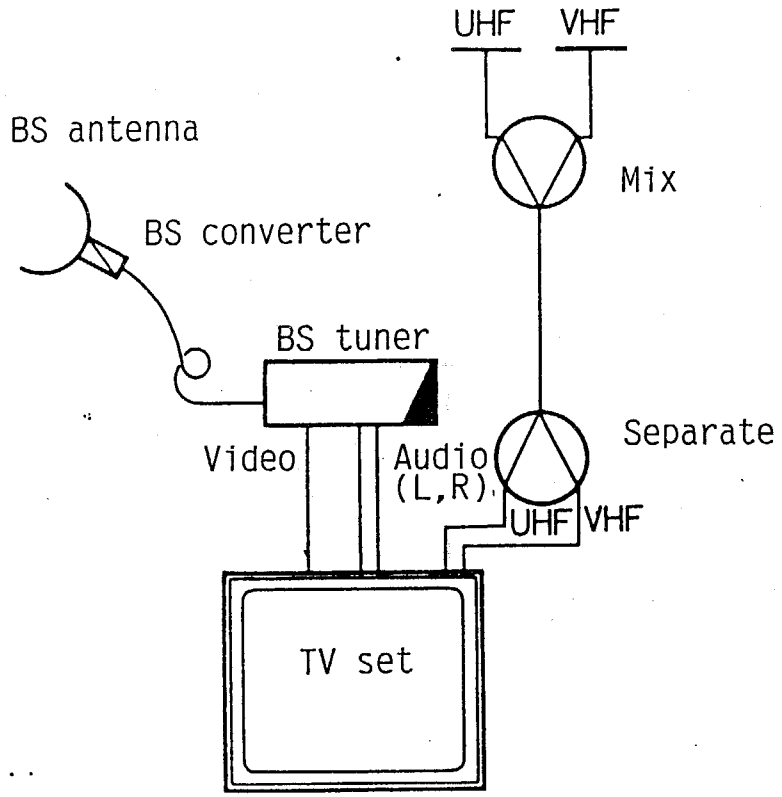

Fig. 1-3. Receiving system for DBS (from Kenmochi [4]).

Table 1-2. Parameters for C/N calculation (BS-3, Tokyo).

Frequency f [GHz]	11.85
Transmission power P_o [w]	120
Gain of transmisson antenna G_t [dB] [6]	40
Loss of transmission circuit L_t [dB] [5]	2.8
Loss of receiving circuit L_r [dB]	0
Loss of propagation (rain) L [dB] [5]	2
Distance between satellite and receiver d [km]	3.7×10^4
Noise tempereture of antenna (rain) T_a [K] [7]	145
Noise tempereture of transmission line T_l [K] [7]	20

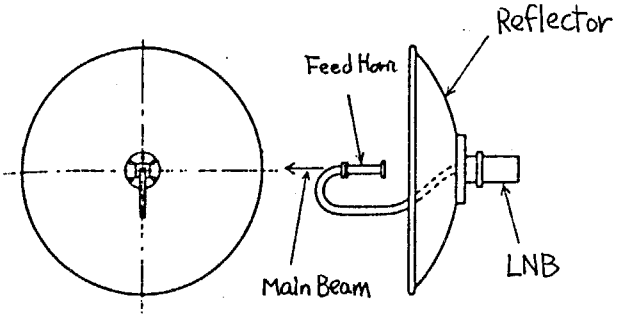

(a) Center feed parabola (from Konno [38]).

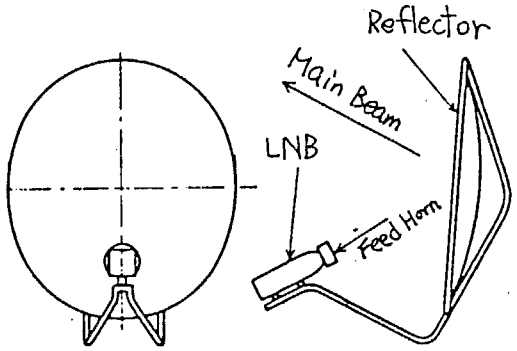

(b) Offset parabola (from Konno [38]).

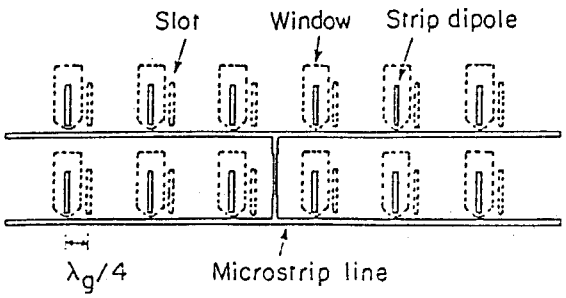

(d) Strip-dipole and slot array (from Ito [13]).

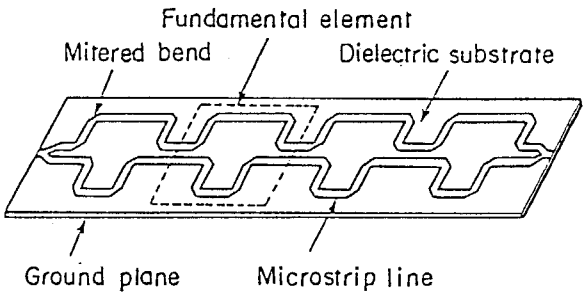

(c) Crank-type microstrip array (from Ito [13]).

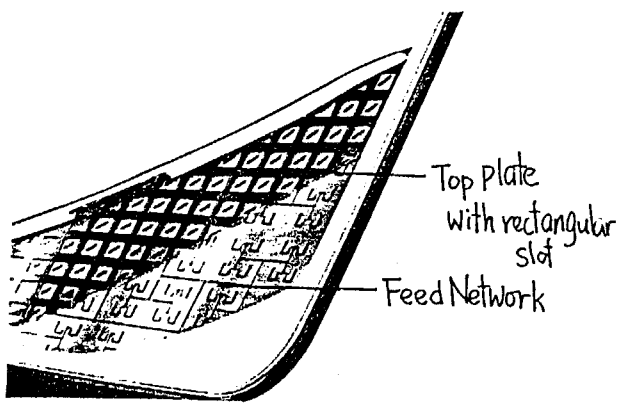

(e) Rectangular slot array (from Matsushita Electric Works [39]).

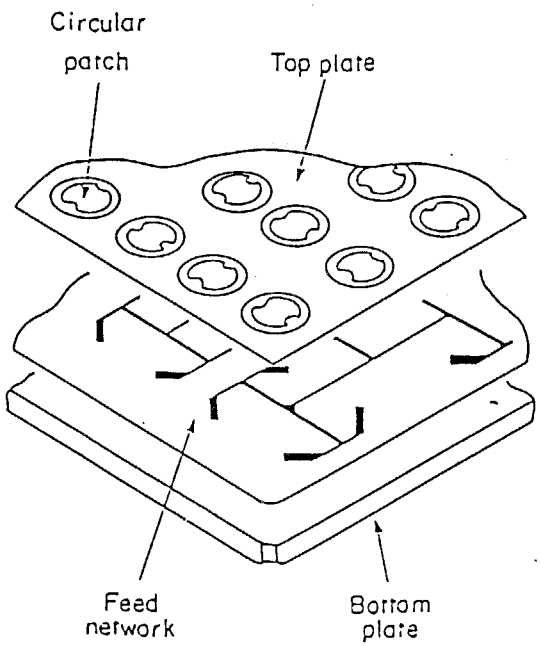

(f) Circular-patch array (from Ito [13]).

Fig. 1-4. Subscriber antennas for DBS.

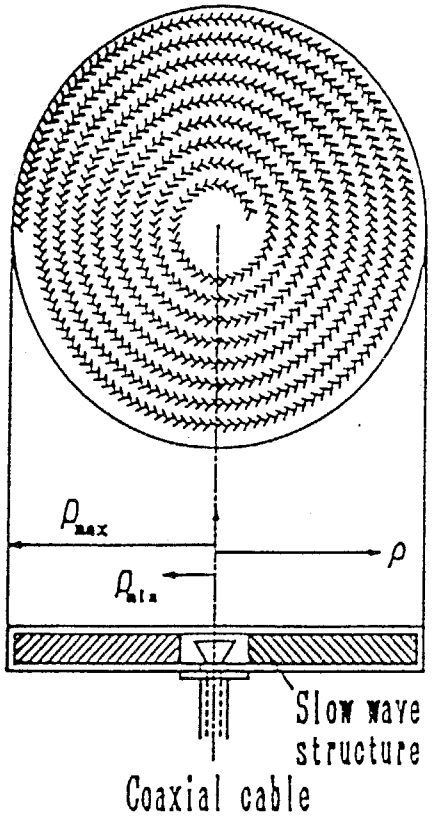

(g) Radial line slot antenna.

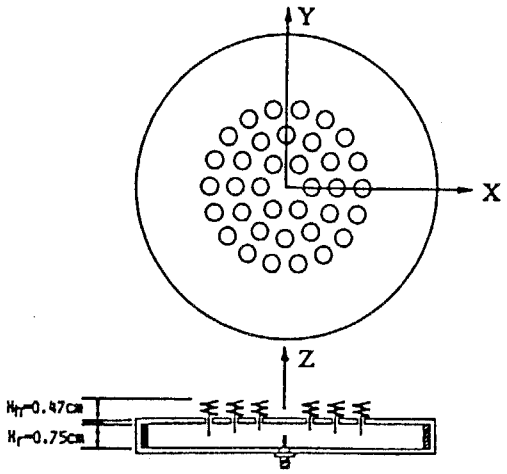

(h) Helical array fed by radial line (RLH) (from Nakano, et. al. [16]).

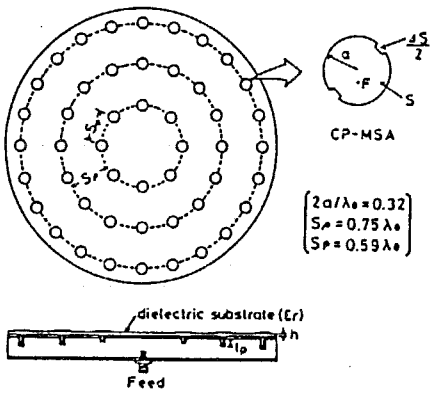

(i) Radial line microstrip patch array (RLP) (from Saito and Haneishi [17]).

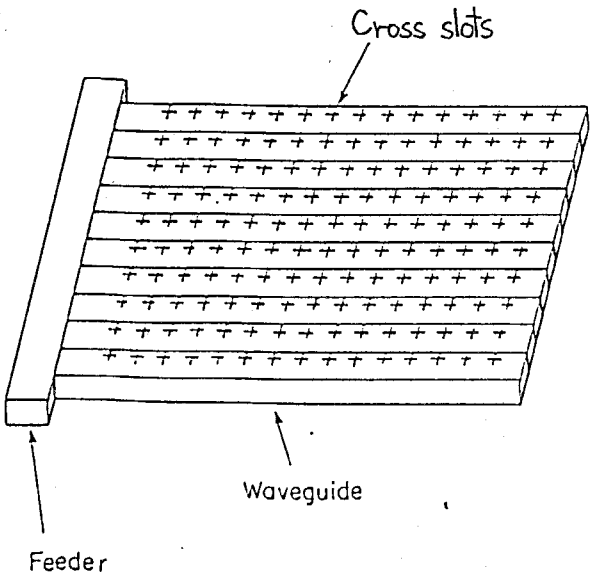

(j) Leaky-wave cross slot array (from Ito [13]).

Fig. 1-4. Subscriber antennas for DBS (continued).

Table 1-3. Losses of the feeding lines.

Feeder	Loss [dB/m] [18]
Waveguide	0.2
Suspended line	1.8~3.0
Triplate line	2.7~5.6
Microstrip line	4~6

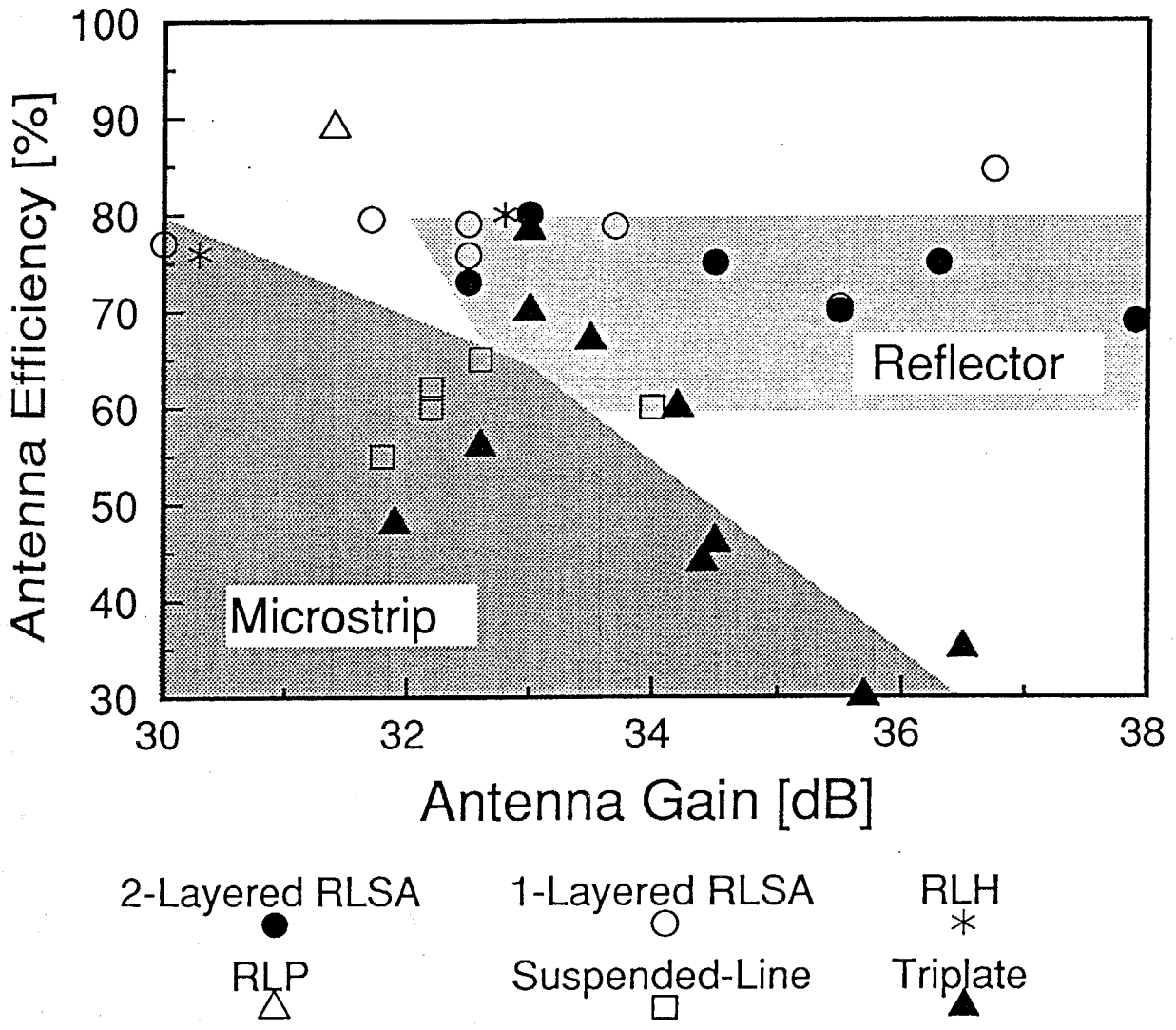

Fig. 1-5. Efficiency of commercial DBS antennas.

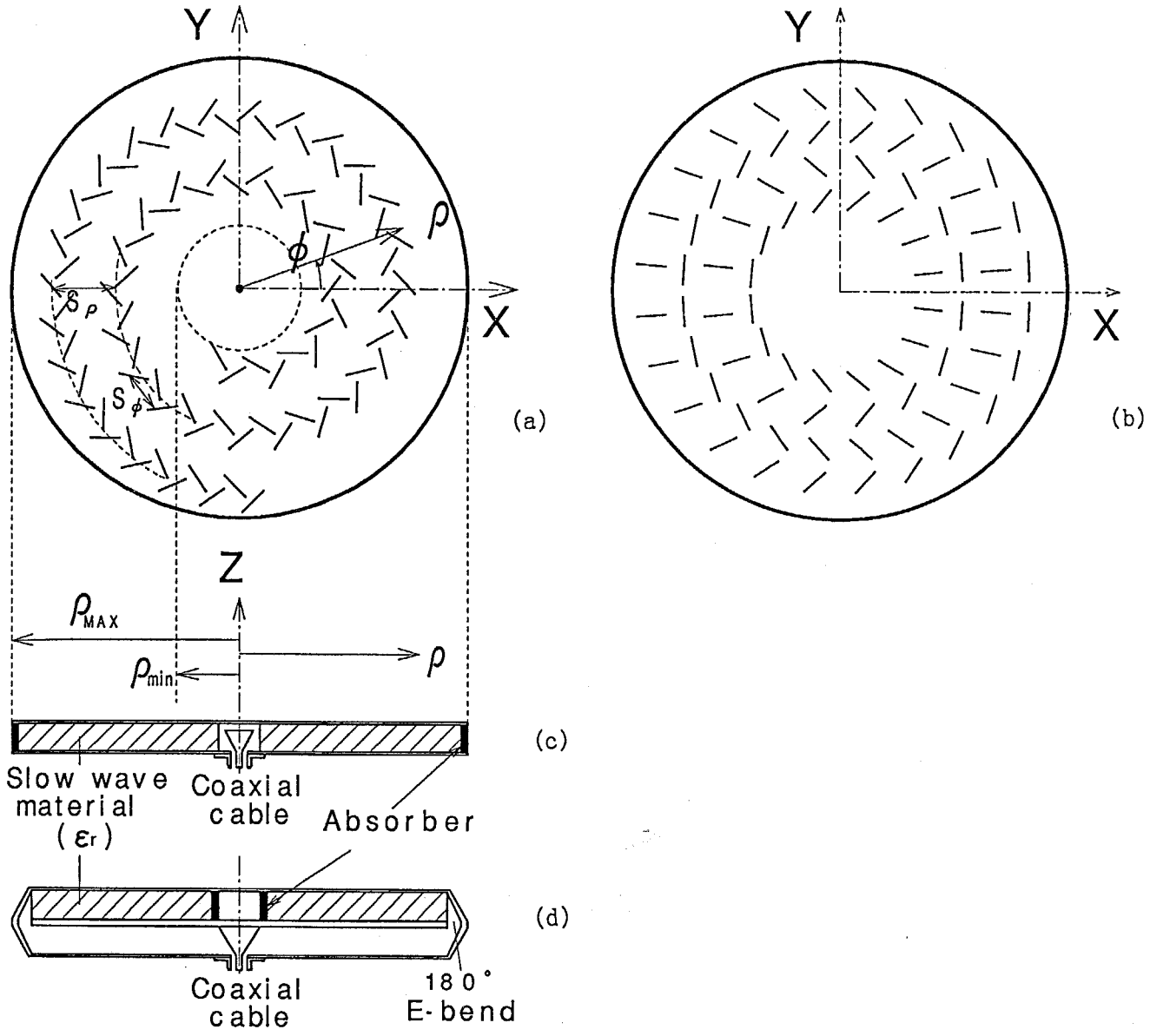

Fig. 1-6. Radial line slot antenna before this study.

(a) Plan of circularly-polarized RLSA.

(b) Plan of linearly-polarized RLSA.

(c) Cross section of single-layered RLSA.

(d) Cross section of double-layered RLSA.

PART. 1 BASIC DISCUSSION ON THE ANALYSES OF RLSA

CHAPTER 2. ANALYTICAL TECHNIQUE

2-1. Introductory Remarks

Considering the practical use of antenna, the final parameter to be improved is the antenna gain as a function of return loss, radiation pattern, cross polarization ratio and so on. This chapter presents the basic analytical techniques, which are common in this paper.

The analytical technique to calculate the gain of RLSA is divided into two parts. One is the estimation of the excitation coefficients of the slots, together with the return loss and termination loss (2-2. Slot Coupling Analysis by Moment Method). The other is the calculation of the directive gain and radiation pattern from the given excitation coefficients (2-3. Array Gain Calculation using Induced Electromotive Force Method). This chapter summarizes these techniques.

2-2. Slot Coupling Analysis by Moment Method

2-2-1. Analysis Model

Figure 2-1 shows the structure of RLSA together with its design parameters. The parameters which affect the slot coupling are listed in Table 2-1. However, it is impossible to analyse the whole antenna structure with more than thousand slots as it is. Instead, the rectangular waveguide model with periodic boundary conditions has

been presented to simulate the slot coupling in CP-RLSA [1]. This model is applicable to RLSA of wider class under the following assumption:

i) The slot coupling angle changes gradually in angular direction.

ii) The slot coupling is weak enough so as not to disturb the rotational symmetry of inner field seriously.

iii) S_ϕ should be much smaller than the radius ρ and the circular array is regarded as the linear one.

Figure 2-2 shows the analysis model. The slots are cut on the infinite rectangular waveguide with periodic boundary walls. The x- and z-direction correspond to the ϕ- and the ρ-direction in Fig. 2-1, respectively. The slots (number = i, length = L_i, width = W (fixed), coupling angle = θ_i) are located on the conductor wall of the guide (width = S_ϕ, height = du). The waveguide is filled with dielectric material (relative permittivity = ε_r). An incident TEM wave propagates in the $\pm$z-direction.

2-2-2. Analysis

The aim of this analysis is to estimate the excitation coefficients of slots together with the reflection and transmission characteristics in the waveguide.

[Slot Excitation]

To derive a set of integral equations for electric fields on the slots, the field equivalence theorem is applied. The slots are replaced with an unknown equivalent magnetic current sheet backed with a perfectly conducting wall; the analysis model is divided into two regions, a half free space (region 1) and the waveguide inside region (region 2). For respective regions, the dyadic Green's functions $\bar{G}_{out}$ and $\bar{G}_{in}$ for the magnetic field produced by a unit magnetic current are formulated [1] (APPENDIX A). The continuity of tangential magnetic field on the slot requires the following

integral equations;

$$\sum_{i=1}^{n} \iint_{S_i} \bar{G}_{out} \cdot (E_i \times (-\hat{y})) dS = H_{in} + \sum_{i=1}^{n} \iint_{S_i} \bar{G}_{in} \cdot (E_i \times \hat{y}) dS \qquad (2\text{-}1),$$

where E_i, $\hat{y}$ and H_{in} are the unknown electric field on the #i slot, a unit vector on the y-direction and the incident TEM magnetic field, respectively.

For the reduction of Eq. (2-1) to a linear equation, Galerkin's method is applied. As the slots are narrow ($W \approx 1/10 L_i$), only one component of E_i along the slot width is considered. When the slot length L_i is smaller than the resonant length, E_i can be approximately expressed in terms of one unknown coefficient v_i as

$$E_i = v_i f_i(\xi_i) g(\eta_i) \hat{\eta}_i = v_i e_i \qquad (2\text{-}2),$$

where the coordinates ξ_i and η_i are the local coordinates on the #i slot, in the length and width direction respectively, as shown in Fig. 2-2(b). Functions $f_i(\xi_i)$ and $g(\eta_i)$ are defined as [1];

$$f_i(\xi_i) = \frac{sin\{k_0(L_i/2 - |\xi_i|)\}}{sin(k_0 L_i/2)} \qquad (2\text{-}3),$$

$$g(\eta_i) = \frac{1}{\sqrt{(W/2)^2 - \eta_i^2}} \qquad (2\text{-}4).$$

The integral equation (2-1) is multiplied with the basis function of slot #j $e_j \times \hat{y}$ and is integrated over the slot aperture. A set of linear equations for the unknown excitation coefficient v_j is given by

$$\sum_{i=1}^{n} v_i \iint_{S_j} \iint_{S_i} (e_j(r_j) \times \hat{y}) \cdot (\bar{G}_{out} + \bar{G}_{in}) \cdot (e_i(r_i) \times \hat{y}) dS_i dS_j$$

$$= -\iint_{S_j} (e_j(r_j) \times \hat{y}) \cdot H_{in} dS_j \qquad (j=1 \sim n) \qquad (2\text{-}5).$$

The integrals in both sides contain only known functions $\bar{G}_{out}$, $\bar{G}_{in}$, $e \times \hat{y}$ and H_{in}, and then the excitation coefficients of all the slots v_j (j=1~n) are determined.

[Scattering Matrix]

The scattering matrix of slot array is derived from the result of moment analysis. The reference plane is considered at the origin of z-axis (z=0) in Fig. 2-2. Port 1 and port 2 are determined for the incidence from -z and +z-direction, respectively. Using the excitation coefficients v_i obtained from Eq. (2-5), the inner field H is given as

$$H=H_{in}+\sum_{i=1}^{n} v_i \iint_{S_i} \bar{G}_{in}\cdot(e_i(r_i)\times\hat{y})\,dS_i \qquad (2\text{-}6).$$

The moment of the dominant mode propagating in the ±z-direction is now defined as

$$c_i^{(\pm)}=Z_o \iint_{S_i} H_i^{(\pm)}(r_i)\cdot(e_i\times\hat{y})\,dS_i \qquad (2\text{-}7),$$

where $H_i^{(\pm)}(r)$ is the dominant mode magnetic function propagating in the ±z-direction and Z_o is the free space impedance.

To derive the scattering matrix, the explicit form of $\bar{G}_{in}$ (Appendix A) is applied;

$$\bar{G}_{in}(r|r_o)=\begin{cases}\dfrac{1}{2}\sum_{\nu} H_\nu^{(-)}(r)H_\nu^{(+)}(r_o) & (z<z_o)\\ \dfrac{1}{2}\sum_{\nu} H_\nu^{(+)}(r)H_\nu^{(-)}(r_o) & (z>z_o)\end{cases} \qquad (2\text{-}8),$$

where $H_\nu^{(\pm)}(r)$ is the normalized magnetic fields propagating in the ±z-direction and ν is the mode number (ν=1: dominant) [1]-[3].

Considering the incident wave from port 1 as

$$H_{in}=H_1^{(+)}(r) \qquad (2\text{-}9).$$

Substituting Eqs. (2-7) ~ (2-9) into Eq. (2-6), the total inner field H is given as follows;

$z<z_o$ region:

$$H(r)=H_1^{(+)}(r)+\left\{\frac{1}{2Z_o}\sum_{i=1}^{n} c_i^{(+)}v_i^{(+)}\right\}H_1^{(-)}(r)$$

$$+(\text{higher order modes}) \qquad (2\text{-}10),$$

$z>z_0$ region:

$$H(r)=\left\{1+\frac{1}{2Z_0}\sum_{i=1}^{n} c_i^{(-)} v_i^{(+)}\right\} H_1^{(+)}(r)$$

$$+(\text{higher order modes}) \qquad (2\text{-}11).$$

S_{11} and S_{21}, which are defined as the coefficients for the dominant modes of H, are given as

$$S_{11}=\frac{1}{2Z_0}\sum_{i=1}^{n} c_i^{(+)} v_i^{(+)} \qquad (2\text{-}12),$$

$$S_{21}=1+\frac{1}{2Z_0}\sum_{i=1}^{n} c_i^{(-)} v_i^{(+)} \qquad (2\text{-}13).$$

In the same manner, considering the incident wave from port 2 as

$$H_{1n}=H_1^{(-)} \qquad (2\text{-}14),$$

the rest of matrix elements S_{*2} are given as follows;

$$S_{12}=1+\frac{1}{2Z_0}\sum_{i=1}^{n} c_i^{(+)} v_i^{(-)} \qquad (2\text{-}15),$$

$$S_{22}=\frac{1}{2Z_0}\sum_{i=1}^{n} c_i^{(-)} v_i^{(-)} \qquad (2\text{-}16).$$

2-3. Array Gain Calculation using Induced Electromotive Force Method

It is difficult to calculate the directive gain of RLSA strictly, because all the slots are in different lengths and then have different directivities. Fourier transform method for aperture antenna analysis [4] is not applicable, because it can not estimate the grating lobes caused by discrete arrangement of slots.

This section summarize the simplified calculation method of array directivity and gain [5][6]. In this analysis, the directivity of each slot is approximated by that of electrically small magnetic dipole. In the calculation, the duality of the electric and mangetic source is used.

2-3-1. Analysis Model

Figure 2-3(a) shows the slot arrangement of array and coordinates in this analysis. Each slot is in different length and has the different directivity. However, the difference of directivity is rather small even comparing with that of small magnetic dipole, at the macroscopic view of the array with thousands of slots. Therefore, the original problem can be reduced to the analysis model that all the slots are replaced by small dipoles located at their center as in Fig. 2-3(b), where the electric field in the model corresponds to the original magnetic field and vice versa. The equivalent magnetic current of #i slot M_i is defined by using the excitation coefficient v_i of Eq. (2-6) and expansion function $\mathbf{e}_i$ in Eq. (2-2) as

$$M_i = v_i \iint_{S_i} \mathbf{e}_i \times \hat{Z} \, dS_i \qquad (2\text{-}17),$$

where $\hat{Z}$ is a unit vector along Z-direction.

2-3-2. Analysis [5]

The radiation field of the antenna $E(r,\phi,\theta)$ is generally given by

$$E(r,\phi,\theta) = \frac{e^{-jkr}}{r} \mathbf{e}(\phi,\theta) \qquad (2\text{-}18),$$

where $\mathbf{e}(\phi,\theta)$ is the directivity of electric field. The directive gain G of the antenna in (ϕ,θ) is defined as

$$G(\phi,\theta) = \frac{4\pi |\mathbf{e}(\phi,\theta)|^2}{\int_0^{2\pi} d\phi \int_0^{\pi} |\mathbf{e}(\phi,\theta)|^2 \sin\theta \, d\theta} \qquad (2\text{-}19).$$

However, the denominator of Eq. (2-19) is difficult to calculate especially when the number of slot is large. Not only the time to calculate each point of $\mathbf{e}(\phi,\theta)$ increases but also the number of points in quadrature should be increased with the increase of slot

number ($\propto$ (antenna diameter)^2).

To reduce the amount of calculation, the denominator of Eq. (2-19) is replaced by the total radiated power P_r given as follows;

$$P_r=\frac{1}{2}\oint_{\Omega}(E\times H^*)\cdot d\Omega=\frac{1}{2Z_0}\int_0^{2\pi}\int_0^{\pi}|e(\phi,\theta)|^2\sin\theta d\theta d\phi \quad (2\text{-}20),$$

where Ω is solid angle. By substituting P_r, Eq. (2-19) is reduced to

$$G(\phi,\theta)=\frac{2\pi|e(\phi,\theta)|^2}{Z_0P_r} \quad (2\text{-}21).$$

On the other hand, the total radiated power of array antenna in the free space P_{rf} can be obtained from the mutual resistance between two elements R_{ij} and the excitation current I_i as

$$P_{rf}=\frac{1}{2}\sum_{i=1}^{n}\sum_{j=1}^{n}R_{ij}I_iI_j^* \quad (2\text{-}22).$$

Equation (2-22) indicates the free space radiated power assuming the dipole radiation, but in RLSA, the power is only radiated to half free space $Z>0$, and therefore the radiated power P_r is

$$P_r=\frac{1}{2}P_{rf} \quad (2\text{-}23).$$

The mutual resistance is calculated by induced electromotive force method as

$$R_{ij}=\frac{Z_0k_0^2\delta^2}{4\pi\bar{R}^3}\{2(\sin\bar{R}-\bar{R}\cos\bar{R})\cos\alpha\cos\beta + (\bar{R}\cos\bar{R}+(\bar{R}^2-1)\sin\bar{R})\sin\alpha\sin\beta\} \quad (2\text{-}24),$$

$$R_{ii}=\frac{Z_0k_0\delta^2}{6\pi} \quad (2\text{-}25),$$

where $\bar{R}=k_0R$ is normalized distance, α, β and R are defined in Fig. 2-4, δ is the length of small dipole [7] (see Appendix B for detailed feature).

Considering the duality, electric current I_i in this model is replaced by the equivalent magnetic current M_i in the original

problem, and substituting Eqs. (2-22) and (2-23) into Eq. (2-21), the final expression of directive gain is given as

$$G(\phi,\theta)=\frac{8\pi|e(\phi,\theta)|^2}{Z_0\sum_{i=1}^{n}\sum_{j=1}^{n}R_{ij}M_iM_j^*} \qquad (2\text{-}26).$$

This analysis has already been proved to agree well with the exact calculation considering the slot length [6].

2-4. Concluding Remarks

This chapter has summarized basic, but important numerical techniques for the analysis of RLSA, slot coupling analysis and array gain analysis. The reliabilities of these analyses are already discussed in reference [1] and [5], respectively, although the equivalent scattering matrix in the slot coupling analysis is newly introduced to the analysis of RLSA.

References

[1] J. Hirokawa, M. Ando and N. Goto, "Analysis of Slot Coupling in a Radial Line Slot Antenna for DBS Reception," IEE Proc., vol. 137, pt. H, no. 5, pp. 249-254 (Oct. 1990).

[2] H. Seki, "Moment and Variational Analysis of Slotted Waveguide Antennas and Its Applications," Doctoral Dissertation, Tokyo Inst. of Tech. (Dec. 1981).

[3] R. E. Collin, "Field Theory of Guided Waves," Sec. 5.6, McGraw-Hill, New York (1960).

[4] R. E. Collin, "Antennas and Radiowave Propagation," Sec. 4.1, McGraw-Hill, New York (1985), for example.

[5] T. Nagatshuka, "A Calculation of the Directive Gain of a Radial Line Slot Antenna," Graduation Thesis, Tokyo Inst. of Tech. (Feb. 1985).

[6] T. Nagatshuka, M. Ando and N. Goto, "A Calculation of the Directive Gain of a Radial-Line Slot Antenna," 1985 Natl. Conv. IECE, 747 (Mar. 1985).

[7] N. Goto, "New Antenna Technology," Ohm Co., Tokyo (1986).

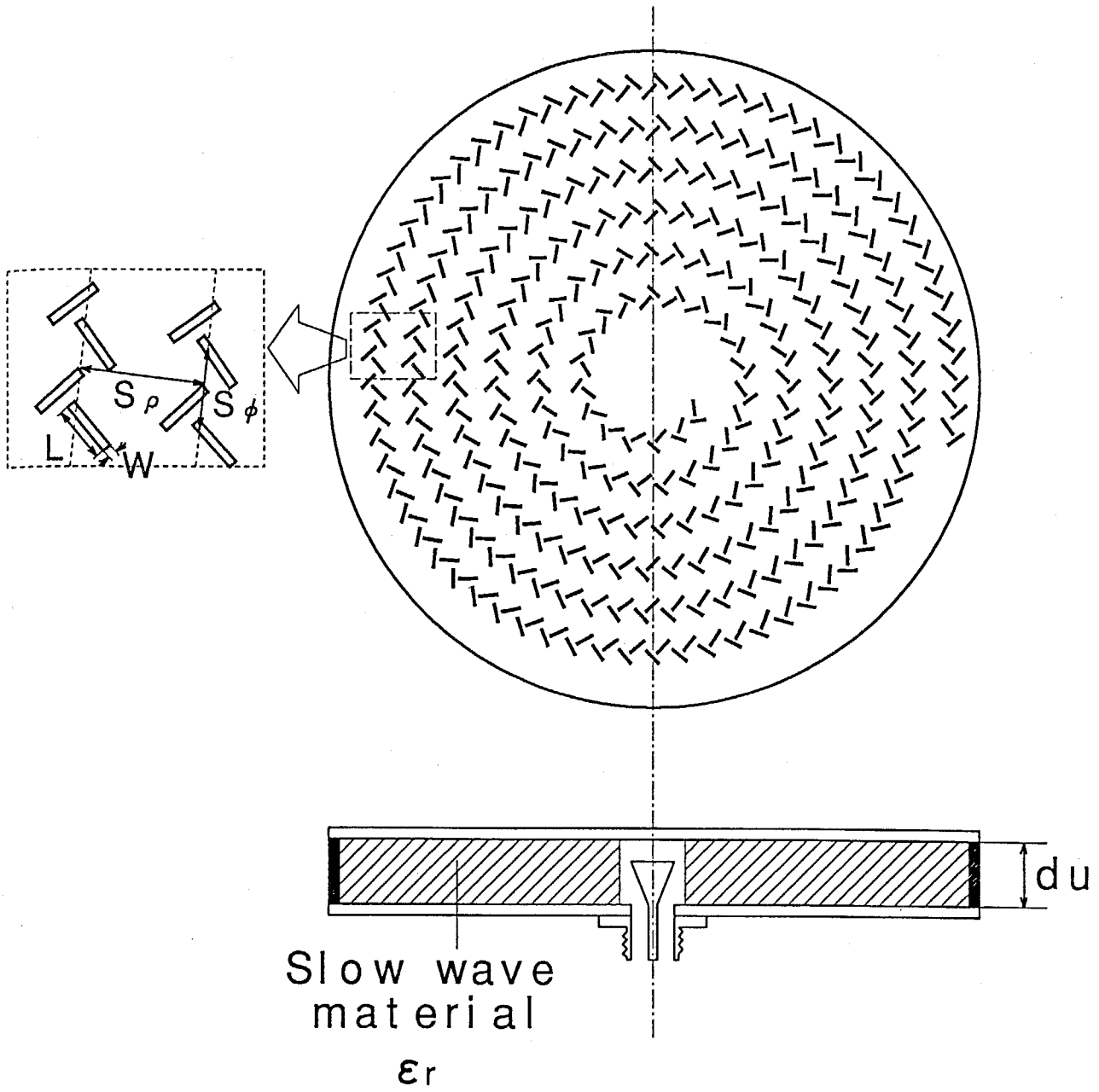

Fig. 2-1. Radial Line Slot Antenna (RLSA) and its design parameters.

Table 2-1. Design parameters and their effects on the slot coupling.

waveguide height du	basic tendency of resonance
permittivity ε_r	
slot angular spacing S_ϕ	
slot radial spacing S_ρ	excitation phase
slot length L	coupling strength

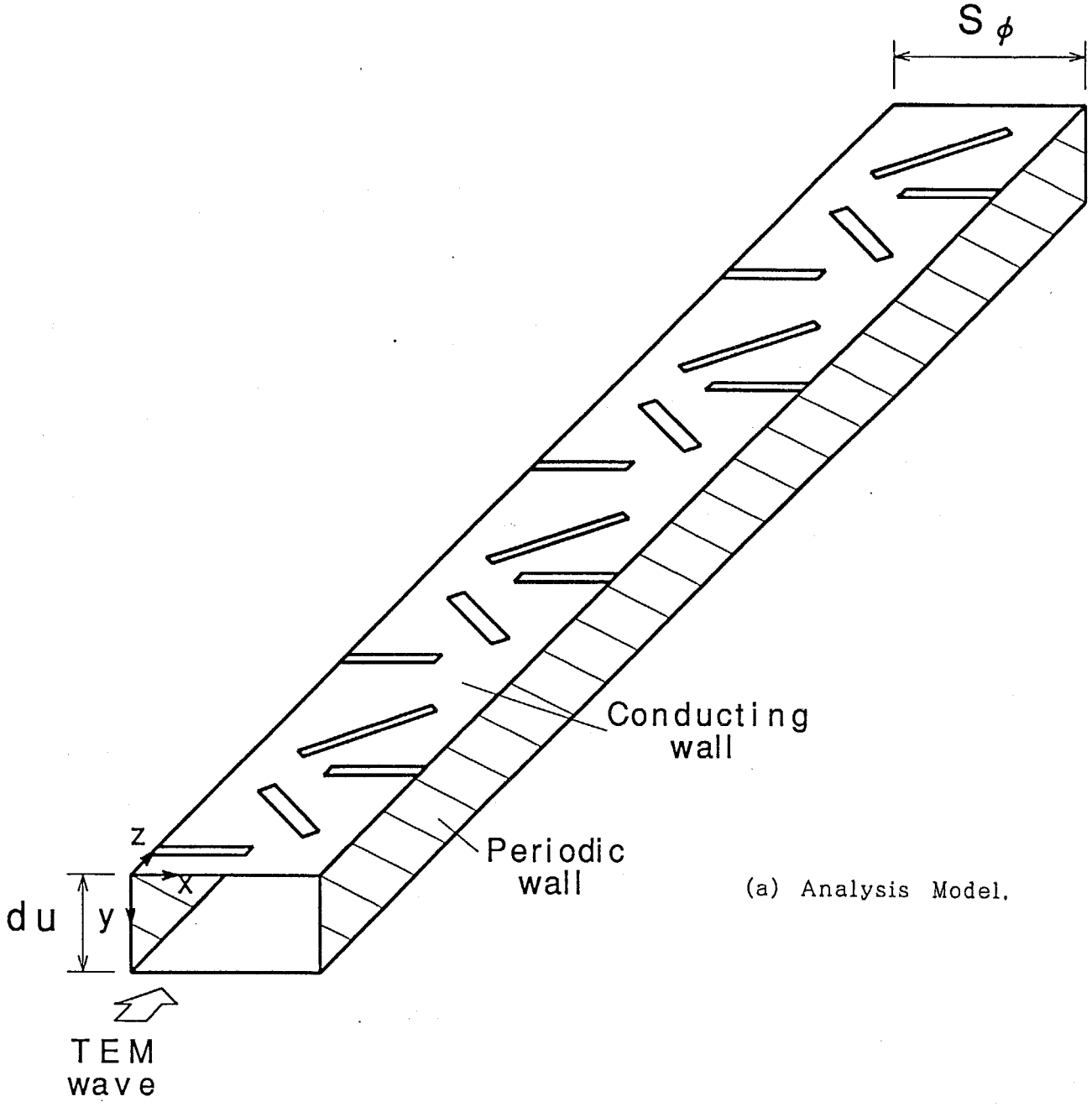

(a) Analysis Model.

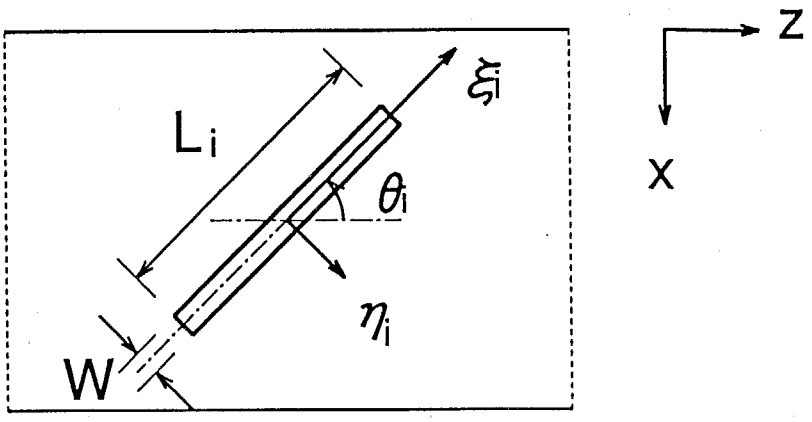

(b) Local coordinates on the #i slot.

Fig. 2-2. Analysis model for slot coupling estimation.

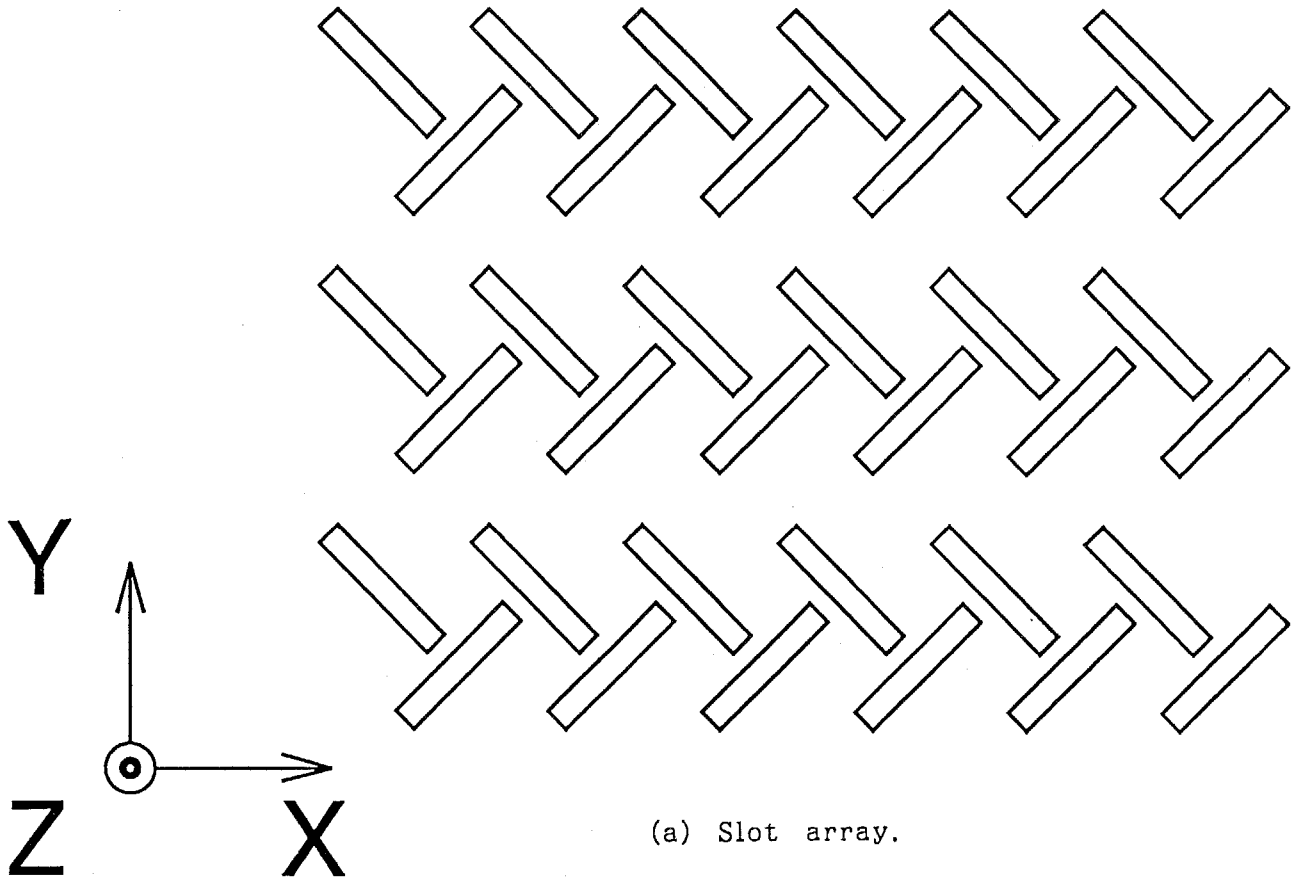

(a) Slot array.

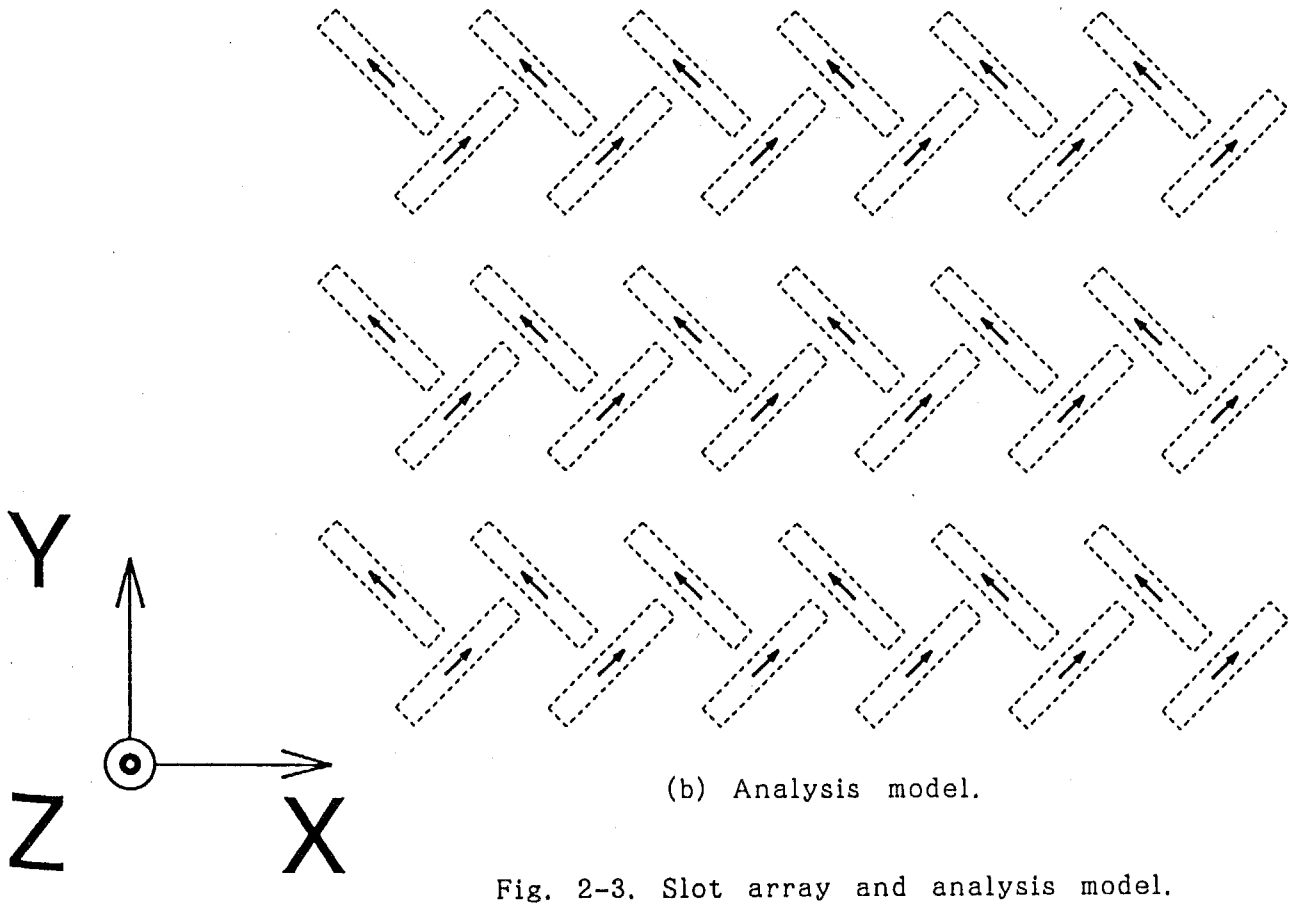

(b) Analysis model.

Fig. 2-3. Slot array and analysis model.

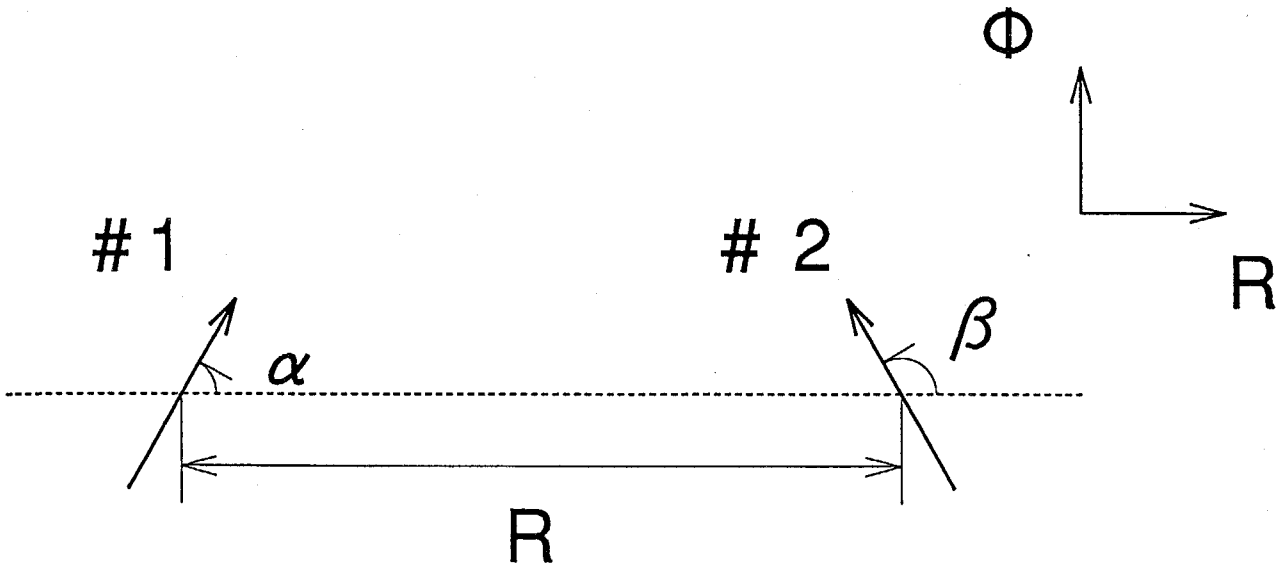

Fig. 2-4. Coordinates in the calculation of mutual impedance.

CHAPTER 3. BASIC CHARACTERISTICS OF A SLOT ON RADIAL WAVEGUIDE
- AN EQUIVALENT CIRCUIT -

3-1. Introductory Remarks

Before the discussion of antenna design, the radiation, the reflection and the transmission characteristics of a slot should be known for the design of a slot set. Especially in the design of LP-RLSA [1], the reflection from a slot perturbs the antenna operation.

This chapter discuss about an equivalent circuit of a slot on the radial waveguide [2]. The analysis model given in Sec. 2-2 is applied. Radiation and reflection coefficients are estimated in the form of S-matrix. The dependence of the matrix element upon the two major design parameters, the length L and the angle θ of a slot, is evaluated and characterized. An alternative impedance expression is also introduced for the practical antenna design where the angle θ is specified a priori from polarization requirement.

3-2 Model and Analysis

Figure 3-1 shows the analysis model. The basic structure is the same as discussed in Sec. 2-2. In this analysis, the slot is set at the center of the waveguide broadwall and the origin of the coordinate is set at the slot center.

First of all, the equivalent S-matrix circuit given in Fig. 3-2(b) is estimated. Considering the slot is located at the origin of the coordinate, Eq. (2-7) gives the following relation;

$$c^{(-)}=-c^{(+)}=(\text{real value})\triangleq c \qquad (3-1).$$

Substituting Eq. (3-1) into Eq. (2-5), another symmetrical expression about the excitation coefficient v is obtained:

$$v^{(-)}=-v^{(+)}\triangleq v \qquad (3-2).$$

The elements of S-matrix given in Eq. (2-12), (2-13), (2-15) and (2-

16) are simplified as follows;

$$S_{11}=S_{22}=\frac{vc}{2Z_o} \qquad (3-3),$$

$$S_{21}=S_{12}=1-\frac{vc}{2Z_o} \qquad (3-4).$$

Thus the resultant S-matrix is expressed in terms of only one parameter of S_{11} as

$$[S]=\begin{bmatrix} S_{11} & 1-S_{11} \\ 1-S_{11} & S_{11} \end{bmatrix} \qquad (3-5).$$

Another important parameter in the antenna design is the radiation from slots. Assigning the slot as port #3, which corresponds to the real radiation power from the slot, we can expand the S-matrix to three dimensional one as [3]

$$[S_e]=\begin{bmatrix} S_{11} & 1-S_{11} & S_{13} \\ 1-S_{11} & S_{11} & S_{23} \\ S_{13} & S_{23} & S_{33} \end{bmatrix} \qquad (3-6),$$

where the reciprocity principle of $S_{13}=S_{31}$ and $S_{23}=S_{32}$ are used implicitly. The structural symmetry requires

$$S_{23}=-S_{13} \qquad (3-7).$$

Therefore, the matrix $[S_e]$ is reduced to

$$[S_e]=\begin{bmatrix} S_{11} & 1-S_{11} & S_{13} \\ 1-S_{11} & S_{11} & -S_{13} \\ S_{13} & -S_{13} & S_{33} \end{bmatrix} \qquad (3-8).$$

Neglecting the conductor loss, we can impose the relation

$$[S_e][\overline{S_e}]^t=[I] \qquad (3-9),$$

where ^{t} and $\overline{\ }$ indicate the transposition and complex conjugate, respectively. [I] is the unit matrix. This condition leads us to the relations as (see appendix C)

$$S_{13}=\sqrt{1-|S_{11}|^2-|1-S_{11}|^2}\,exp(j\angle S_{11}) \qquad (3-10),$$

$$S_{33}=(1-2S_{11}^*)exp(j2\angle S_{11}) \qquad (3-11),$$

though S_{33} does not appear in the antenna design, for there is no incidence supposed from outside. Consequently, all the matrix elements are completely determined by only one parameter of S_{11} defined in Eq. (3-3).

The relation between the two parameters, the coefficient v and the S-matrix element S_{13}, is discussed. The v denotes the excitation coefficient of slot aperture field, while $|S_{13}|$ indicates the square root of total radiated power to half free space or the aperture illumination.

S_{13} can be expressed in terms of v by using Eq. (3-3) and (3-10) as

$$S_{13}=\sqrt{\left|\frac{(v+v^*)c}{2Z_0}+\frac{vv^*c^2}{2Z_0^2}\right|}\,exp(\angle v) \qquad (3\text{-}12).$$

To interpret this relation, the effective voltage v_e is introduced as

$$v_e\triangleq\int_{-L/2}^{L/2} vf(\xi)d\xi=\frac{2(1-\cos k_0L/2)}{k_0\sin k_0L/2}v \qquad (3\text{-}13).$$

Figure 3-3 shows $|v_e|$ vs $|S_{13}|$ for various combination of L and θ. It firmly confirms the proportionality between v_e and S_{13}. In the original analysis [4], the aperture illumination has been estimated by v, but it is not correct when the slot length is non-uniform over the aperture. It should be estimated by v_e (or S_{13}).

For the compatibility with the conventional design of general slot array [5], the slot is expressed in an alternative form of the series impedance circuit Z_s shown in Fig. 3-2(c). The relation between S_{11} and Z_s is

$$Z_s=\frac{2S_{11}}{1-S_{11}}Z_1 \qquad (3\text{-}14),$$

where Z_1 $(=Z_0/\sqrt{\varepsilon_r})$ is the wave impedance in the guide.

The following relation between total excitation coefficient of

slot v_o and excited voltage V on the impedance circuit in Fig. 3-2(c) is derived (see appendix D in detail);

$$v_o=\frac{Z_o}{c\sqrt{Z_1}}V=\frac{Z_o}{c\sqrt{Z_1}}Z_s I \qquad (3-15),$$

where I is the current flowing through the impedance circuit. Since Z_o, c and Z_1 are all real values in Eq. (3-15), the excitation phase of slot ϕ_s is given as

$$\phi_s \triangleq \angle v_o = \angle V = \angle(Z_s I) \qquad (3-16).$$

On the other hand, the power radiated from slot P_s is equivalent to the power dissipated at Z_s as

$$P_s = Re(Z_s)|I|^2 \qquad (3-17).$$

3-3. Numerical Results

Figure 3-4 shows examples of frequency characteristics of Z_s for a slot specified as sample #1 in Table 3-1. It is similar to the parallel LCR resonance.

A slot has two structural parameters, coupling angle θ and slot length L. In practical design, θ is usually fixed from polarization requirement. Therefore, two important characteristics, radiation and reflection, are discussed as functions of L for the fixed angle θ in this section.

<u><reflection></u> Figure 3-5 shows the locus of the matrix element S_{11}, which equals to the reflection coefficient in the guide, for various slot length L. The key feature of the trace in Fig. 3-4 is its circular shape which passes just on the origin, with its center on the real-axis. Therefore, the trace is characterized by

$$S_{11}=C_{11}(\theta)(1+e^{j\psi(\theta,L)}) \qquad (3-18),$$

where C_{11} is a real constant determined by slot coupling angle θ and is independent of slot length L. The phase ψ is a function of both θ and L. Figure 3-6(a) shows the θ dependence of C_{11} for two different

structures. In both cases, C_{11} increases monotonously with the increase of θ. On the other hand, the contour of $\psi(\theta,L)$ for sample #1 is shown in Fig. 3-7. Though it is slightly affected by θ, the effect of L, which correspond to the resonant characteristics, is dominant.

<radiation> Substituting Eq. (3-18) into Eq. (3-10), the matrix element S_{13}, which corresponds to the slot illumination for the unit incidence of traveling wave from -z-direction, is expressed as

$$S_{13}=\sqrt{C_{11}(1-2C_{11})}(1+e^{j\psi(\theta,L)})$$
$$\triangleq C_{13}(\theta)(1+e^{j\psi(\theta,L)}) \quad (3-19).$$

$C_{13}(\theta)$ is presented in Fig. 3-6(b). The illumination $|S_{13}|$ takes its maximum when

$$2C_{11}=0.5 \quad (3-20),$$
$$\psi(L)=0 \ (\text{resonance}) \quad (3-21)$$

and

$$|S_{13}|_{max}=2C_{13max}\fallingdotseq 0.7071 \quad (3-22).$$

In sample #1 in Fig. 3-6(b), C_{13} is saturated around $\theta=80^{\circ}$. In sample #2, C_{13} takes its maximum at $\theta=50^{\circ}$. In the previous design [1] it was assumed that slot coupling strength is in proportion to $sin\theta$. Figure 3-6(b) points out that it is not correct rigorously, a t least around the resonance where $|S_{13}|\approx 2C_{13}$.

This phenomena is easily explained by impedance equivalent circuit shown in Fig. 3-8. If the slot is terminated by matched load Z_1, the maximum power-transfer condition at Z_a is realized when

$$Z_a=2Z_1 \quad (3-23).$$

The substitution of Eq. (3-23) into Eq. (3-14) results in Eq. (3-20). Therefore, impedance matching rather than coupling angle directly affects the maximum coupling.

In the antenna design, once the design parameters of antenna are determined, such as frequency f, waveguide height du, equivalent

guide width S_ϕ and relative permittivity ε_r, $C_{11}(\theta)$ is determined numerically, first. To this end, the calculation for some L_1 is sufficient, which determines the circle in Fig. 3-5 uniquely. In the special case of CP-RLSA, the slots have the angle $\theta=45^\circ$ and the design is drastically simplified; the maximum coupling is also estimated at this stage. In the final stage of the slot design, the slot lengths are determined to realize the required loci on the circle.

3-4. Concluding Remarks

This chapter discussed about the equivalent circuit of a slot on the radial waveguide. Reflection and radiation characteristics of slots are surveyed.

In antenna design, slot coupling is controlled by the slot length L and the angle θ. The relation between the reflection, radiation and these parameters are discussed in this chapter. The reflection and radiation coefficients are given in particular circles on the complex plane for fixed θ. As for the θ dependence, the conventional assumption that coupling strength is in proportion to $sin\theta$ is not accurate. The impedance matching plays another important role in the slot coupling.

References

[1] M. Ando, T. Numata, J. Takada and N. Goto, "A Linearly-Polarized Radial Line Slot Antenna," IEEE Trans. Antennas & Propag., vol. AP-36, no. 12, pp. 1352-1357 (Dec. 1985).

[2] J. Takada, M. Ando and N. Goto, "An Equivalent Circuit of a Slot in Radial Line Slot Antennas," IEICE Trans., vol. E74, no. 9, pp. 2922-2928 (Sep. 1991).

[3] Y. Konishi, H. Mizutamari, H. Sato, S. Mano and T. Katagi,

"Analysis and Design Methods of Planar Array Antenna with Slotted Waveguides Taking into Account Mutual Coupling," Trans. IEICE, vol. J71-B, no. 11, pp. 1325-1331 (Nov. 1988).

[4] J. Hirokawa, M. Ando and N. Goto, "Analysis of Slot Coupling in a Radial Line Slot Antenna for DBS Reception," IEE Proc., vol. 137, pt. H, no. 5, pp. 249-254 (Oct. 1990).

[5] R. E. Collin and F. J. Zucker (ed.), "Antenna Theory part 1," Sec. 14-8, McGraw-HIll, New York (1969).

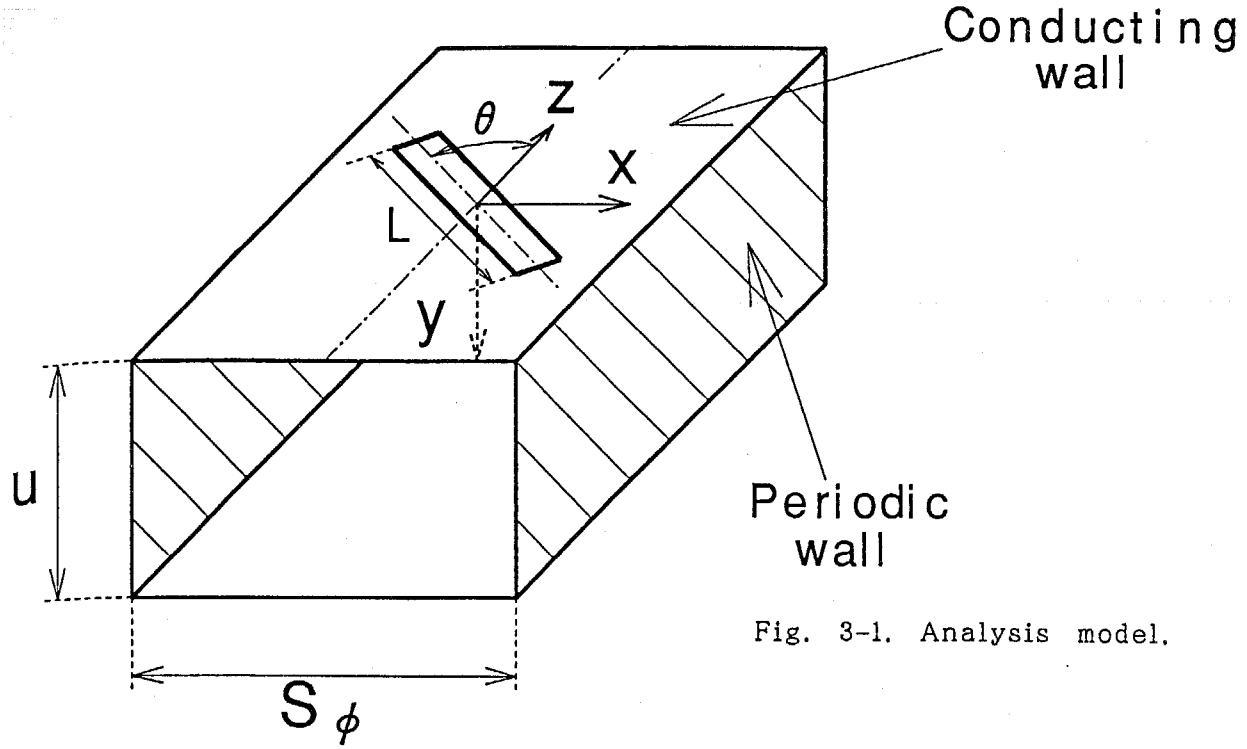

Fig. 3-1. Analysis model.

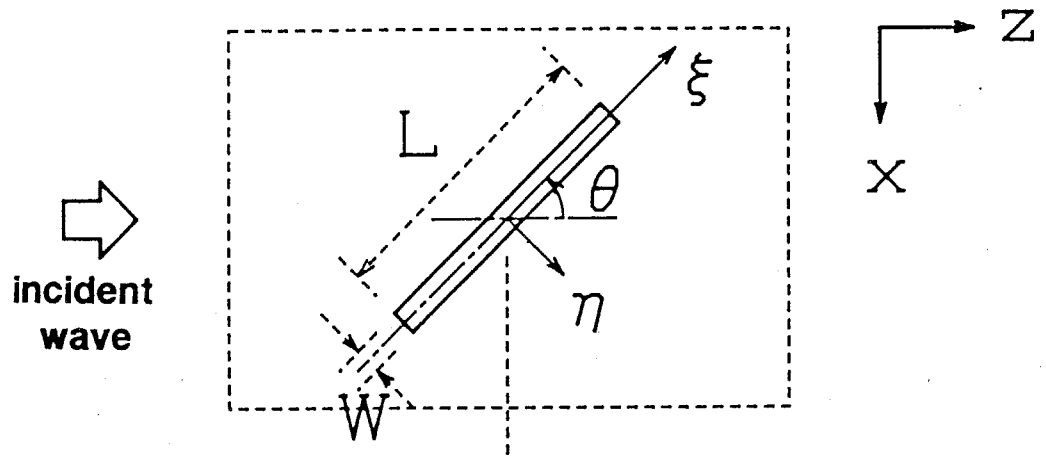

(a) Configuration and coordinates.

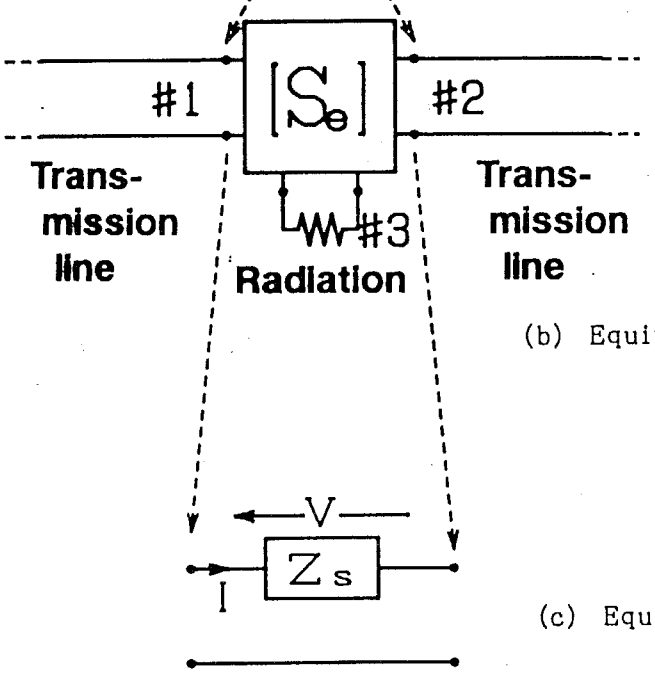

(b) Equivalent S-matrix.

(c) Equivalent impedance.

Fig. 3-2. Equivalent circuit of slot.

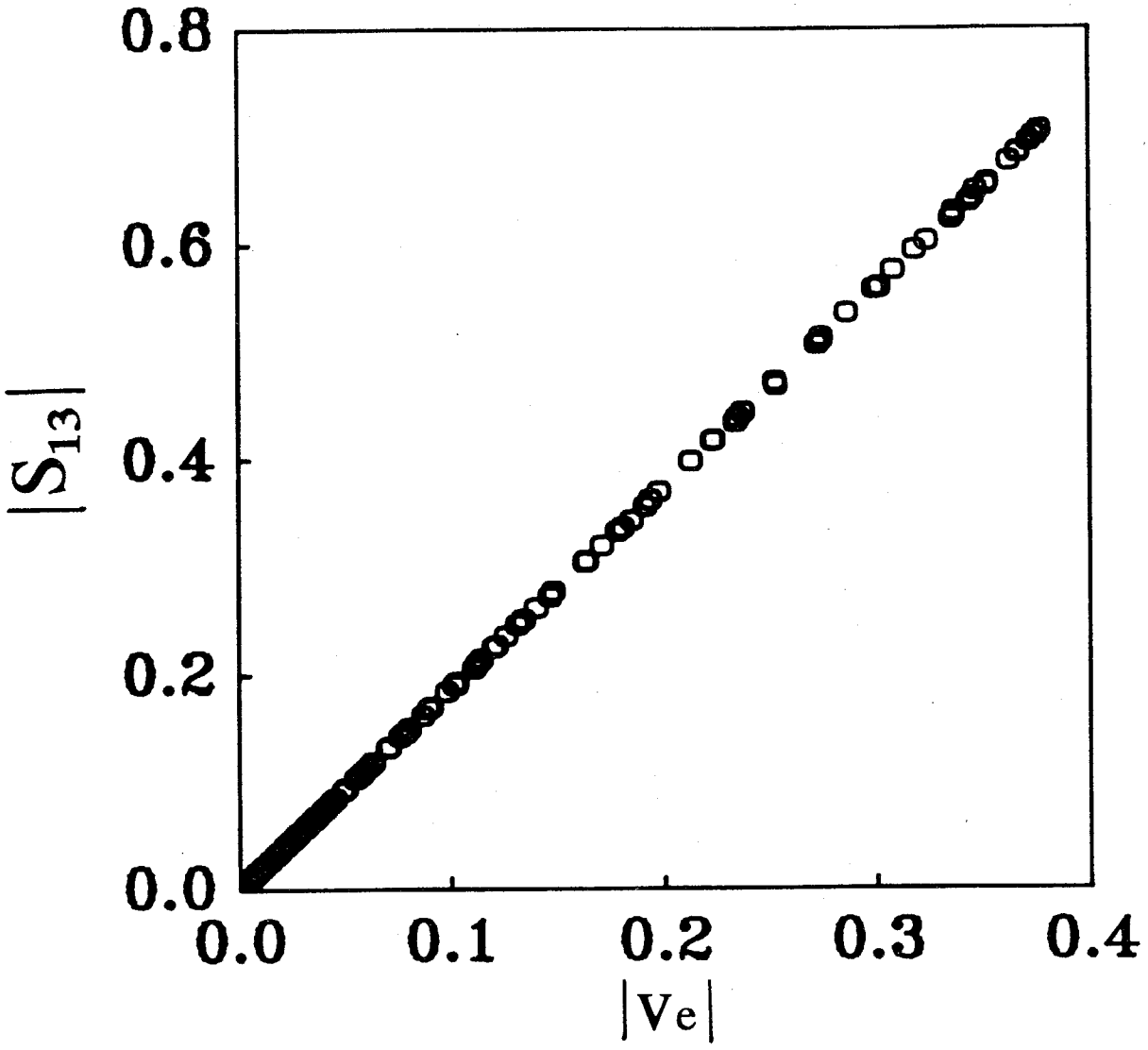

Fig. 3-3. Effctive slot voltage $|v_e|$ vs radiation coefficient $|S_{13}|$.

Table 3-1. Parameters used for numerical examples.

sample No.	#1	#2
frequency f [GHz]*	12.0	
waveguide width S_b [mm]	12.5	10.0
waveguide height du [mm]	7.5	5.0
permittivity ε_r	1.48	2.01
slot length L [mm]*	11.0+	—
slot width W [mm]	1.0	
slot coupling angle θ [deg]*	45+	—

*:varied, +:for Fig. 3-4.

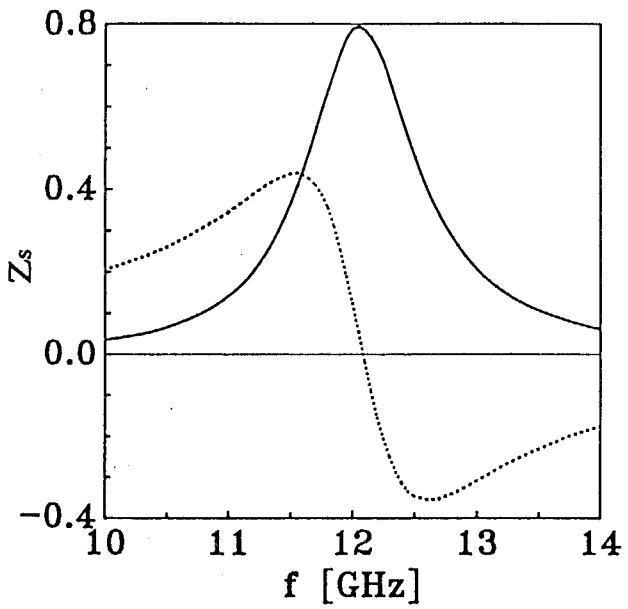

Fig. 3-4. Frequency characteristics of Zs.
solid line: resistance.
dotted line: reactance.

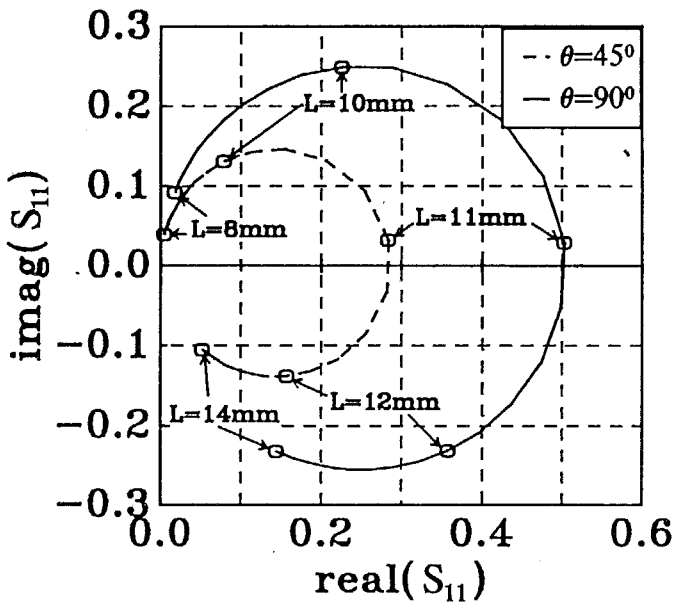

Fig. 3-5. Locus of S_{11} with respect to the slot length L.

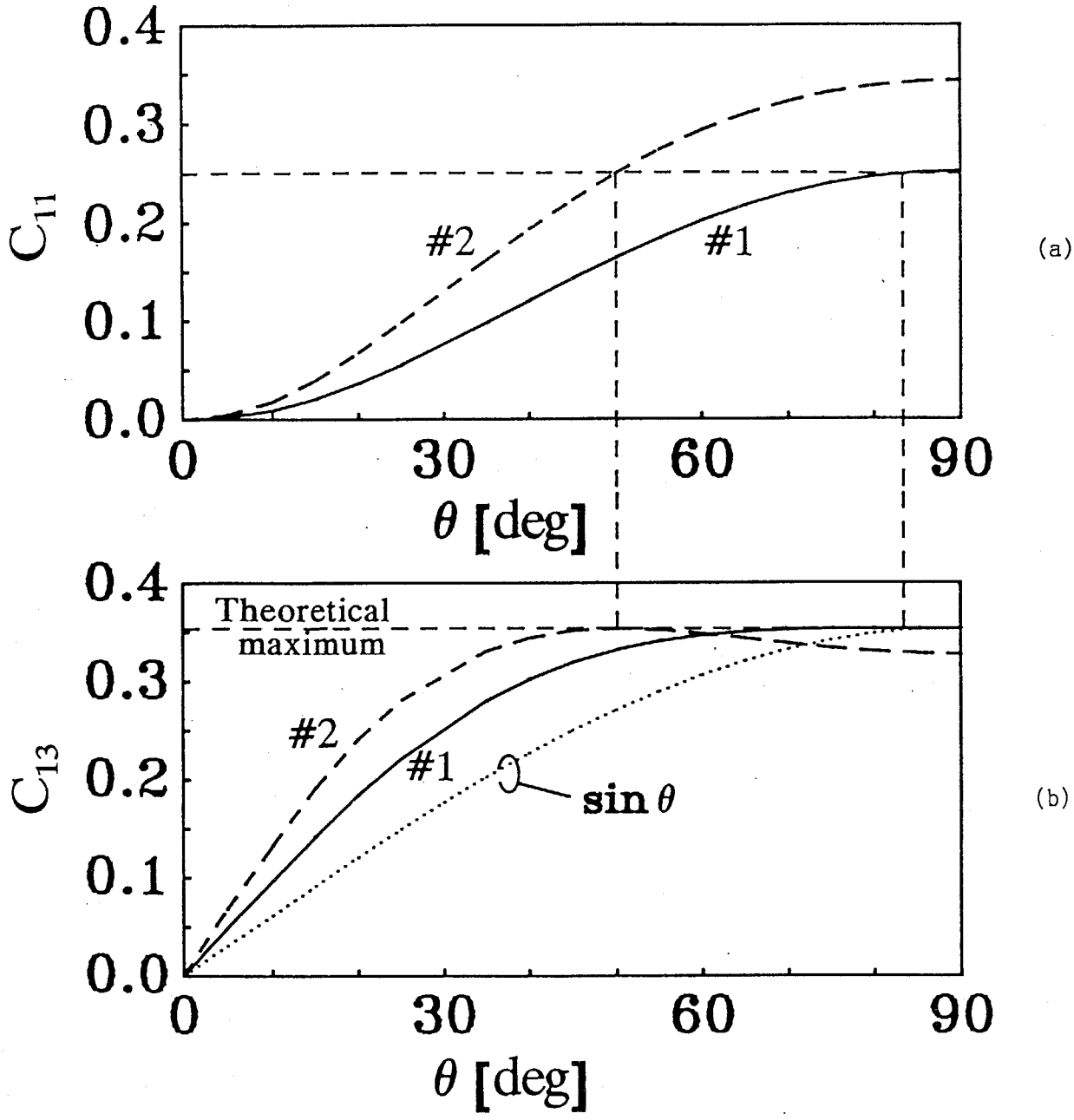

Fig. 3-6. (a) θ dependence of C_{11}.

(b) θ dependence of C_{13}.

solid line: sample #1.

dotted line: sample #2.

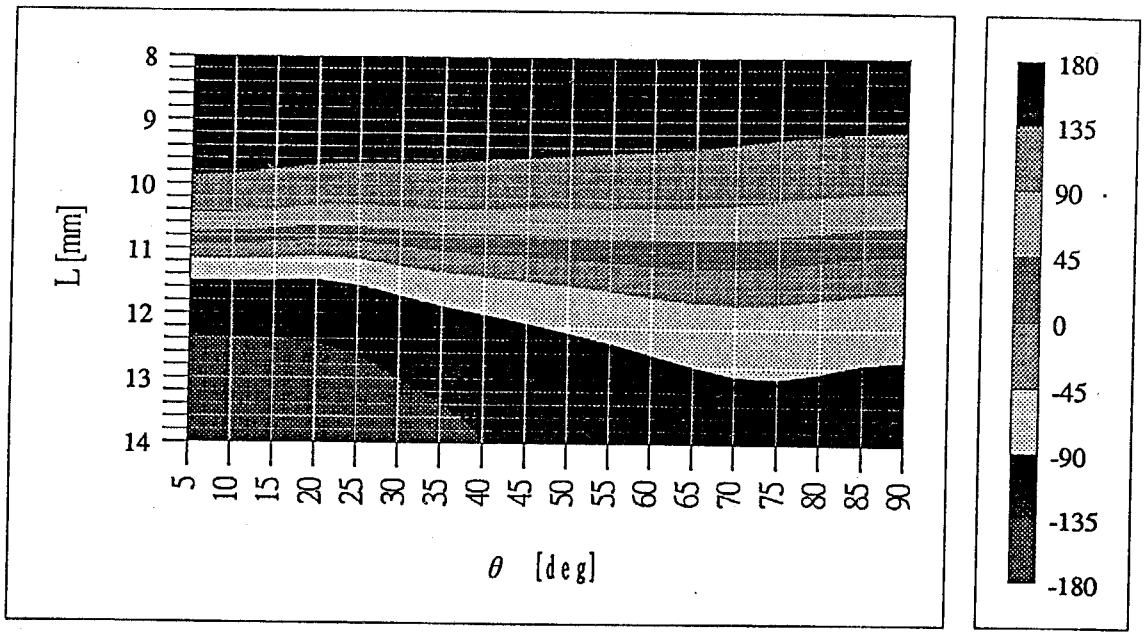

Fig. 3-7. Contour of $\psi(\theta,L)$ for sample #1.

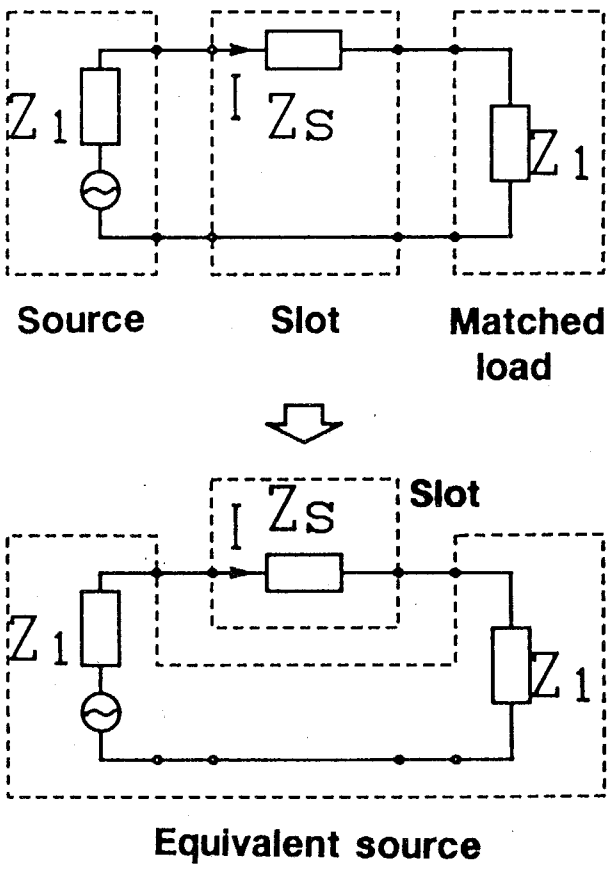

Fig. 3-8. Impedance equivalent circuit for maximum power transfer.

PART. 2 THE ILLUMINATION DESIGN FOR RLSA IN TRAVELLING WAVE OPERATION

CHAPTER 4. AN EQUIVALENT CIRCUIT OF A SLOT SET IN RLSA

4-1. Introductory Remarks

To realize the desired aperture illumination in the design of RLSA, the length and the spacing of each slot should be optimized. For that purpose, the coupling strength and the guide wavelength for each slot should be known. However, it is impossible to simulate the whole antenna structure with thousands of slots as it is. After the trial and error [1]-[3], the analysis model with periodic structure is introduced [4]. The results are in good agreement with the measured value, but it takes a lot of time to simulate, even by the supercomputer. This chapter presents an alternative technique to simulate the slot coupling using an equivalent circuit of a slot set [5]. Under the assumption of the traveling wave operation with small reflection, which is necessary for the stability of rotational symmetry in RLSA, a simplified formulation is presented. This analysis can reduce the CPU time to 1/40 of that for the conventional one. This technique also includes a new and simple design concept, power relation design by using the radiation elements with small reflection, which can be applied generally to the array antenna fed by the traveling wave.

In this section, the word "slot set" includes the slot pair for circular or linear polarization.

4-2. Traveling Wave Operation

Since the radial waveguide is an oversized one, the local reflection perturbs the axial symmetry of inner field, even the total return loss is reduced [6]. Therefore, the generally used beamtilt technique to suppress the reflection from slots in the slotted waveguide array [7] is not appropriate to reduce the return-loss in RLSA. Instead, each slot set must be optimized to suppress the local reflection. Then the antenna is operating with the traveling wave, where the power relation design neglecting the reflection becomes effective [8]. Under the traveling wave operation, the excitation of slots are expressed by the following parameters.

<amplitude> When the reflection from a slot set is sufficiently small, the radiation from slots is expressed by the attenuation of inner power attenuation. Applying the continuous attenuation model shown in Fig. 4-1, the inner power density $P(\rho)$ for outward propagating wave is expressed from the power relation in $\Delta\rho$ segment as

$$2\pi\rho P(\rho)-2\pi(\rho+\Delta\rho)P(\rho+\Delta\rho)=2\pi\rho\Delta\rho\{2\alpha(\rho)\}P(\rho) \qquad (4-1),$$

where α is defined as the coupling factor, which correspond to the inner field attenuation for unit ρ segment. The left side of Eq. (4-1) shows the difference between the incident power and the transmit power, while the right side denotes the radiated power. Assuming $\Delta\rho\to 0$, the following differential equation is obtained;

$$\frac{d}{d\rho}\{\rho P(\rho)\}=-2\alpha(\rho)\rho P(\rho) \qquad (4-2).$$

From Eq. (4-1), the aperture power density is proportional to $\alpha(\rho)P(\rho)$. Substituting the desired aperture illumination into Eq. (4-2), α distribution as a function of ρ is obtained. Assuming

the uniform aperture illumination, for example, $\alpha(\rho)$ is given as

$$\alpha(\rho)=\frac{\rho}{\frac{\rho_{max}}{\alpha_{max}}+\rho_{max}^2-\rho^2} \qquad (4-3),$$

where ρ_{max} and α_{max} are the radius of aperture and the maximum coupling factor, respectively.

The same discussion is valid for the inward traveling wave by replacing the power relation of Eq. (4-1) with

$$2\pi(\rho+\Delta\rho)P(\rho+\Delta\rho)-2\pi\rho P(\rho)=2\pi\rho\Delta\rho\{2\alpha(\rho)\}P(\rho) \qquad (4-4).$$

<phase> On the other hand, the phase distribution is controlled by S_ρ, the spacing of adjacent slot set in ρ-direction. Assuming the uniform phase distribution,

$$S_\rho=\lambda_g\triangleq\zeta\lambda_o \qquad (4-5),$$

where λ_g is the guide wavelength considering the slot coupling, λ_o is the free space wavelength and ζ is the slow wave factor defined as

$$\zeta=\frac{\lambda_g}{\lambda_o} \qquad (4-6).$$

Equation (4-5) is accurate only when the adjacent slot sets in the ρ-direction are identical. The different case is discussed later.

Therefore, once the coupling factor and the slow wave factor for a slot set are known, the slot arrangement can be designed. In the design of double-layered CP-RLSA with uniform slots, the coupling analysis was not necessary because the reflection from each slot pair is small in nature, and the power relation design is easily applied with constant α and ζ.

4-3. Conventional Analysis

In reference [4], the analysis model of 2-dimensional uniform slot array shown in Fig. 4-2 is assumed. Slot sets are arranged on

the parallel plate waveguide with the periods of S_ρ and S_ϕ along x- and z-direction, respectively. The incident TEM wave is propagating in +z-direction. As is discussed in Sec. 2-2, the periodic boundary condition with the period of S_ϕ is assumed inside the waveguide. On the other hand, the periodicity outside is also considered by assuming that all the slots on the equal-wavefront (eg. z=constant) are excited in the equal complex amplitude. This periodicity is reflected in the Green's function for external region. In the practical calculation, the number of the period is increased until the excitation coefficients converge.

The design parameters α and ζ are estimated from the excitation coefficients of slots. The complex amplitude of principal polarization from #j slot set E_j is defined as

$$E_j=\sum_{i=1}^{n} v_{ej i}^{(+)}\cdot\hat{\beta}^* \qquad (4-7),$$

where $\hat{\beta}$ indicates the unit vector of principal polarization (see Appendix E) and * indicates the complex conjugate. $v_{ej i}^{(+)}$ is the electric field vector radiated from slot #i in slot set #j, which is defined in the same manner as Eq. (3-13);

$$v_{ej i}^{(+)}=v_{j i}^{(+)}\iint_{S_{j i}} e_{j i}\,dS \qquad (4-8),$$

where $e_{j i}$ is defined in Eq. (2-2). Considering the traveling wave operation, E_j is approximated in the manner of least mean square as

$$E_j\propto exp\{-(\alpha+j\beta)z_j\} \qquad (4-9),$$

where α is the coupling factor defined in Eq. (4-1), β is the aperture phase gradient which related to the slow wave factor ζ defined in Eq. (4-6) as [1]

$$\beta=\left\{\frac{1}{\zeta\lambda_0}-\frac{1}{S_\rho}\right\}\cdot 2\pi \qquad (4-10),$$

and z_j is the z-location of the center of the slot set.

The result of analysis agrees well with the experimental results [5]. However, since 9×9 slot sets are assumed in the analysis, it takes a lot of time for calculation.

4-4. Equivalent Circuit and Antenna Design Parameters

4-4-1. Analysis Model

The analysis model is composed of one slot set on the rectangular waveguide with periodic boundary condition as is shown in Fig. 4-3. The excitation coefficients of slots together with the 2-port S-matrix of a slot set are calculated in the manner discussed in Sec. 2-2. In the analysis, the periodicity of external region along x-direction is considered by using the Green's function for periodic structure (Appendix A).

Taking account of the radiation phase, port #3 in the S-matrix equivalent circuit is defined as the radiation of principal polarization similar to Eq. (4-7);

$$S_{31} \propto \sum_{i=1}^{n} v_{ei}^{(+)} \cdot \hat{\beta}^{*} \qquad (4\text{-}11),$$

where $v_{ei}^{(+)}$ is the electric field vector radiated from slot #i defined in the same manner as Eq. (4-8).

4-4-2. S-Parameters and Design Parameters

The relation among the S-parameters and the slot design parameters α and ζ are discussed in this section [5].

Once the reflection from a slot set $|S_{11}|$ is sufficiently reduced, the radiation from a slot set is approximated by the continuous attenuation model discussed in the previous section. The power relation for a slot set is given by replacing $\Delta\rho$ in Eq. (4-1) by S_ρ. Since the equivalent S-matrix is defined for plane wave incidence, $\rho \to \infty$ is assumed and

$$P(\rho) - P(\rho + S_\rho) = 2 S_\rho \alpha P(\rho) \qquad (4\text{-}12),$$

where $P(\rho+S_\rho)$ is determined from the definition of S-matrix as

$$P(\rho+S_\rho)=|S_{21}|^2P(\rho) \qquad (4-13).$$

Substituting Eq. (4-13) into Eq. (4-12), the coupling factor α is given as

$$\alpha=\frac{1-|S_{21}|^2}{2S_\rho} \qquad (4-14).$$

On the other hand, the phase distribution on the equivalent network is shown in Fig. 4-4. The phase discontinuity of $\angle S_{21}$ occurs at the equivalent S-matrix for a slot set. The equivalent guide wavelength λ_g is defined from the phase difference between the incident and transmit phase as

$$\lambda_g=\frac{\theta_1-\theta_0}{2\pi}S_\rho \qquad (4-15).$$

Replacing θ_1 and θ_0 by $\angle S_{21}$ in Eq. (4-15), the slow wave factor ζ is given as

$$\zeta=\frac{2\pi S_\rho}{\left|\dfrac{2\pi S_\rho}{\lambda_g}-\angle S_{21}\right|\lambda_0} \qquad (4-16),$$

where $\lambda_g=\lambda_0/\sqrt{\varepsilon_r}$ is the unperturbed guide wavelength without slot.

In the rigorous phase design for non-uniform slot arrangement, Eq. (4-5) is invalid because the radiated phase varies with the admittance of the slot. The more accurate design is discussed by considering two adjacent slot sets a and b put in ρ-direction shown in Fig. 4-5. Firstly, two slot sets are connected together by the transmission line with the length of $S_{\rho a}=\zeta_a\lambda_0$ according to the definition of slow wave factor, when the radiated phase of principle polarization ψ_a and ψ_b are given as

$$\psi_a=\angle S_{31a}+\theta_a \qquad (4-17),$$

$$\psi_b=\angle S_{31b}+\theta_b \qquad (4-18).$$

However, as $\angle S_{31}$ generally varies with the slot length, ψ_a and ψ_b

are out of phase though $\theta_a=\theta_b$. To compensate the phase difference, S_{pa} is modified as

$$S_{pa}' = S_{pa} + \frac{\angle S_{31b} - \angle S_{31a}}{2\pi}\lambda_g$$

$$= \left\{ 1 + \frac{\angle S_{21a} + \angle S_{31b} - \angle S_{31a}}{2\pi} \right\} \lambda_g \qquad (4\text{-}19)$$

or

$$S_{pa}' = \zeta\lambda_0 + \frac{\Delta\psi_b - \Delta\psi_a}{2\pi}\lambda_g \qquad (4\text{-}20),$$

where $\Delta\psi=\psi-\theta$ is the difference between the radiated phase and the incident phase.

The S-parameters in the equivalent circuit and design parameters for aperture illumination are related by Eq. (4-14) and (4-16). The slot arrangement is designed by use of Eq. (4-2) and {(4-5) [uniform slot] / (4-20) [non-uniform slot]}.

This design using the equivalent circuit is more advantageous than the conventional analysis [2], for the radiated phase ψ can not be estimated in the latter.

4-5. Numerical Results

The numerical examples are presented to show the validity of this analysis. They are compared with the results of conventional analysis expressed in Sec. 4-3, which has already proved to be in good agreement with the experiments [2].

The circular-polarized slot pair is analysed. Table 4-1 shows the design parameters of structure. Figures 4-6(a) and (b) show the coupling factor and the slow wave factor as functions of slot length L, respectively. In the practical design, the slot length is set

shorter than the resonant length, where the results by both analyses are in good agreement. While the length is approaching or over the resonant length, the accuracy of both analyses are degraded by the increase of local reflection from a slot set. In the conventional array analysis, the approximation by the traveling wave attenuation becomes invalid. On the other hand, in the equivalnet circuit, the effect neglecting the reflection in Eq. (4-14) and (4-16) becomes obvious.

The numerical results indicate that this analysis is effective in the slot design. For example, the CPU time of this analysis is reduced to 1/40 that of conventional one by the supercomputer ETA10, where even the personal computer is applicable for the calculation.

4-6. Concluding Remarks

This chapter presented a new technique to estimate the slot coupling using an equivalent circuit of a slot set. The S-parameters for the equivalent circuit are related to the slot design parameters under the assumption of small reflection from each slot set. The numerical results are in good agreement with the conventional ones, while the CPU time for calculation is reduced to 1/40 by supercomputer ETA10. The power relation design presented in this chapter is applicable to the general array antenna fed by the traveling wave. The key point in this design is is to reduce the reflection from each element, which is a new design concept in the traveling wave array.

References

[1] M. Ando, H. Sasazawa, S. Nishikata and N. Goto, "A Slot Design of Radial Line Slot Antennas," Trans. IEICE, vol. J71-B, no. 11, pp. 1345-1351 (Nov. 1988).

[2] J. Hirokawa, M. Ando and N. Goto, "An Analysis of Slot Coupling on a Radial Waveguide," IEICE Technical Report, AP88-76 (Oct. 1988).

[3] J. Hirokawa, M. Ando and N. Goto, "An Analysis of Slot Radiation on the Waveguide with a Magnetic Wall for a RLSA", 1989 Spring Natl. Conv. Rec., IEICE, B-67. (Mar. 1989).

[4] J. Hirokawa, M. Ando and N. Goto, "Analysis of Slot Coupling in a Radial Line Slot Antenna for DBS Reception," IEE Proc., vol. 137, pt. H, no. 5, pp. 249-254 (Oct. 1990).

[5] J. Takada, M. Takahashi, M. Ando and N. Goto, "An Equivalent Circuit of Slot-Pair for Circularly-Polarized Radial Line Slot Antennas," 1990 Spring Natl. Conv. Rec., IEICE, B-137 (Mar. 1990).

[6] J. Takada, M. Ando and N. Goto, "A Beam-Tilted Linearly Polarized Radial Line Slot Antenna," Trans. IEICE, vol. J71-B, no. 11, pp. 1352-1357 (Nov. 1988).

[7] R. E. Collin and F. J. Zucker (ed.), "Antenna Theory part 1," Sec. 14-8, McGraw-Hill, New York (1969).

[8] M. Ando, K. Sakurai, N. Goto, K. Arimura and Y. Ito, "A Radial Line Slot Antenna for 12GHz Satellite TV Reception," IEEE Trans. Antennas & Propag., vol. AP-33, no. 12, pp. 1347-1353 (Dec. 1985).

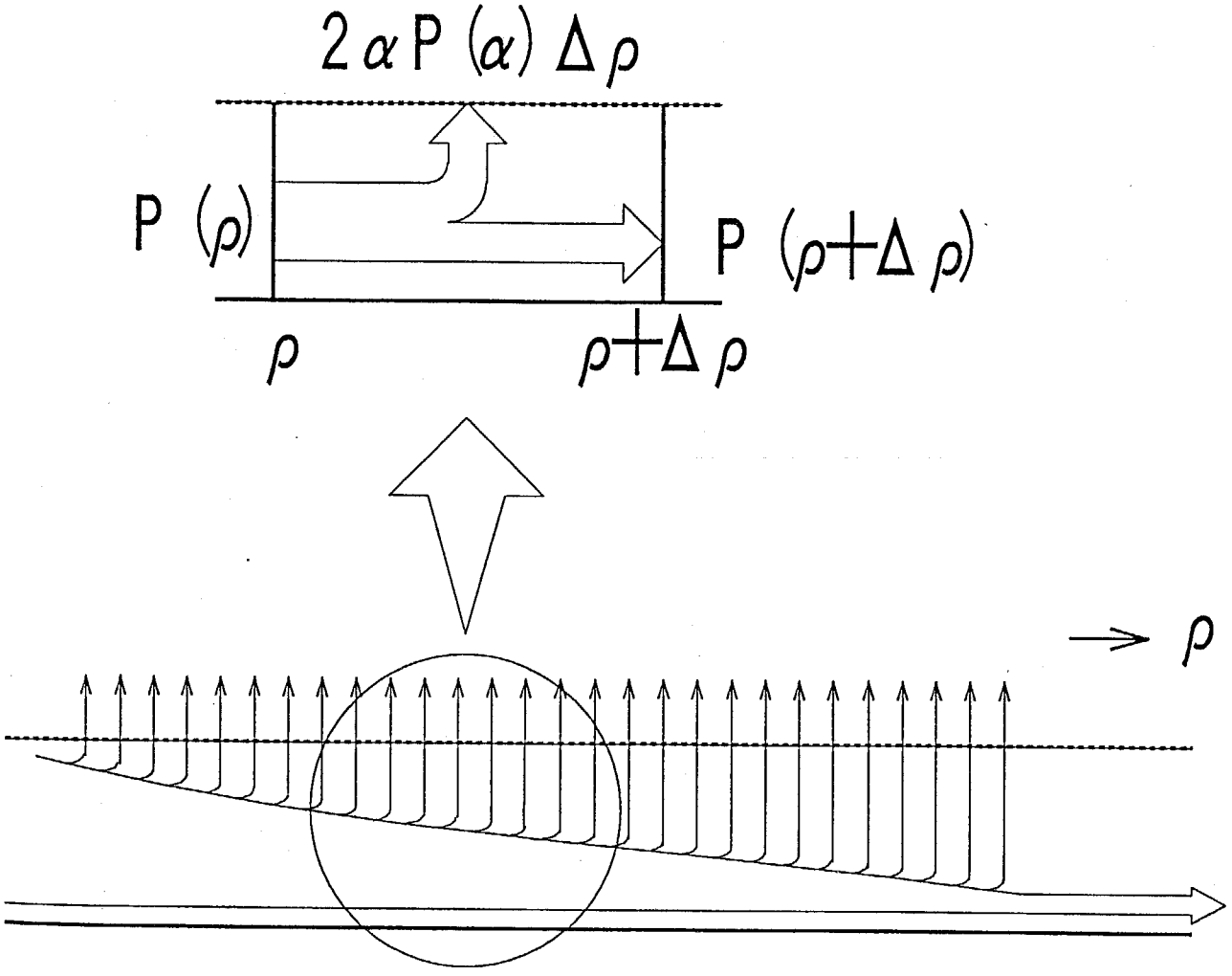

Fig. 4-1. Continuous attenuation model of inner power for cylindrical wave.

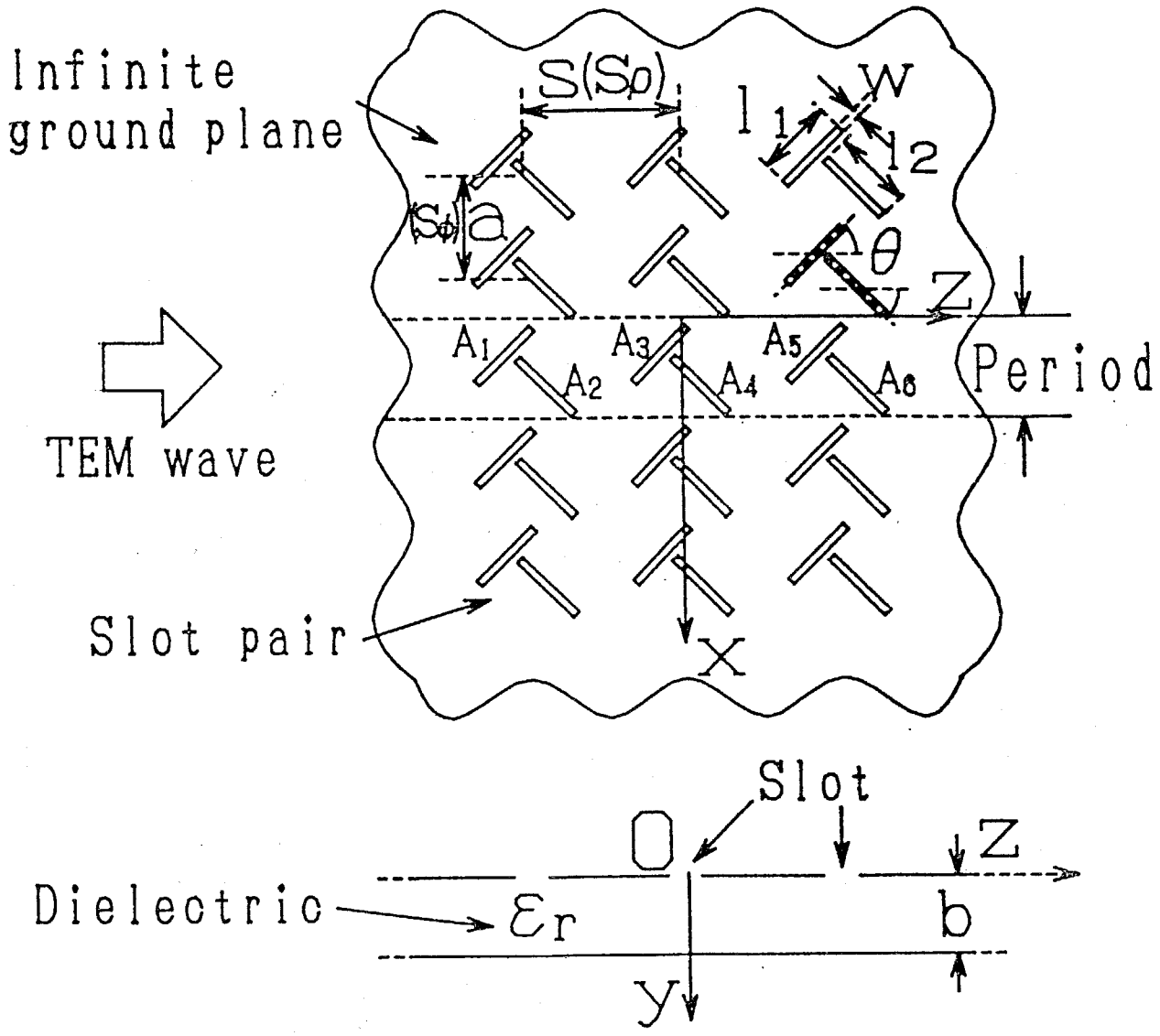

Fig. 4-2. 2-dimensional uniform slot array (conventional analysis model).

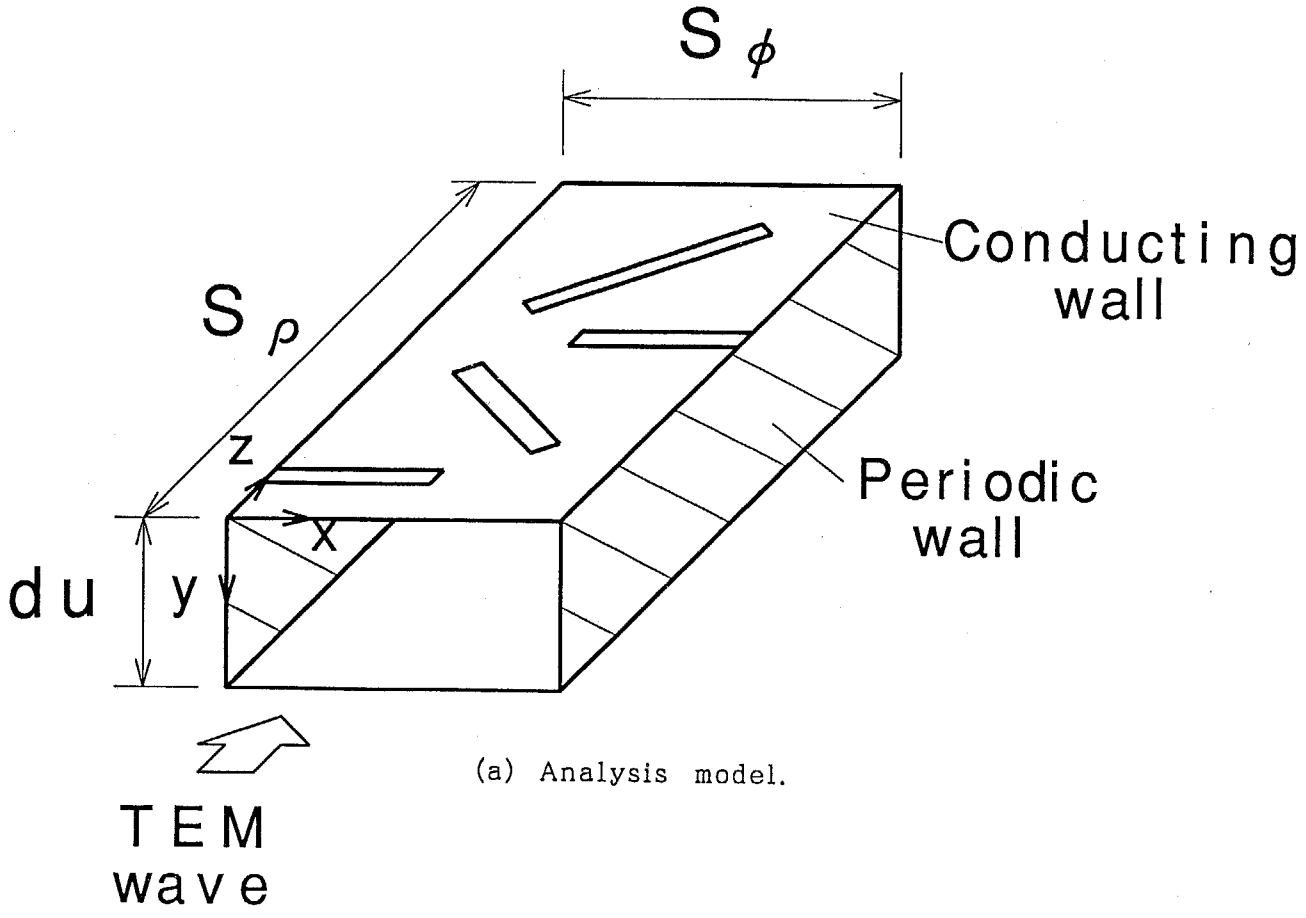

(a) Analysis model.

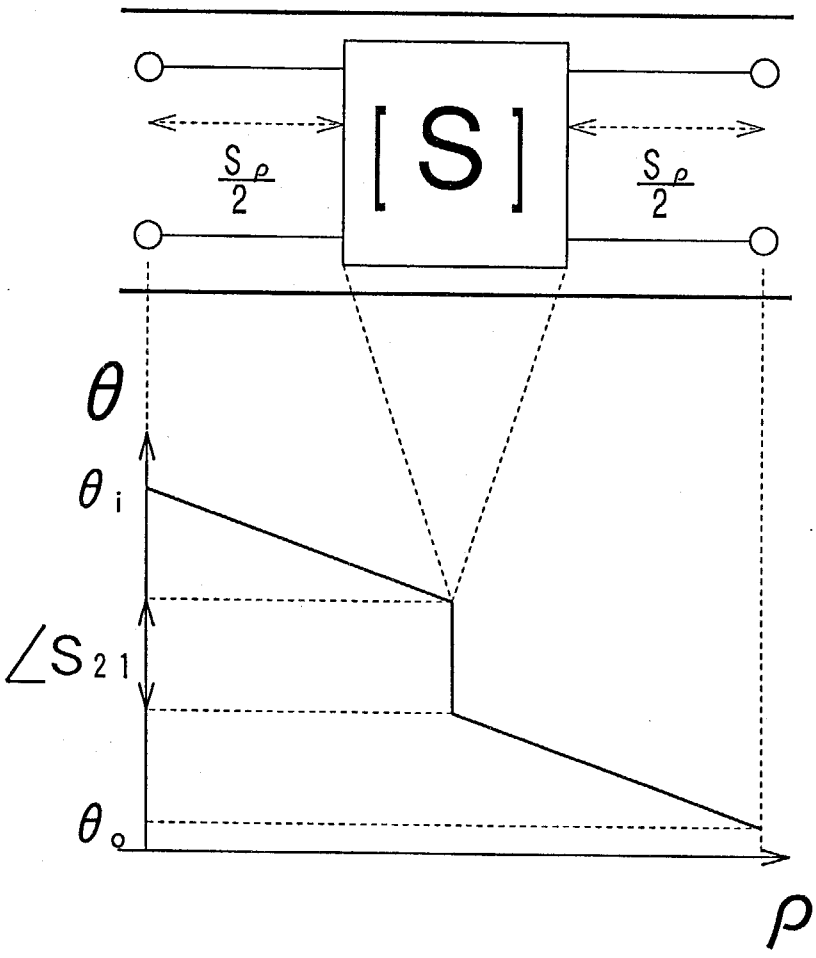

(b) Equivalent network; transmission line and equivalent S-matrix for a slot set.

(c) Phase distribution on the equivalent network.

Fig. 4-3. Analysis model and equivalent network of a slot set.

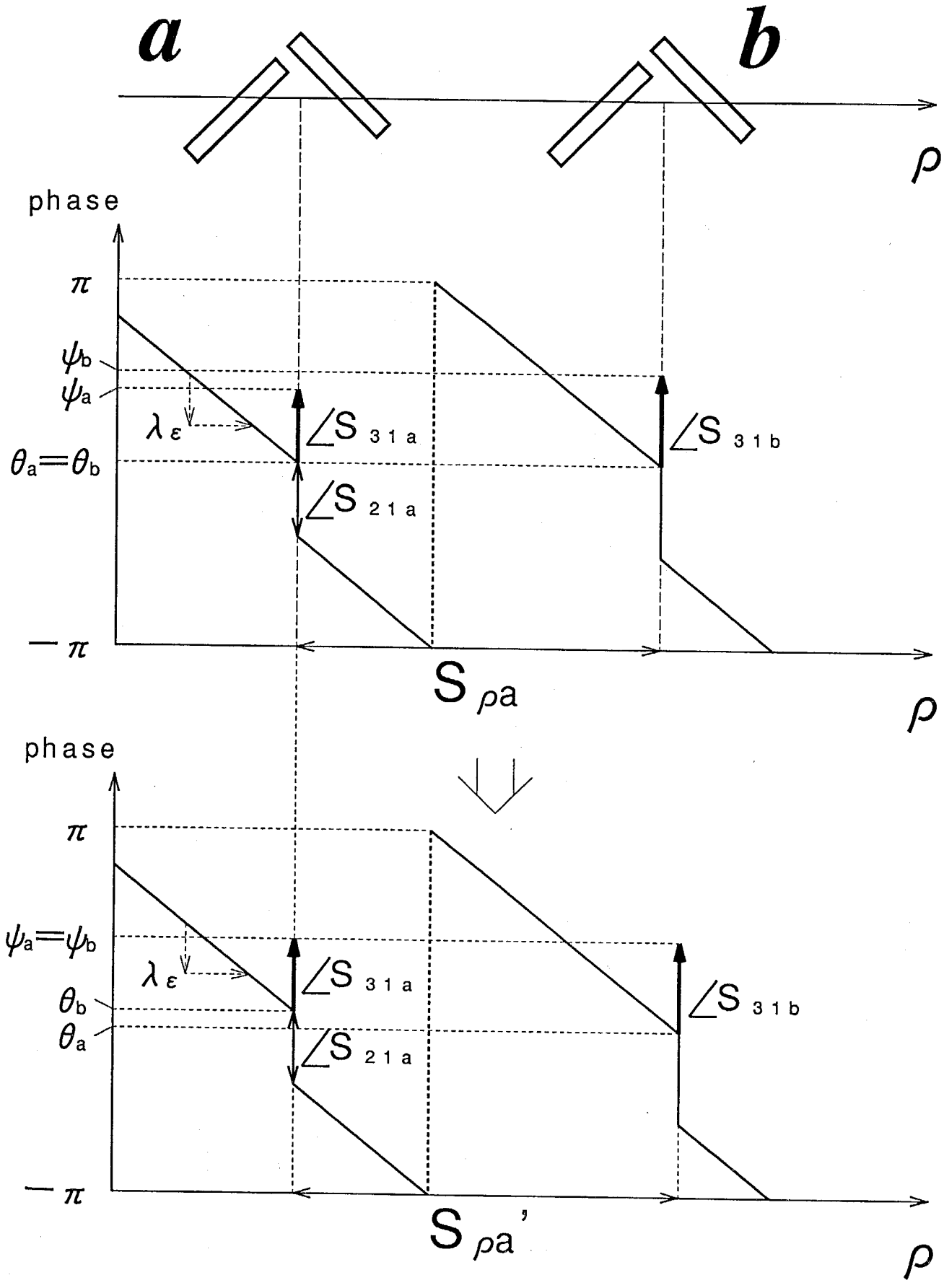

Fig. 4-4. Two adjacent slot sets put in ρ-direction.

Table 4-1. Design parameters for the analysis.

frequency f [GHz]*	11.85
waveguide width S_ϕ [λ_o]	0.5
waveguide height du [mm]	5.0
permittivity ε_r	1.5

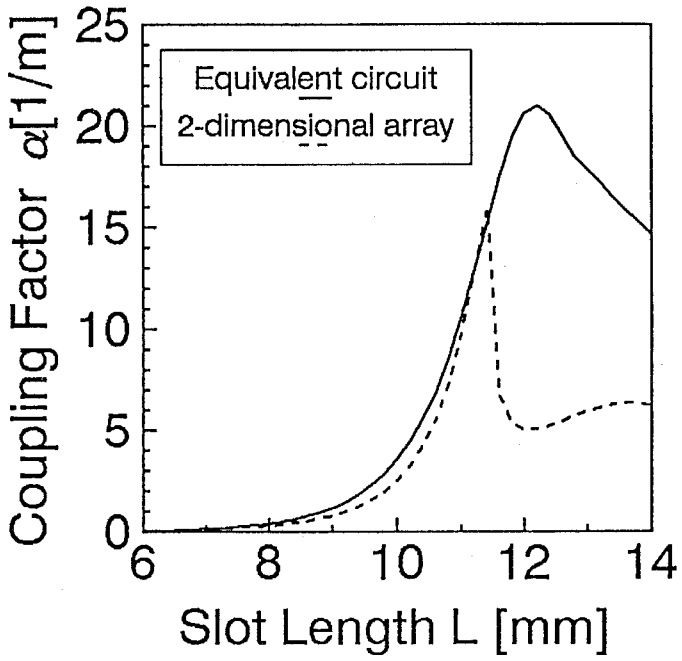

(a) Coupling factor.

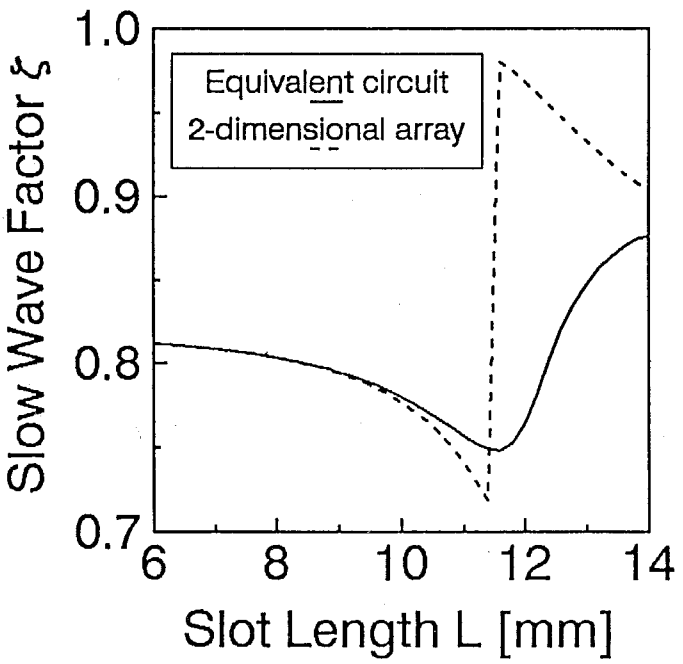

(b) Slow wave factor.

Fig. 4-5. Design parameters analysed by equivalent circuit and 2-dimensional array.

CHAPTER 5. FREQUENCY CHARACTERISTICS OF DOUBLE-LAYERED RLSA

5-1. Introductory Remarks

The RLSA is originally presented in the single-layered structure [1]. But the tapered apeture illumination degraded the aperture efficiency, since the slot coupling could not be theoretically estimated. The alternative configuration of double-layered RLSA is then presented [2]. Its advantage is that the uniform slot arrangement can realize the uniform apeture illumination. In spite of the structural complexity, the design is far simpler than that of the single-layered RLSA discussed in Chap. 6.

The bandwidth of RLSA decreases with the antenna diameter due to well known long-line effects of traveling wave antennas. Hence, the antenna diameter plays an important role in the design of RLSA.

The objective of this chapter is to predict the performance of double-layered RLSA as functions of antenna design parameters, especially of the diameter [3][4]. Firstly, the design of CP-RLSA with uniform slot density is surveyed. Then, the bandwidth and the gain of the antenna are calculated for the actual array as shown in Sec. 2-3. In the analysis, the slot coupling is evaluated on the basis of full wave analysis shown in Sec. 2-2 where the effects of all the design parameters are taken into account. The super-computer enables us to handle more than five thousand elements arranged spirally.

5-2. Design of Double-Layered RLSA

5-2-1. Structure

Figure 5-1 shows the double-layered CP-RLSA and its power-flow. Three circular plates compose a two-fold radial line waveguide. The shapes of the 180° E-bend at the outer part and the coaxal-to-

radial line adaptor at the center are numerically optimized to reduce reflections [5]. The upper guide is filled with dielectric material as a slow wave structure to suppress the grating lobes from the array. The power is fed from the coaxial cable at the center and transformed into a rotationally-symmetrical radially outward traveling wave in the lower guide. It is again transferred at the 180° E-bend into a inward traveling wave in the upper guide. The slots with constant length L are arrayed on the top plate. Two slots form a slot pair as a unit radiator of circular polarization. The slot pairs are arrayed spirally so that their radiation is added in phase; a small unused area exists in the circular aperture because of the spiral arrangement of slots. S_ρ and S_ϕ are the spacing between adjacent pair in the ρ and ϕ direction, respectively. In this paper, these are constant all over the aperture and the slot pair density is almost uniform. Most of the power is coupled to slots gradually and is radiated in the desired polarization producing a boresight beam, while the rest of the power is absorbed by the absorber at the center. A typical example of structural parameters is shown in table 5-1, which are used in the calculations in this paper.

5-2-2. Aperture Illumination

Let us assume the rotational symmetry of the inner field and the traveling wave operation discussed in Sec. 4-2, the apeture radiated field is approximated as [6][7]

$$f(\rho)=\frac{\exp(\alpha\rho)}{\sqrt{\rho}}\cdot\exp\left\{j2\pi\left(\frac{1}{\zeta\cdot\lambda_o}-\frac{1}{S_\rho}\right)\rho\right\} \qquad (5-1),$$

where α and ζ are the coupling factor and the slow wave factor, respectively. In this chapeter, the spacing S_ρ and the slot length L are constant, then α and ζ are assumed to be constant all over the aperture. Figure 5-2 shows an example of measured frequency

characteristics of α and ζ together with the predicted ones. In this chapter, the analysis explained of Sec. 4-3 is applied. They are in good agreement. Around the resonant frequency, α increases and ζ varies rapidly. When α is too large (~20[1/m]), the rotational symmetry of the traveling wave is excessively disturbed.

5-2-3. Optimum Coupling Factor

Antenna efficiency η is determined by

$$\eta=\eta_D \cdot \eta_R \qquad (5-2),$$

where η_D (<1) is the aperture efficiency concerning to the directive gain and η_R (<1) is the radiation efficiency accounting for the power absorption at the terminator. To increase the aperture efficiency η_D, the coupling factor should be chosen properly so that the aperture field distribution given by Eq. (5-1) may approach to uniform. On the other hand, to reduce the loss power at the absorber and increase the radiation efficiency η_R, the coupling should be strong to some extent. The radiation efficiency η_R is determined by the sizes of the aperture and absorber as

$$\eta_R=1-\exp(2\alpha(\rho_{min}-\rho_{max})) \qquad (5-3),$$

where ρ_{max} is the radius of antenna (=D/2) and ρ_{min} is the radius of absorber [8]. Taking into account all of them, the gain of CP-RLSA as a function of coupling factor α and antenna diameter D is calculated as shown in Fig. 5-3. From this figure, the coupling factor α has the optimum value α_{opt} in terms of gain. For D=600mm for example, α_{opt} is about 5.3 [1/m]. Decrease of the efficiency for $\alpha<\alpha_{opt}$ is due to the power loss in the absorber, while that for $\alpha>\alpha_{opt}$ is due to the the nonuniform aperture distribution where the amplitude distribution decreases too rapidly toward its center. From this figure, the optimum value of α is given as a function of antenna diameter. Figure 5-4 shows the optimum coupling factor α and the range of α which gives the gain degradation of less than

0.5dB. The optimum α[1/m] is almost inversely proportional to aperture diameter D[m] as

$$\alpha_{opt} \simeq \frac{3.2}{D} \qquad (5\text{-}4).$$

Figure 5-4 also shows the maximum antenna efficiency η retained for α_{opt}. The efficiency of RLSA with uniform slots decreases with the antenna diameter. The behavior η_R accounts for this phenomena. Substituting (5-4) into (5-3), we can show that η_R decreases monotonously as the antenna diameter decreases.

In addition to this quantitative prediction, we have to be reminded that excessive values of α degrade the rotational symmetry of the field. In wide variety of experiments, the desired operation with rotational symmetry has been observed for $\alpha \leqq 10$ at least.

Those results give the lower limitation for antenna diameter of RLSA; a small RLSA of 300mm in diameter still has the potential of the efficiency of 65% or the gain of 30dBi where $\alpha_{opt} \simeq 10$.

If α is varied as a function of ρ by arranging slots with different length, perfectly uniform aperture distribution can be realized, but in double-layered RLSA using radially inward traveling wave as excitation, the improvement is within a few percents in efficiency [9][10].

5-2-4. Antenna Design Procedure

Once the design parameters are determined, the desired slot length L to realize the optimum coupling factor α_{opt} at the design frequency is obtained by the analysis, together with the slow wave factor ζ. The slot pair radial spacing S_ρ is then set equal to λ_g $(=\zeta \cdot \lambda_0)$ to realize the uniform phase distribution.

In the following results of calculations, slot length L and radial spacing S_ρ are optimized by this procedure for each set of design parameters.

5-3. Bandwidth of Double-Layered CP-RLSA

The bandwidth of double-layered CP-RLSA is evaluated by taking account of the frequency characteristics of slot coupling.

The frequency characteristics of coupling factor α and slow wave factor ζ are obtained by the slot coupling analysis. The complex excitation coefficient of each slot on the array is determined by α and ζ, and then the array gain can be calculated.

Figure 5-5 shows the -3dB bandwidth and the maximum gain of double-layered CP-RLSA as functions of aperture diameter D. As the RLSA is a traveling-wave antenna, the bandwidth is limited due to the long line effect and is inversely proportional to D. A dashed line indicates the bandwidth determined by this effect. The actual bandwidth of RLSA is limited further due to the resonant characteristics of slots, that is, the changes in α and ζ from optimum ones. The overall bandwidth is shown in a solid line. It is less dependent of the antenna diameter. For example, the bandwidth is about 750MHz for D=400mm, and about 400MHz for D=1000mm.

Figure 5-5 also shows the maximum gain of double-layered RLSA. Using this figure, we can select the appropriate size of the antenna for each application, taking account of the bandwidth.

5-4. Effects of Other Design Parameters

Now, the effects of other structural parameters on bandwidth and maximum gain of the antenna are discussed. Calculations are done for the antenna diameter of 600mm. In the following graphs, solid lines indicate the -3dB bandwidth and dotted lines indicate the maximum gain.

5-4-1. Relative Permittivity of Slow Wave Structure ε_r

The relative permittivity of slow wave structure ε_r is determined

by the dielectric constant of material and expansion ratio [11]. It influences the frequency characteristics of slot coupling. Thus the antenna design, especially S_ρ, varies as well as the antenna performances. As the dielectric loss tanδ is negligibly small for the expanded dielectric, the loss is neglected in this calculation.

Figure 5-6 shows the -3dB bandwidth and maximum gain of CP-RLSA as functions of relative permittivity ε_r. The bandwidth, shown in the solid line, decreases with the increase of ε_r, for the electrical length of the waveguide is increased and the long line effect becomes notable. The maximum gain, indicated in the dashed line, slightly increases because of the following two reasons. One is that S_ρ decreases and unused spiral area at the outermost aperture (hatched in Fig. 5-1) is reduced. The other is that larger ε_r accounts for better suppression of grating lobes. Thus the compromise of bandwidth and gain determines ε_r. The practical value is about 1.4 - 1.8.

5-4-2. Height of Waveguide du

The height of upper waveguide or the thickness of dielectric sheet (slow wave structure) also changes the antenna performances via the slot coupling.

Figure 5-7 shows the -3dB bandwidth and maximum gain of CP-RLSA as functions of the waveguide height du. When the height is small, the slot coupling becomes larger. Hence, the separation between the resonance and the operation frequency can be set larger in the design. At the operation frequency, the variations of α and ζ ($d\alpha/df$ and $d\zeta/df$) become small and the bandwidth increases. The gain remains almost unchanged, but the guide wavelength becomes slightly short and the unused spiral area decreases, which results in the small increase of the gain. If the height becomes excessively smaller, however, the design of reflectionless radial-coaxial

adaptor or 180° E-bend become more difficult, though it is not included in this analysis.

5-4-3. Slot Pair Angular Spacing S_ϕ

The slot pair radial spacing S_ρ is set to be equal to the guide wavelength, but the angular spacing S_ϕ can be varied in the design. For the larger angular spacing, higher modes are excited and disturb the rotational symmetry of the field. The smaller angular spacing have been preferred from this point of view.

Figure 5-8 shows the -3dB bandwidth and maximum gain of CP-RLSA as functions of slot pair angular spacing S_ϕ. S_ϕ has little effects on the bandwidth and the maximum gain.

5-5. Concluding Remarks

This chapter surveyed the design and the performances of double-layered CP-RLSA and predicts the gain and the bandwidth as functions of the antenna diameter. Theoretical bandwidth due to the long line effect decreases monotonously with the antenna diameter. In practice, the bandwidth of RLSA is limited by slot resonance as well; the resultant antenna bandwidth is smaller and the dependence on the antenna diameter is reduced a little.

This chapter also presented the effects of design parameters of double-layered CP-RLSA (ε_r, du, S_ϕ) on the antenna gain and bandwidth, considering the slot coupling exactly. Relative permittivity of slow wave structure affects the bandwidth and gain considerably, and ε_r=1.4-1.8 is favorable value. The height of waveguide and the slot pair angular spacing have little influence on bandwidth or gain. However, it is preferred for stable rotationally symmetric field to use lower waveguide and smaller spacing.

The results in this chpater stimulates the future development of RLSA with wide varieties of diameters.

Similar discussions for single-layered structure with nonuniform slot distribution has been done about the antenna diameter [12], where the frequency characteristics are almost the same as double-layered one. Consequently, the effects of ε_r, du and S_ϕ are expected to be similar, though they are left for future study.

References

[1] N. Goto and M. Yamamoto, "Circularly Polarized Radial Line Slot Antennas," IECEJ Technical Report, AP80-57 (Oct. 1980).

[2] M. Suzuki and N. Goto, "A Matched Load of Radial Line Slot Antenna," IECEJ Technical Report, AP82-100 (Nov. 1982).

[3] M. Ando, J. Takada and N. Goto, "Aperture-Diameter Dependence of Efficiency of RLSA," 1989 Spring Natl. Conv. Rec., IEICE, SB-1-3 (Mar. 1989).

[4] J. Takada, M. Ando and N. Goto, "The Bandwidth and the Gain of Radial Line Slot Antenna with Uniform Slot Density," Trans. IEICE, vol. E73, no. 8, pp. 1372-1377 (Aug. 1990).

[5] M. Ando, S. Ito, K. Kawasaki and N. Goto, "A Design of a Radial Line Slot Antenna with Improved Input VSWR," Trans. IEICE, vol. J70-B, no. 4, pp. 495-504 (Apr. 1987).

[6] H. Sasazawa, S. Nishikata, J. Takada, M. Ando and N. Goto, "A High Efficiency Flat Antenna for Satellite Communication," IECEJ Technical Report, AP87-115 (Jan. 1988).

[7] H. Sasazawa, Y. Oshima, K. Sakurai, M. Ando and N. Goto, "Slot Coupling in a Radial Line Slot Antenna for 12-GHz Band Satellite TV Reception," IEEE Trans. Antennas & Propag., vol. AP-36, no. 9, pp. 1221-1226 (Sep. 1988).

[8] M. Ando, K. Sakurai, N. Goto, K. Arimura and Y. Ito, "A Radial Line Slot Antenna for 12GHz Satellite TV Reception," IEEE Trans. Antennas & Propag., vol. AP-33, no. 12, pp. 1347-2353 (Dec.

1985).

[9] H. Sasazawa, M. Ando and N. Goto, "Efficiency Optimizing Slot Arrangements in Radial Line Slot Antennas," IECEJ Technical Report, AP86-105 (Nov. 1986).

[10] M. Takahashi, J. Takada, M. Ando and N. Goto, "A Design of a Radial Line Slot Antenna with Uniform Aperture Distribution," 1989 Autumn Natl. Conv. Rec., IEICE, B-34 (Oct. 1989).

[11] H. Moriyama, J. Takada, M. Ando and N. Goto, "A Radial Line Slot Antenna with an Expanded Polyethylene Slow Wave Structure," Trans. IEICE, vol. E71, no. 10, pp. 968-971 (Oct. 1988).

[12] K. Yamamoto, M. Takahashi, M. Ando and N. Goto, "Frequency Characteristics of Radial Line Slot Antennas," IEICE Technical Report, AP91-45 (July 1991).

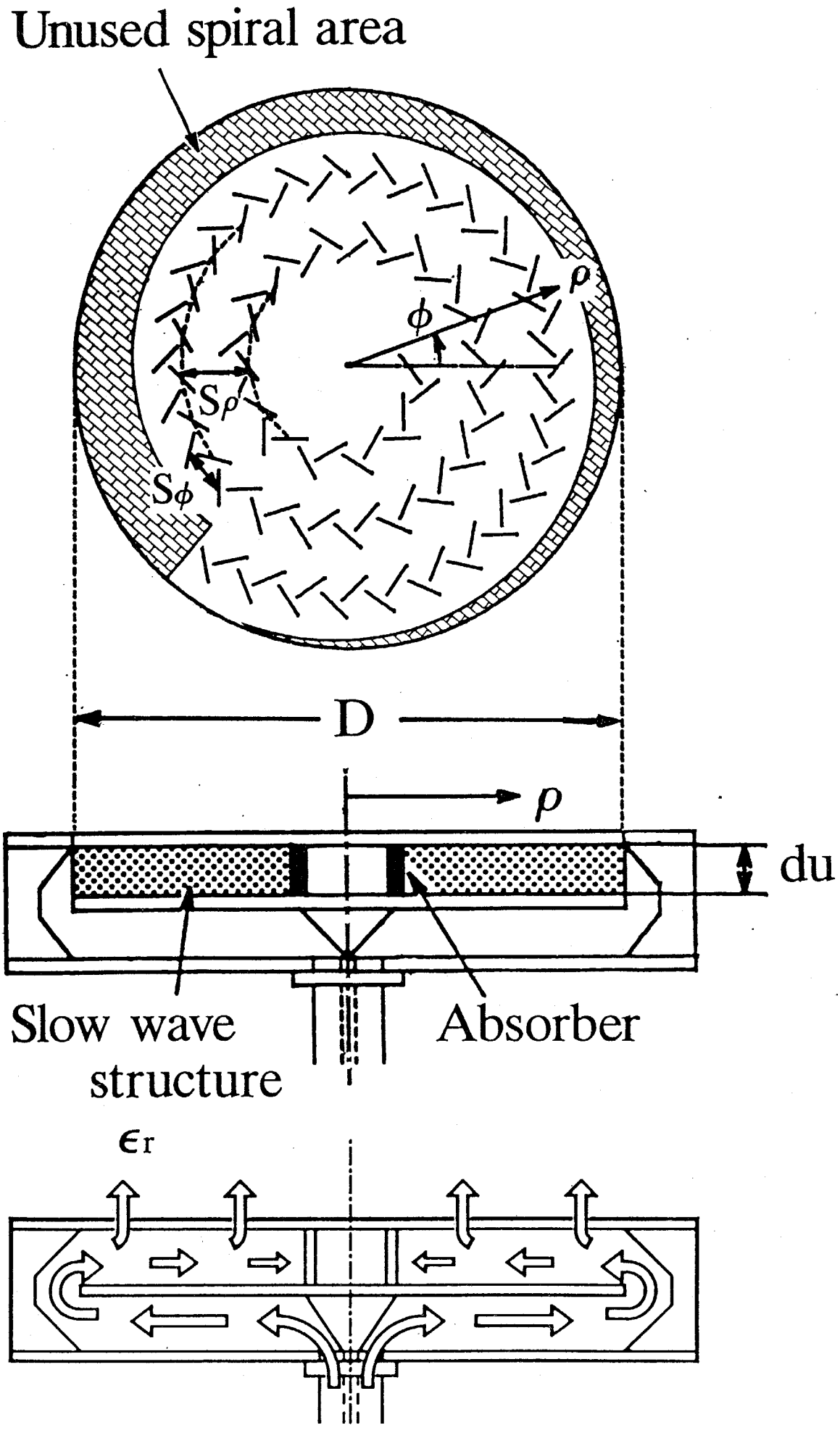

Fig. 5-1. Double-layered CP-RLSA.

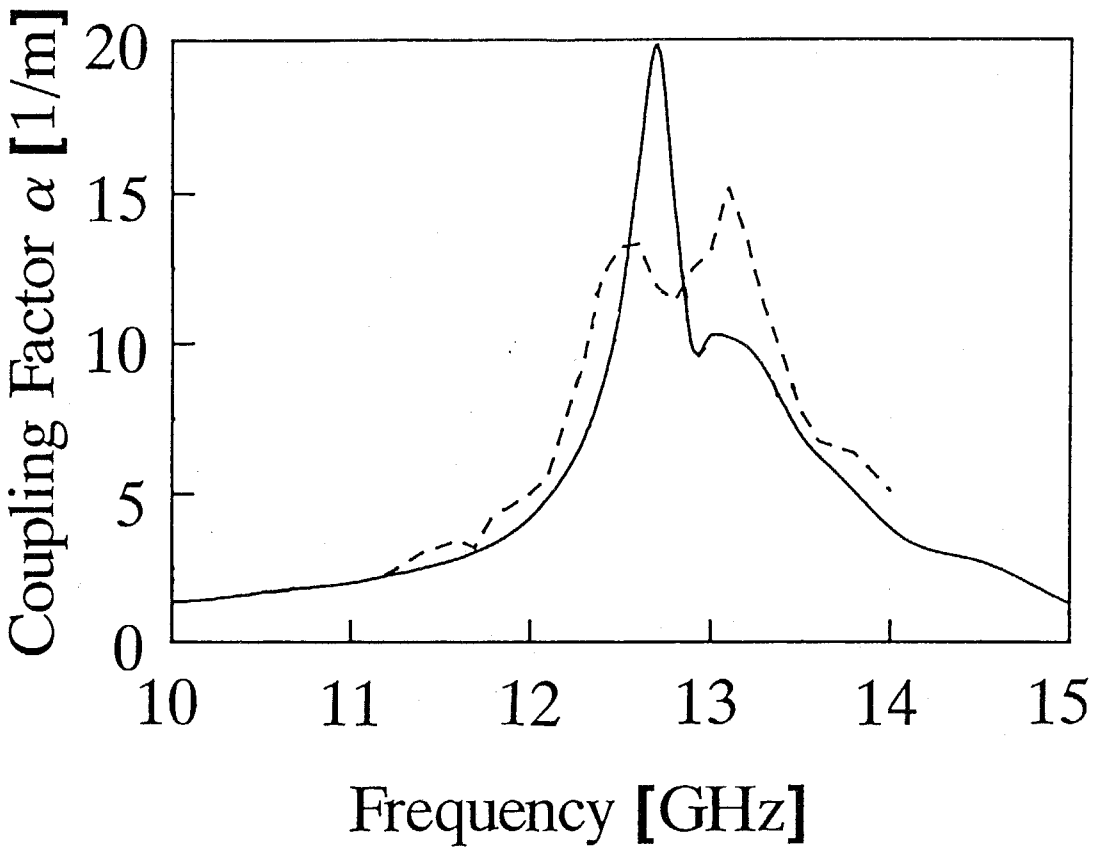

(a) Coupling factor α.

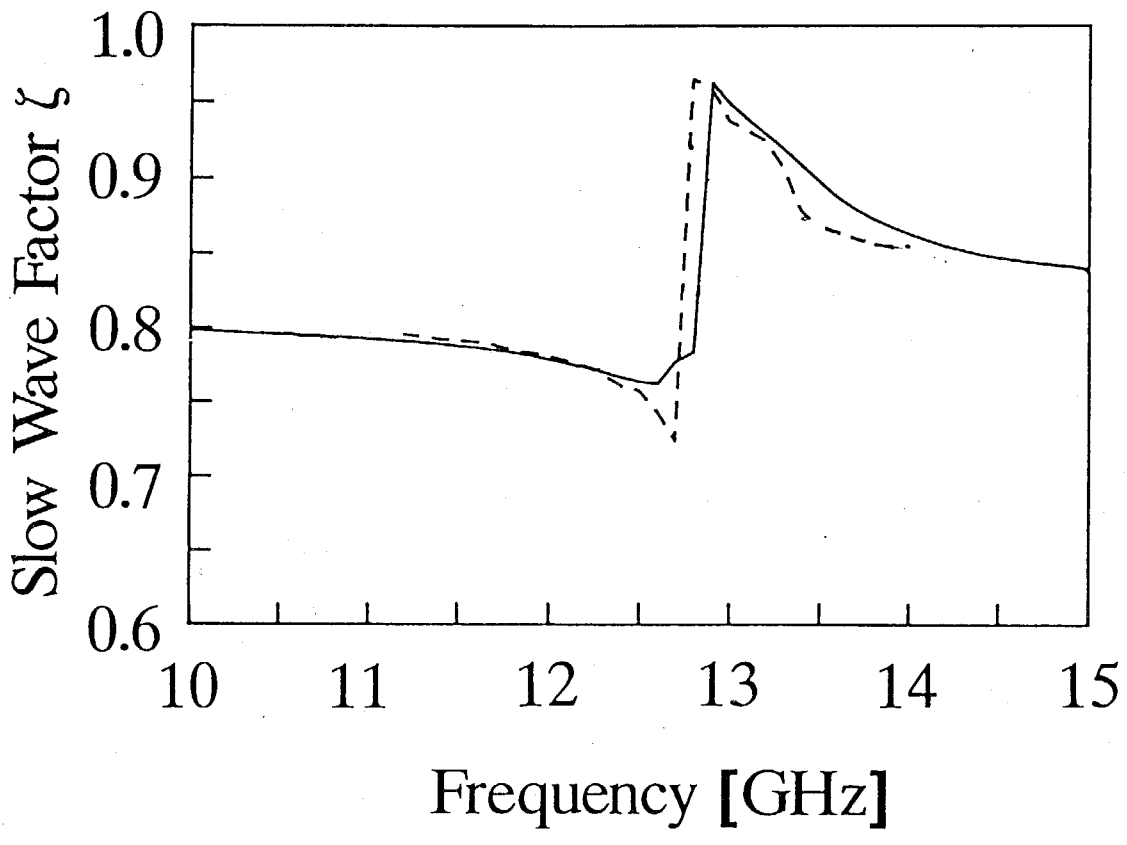

(b) Slow wave factor ζ.

Fig. 5-2. Frequency characteristics of CP-RLSA.

solid line: theory, dashed line: measured.

Table 5-1. An example of antenna design parameters.

frequency f_o [GHz]		12.0
slot pair radial spacing S_ρ	[mm]	18.85*
	[λ_o]	0.754
slot pair angular spacing S_ϕ	[mm]	12.5
	[λ_o]	0.5
slot length L	[mm]	9.85*
	[λ_o]	0.394
antenna diameter D [mm]		600
waveguide height du [mm]		7.5
permittivity ε_r		1.56

*:nominal value, and varied in optimization.

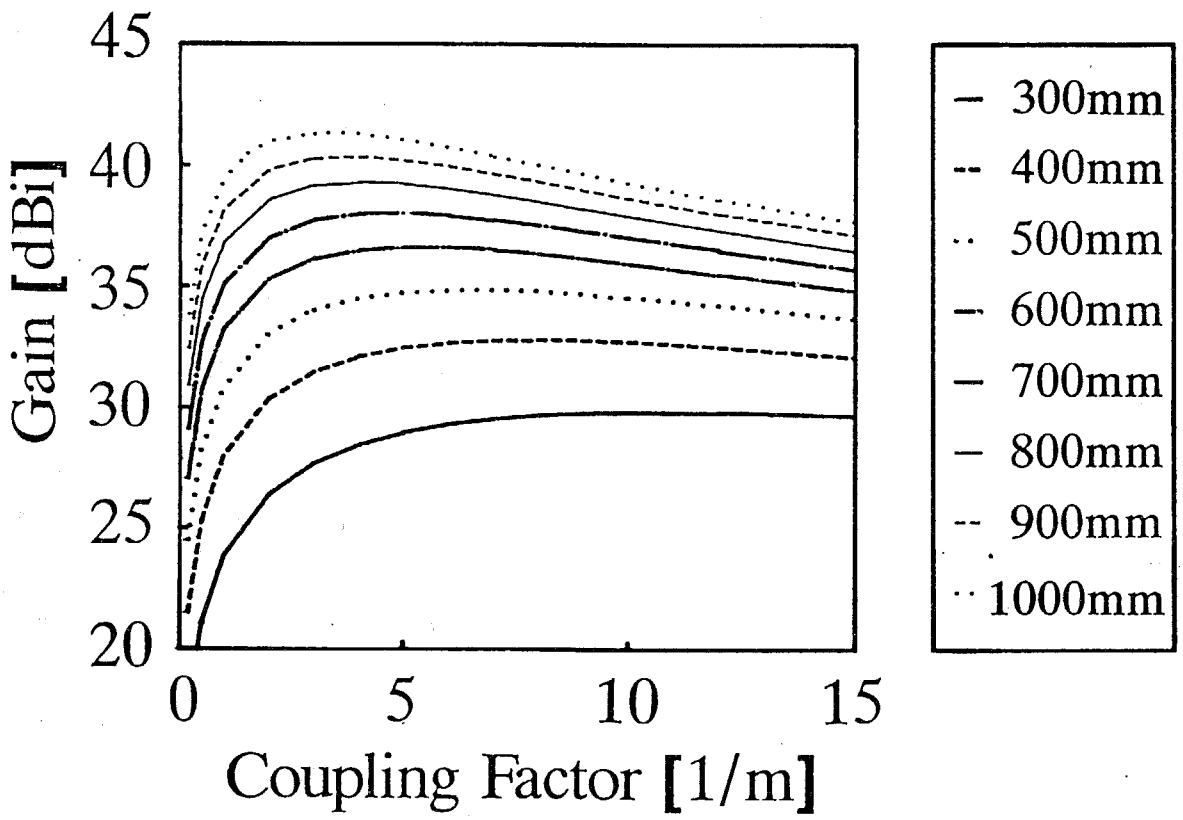

Fig. 5-3. The coupling factor and the gain of CP-RLSA as functions of antenna diameter D.

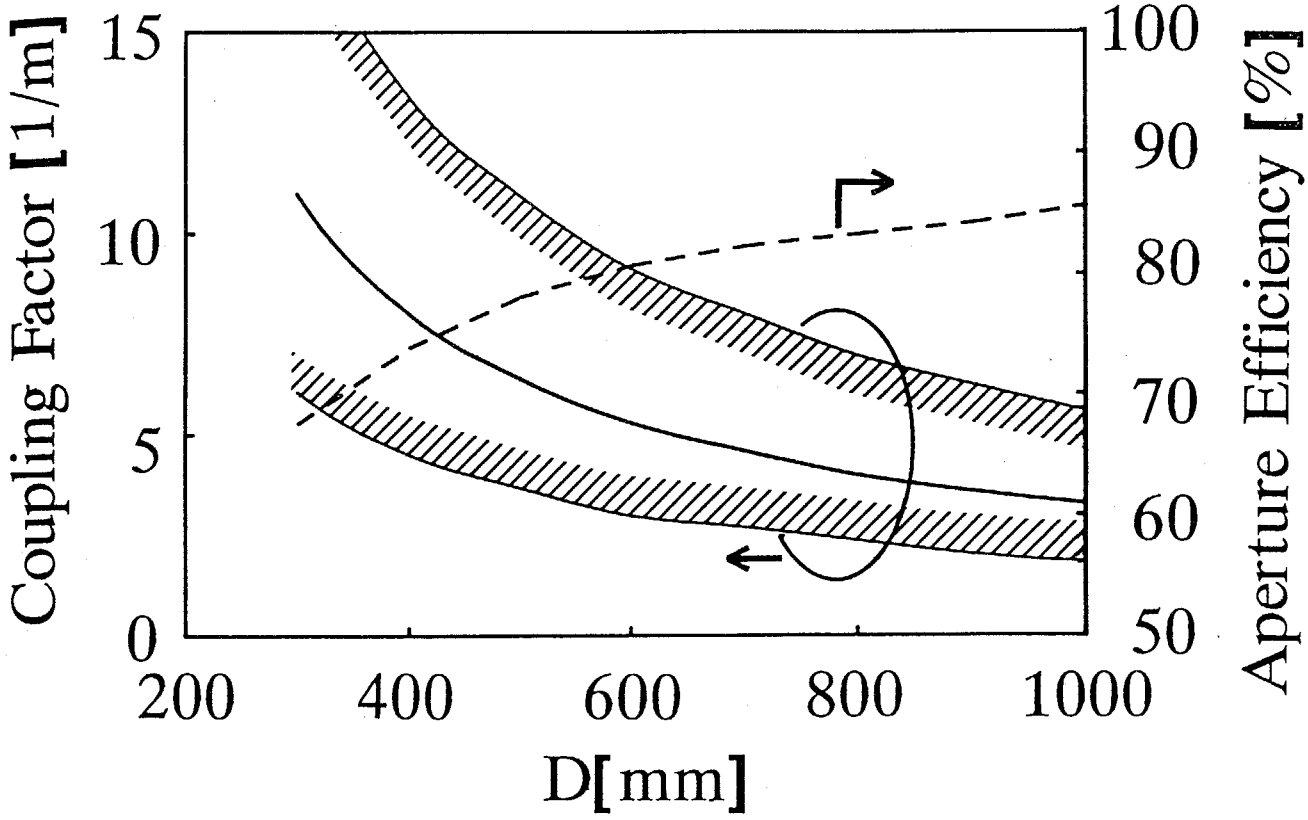

Fig. 5-4. Optimum coupling factor and maximum gain of CP-RLSA vs. antenna diameter.

——: optimum coupling factor,

▨: range of coupling factor with gain degradation of less than 0.5dB,

- - : maximum gain.

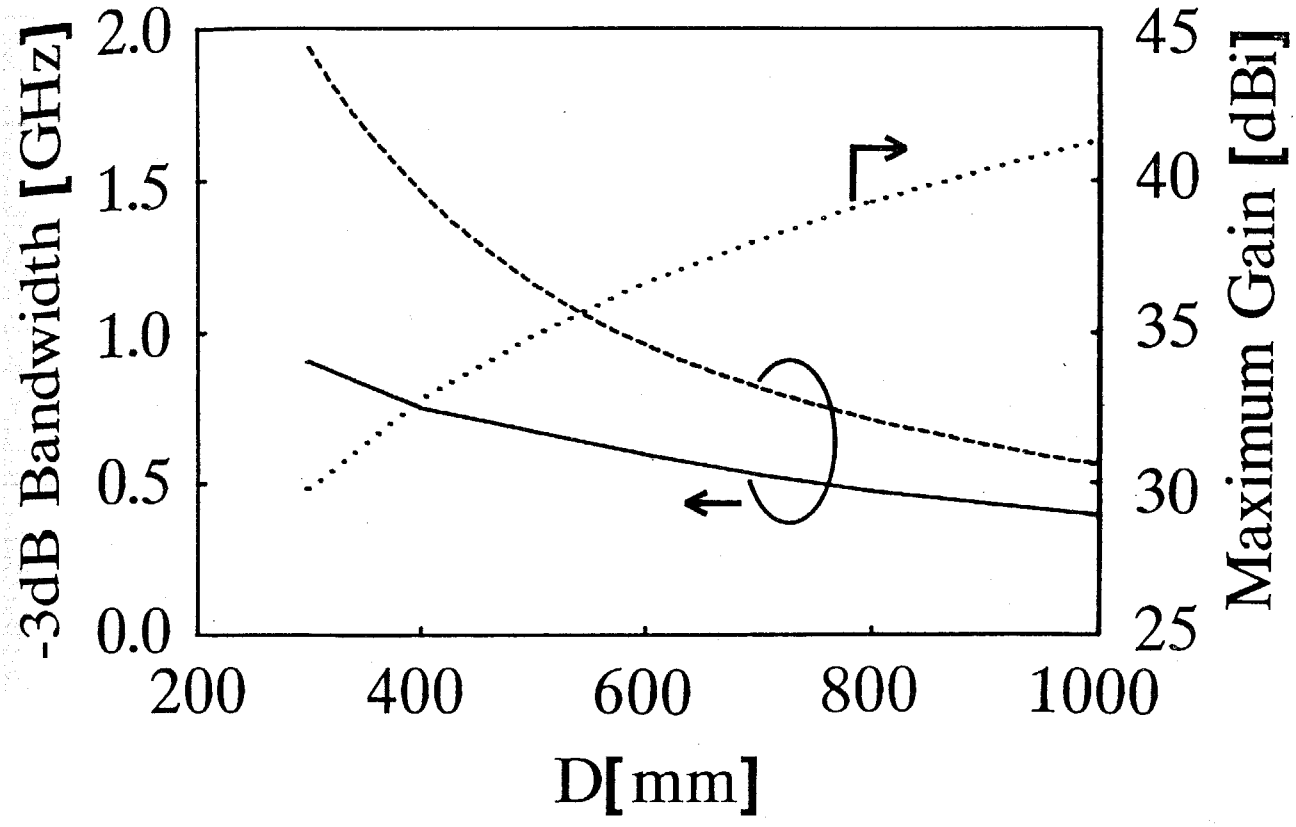

Fig. 5-5. -3dB bandwidth and maximum gain of CP-RLSA vs. antenna diameter D.

- - : ideal bandwidth considering long line effect only,

——: real bandwidth consdering slot resonance,

····: maximum gain.

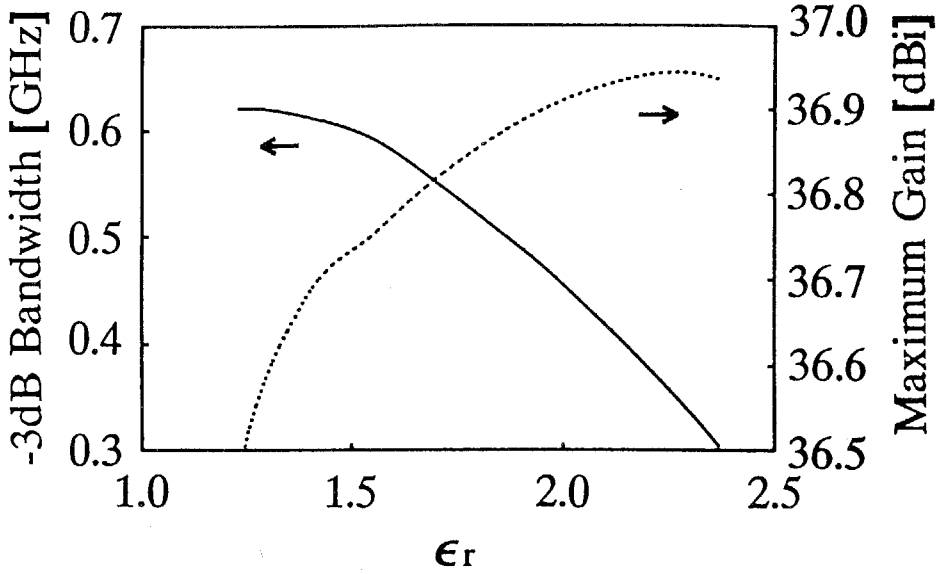

Fig. 5-6. -3dB bandwidth and maximum gain of CP-RLSA vs. relative permittivity ε_r.

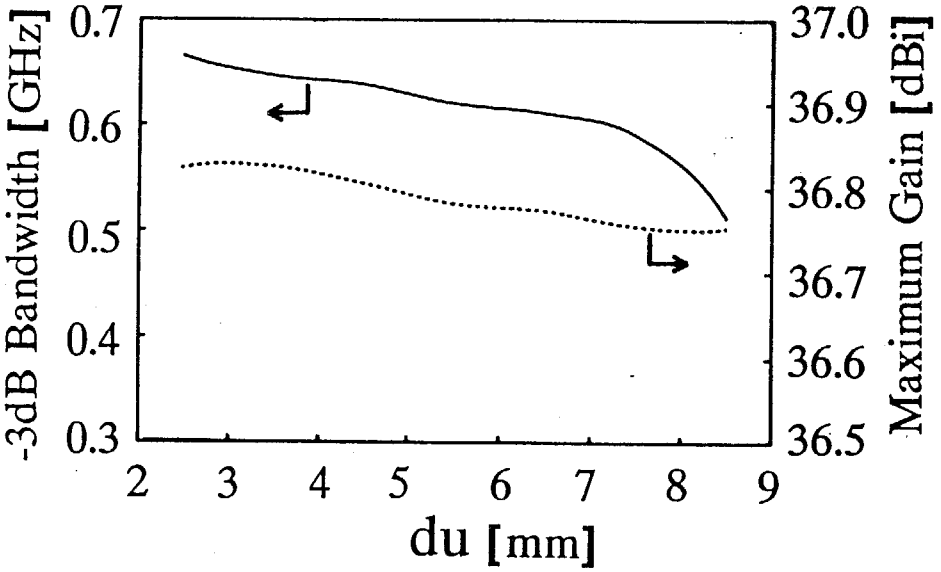

Fig. 5-7. -3dB bandwidth and maximum gain of CP-RLSA vs. waveguide height du.

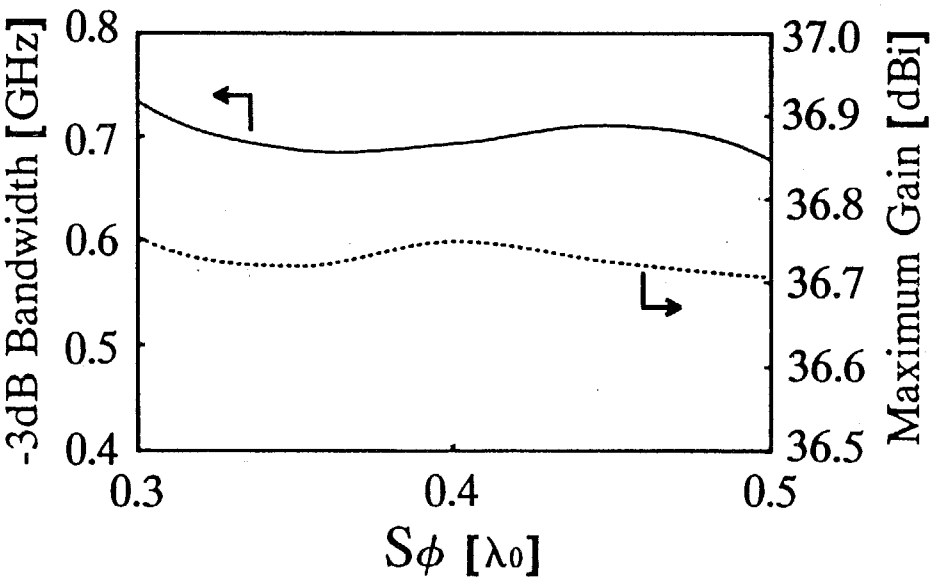

Fig. 5-8. -3dB bandwidth and maximum gain of CP-RLSA vs. slot pair angular spacing S_ϕ.

CHAPTER 6. THE DESIGN OF SINGLE-LAYERED RLSA

6-1. Introductory Remarks

After the slot coupling analysis was founded [1], the single-layered RLSA became considerable again. The relation between the slot length and the coupling strength is theoretically given, and the uniform aperture illumination can be realized by varying the slot length over the aperture.

This chapter summarizes the problem of the original single-layered RLSA and the basic design concept of new one [2]. The experimental results comparative or even superior to those of double-layered ones confirm the design [3].

6-2. Configuration of Single-Layered RLSA and Its Problem

6-2-1. Configuration

Figure 6-1 shows the configuration of a single-layered CP-RLSA. Two conductor disks form a radial waveguide. The power is fed at the center and transferred into the outward traveling wave. The slots are cut on the upper conductor and the power is gradually radiated from these slots while propagating. The slots, consisting of many pairs each one of which is a unit radiator of circular polarization, are arrayed along a design spiral. S_ρ and S_ϕ are the spacings between adjacent slot pairs along the ρ and the ϕ directions, respectively. S_ρ is designed to be equal to guide wavelength λ_g while S_ϕ is determined arbitrarily. To suppress the grating lobes from the array, the waveguide is filled with dielectric material and λ_g is set smaller than λ_o. The residual power unradiated from slots is terminated by the absorber at the outermost part.

6-2-2. Problem of Single-Layered RLSA

The outward propagating wave in the radial waveguide without

slots are represented as [6]

$$E_z = E_o H_o^{(2)}(k_o \rho) \qquad (6\text{-}1),$$

$$H_\phi = j\frac{E_o}{Z_o} H_1^{(2)}(k_o \rho) \qquad (6\text{-}2),$$

where Z_o is characteristic impedance in the free space. Their amplitudes are propotional to $1/\sqrt{\rho}$.

In the original design, the uniform slots are arranged [4][5]. Using the continuous attenuation model explained in Sec. 4-2, the aperture power density $P_a(\rho)$ is given as

$$P_a(\rho) = \frac{1}{\rho} e^{-2\alpha\rho} \qquad (6\text{-}3),$$

where the attenuation due to slot radiation accelerates the amplitude taper of cylindrical wave and the aperture illumination is steeply tapered. The double-layered RLSA discussed in Chap. 5 is presented to cancel these effects.

Therefore, slot coupling control for uniform aperture illumination is the most important technology in the design of a single-layered RLSA. The basic concept is to adopt non-uniform slots which couple weakly in the inner and strongly in the the outer portions of the aperture.

6-3. Design Procedure for Uniform Aperture Illumination

Since the slot coupling is established, the aperture illumination can be controlled by the slot length. Based on the discussion in Chap. 4, the uniform aperture illumination design is done for single-layered RLSA in the following procedure. The numerical example are also shown for CP-RLSA. The design parameters for the example are shown in Table 6-1.

First, the coupling between slot set and the radial waveguide is estimated by the slot coupling analysis. The coupling factor α, the

slow wave factor ζ and the radiated phase $\Delta\psi$ for a slot set are calculated by the full wave analysis discussed in Chap. 4. They are predicted for given slot length L. Figure 6-2(b)~(d) show the L dependences of α, ζ and $\Delta\psi$, respectively. To obtain large coupling, near resonant, i.e. longer, slots are used.

In the next step, the coupling factor $\alpha(\rho)$ for uniform aperture illumination is introduced. Assuming the continuous attenuation model, $\alpha(\rho)$ for uniform illumination is obtained by substituting $\alpha(\rho)P(\rho)$=const. into Eq. (4-2) as

$$\alpha(\rho)=\frac{\rho}{\frac{\rho_{max}}{\alpha_{max}}+\rho_{max}^2-\rho^2}$$

$$=\frac{\rho}{\frac{\rho_{max}^2-\rho_{min}^2}{1-t}-\rho^2} \qquad (6-4),$$

which is the same equation as Eq. (4-3). In Eq. (6-4), the slots are arranged in the region $\rho_{min}<\rho<\rho_{max}$. Since the slot coupling cannot be increased arbitrarily to prevent disturbing the rotational symmetry of the inner field excessively, the maximum coupling factor α_{max} is limitted to some extent. Consequently, termination loss power t does not vanish; it becomes notable as the aperture diameter decreases. Figure 6-2(a) shows a numerical example. The coupling factor is small at the inner part and large at the outer part. The termination loss is about 14% in this example.

Finally, the slot length and the position are determined over the aperture. For some point at ρ, slot length L is determined to realize $\alpha(\rho)$. Then, the corresponding slow wave factor ζ and the radiated phase $\Delta\psi$ are used to set the slot radial spacing S_ρ as in Eq. (4-20). In the practical design, however, the following equations are used instead of Eq. (4-20):

$$\rho_{b0}=\rho_{a0}+\zeta_a\cdot\lambda_0 \qquad (6-5),$$

$$\rho_a=\rho_{a0}+\frac{\Delta\phi_a-\Delta\phi_0}{2\pi}\lambda_g \qquad (6-6),$$

where $\Delta\phi_0$ indicates the $\Delta\phi$ of the innermost slot set. ρ_0 is the initial value of ρ defined by Eq. (6-5), which should be modefied by Eq. (6-6) later. In both equations, the objective values in the left side are given as functions of slot set α only, and the design can be carried out incrementally to cover all the aperture. The whole of Fig. 6-2 explains this incremental loop of the design.

The resultant L and S_ρ are given in Fig. 6-3. The longer slots are applied to the outer part with smaller spacing.

The procedure of the design is summarized in a flow chart shown in Fig. 6-4. All the design procedures are carried out theoretically.

6-4. Measurements

Based upon the above design, the model antennas shown in Table 6-1 were fabricated. No abosorber is used and the residual power is reflected at the conducting wall in these models [7][8].

In every model, the aperture amplitude and phase are uniform all over the aperture at the design frequency. Figure 6-5 shows the aperture distribution for 0.4mϕ antenna (sample d). The radiation pattern is symmetrical and the first sidelobe level of about -17dB indicates the normal antenna operation. The grating lobes, to the endfire direction, are suppressed to less than -35dB, which does not degrade the antenna gain. Figure 6-6 shows the radiation pattern for 0.4mϕ antenna (sample d). The axial ratio is excellent and is below -1dB, since slot pairs are arranged sequentially and cross polarization is canceled. Figure 6-7 shows the frequency characteristics of the antenna gain. The measured results indicated

by solid lines agree beautifully with the theoretical values in dotted lines [3]. The predicted antenna efficiency of model antennas is shown in Fig. 6-8 as a function of antenna gain, together with the measured ones plotted by ○. It also shows the predicted termination loss, which is the dominant loss factor in RLSA. Antenna efficiency increases as the diameter becomes large, since the termination loss becomes smalle. It is emphasized that the 70~84% efficiency realized here is comparable to, or even higher than, that of double-layered one. The high potential of single-layered RLSAs as well as the validity of its design and the analysis are presented.

6-5. Concluding Remarks

This chapeter summarized the slot design for single-layered RLSA with uniform aperture illumination. The key technology is the non-uniform slot arrangement. The weak and strong coupling slots are arranged at the inner and outer part, respectively. The model antennas with various diameters are fabricated. The measured results agrees beatifully with the predicted value and confirms the design.

The reuse of residual power is left for future study [9]. There will be two solutions for CP-RLSA presented by now.

One is the matching element to radiate all the residual power. Figure 6-9(a) and (b) show the spiral slit [2] and matching slots [10], respectively. The former slit is in spiral shape and operates as a circular-polarized element, while the latter slots are arranged spirally to be excited in phase with slot pairs. They are examined theoretically, but the model antennas are difficult to be fabricated and the effects are not yet confirmed experimentally. The alternative solution is the aperture illumination control. Taking the termination loss into account, the uniform aperture illumination

is not the optimum one for the high gain. By increasing the coupling strength in the inner part, the termination loss is reduced. Even the illumination level at the outer part decreases, the total efficiency is improved. Figure 6-10 shows the coupling factor and the apeture illumination for maximum gain. However, the stronger coupling disturbes the rotational symmetry of the inner field and the desired operation is not realized. These problems are now studied by other candidate.

References

[1] J. Hirokawa, M. Ando and N. Goto, "Analysis of Slot Coupling in a Radial Line Slot Antenna for DBS Reception," IEE Proc., vol. 137, pt. H, no. 5, pp. 249-254 (Oct. 1990).

[2] M. Takahashi, J. Takada, M. Ando and N. Goto, "A Slot Design for Uniform Aperture Distribution in Single-Layered Radial Line Slot Antennas," IEEE Trans. Antennas & Propag., vol. AP-39, no. 7, pp. 954-959 (July 1991).

[3] M. Takahashi, J. Takada, M. Ando and N. Goto, "Characteristics of Single-Layered Radial Line Slot Antennas," IEICE Technical Report, AP90-129 (Feb. 1991).

[4] N. Goto and M. Yamamoto, "Circularly Polarized Radial-Line Slot Antennas," IECEJ Technical Report, AP80-57 (Aug. 1980).

[5] N. Goto, N. Miyahara and K. Arimura, "Radiation Pattern of a Radial Line Slot Antenna," IECEJ Technical Report, AP81-90 (Oct. 1981).

[6] N. Marcuvitz, "Waveguide Handbook," Sec. 1-7, McGraw-Hill (1951) / Peter Peregrius (re-issued, 1986).

[7] M. Takahashi, J. Takada, M. Ando and N. Goto, "Characteristics of Small Aperture Single-Layered Radial Line Slot Antennas," IEE Proc., vol. 138 or 139, pt. H (to be published; 1991 or 1992).

[8] J. Takada, M. Takahashi, M. Ando and N. Goto, "Radial Line Slot Antennas," Denshi Tokyo, no. 30 (to be published; Feb. 1992).

[9] S. Sumikawa, M. Takahashi, J. Takada, M. Ando and N. Goto, "High Efficiency Single-Layered Radial Line Slot Antennas," 1991 Spring Natl. Conv. Rec., IEICE, B-143 (Mar. 1991).

[10] S. Hagiwara, J. Takada, M. Ando and N. Goto, "A Matching Slot in Single-Layered Radial Line Slot Antennas," 1990 Autumn Natl. Conv. Rec., IEICE, B-40 (Oct. 1990).

Table 6-1. Design parameters for numerical examples.

frequency f_o [GHz]		11.85
slot pair angular spacing S_ϕ	[mm]	12.66
	[λ_o]	0.5
slot arranged region [mm]	ρ_{min}	30
	ρ_{max}	300
waveguide height du [mm]		5.0
permittivity ε_r		1.5
maximum coupling factor α_{max} [1/m]		20.0

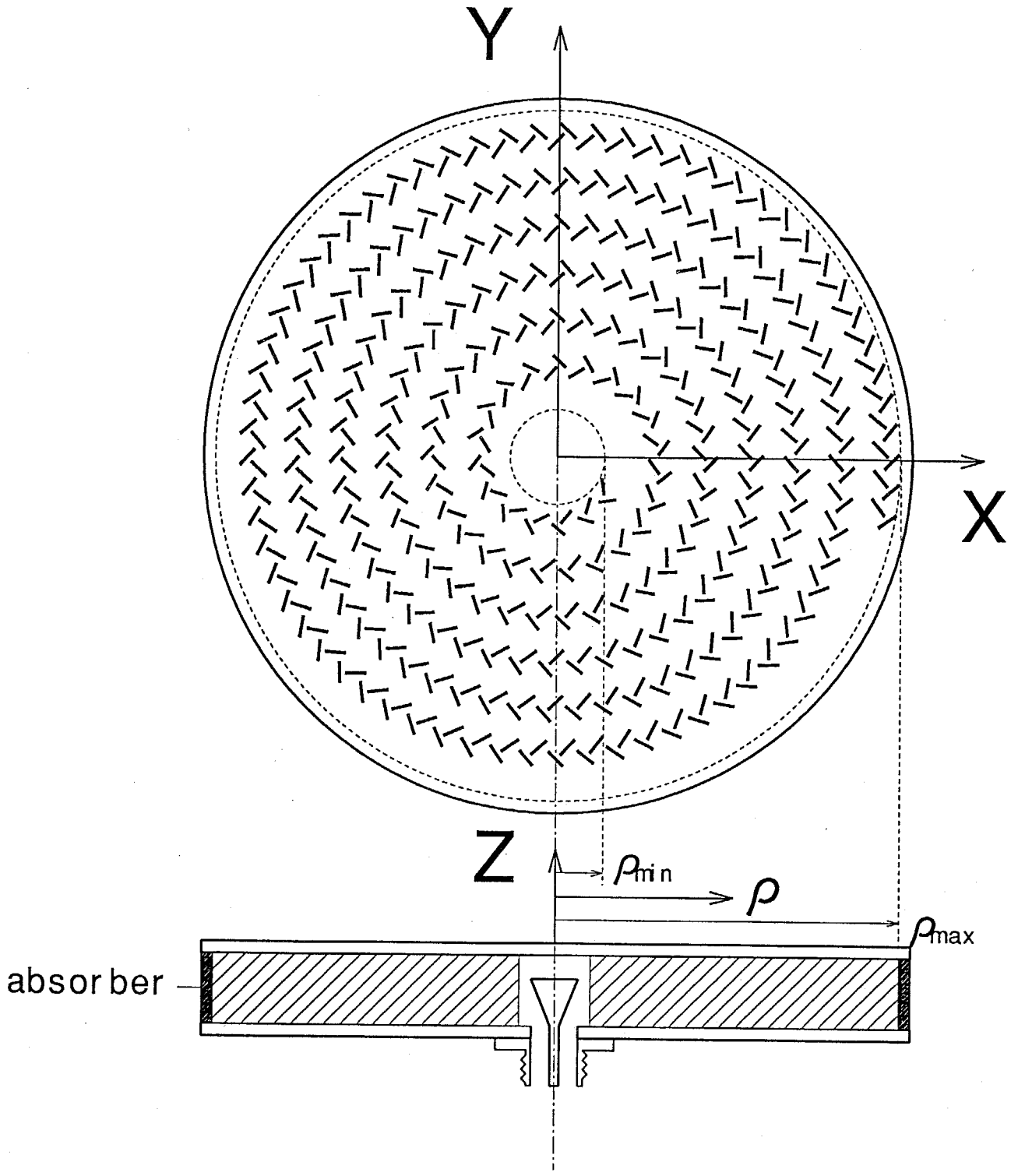

Fig. 6-1. Single-layered CP-RLSA.

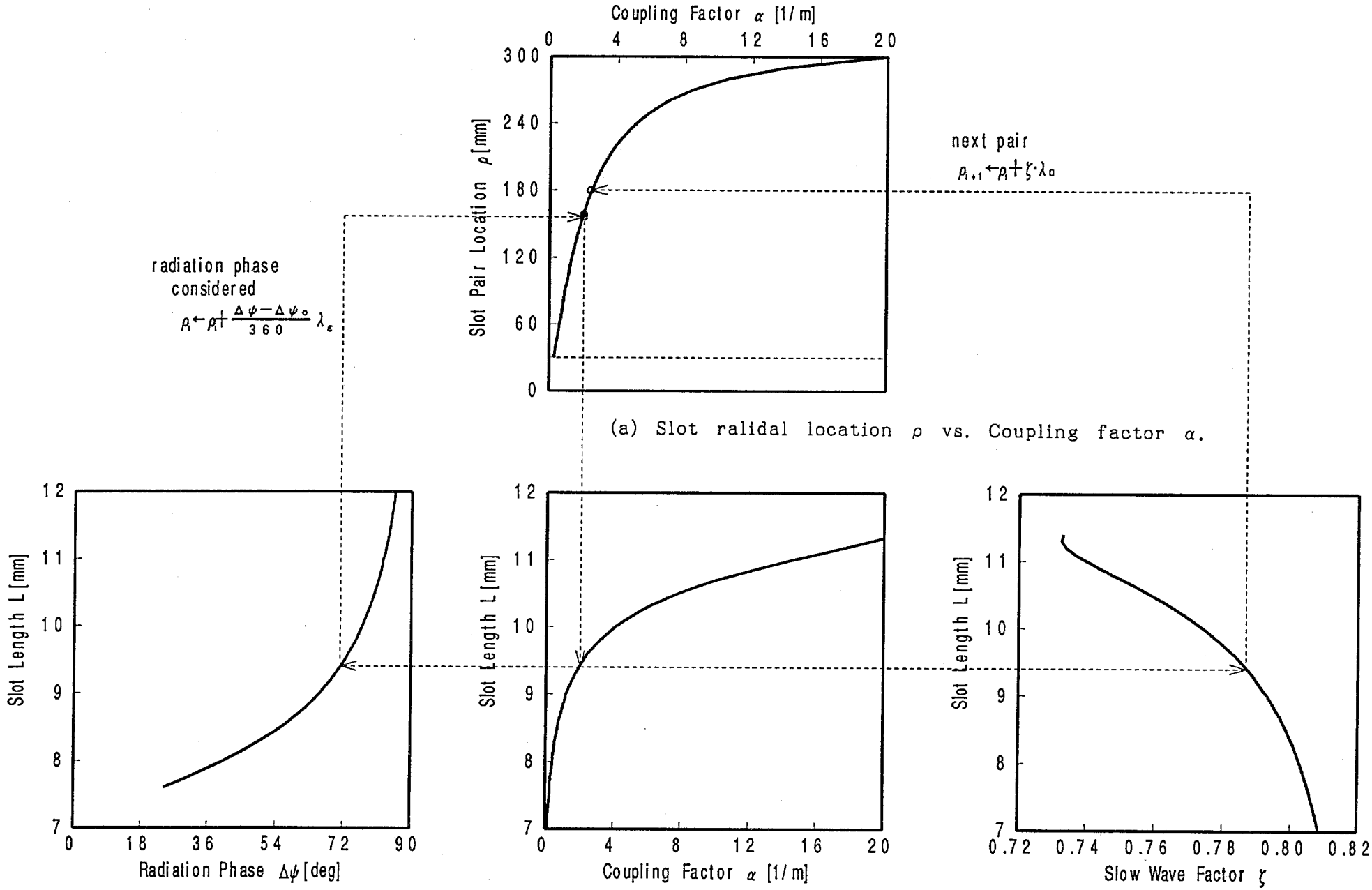

Fig. 6-2. Numerical examples and design process.

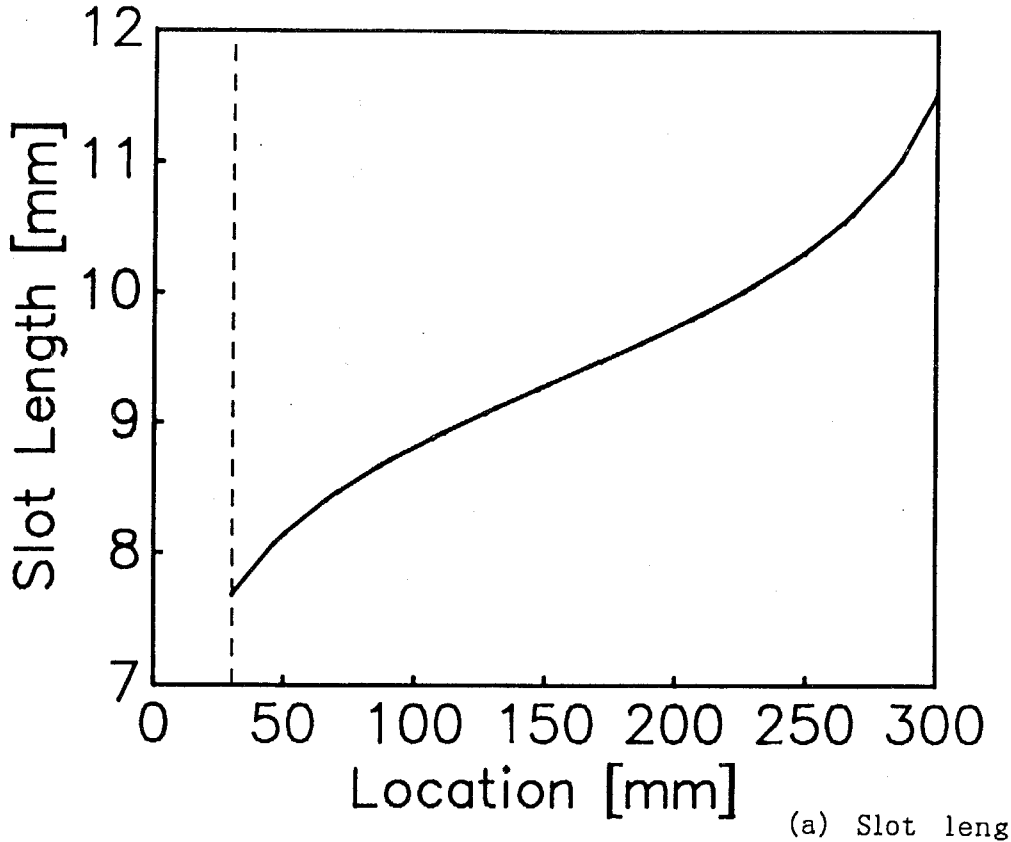

(a) Slot length.

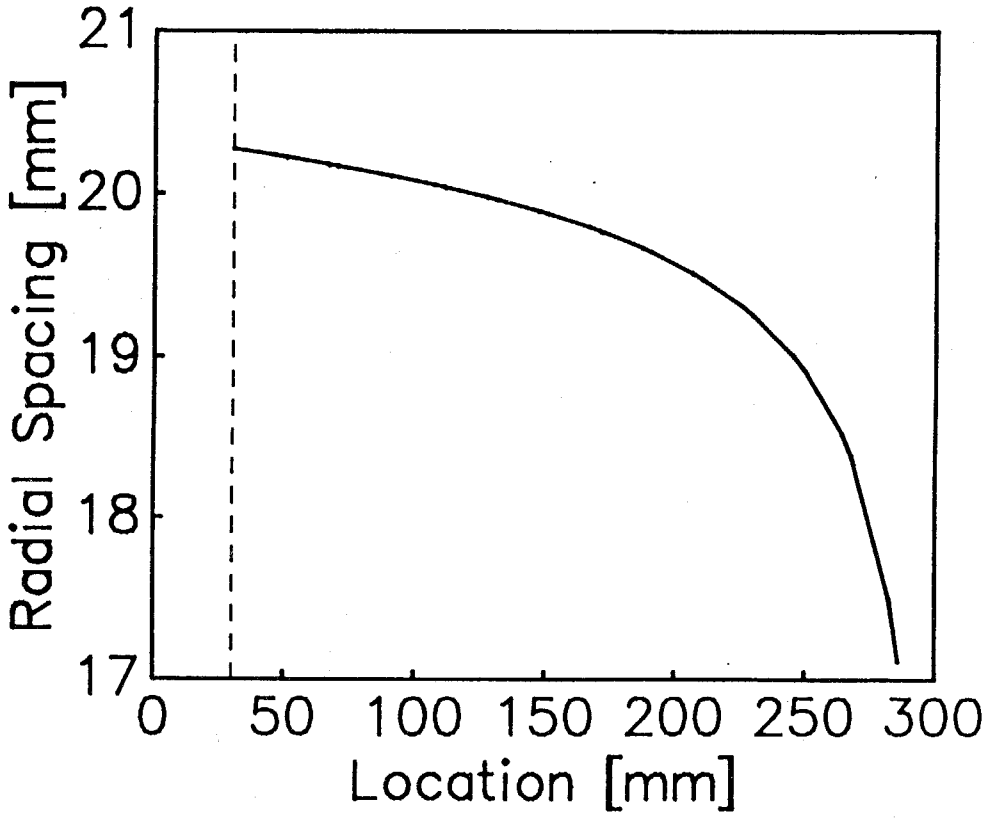

(b) Slot pair radial spacing.

Fig. 6-3. Slot length and radial spacing for uniform aperture.

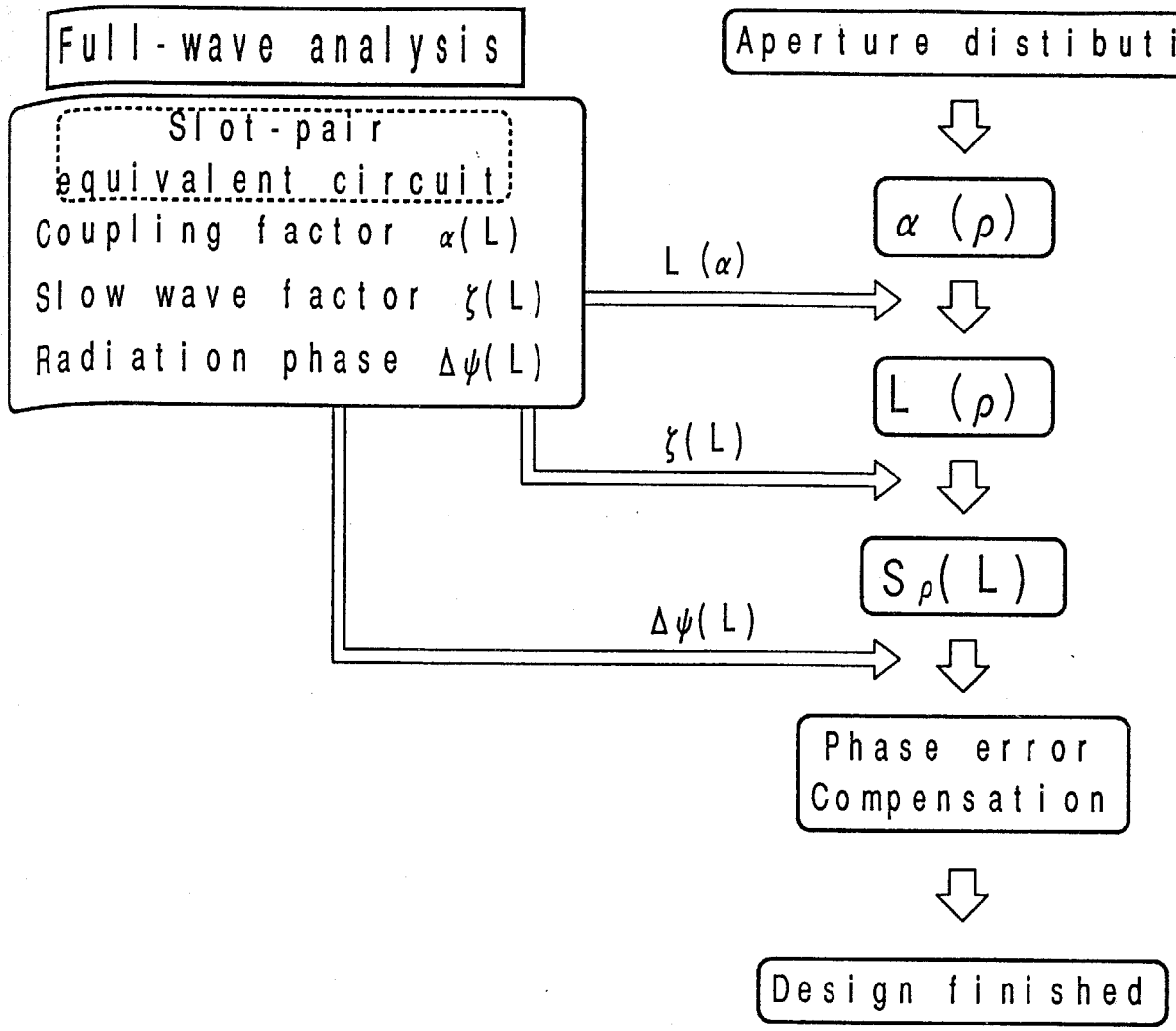

Fig. 6-4. Flow chart of the slot design procedure.

Table 6-2. Design parameters of model antennas.

Model Antenna	Diameter $D=2\rho_{max}$ [m]	Waveguide height du [mm]	ε_r	α_{max} [1/m]
a	0.25	5.00	1.50	17.2
b	0.30	5.00	1.50	17.2
c	0.35	5.00	1.50	17.2
d	0.40	7.50	1.55	23.4
e	0.45	3.00	1.29	24.4
f	0.60	3.75	1.53	23.4

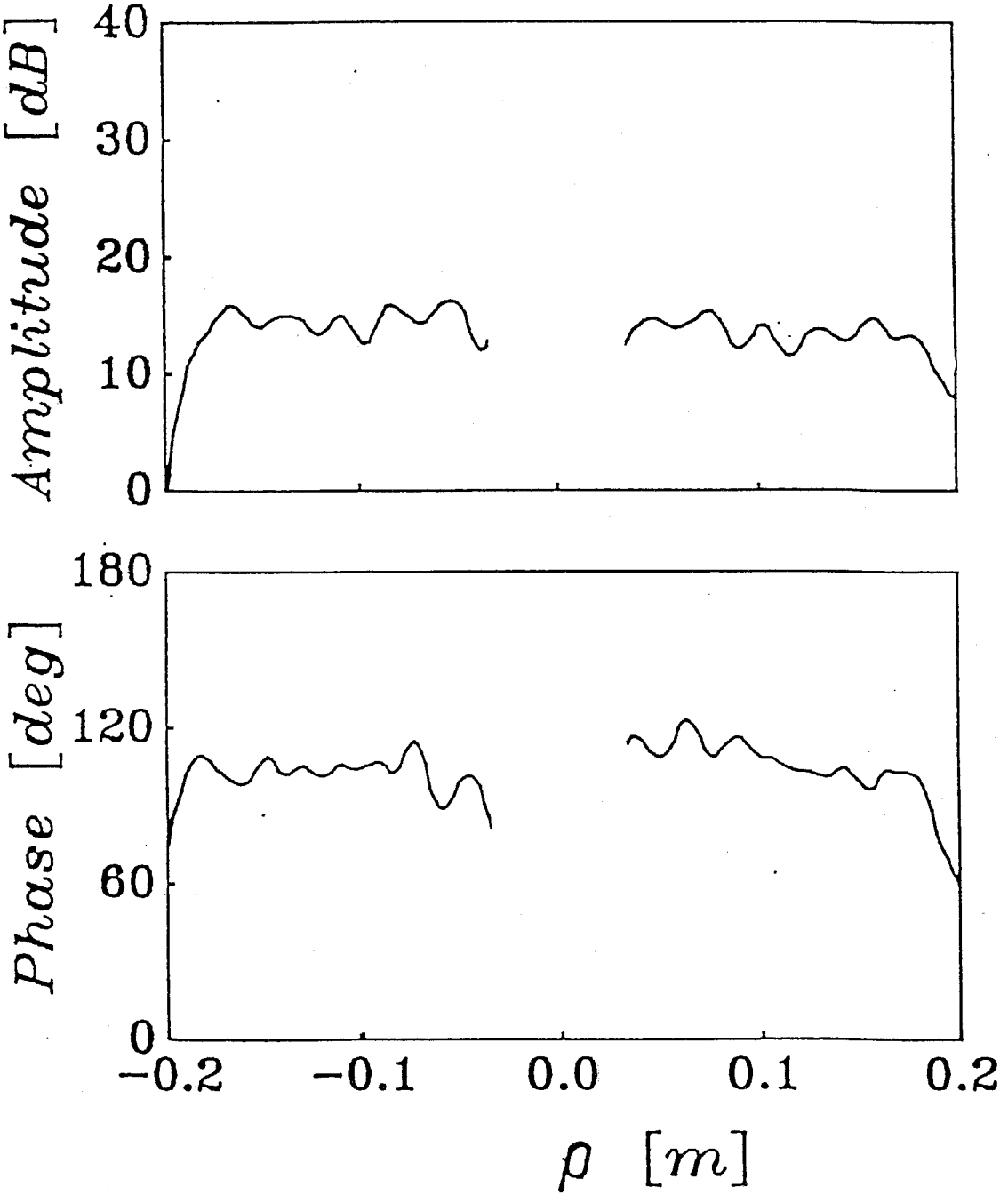

Fig. 6-5. Aperture distribution for 0.4mϕ model antenna.

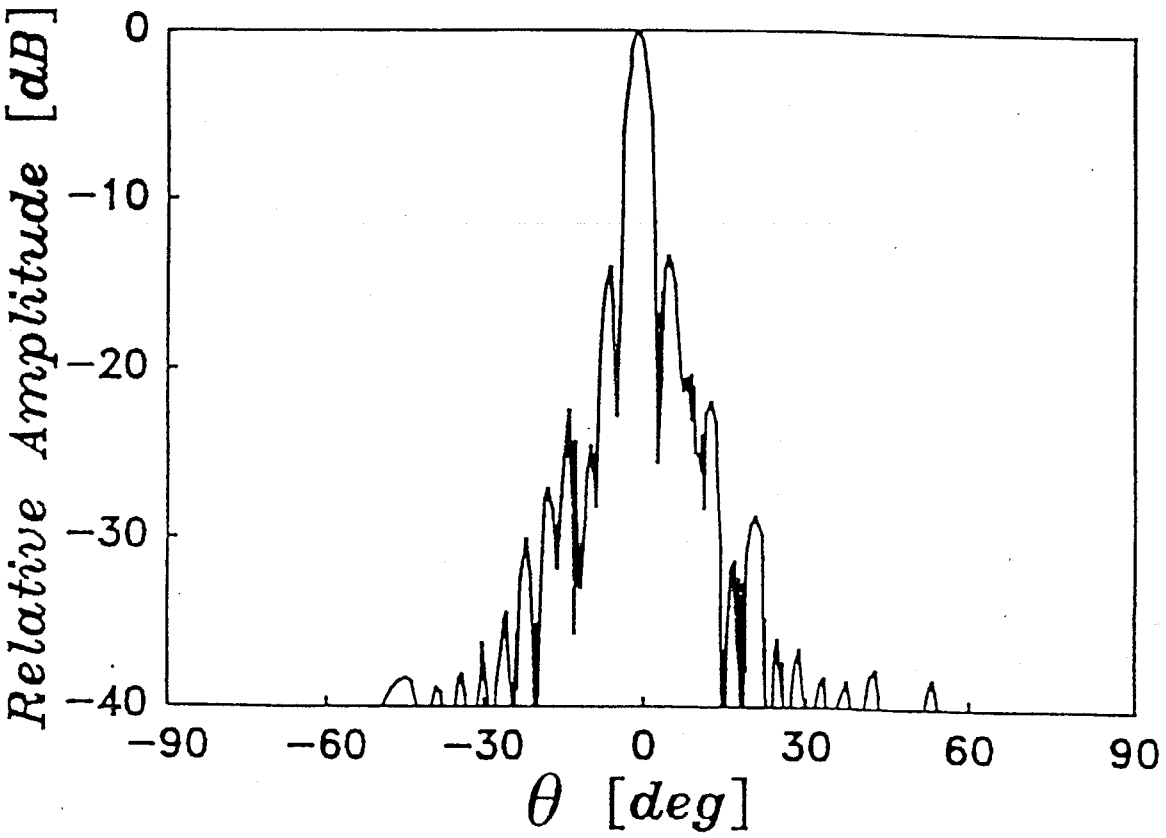

Fig. 6-6. Radiation pattern for 0.4mϕ model antenna.

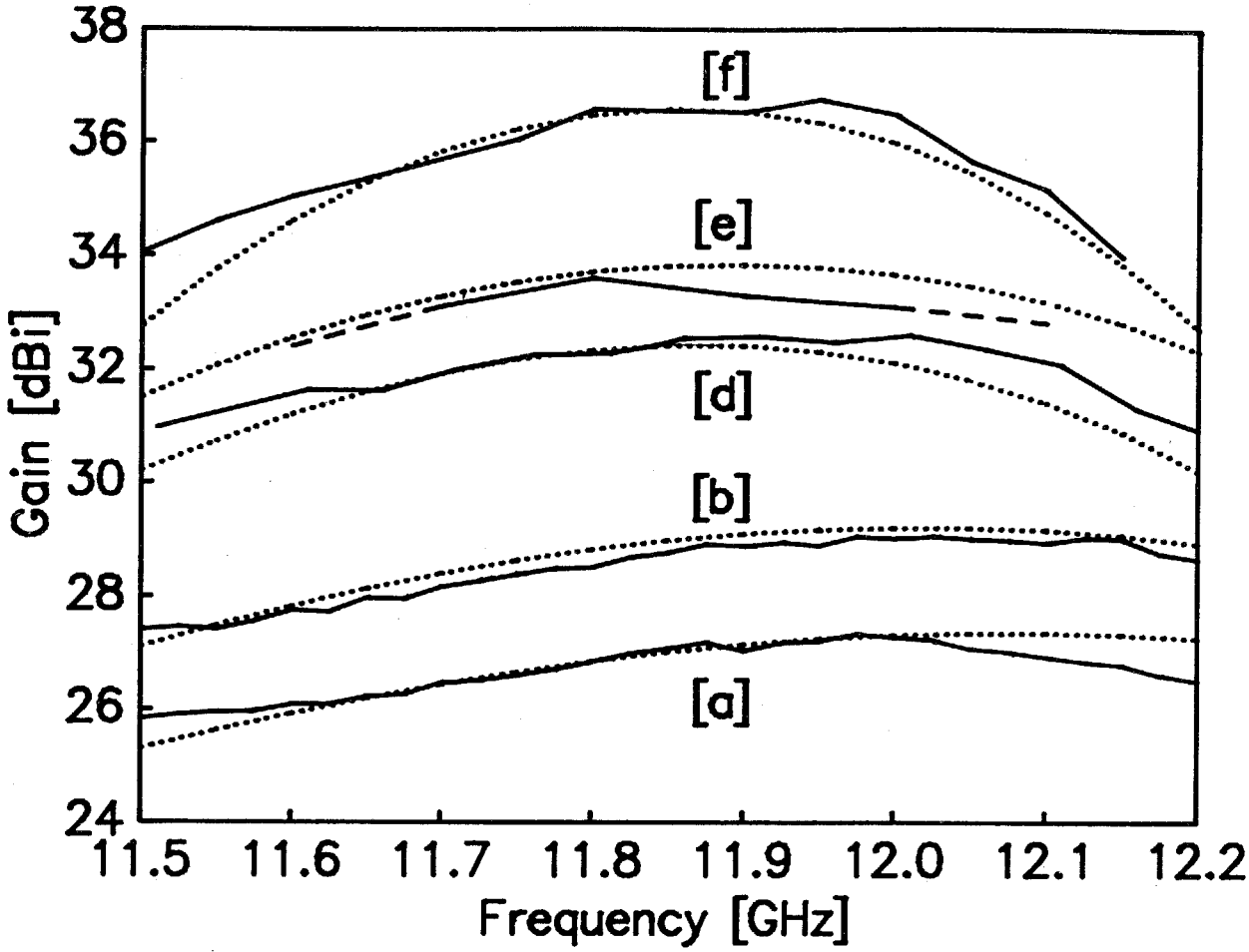

Fig. 6-7. Antenna gain for various model antennas (——: experiments, ····: theory).

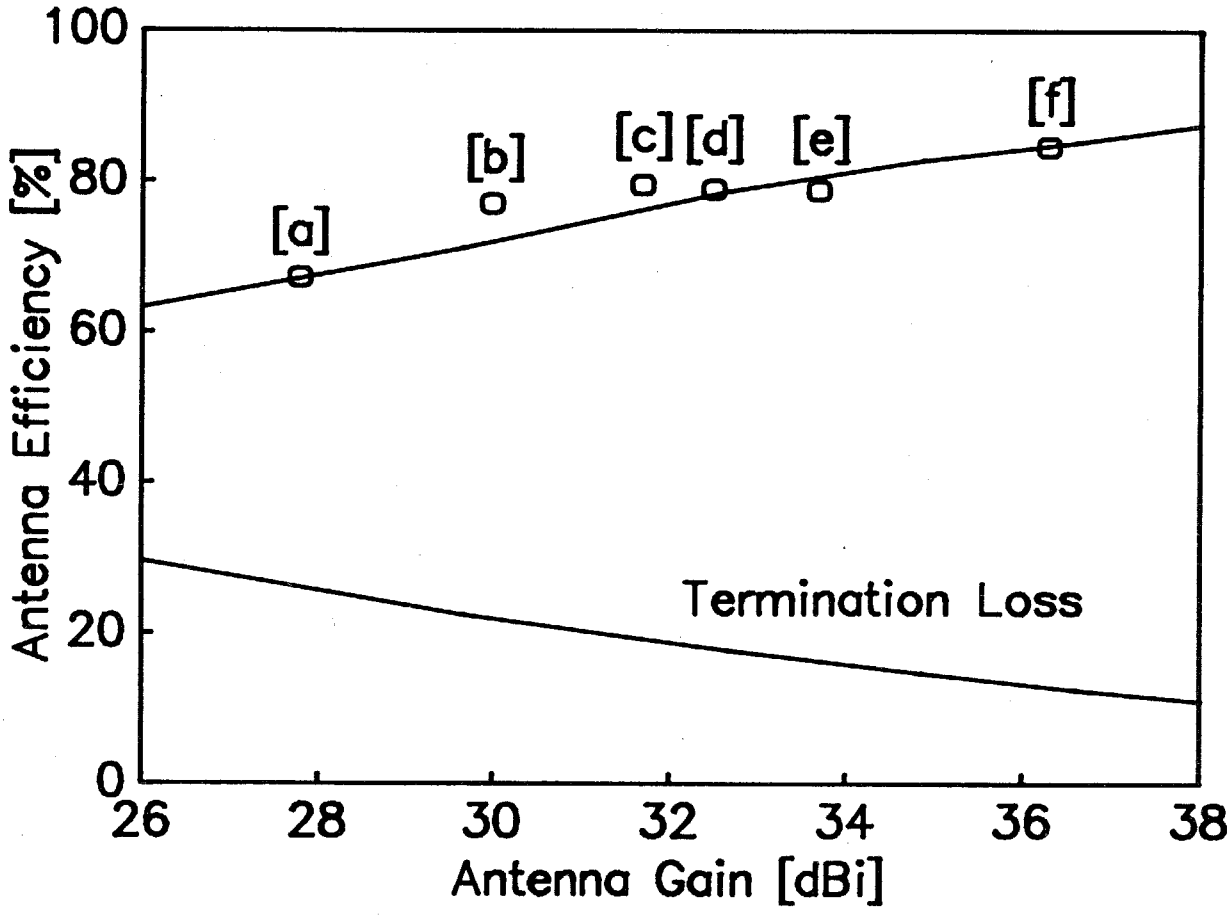

Fig. 6-8. Antenna gain vs. antenna efficiency (——: theory, ○: experiments).

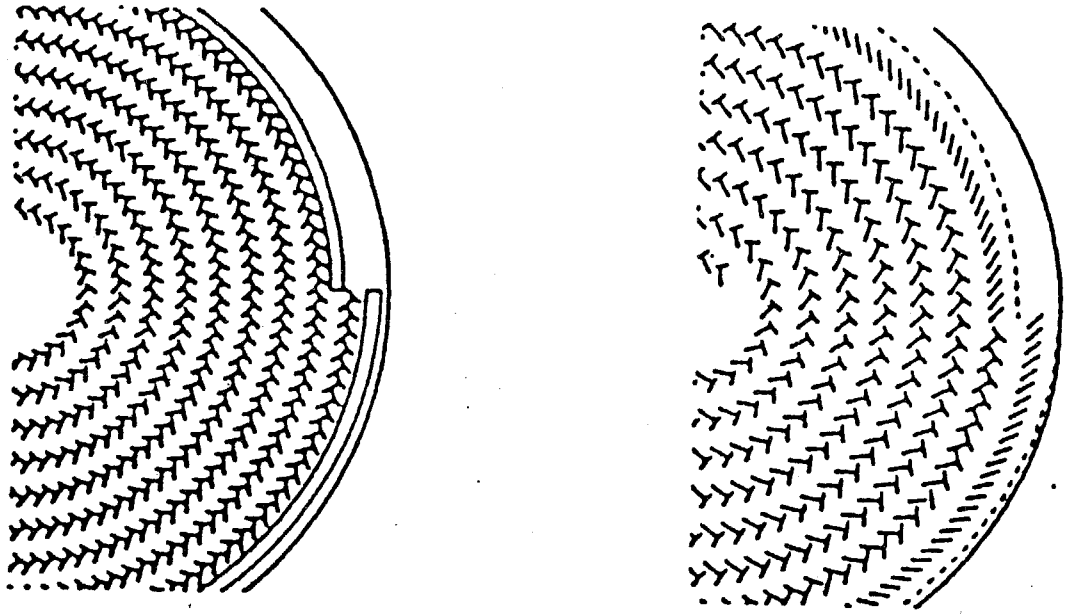

(a) Spiral slit. (b) Matching slots.

Fig. 6-9. Matching elment for the reuse of residual power.

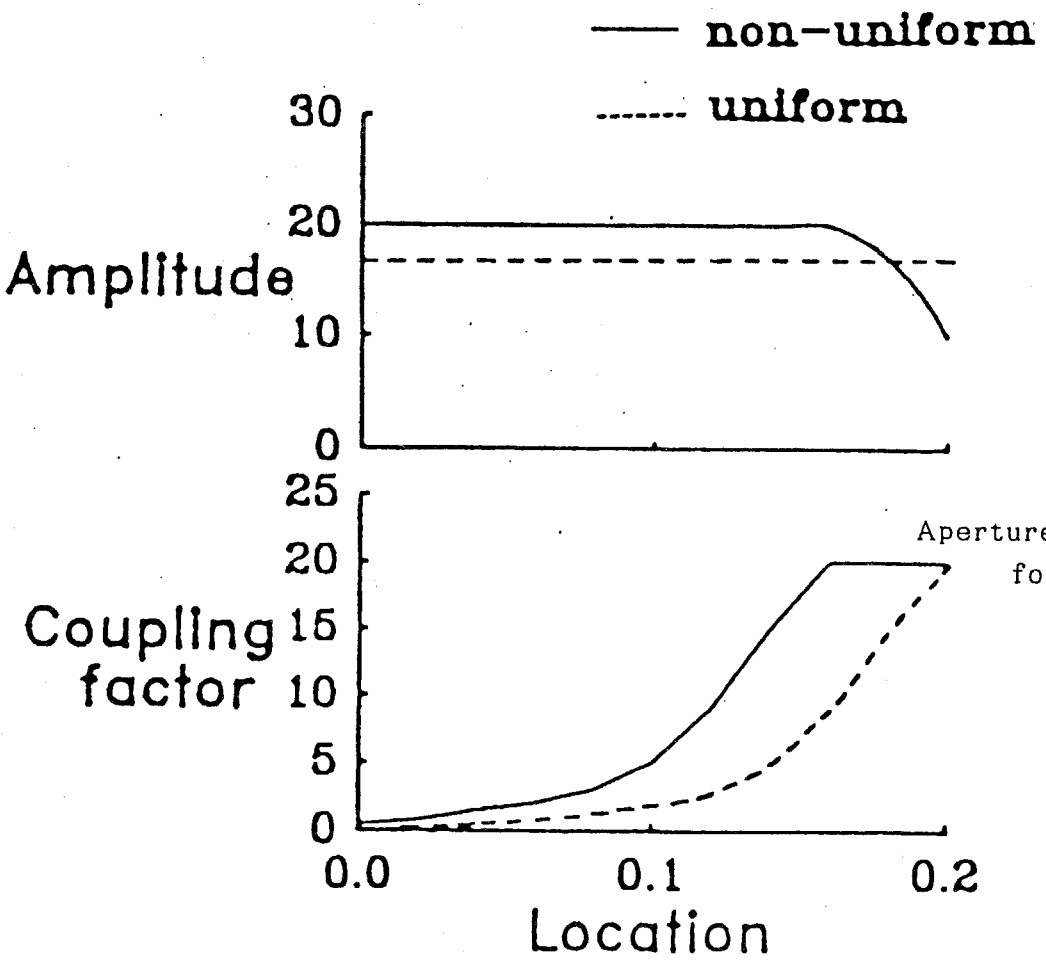

Fig. 6-10.
Aperture illumination control for the reduction of the residual power

PART. 3 SUPRESSION OF REFLECTION FROM SLOTS IN LINEARLY-PORALIZED RLSA

CHAPTER 7. ADDTIONAL REFLECTION CANCELING SLOTS FOR LP-RLSA [SOLUTION #1]

7-1. Introductory Remarks

The basic concept of a linearly-polarized RLSA (LP-RLSA) was presented in 1987 [1][2]. In LP-RLSA, however, the slots are arrayed annularly with the radial spacing of half the guide wavelength, which results in the serious degradation of return loss characteristics. To remedy these problems, a beam-tilt design [3] and the use of reflection canceling slot set [4][5] have been proposed. But the predicted antenna operation has not been realized because these ideas were only conceptual but were not quantitative.

This chapter first clarify the problem of original LP-RLSA. Then a slot set using additional reflection canceling slots is presented as a solution for it. The design parameters are numerically optimized. The experimental results confirm the design.

7-2. Conventional Design and Problems

Figures 7-1(a) and (e) show a plan and a cross-section of an original LP-RLSA [2]. The rotationally symmetrical outward traveling wave excites the slots arranged on the top plate.

Two slots of equal length L form a slot pair as a unit radiator of linear polarization, and the pairs are arranged with spacing S_p

and S_ϕ in ρ and ϕ direction, respectively. Figure 7-1(b) shows a slot pair configuration. This design is based on two assumptions, that is, the traveling wave operation propagating in the $+\rho$ direction and the slot excitation in proportion to $\sin\theta$, where θ is the coupling angle. To radiate the linear polarization along the X direction, two slots should satisfy the following equations:

[alternating phase excitation]

$$d_1=\frac{\lambda_g}{2} \qquad (7-1),$$

[suppression of cross polarization]

$$L_1=L_2(\triangleq L_R) \qquad (7-2),$$

$$\theta_1=-\frac{\phi}{2} \qquad (7-3),$$

$$\theta_2=\frac{\pi}{2}-\frac{\phi}{2} \qquad (7-4),$$

where λ_g is the guide wavelength. The configuration of a slot pair varies with the slot location ϕ in the antenna aperture. To excite all the pairs in phase, they are arranged annularly with the radial spacing $S_\rho=\lambda_g$.

Unfortunately, the return loss characteristic of the LP-RLSA thus designed is seriously degraded for the following two reasons:

(i) Two slots in a pair are spaced by $\lambda_g/2$ along the ρ direction, and then the reflected waves from two slots are in phase. (Fig. 7-2(a))

(ii) All the slot pairs are arrayed annularly with the spacing of λ_g, and then the reflected waves from all the pairs are in phase at the input port. (Fig. 7-2(b))

These situations are undesirable in contrast with these for CP-RLSA where

(iii) Two slots in a pair are spaced by $\lambda_g/4$, and the reflected

waves from these are out of phase and cancelled with each other.

(iv) The slot pairs are arrayed spirally, and the total sum of the reflected waves from the pairs are almost vanishing at the input port.

The problems (i) and (ii) must be solved to realize the high efficiency LP-RLSA. We have already presented a beam tilt design to solve (ii) [3]; the main beam is tilted from boresight by deforming the array arrangement of slot pairs from annular shape to offset elliptical one. The experiments using a model antenna confirmed the improvement of input VSWR. However, slot reflections still disturb the rotational symmetry of the inner field as well as the uniformity of aperture illumination. For the stable antenna operation, it is necessary to suppress the reflection from slot pairs (i).

In this chapter, the reflection cancelling slots suggested in reference [4] are adopted to suppress the reflection from a unit pair. The resultant slot arrangement is given in Fig. 7-1(c).

7-3. The Design of Reflection Canceling Slot Sets

7-3-1. Configuration

A unit radiator for linear polarization consists of four slots, which are two radiating and two additional ones.

Figure 7-1(d) shows a slot set. The slots #1 and #2 are the radiation slots, which are arranged so as to satisfy the Eqs. (7-2)~(7-4) and radiate the desired linear polarization to broadside. The slots #3 and #4 are the additional slots to cancel the reflection from radiation slots. The design of slots #3 and #4 are the objective of this chapter.

The basic concept for suppressing the reflection is expressed as follows:

[radiation cancellation in boresight]

$$d_2=\frac{\lambda_g}{2} \qquad (7\text{-}5),$$

$$\theta_3=\theta_4\left(=\frac{\pi}{2}\right) \qquad (7\text{-}6),$$

[reflection cancellation]

$$d_3\simeq\frac{\lambda_g}{4} \qquad (7\text{-}7).$$

The radiation from the additional slot pair (#3 and #4) is small everywhere, because they are separated by d_2 which is less than $\lambda_0/2$ and are excited in alternating phase.

The above conditions are only conceptual and the parameters L_1, L_2, L_3, L_4, d_1, d_2 and d_3 should be optimized independently. For the simplicity of the design, weak slot coupling is assumed in this design and the following are specified in addition to Eqs. (7-1)~(7-6).

$$L_3=L_4=L_D \qquad (7\text{-}8),$$

$$d_2=d_1 \qquad (7\text{-}9).$$

Consequently, only two parameters of L_D/L_R and d_3 ($\triangleq\lambda_g/4+\Delta\rho$) are optimized in the full wave analysis of slots coupling to the waveguide discussed in Sec. 2-2.

To avoid the physical overlap of slots, the additional slots are displaced in the ϕ direction according to the following rules:

i) $0° < \phi < 90°$

Slot #1 may overlap with the #3 in the seme set and #4 in the inner adjacent set. They are displaced as

$$t_3^{\,i}=-\frac{S_\phi}{2}-\left(\frac{1}{4}\lambda_g-\Delta\rho\right)\tan\theta_1 \qquad (7\text{-}10),$$

$$t_4^{\,i-1}=+\frac{S_\phi}{2}+\left(\frac{1}{4}\lambda_g+\Delta\rho\right)\tan\theta_1 \qquad (7\text{-}11),$$

where t is the displacement along ϕ direction as is shown in Fig. 7-3(a) and the superscript on t indicate the number of slot set in ρ direction, starting with the innermost set. In the practical slot arrangement, slots $\#1^i$, $\#2^i$, $\#3^i$ and $\#4^{i-1}$ are considered to make up #i slot set. Consequently, the innermost slot set #1 consists of three slots, $\#1^1$, $\#2^1$ and $\#3^1$, and the outermost slot set #n consists of five slots, $\#1^n$, $\#2^n$, $\#3^n$, $\#4^{n-1}$ and $\#4^n$.

ii) $90° < \phi < 180°$

Slot #2 may overlap with the #3 and #4 in the same set. They are displaced as

$$t_3 = +\frac{S_\phi}{2} - \left(\frac{1}{4}\lambda_g - \Delta\rho\right)\tan\theta_2 \qquad (7\text{-}12),$$

$$t_4 = -\frac{S_\phi}{2} + \left(\frac{1}{4}\lambda_g + \Delta\rho\right)\tan\theta_2 \qquad (7\text{-}13),$$

as shown in Fig. 7-3(b).

iii) $180° < \phi < 360°$

Since the slot arramengement is symmetrical about X-axis, the slot sets in this region is not independently designed.

Therefore, overlap of slots is avoided all over the aperture.

7-3-2. Design of a Slot Set

To suppress the reflection, the slot lengths L_R, L_D and the relative location of additional slots $\Delta\rho$ should be optimized. An S-matrix equivalent circuit for a slot set explained in Chap. 4 is derived. The parameters L_D and $\Delta\rho$ are optimized to minimize the reflection coefficient $|S_{11}|$.

The optimization is done for given L_R and ϕ, which are specified from the requirement of the coupling strength and polarization in aperture illumination design. The final solutions of S-parameters are therefore given as functions of L_R and θ. The coupling factor α

is directly related to $|S_{21}|$ (Eq. (4-14)). After intensive numerical studies and interpolation, the parameters L_R and θ as well as the optimum L_D and $\Delta\rho$ are given as functions of α and ϕ.

7-3-3. Design of an Array

Once the reflection from a slot set is suppressed, the array design procedure is just the same as that of CP-RLSA, which is explained in Chap. 6. The difference is that the configuration of slot set in LP-RLSA varies with ϕ over the aperture. Firstly, the coupling factor α is specified for required aperture illumination as discussed in Chap. 6. Secondly, the parameters L_R, θ, L_D and $\Delta\rho$ are obtained using the results in 7-3-2.

7-4. Numerical Results

Table 7-1 shows the parameters used in the analysis.

The condition for the minimum reflection is discussed first. Figure 7-4 shows the relation between the length L_R of radiation slots and the optimum length L_D of additional slots. Though the optimum L_D is varied a bit for different ϕ, the tendency is the same. When L_R is shorter and the coupling is weak, L_D is significantly less than L_R and short additional slots effectively suppress the reflection. When L_R increases and coupling becomes stronger, on the other hand, L_D is approaching L_R. Figure 7-5 shows the relation between L_R and $\Delta\rho$, the offset of the additional slot. $\Delta\rho$ is largely dependent on ϕ. $|\Delta\rho|$ accounts for the perturbation of slot coupling and increases with the slot length. For L_R>8mm which is usual in the practical antenna, the design neglecting the perturbation due to slot coupling is not valid. The relations differ a little with the angle ϕ.

The parameters used in the aperture illumination control, coupling factor α, slow wave factor ζ and the relative radiation

phase $\Delta\psi$, are given as functions of L_R in Figs. 7-6, 7-7, and 7-8, respectively. They exhibit a resonance curve as is similar to a slot pair of CP-RLSA. This figure is used to determine L_R and S_ρ for given α as is stated in 7-3-3.

Figure 7-9 shows the reflection coefficient $|S_{11}|$ of a slot set as a function of required coupling factor α. The reflections are substantially suppressed, though they increase with the coupling factor α. $|S_{11}|$ of a original slot pair without additional slots is also given for comparison. The reflection of -10dB for a slot pair is reduced to about -40dB in this design at α=10.

Once the design of a slot set is accomplished, the array design along ρ direction for some angle ϕ is straightforward, since reflection from a set is negligible. To check the design sequence, we recall a 1-dimensional array on the rectangular waveguide shown in Fig. 7-10. The slot sets in this array are designed to realize the aperture illumination proportional to $\sqrt{\rho}$ for compensating the attenuation of cylindrical wave in practical antennas. Figure 7-11 shows the calculated reflection coefficient of this 1-dimensional array as a function of ϕ. In this analysis, the design parameters for $90° < \phi \leqq 180°$ are substituted for those for $(180° - \phi)$. The reflection coefficient of -2~-3dB in the original design is improved to the level below -10dB from the original design of about -3dB. The symmetry about ϕ=90° shows that the substitution above is sufficient for the array design. The reflection from an array is larger than that from a slot set in Fig. 7-9 because $S_\rho = \lambda_g$ and all the reflections are in phase. Another reason for it is the fact that the mutual coupling between different slot sets are not considered in the design.

7-5. Experiments

7-5-1. Rotationally Symmetrical Model for Reflection Estimation

The reflection estimation models are fabricated first to confirm the accuracy of design and analysis. In these models, all the slot sets over the aperture are ones for specialized ϕ and they are arranged rotationally symmetric, while the uniform illumination design is done in ρ direction. Table 7-2 summarize the parameters. In these models, however, $\Delta\rho=0$ and L_D is substituted by that of $\phi=90°$ for the simplicity of design. Figs. 7-12 show the slot arrangements.

Figures 7-13 show the measured reflection from slots togeter with the predicted one by array analysis. Time gating technique is used to extract the slot reflection. Though the center frequency is shifted about 300MHz mainly due to the error of permittivity, they are in good agreement and the reflection from slots are sufficiently suppressed, though the approximation of $\Delta\rho=0$ and $\phi=90°$ degrade the reflection.

Figures 7-14 shows the aperture field distribution. Both amplitude and phase are uniform for each model and the aperture illumination design is also confirmed. Since the slot arrangement is rotationally symmetric, the phase is alternating in $\pm\rho$ region.

7-5-2. Model Antennas with Weak Coupling

Two kinds of model antennas (L6:400mmϕ, L7:600mmϕ) are fabricated. To realize the stable antenna operation, the slot coupling is set to be weak at the cost of efficiency ($\eta\leqq70\%$). The design parameters are given in Table 7-3. The slot arrangement of L6 and L7 are shown in Figs. 7-15(a) and (b), respectively. The aperture illumination is uniform. The return loss, the aperture field distribution, the radiation pattern and the gain are measured. The results for the smaller antenna L6 are discussed first.

Figure 7-16 shows the measured reflection from slots by time

gating as well as the predicted one by array analysis. They are in good agreement and the accuracy of the analysis is confirmed for non-symmetrical slot arrangment, too.

Figure 7-17 compares the return loss of the antenna L6 with that of the conventional one without addtional slots. Reflection is suppressed from -2dB to less than -10dB. The reflection from slots in $\phi \simeq 45^{\circ}$ seems to be dominant from Fig. 7-11.

Figures 7-18(a) and (b) show the amplitude and phase distribution of co-pol. electric field over the aperture. The aperture distribution is almost uniform and relatively small ripples due to standing wave confirms the suppression of reflection. The center frequency shifts from design by about 400MHz, which is mainly due to the error in permittivity of the slow wave material and the waveguide height.

Figures 7-19(a) and (b) show the Fresnel radiation patterns in the planes of $\phi=0^{\circ}$ and 90°. The main beam pattern is almost symmetrical and the sidelobe level of about -15dB shows good antenna operation. However, the radiation from additional slots is not negligible in the endfire direction, which may degrade the antenna gain. The cross polarization level is below -20dB.

Figure 7-20 shows the frequency characteristics of the antenna gain and the antenna efficiency for L6. The gain has one peak at the center frequency and the band is limited due to the long line effect of traveling wave antennas. The peak gain of 30.4dBi and the antenna efficiency of 48% is obtained at 11.65GHz. The rigorous analysis of the antenna gain is left for future study, but the antenna efficiency η at the design frequency is roughly estimated as follows:

- Efficiency due to the return loss η_r=90%.
- Efficiency due to the absorber loss η_a=70%.

· Aperture illumination efficiency η_d=75%.

The antenna efficiency η is given as

$$\eta=\eta_i\times\eta_a\times\eta_d=47\%,$$

which accounts for the measured value. The desired operation of the model antenna is partly confirmed.

Figure 7-21 shows the the gain of the larger antenna L7. The peak gain of 34.6dBi and the antenna efficiency of 54% are realized at 11.6GHz, while the predicted efficiency for this antenna is 59%, i.e. η_i=90%, η_a=78% and η_d=83%. The efficiency enhancement of the larger antenna reflects the decrease of absorber loss in Eq. (6-4). The bandwidth is narrower due to the long line effect.

These antennas are the first experimental results to realize the normal operation of LP-RLSA.

7-6. Gain Enhancement - Theory and Experiments -

7-6-1. Gain Enhancement Technique

For the gain enhancement, the efficiencies listed in Sec. 7-5-2 are improved respectively.

(1) Return loss improvement.

(1-1) Beam-tlit technique: As far as the rotational symmetry of inner field is maintained, the sum of the reflected waves at the feed are canceled. It may be effective if it is jointly used with the reflection canceling slot set. Especially when the first null is set normal to the aperture, the reflection is perfectly canceled. Figure 7-22 shows the tilt angle desiring this condition.

(1-2) Reflection of radome: The positive use of the reflection from radome is also attractive. Figure 7-23 shows the mechanism of reflection cancellation and the equivalent S-matrix model. The slot array is replaced by 3-port S-matrix; port #1 as feed, #2 as

termination and #3 as radiation. The matrix elements are calculated by the array analysis. The radome and the free space radiation are replaced together by un-matched load, of which the complex reflection coefficient is Γ. The argument of Γ is varied by the distance d, while the absolute value is constant. By optimizing d, the minimum reflection coefficient $|S_{11}'|$ is given as (see Appendix F in detail)

$$|S_{11}'| \fallingdotseq |S_{11}| - |\Gamma||S_{31}|^2 \qquad (7\text{-}14),$$

by the choice of Γ, the reflection can be sufficiently suppressed.

(2) Termination loss reduction.

(2-1) The increase of maximum coupling factor: It can be increased sence the model antennas in Sec. 7-5-2 are designed with a large termination loss for the stable antenna operation.

(2-2) Non-uniform aperture illumination: As is mentioned in Sec. 6-5, it is effective to reduce the termination loss.

(2-3) The enlargement of the antenna diameter: The radiation area is increased.

(2-4) High-ε_r dielectiric: As the wavelength is reduced, the maximum coupling factor can be increased, with the sacrifice of the frequency bandwidth.

(2-5) Double-layered structure: It is an alternative to reduce the termination loss, since it has natively small losses.

(3) Aperture efficiency improvement.

(3-1) The enlargement of the antenna diameter: The unwanted radiation to the end-fire direction from additional slots is due to the small aperture, where the dicrete source distirbution is not neglegible.

(3-2) High-ε_r dielectiric: Since the number of the slots increases, the unwanted radiation is sufficienly canceled.

(3-3) Minimized S_Φ: To improve the rotational symmetry of inner

field, S_{ϕ} might be reduced.

(3-4) Other slot set configuration: The additional slots radiate the unwanted lobes in the endfire direction, which may degrade the antenna gain. An alternative slot set with small unwanted radiation is presented in Chap. 8.

7-6-2. Experiments

Some of the techniques listed in Sec. 7-6-1, (1-2), (2-1) and (3-3), are examined by model antennas.

(1-2) Reflection of radome: The reflection characteristics of model antenna L6 with the radome is measured. The parameters of radomes are listed in Table 7-4. Figure 7-24 shows the reflection coefficient of slot array with radome R1 ($|\Gamma|$=-18dB) together with the antenna gain as functions of the spacing d. The ripple of the reflection 6dB-pp is almost equal to the predicted -5.4dB by Eq. (7-14). The gain is varying accordingly, but the ripple of 1dB-pp is far larger than the predicted 0.2dB-pp due to the return loss. Figure 7-25 shows another example with radome R2 ($|\Gamma|$=-10dB). In this example, the minimum reflection does not result in the maximum gain. The reflected waves from radome affects not only on the reflection, but also on the excitation coefficients of slots, which may result in the deformation of radiation pattern. The effect of the radome should be therefore quantitatively estimated, though it is left for future study.

(2-1) The increase of maximum coupling factor: The 600mmϕ model antenna L13 is fabricated. The design parameters are given in Table 7-3, which are just the same as model L7, except α_{max} is almost doubled. Figure 7-26 shows the return loss. The maximum value of -8dB is mainly due to the slot reflection. Figure 7-27 shows the aperture field distribution. Though the edge rebel of amplitude is slight lower, the uniformity of the aperture

distribution is rather improved. The Fresnel radiation patterns are shown in Figs. 7-28. Conparing with those of Fig. 7-19, the unwanted radiation to the endfire direction is almost perfectly suppressed. It is mainly due to the larger diameter. The symmatrical patterns indicate the stable antenna operation. Figure 7-29 shows the gain and antenna efficiency. Though the peak frequency is shifted lower, the gain of 35.4dBi and the antenna efficiency of 67% are realized at 11.45GHz.

(3-3) Minimized S_{ϕ}: The minimization of S_{ϕ} is the key technique for CP-RLSA to suppress the higher modes and to keep the rotational symmtry in the radial waveguide. The model antenna L15 is fabricated, in which all the design parameters except S_{ϕ} are the same as those of L6, as shown in Table 7-3. Figure 7-30 shows the apterute distirbution. No significant difference is observed, conparing with Fig. 7-18. The gain and the antenna efficiency are shown in Fig. 7-31, comparing with those of L6. The peak gain is almost equal, while the bandwidth is a bit nallower. This technique seems to be not effective on LP-RLSA.

7-7. Concluding Remarks

The problem of original LP-RLSA is briefly clarified. As a solution, a slot set with small reflection is introduced as a unit radiator of a linearly-polarized radial line slot antenna. The reflection coefficient of a slot set is reduced to -40dB by an optimum choice of slot parameters. The design is confirmed by the experiments using model antennas. The desired operation of LP-RLSA is observed for the first time. The antenna return loss is improved from -2dB to -10dB. The antenna efficiency of 48% and 54% is measured at 12GHz band for the diameters 400mm and 600mm respectively, which agree with the predicted ones.

The techniques for the efficiency enhancement are also listed up. By the 600mmϕ model antenna with strong coupling, the unwanted radiation to the end-fire direction is sufficiently suppressed. The gain of 35.4dBi and the efficiency of 67% are measured at 11.45GHz.

The criterion for the efficiency of LP-RLSA is 80% for the commercial use.

References

[1] M. Ando, T. Numata and N. Goto, "A Linearly-Polarized Radial Line Slot Antenna," IEICE Technical Report, AP87-87 (Oct. 1987).

[2] M. Ando, T. Numata, J. Takada and N. Goto, "A Linearly Polarized Radial Line Slot Antennas," IEEE Trans. Antennas & Propag., vol. AP-36, no. 12, pp. 1675-1680 (Dec. 1988).

[3] J. Takada, M. Ando and N. Goto, "A Beam-tilted Linearly Polarized Radial Line Slot Antenna," IEICE Trans. vol. J71-B, no. 11, pp. 1352-1357 (Nov. 1988).

[4] T. Ikeda, J. Takada, M. Ando and N. Goto, "Slots Reflection Suppression of Linearly-Polarized Radial Line Slot Antennas", 1989 Autumn Natl. Conv. Rec., IEICE, B-42 (Sep. 1989).

[5] M. Ando, J. Takada and N. Goto, "A High Efficiency Radial Line Slot Antenna," ITEJ Technical Report, RE88-30 (Sep. 1988).

Table 7-1. Design parameters in the analysis.

Frequency f[GHz]	12.0
Permittivity ε_r	1.48
Waveguide height du[mm]	7.5
Waveguide width S_ϕ[mm]	12.5
Maximum coupling factor α_{max} [1/m]	12.0+
Antenna radius ρ [mm]	200+

+: in Fig. 7-11.

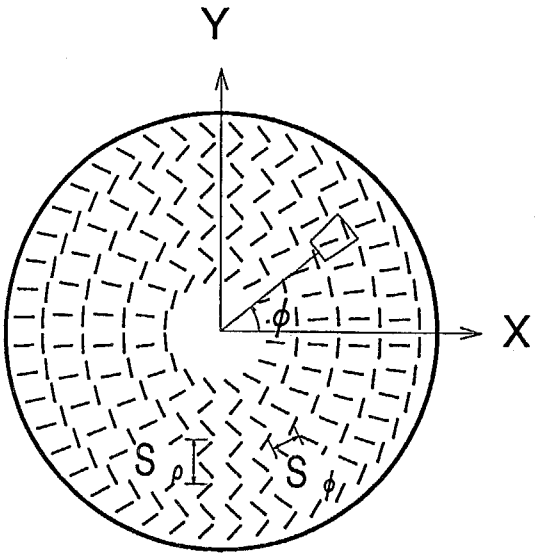

(a) Plan of original LP-RLSA.

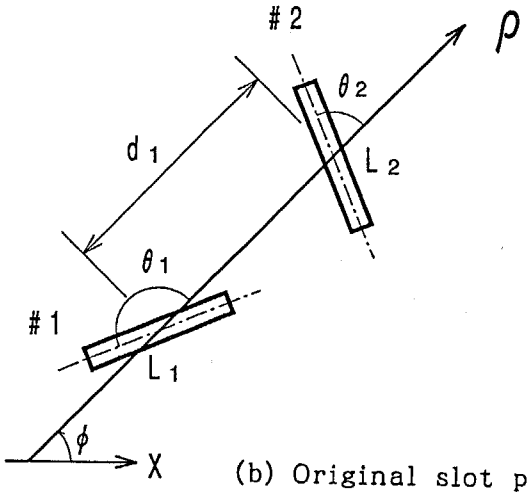

(b) Original slot pair.

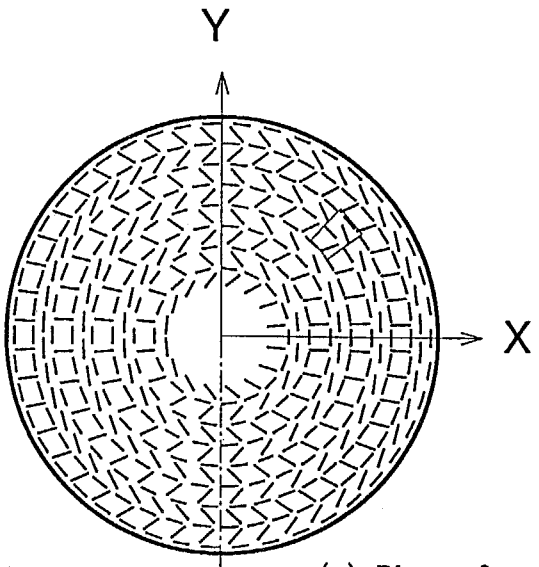

(c) Plan of new LP-RLSA.

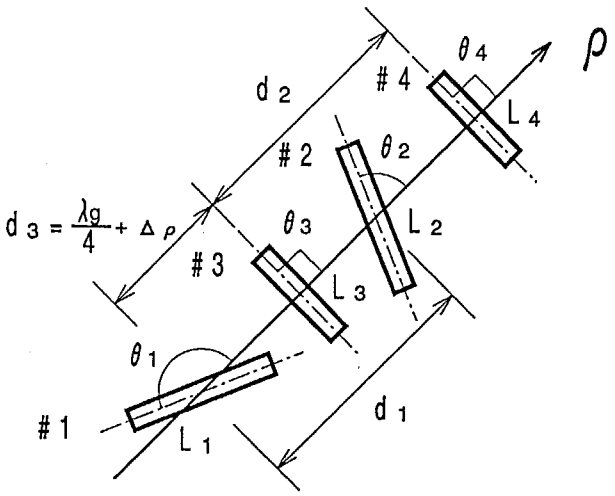

(d) New slot set.

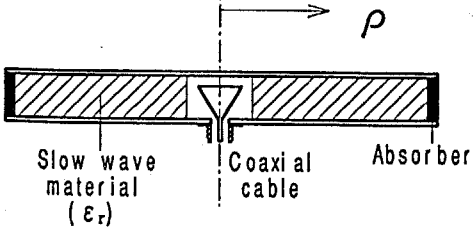

(e) Cross section of LP-RLSA.

Fig. 7-1. Configuration of LP-RLSA.

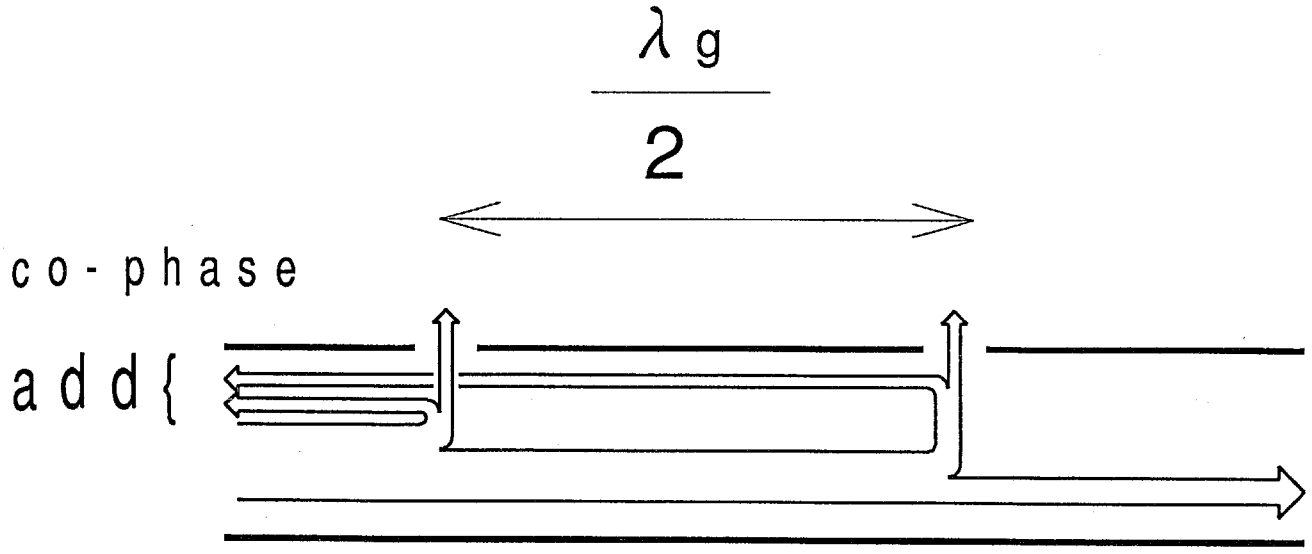

(a) Reflections from adjacent slots.

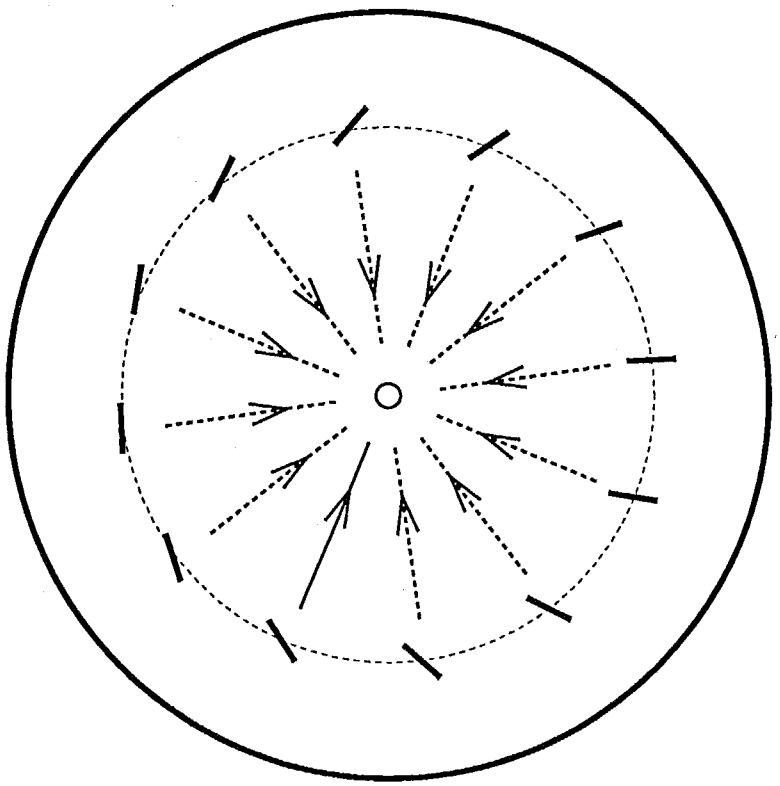

(b) Reflections from all the directions.

Fig. 7-2. Reflection mechanism of original LP-RLSA.

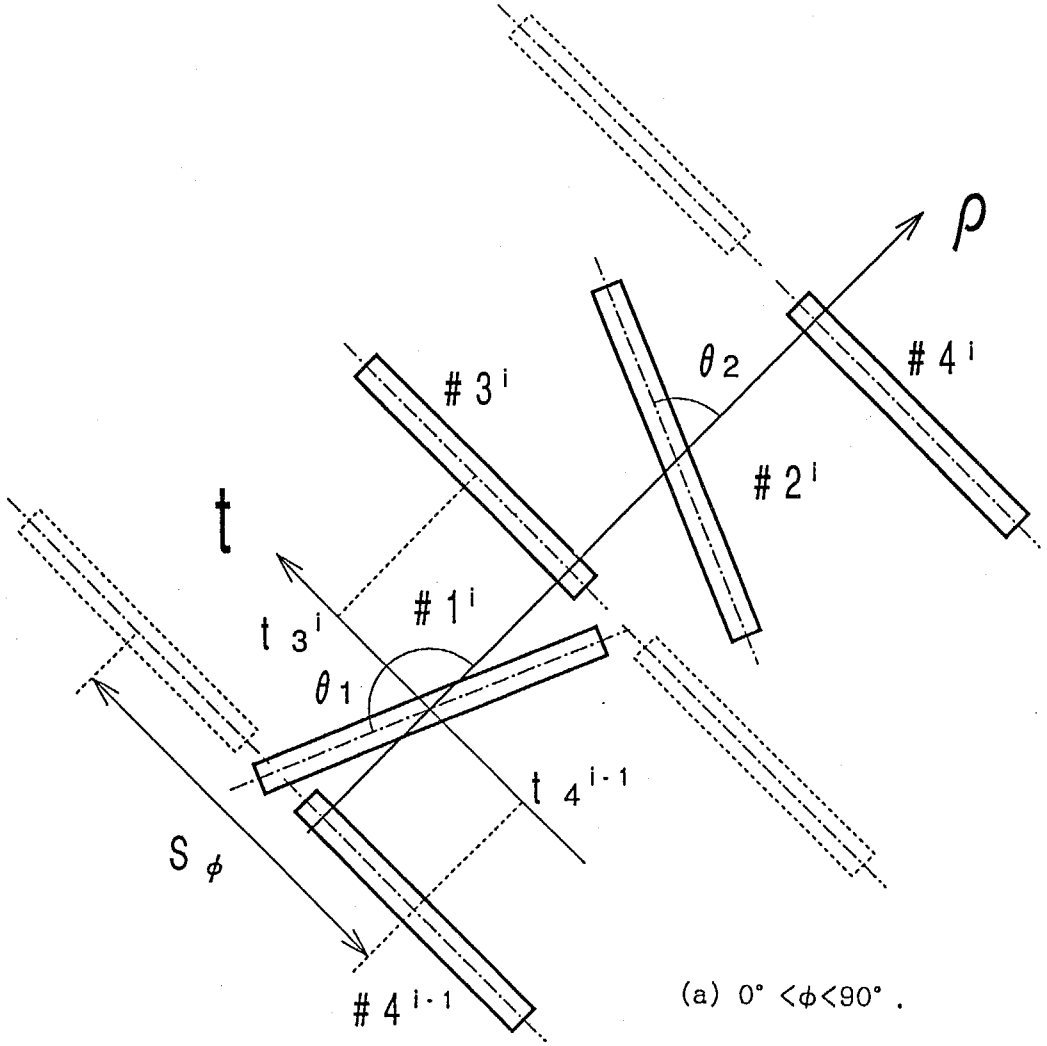

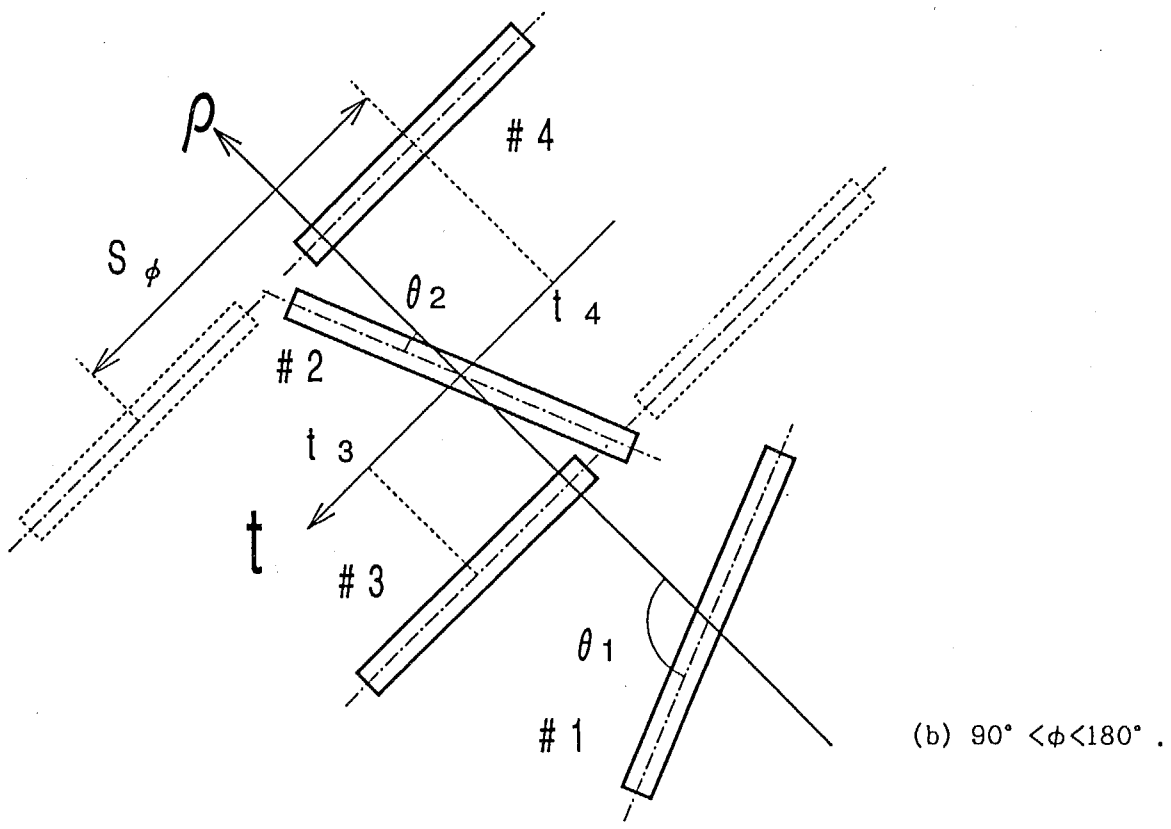

Fig. 7-3. Displacement of addtional slots to avoid the overlap.

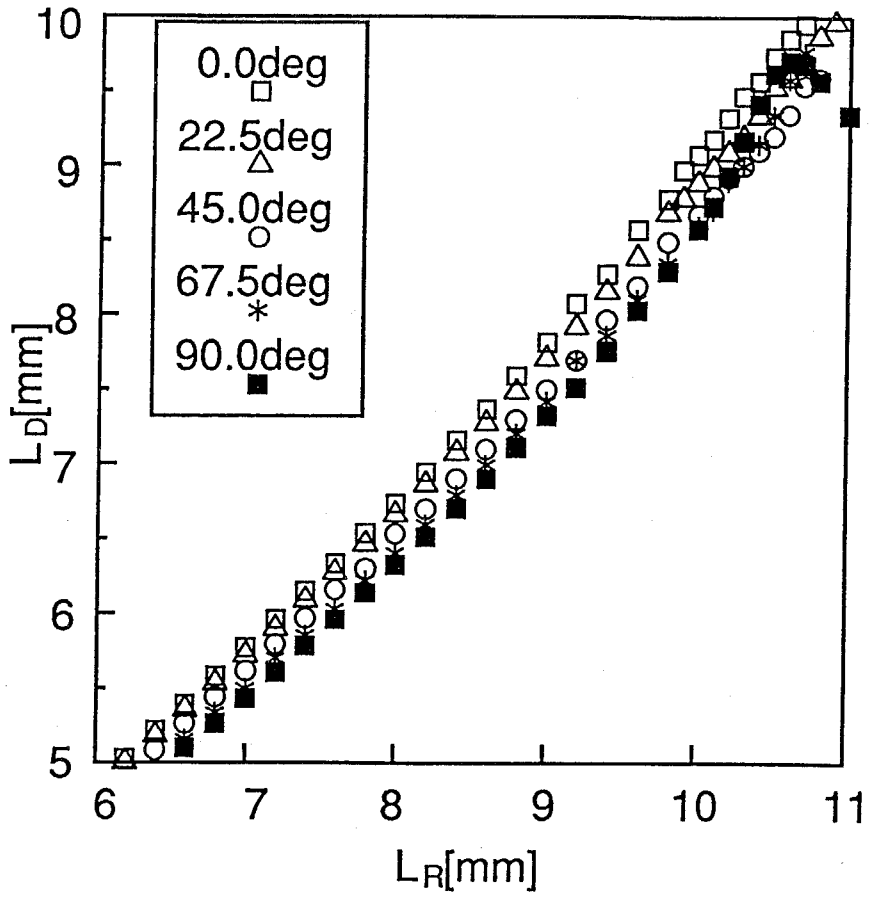

Fig. 7-4. The radiation slot length L_R vs the additional slot length L_D.

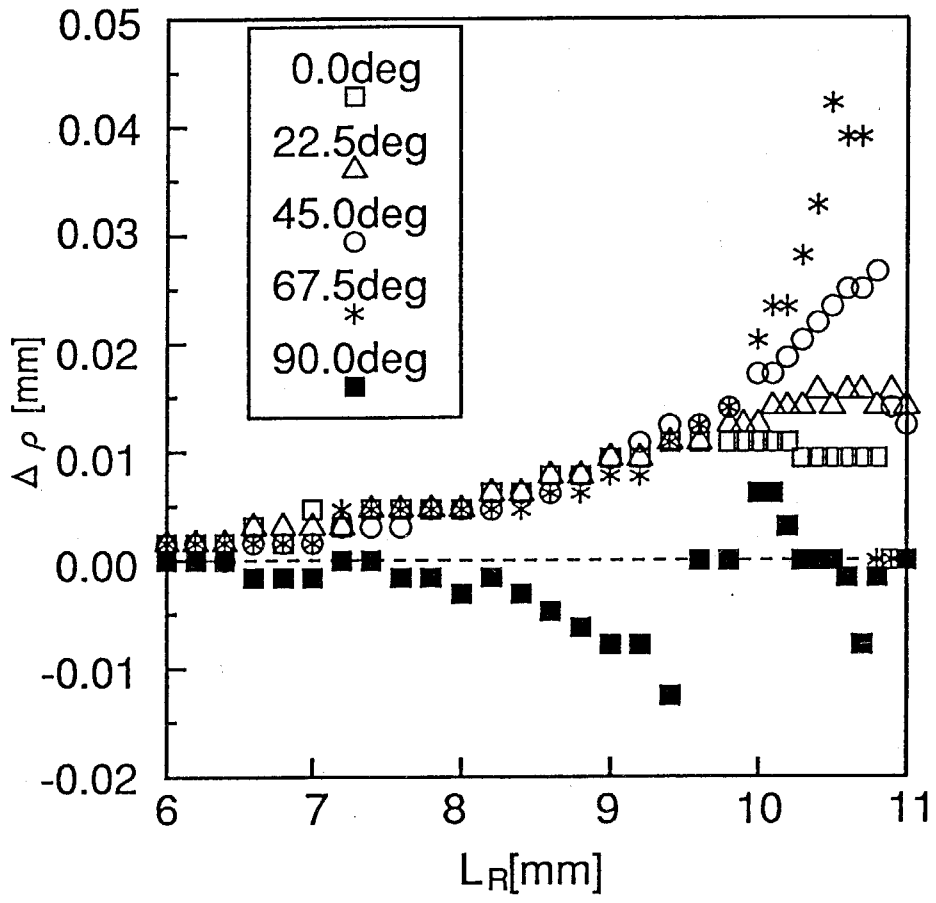

Fig. 7-5. The radiation slot length L_R vs the offset of the additional slot $\Delta\rho$.

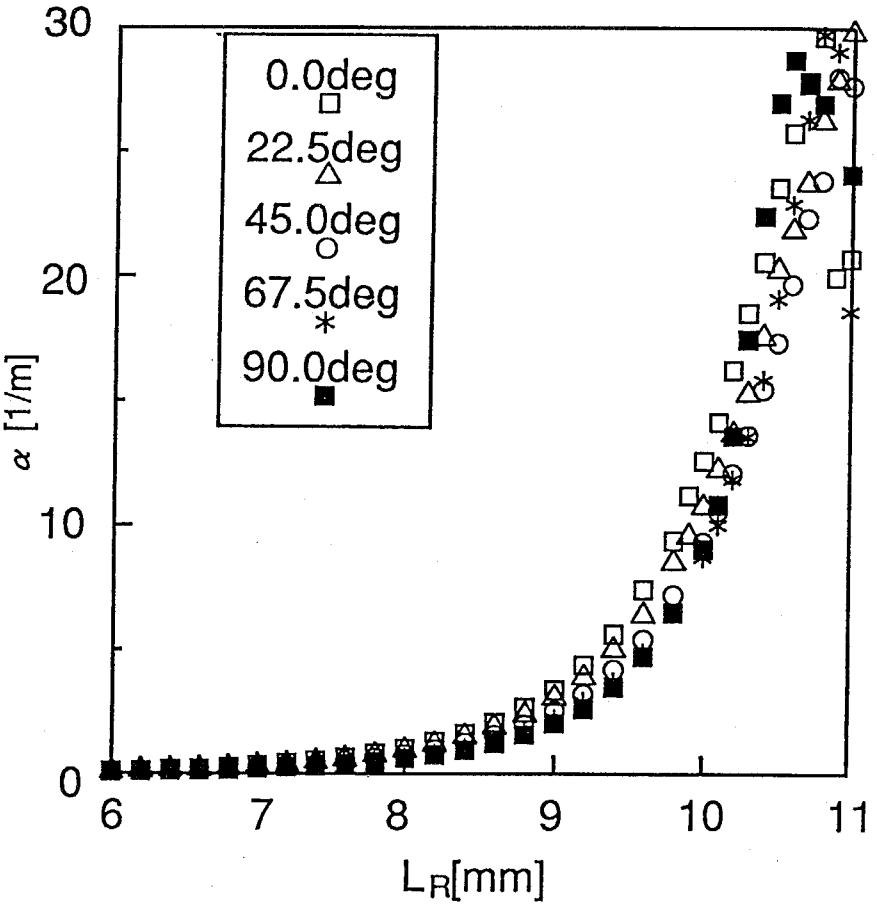

Fig. 7-6. The coupling factor α as a function of the radiation slot length L_R.

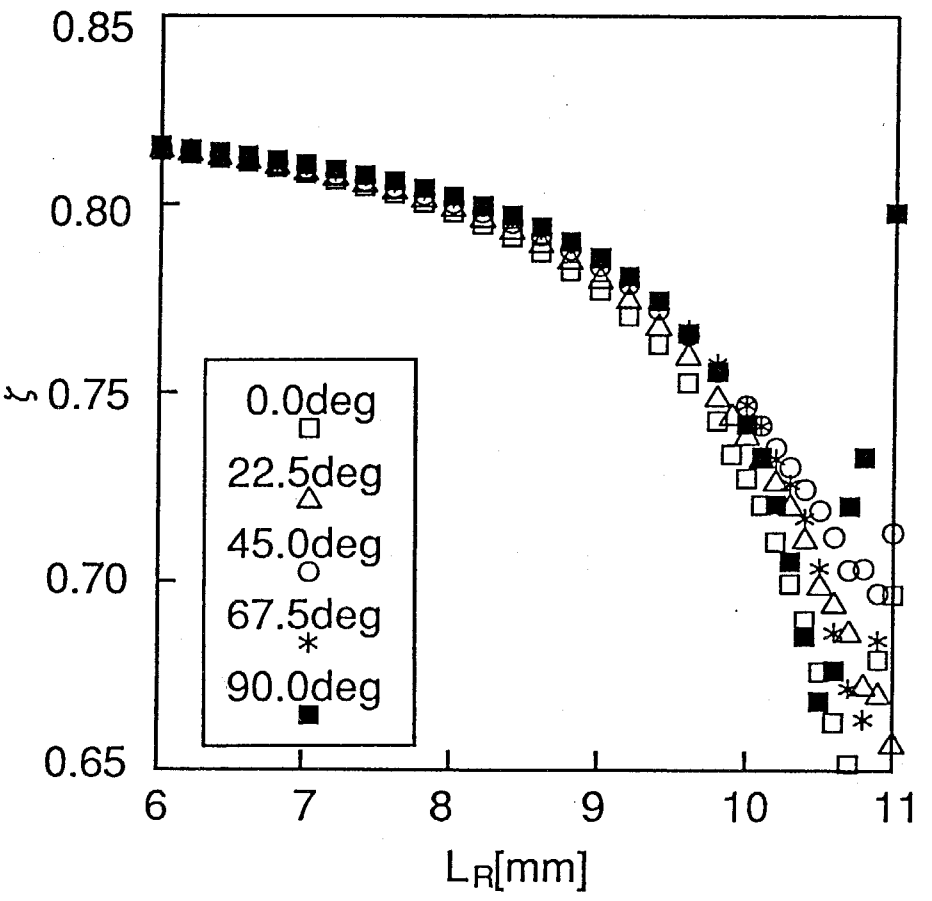

Fig. 7-7. The slow wave factor ζ as a function of the radiation slot length L_R.

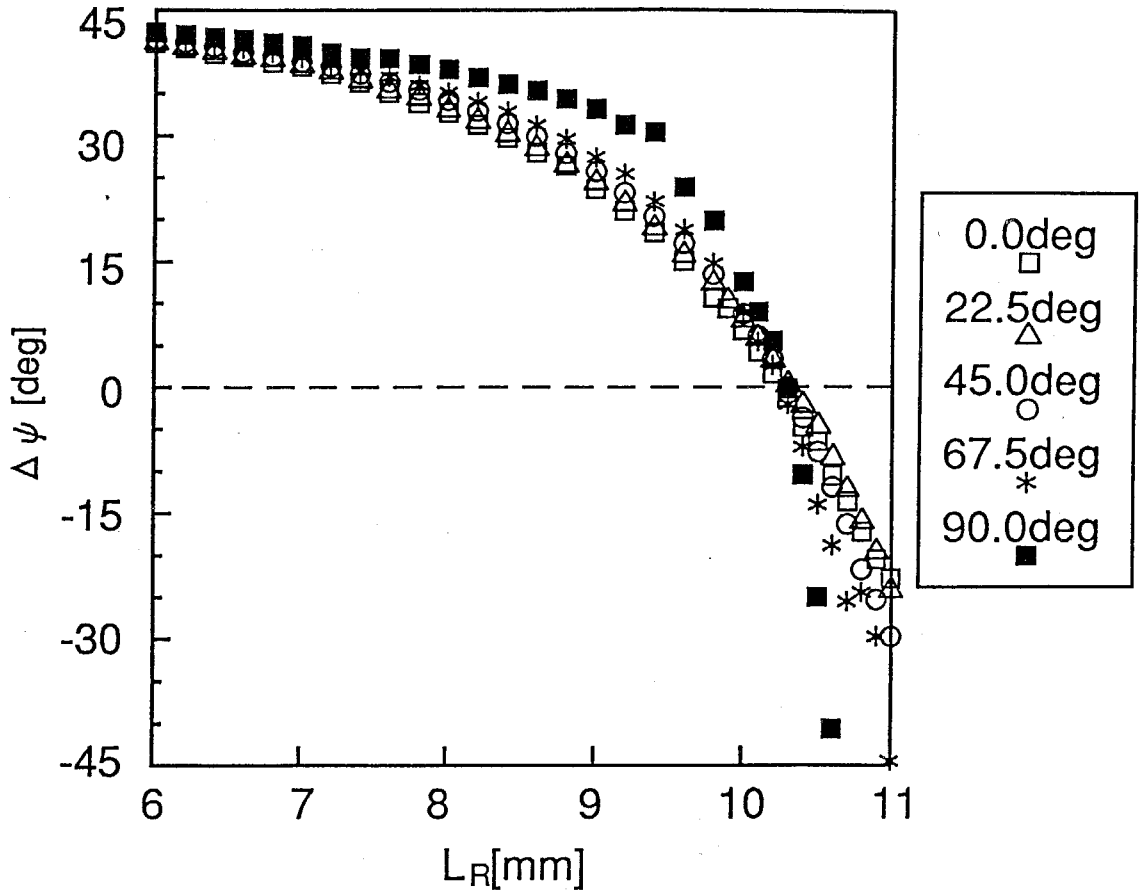

Fig. 7-8. The relative radiation phase $\Delta\psi$ as a function of the radiation slot length L_R.

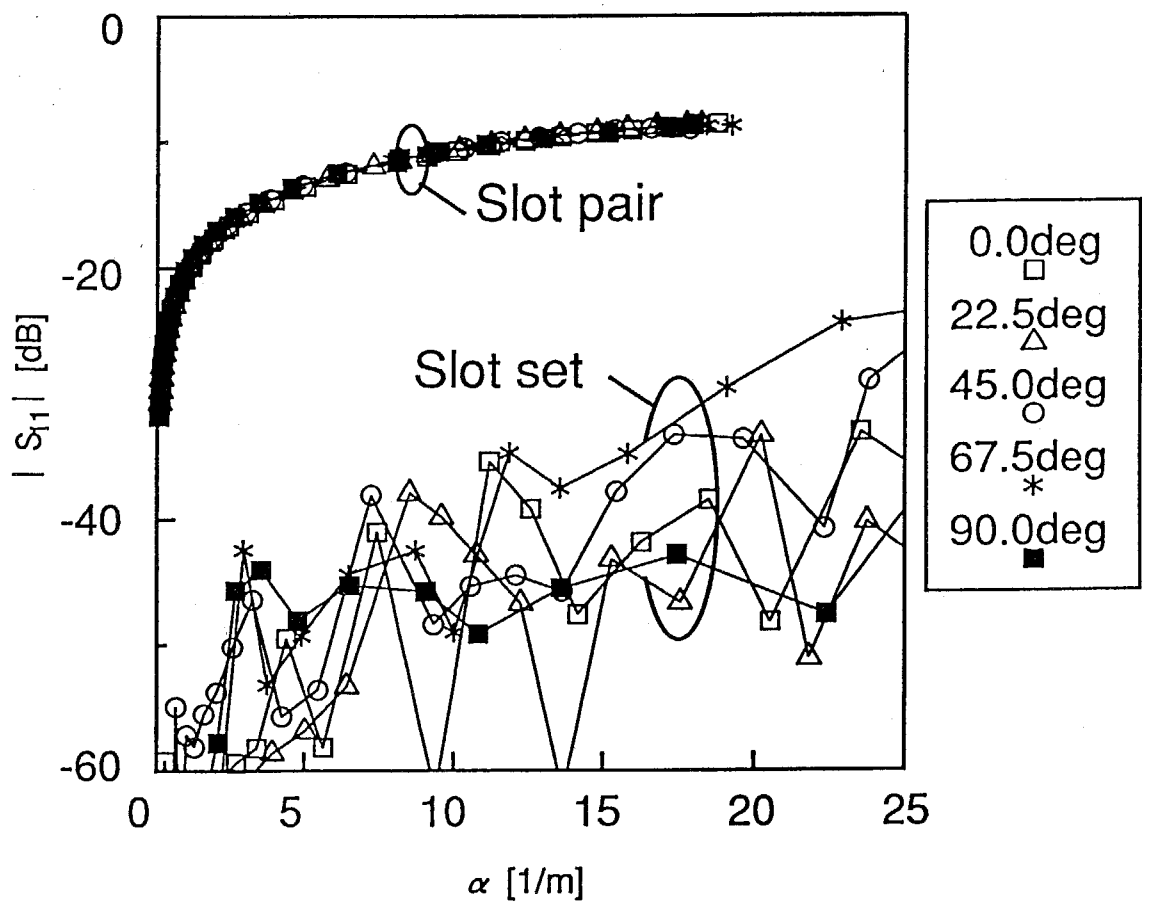

Fig. 7-9. The reflection coefficient $|S_{11}|$ of a slot set.

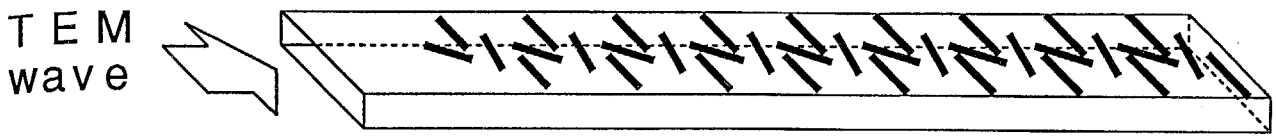

Fig. 7-10. 1-dimensional array.

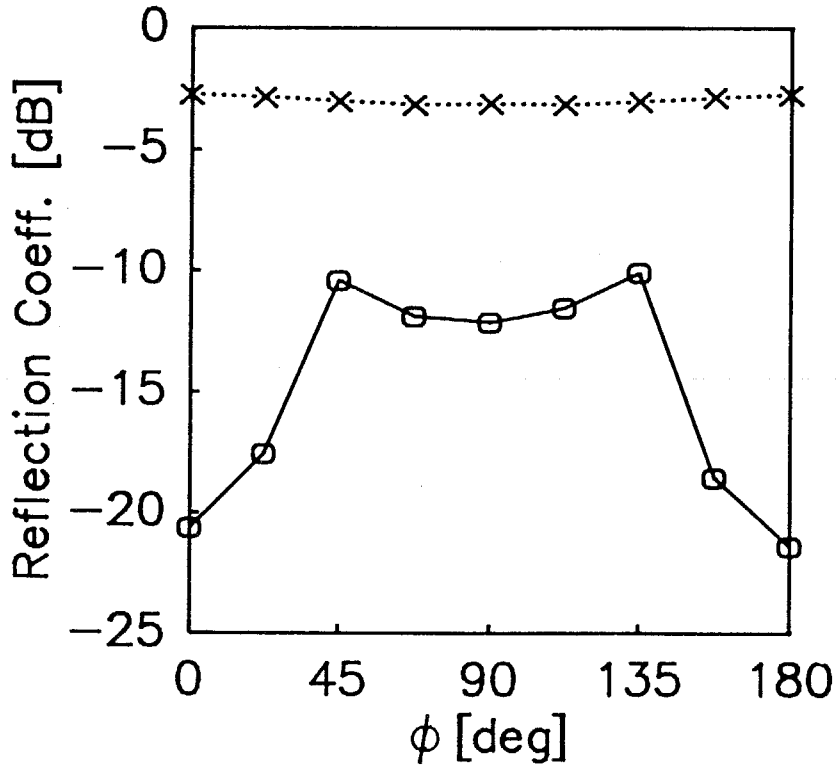

Fig. 7-11. The reflection coefficient of 1-dimensional array.

(—⊖—: this design, ··×··: original design)

Table 7-2. Design parameters for rotationally-symmetrical models.

Name of model	L1	L2	L3
Azimuth angle for slot set design φ [deg]	0	45	90
Frequency f[GHz]	12.0		
Aperture diameter $2\rho_{max}$[mm]	400		
Blocking diameter $2\rho_{min}$[mm]	30		
Waveguide height du[mm]	7.5		
Permittivity ε_r	1.48		
Slot angular spacing S_Φ[mm]	12.5		
Maximum coupling factor α_{max}[1/m]	12		

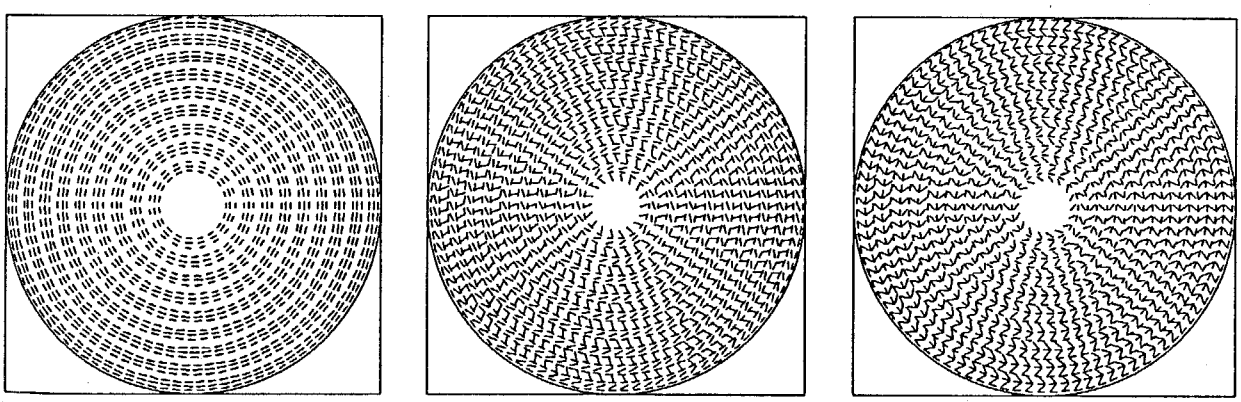

(a) L1(ϕ=0°). (b) L2(ϕ=45°). (c) L3(ϕ=90°).

Fig. 7-12. Slot arrangement for rotationally-symmetrical models.

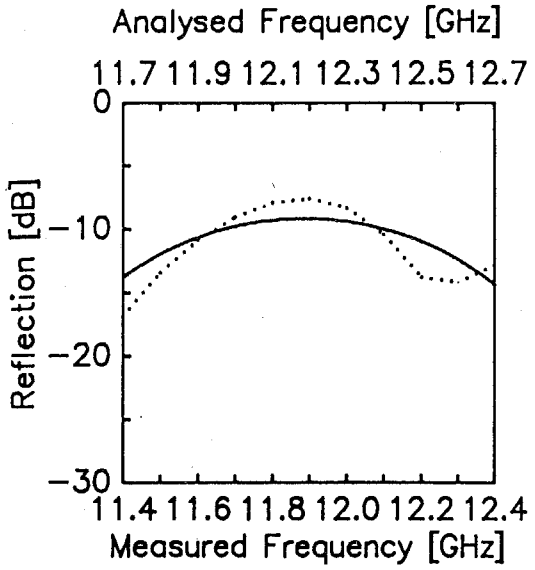

(a) L1(ϕ=0°).

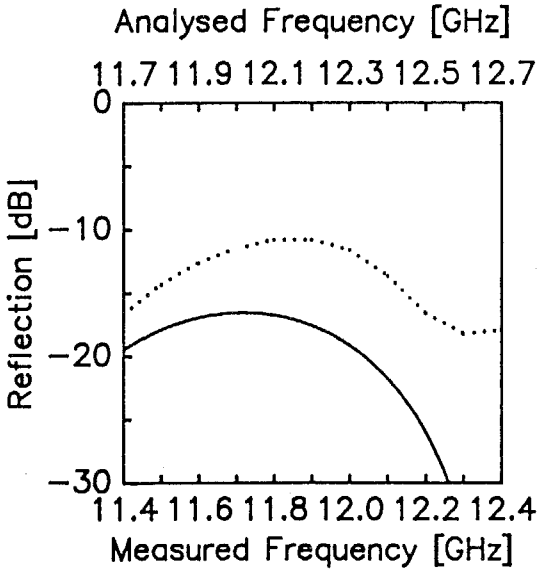

(b) L2(ϕ=45°).

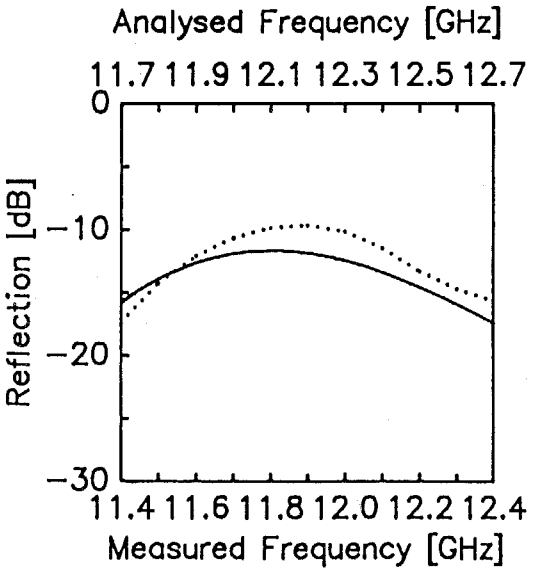

(c) L3(ϕ=90°).

Fig. 7-13. Slot reflection for rotatinally-symmetrical model.

(——: measured, ····: analysed).

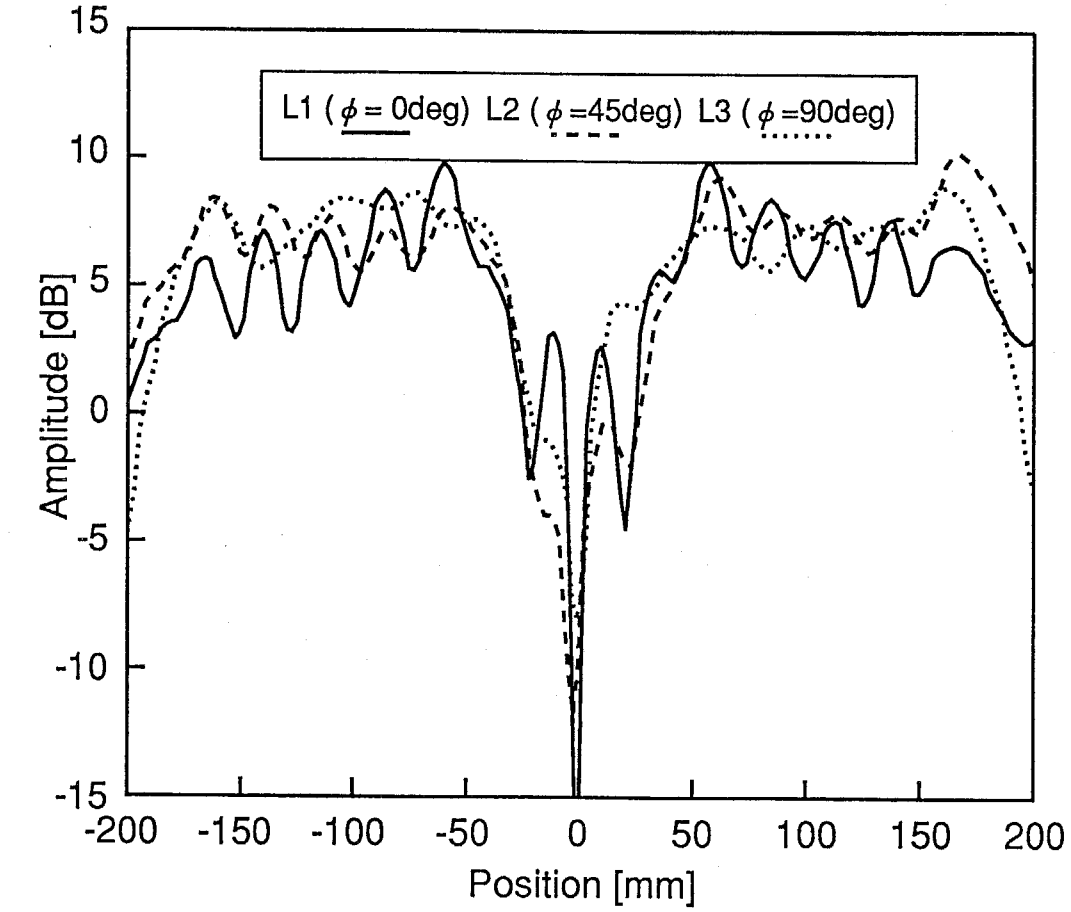

(a) amplitude.

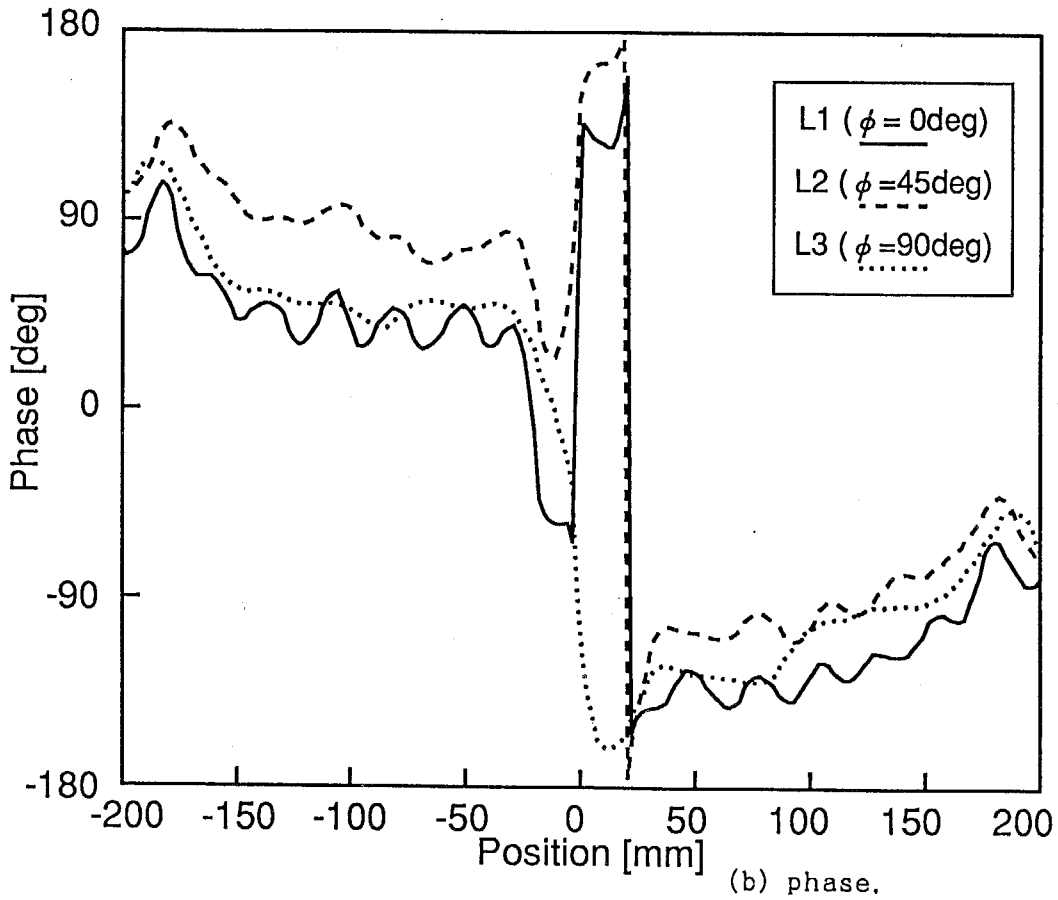

(b) phase.

Fig. 7-14. Aperture distribution for rotationally-symmetrical model.

Table 7-3. Design parameters for model antennas.

Name of model	L6	L7	L13	L15
Frequency f[GHz]	12.0			
Antenna diameter $2\rho_{max}$[mm]	400	600	600	400
Blocking diameter $2\rho_{min}$[mm]	30			
Waveguide height du[mm]	7.5			
Permittivity ε_r	1.48			
Slot angular spacing S_ϕ[mm]	12.5			9.7~12.2
Maximum coupling factor α_{max}[1/m]	12		23.8	12
Radiation slot length L_R[mm]	7.9~10.1		6.9~10.2	7.9~10.1
Additional slot length L_D[mm]	6.6~ 9.2		5.7~ 9.3	6.6~ 9.2
Number of slot N	2022	4592	4592	2246

* L9 is modefied from L6 by deleting the addtional slots.

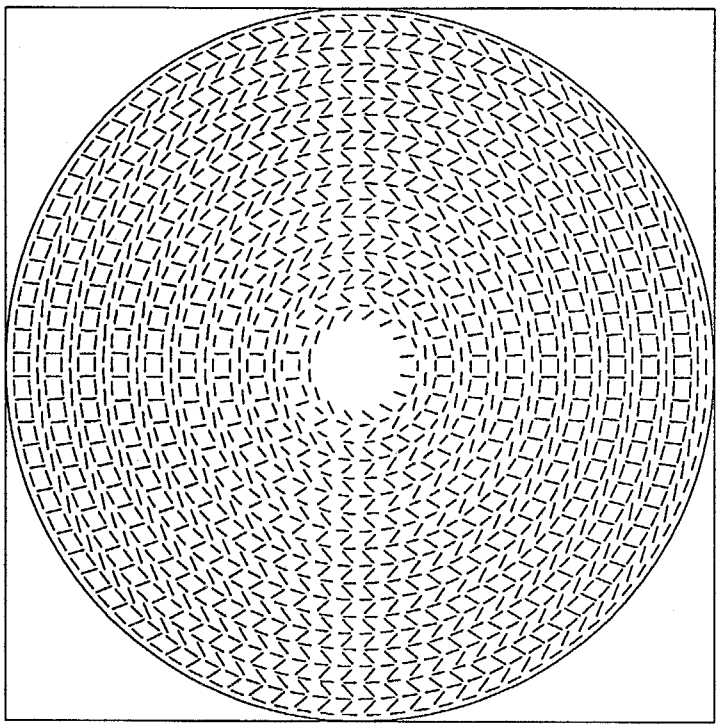

(a) L6 (400mmϕ).

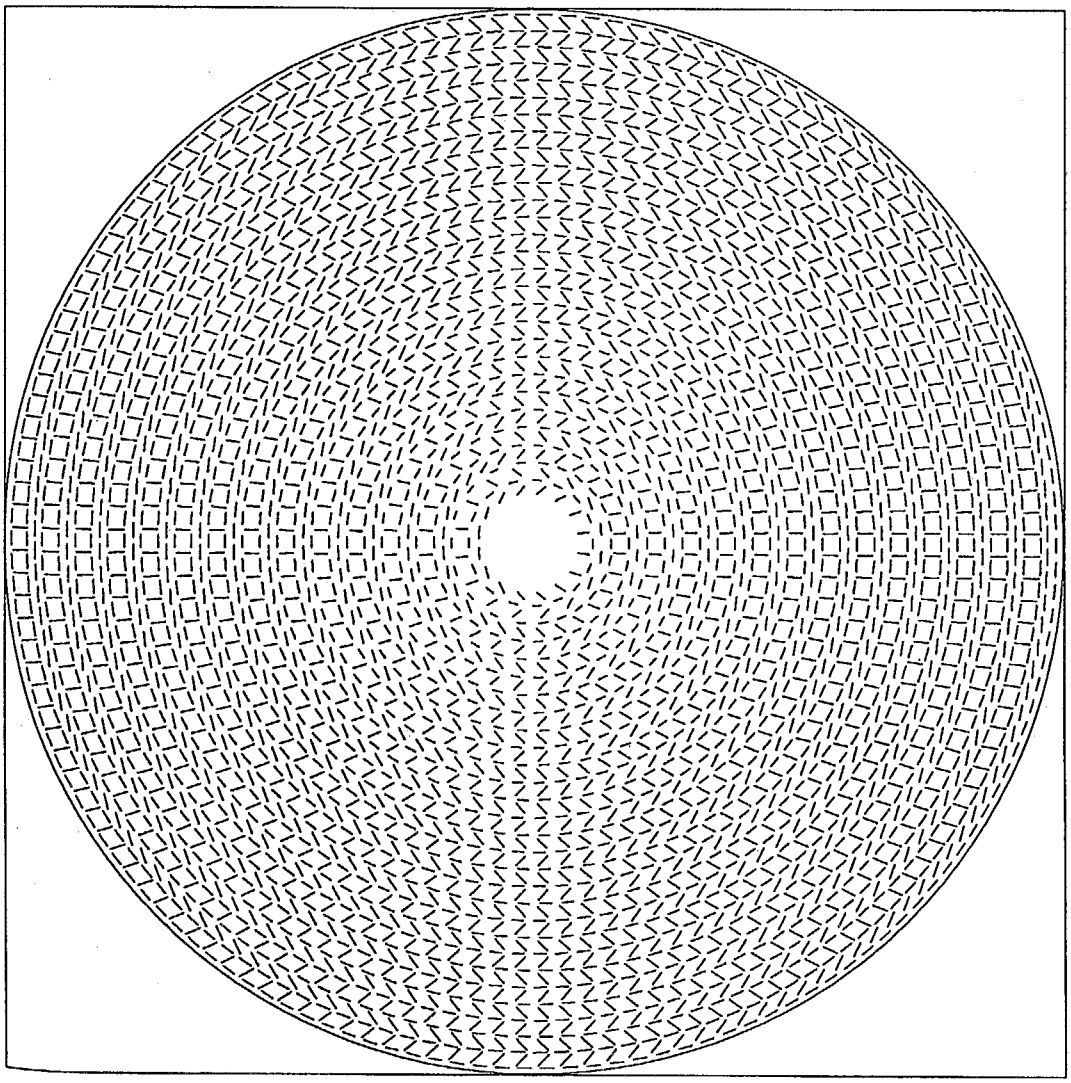

(b) L7 (600mmϕ).

Fig. 7-15. Slot arrangement for model antennas with weak coupling.

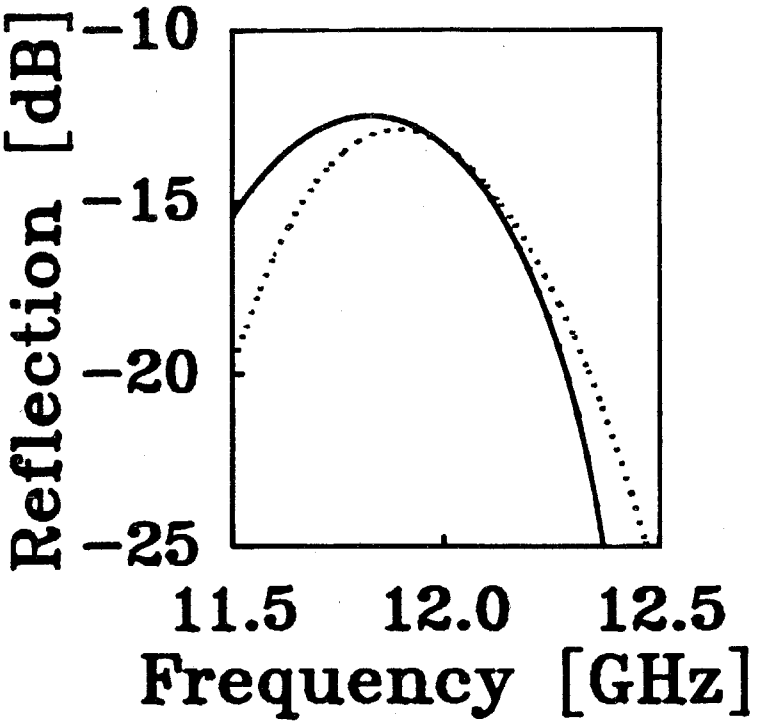

Fig. 7-16. The reflection from slots for antenna L6

(——:measured, ·····:analysed).

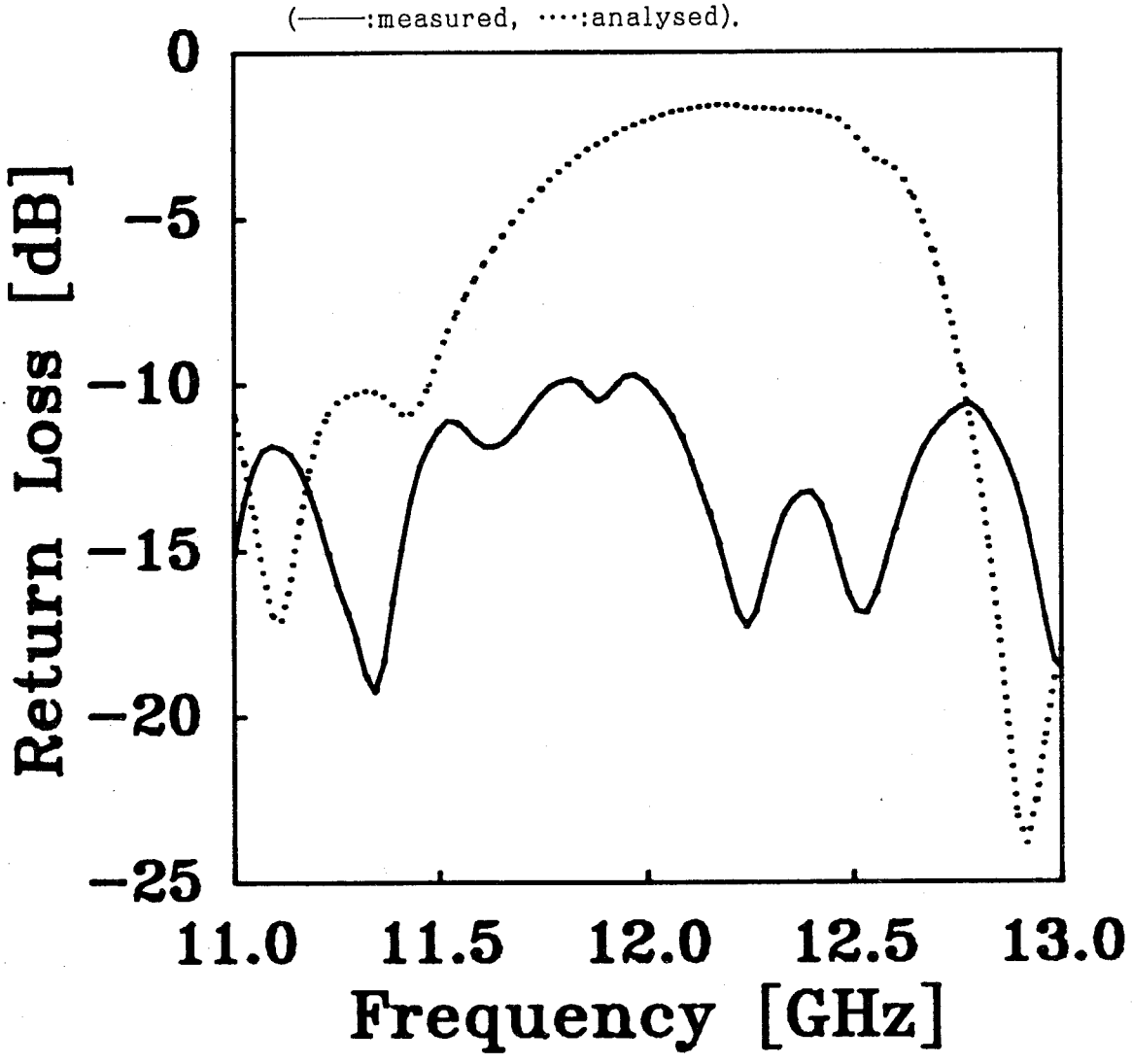

Fig. 7-17. The return loss of antenna L6

(——:antenna L6, ·····:conventional L9).

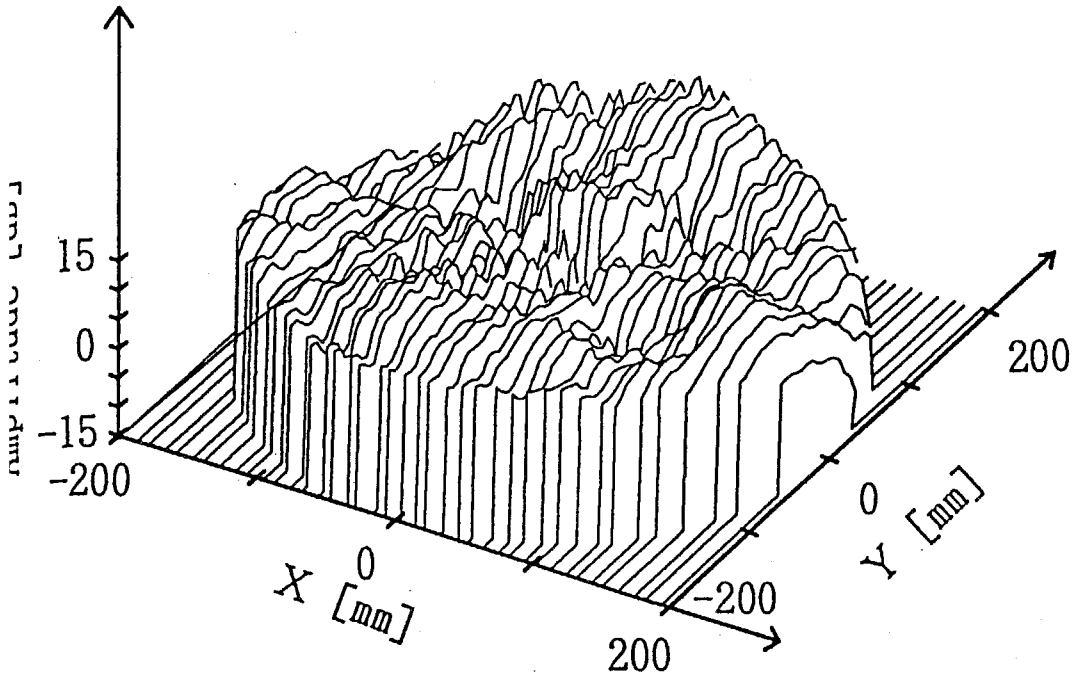

(a) Amplitude.

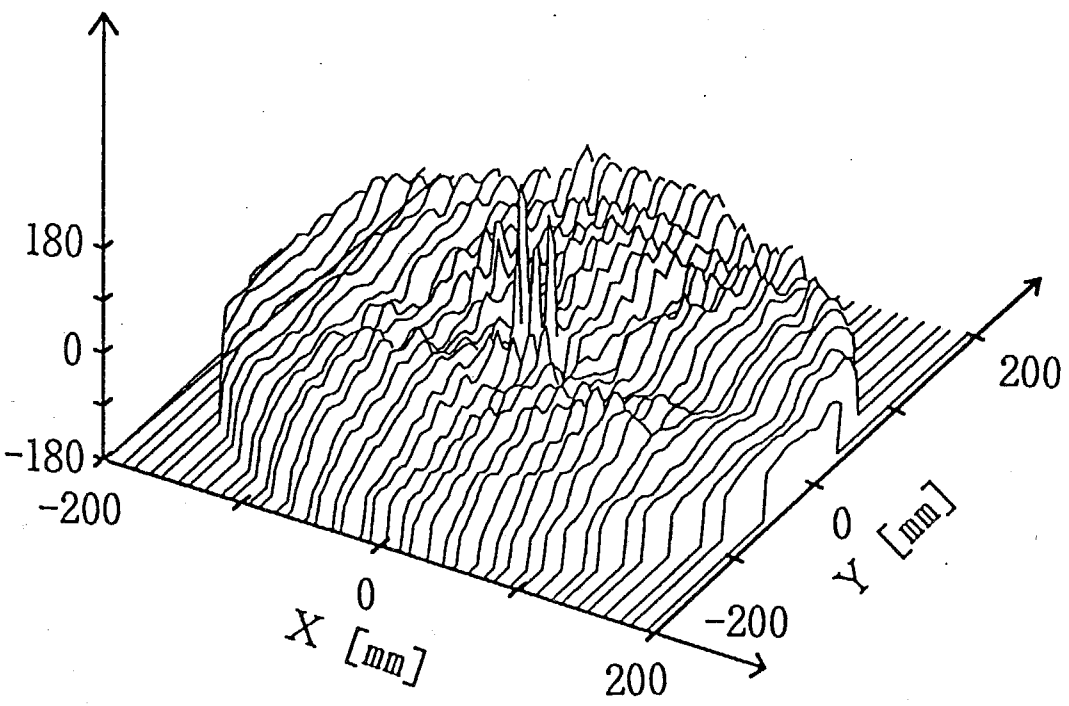

(b) Phase.

Fig. 7-18. The aperture field distribution of antenna L6.

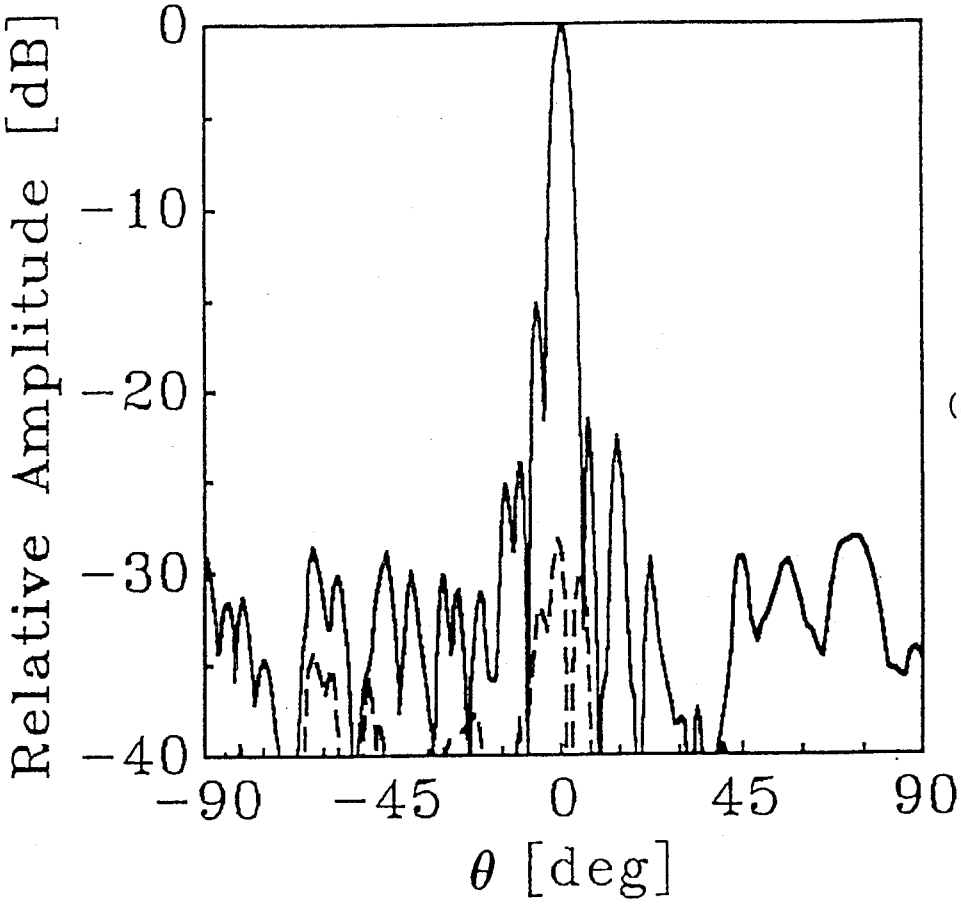

(a) ϕ=0° (E-plane).

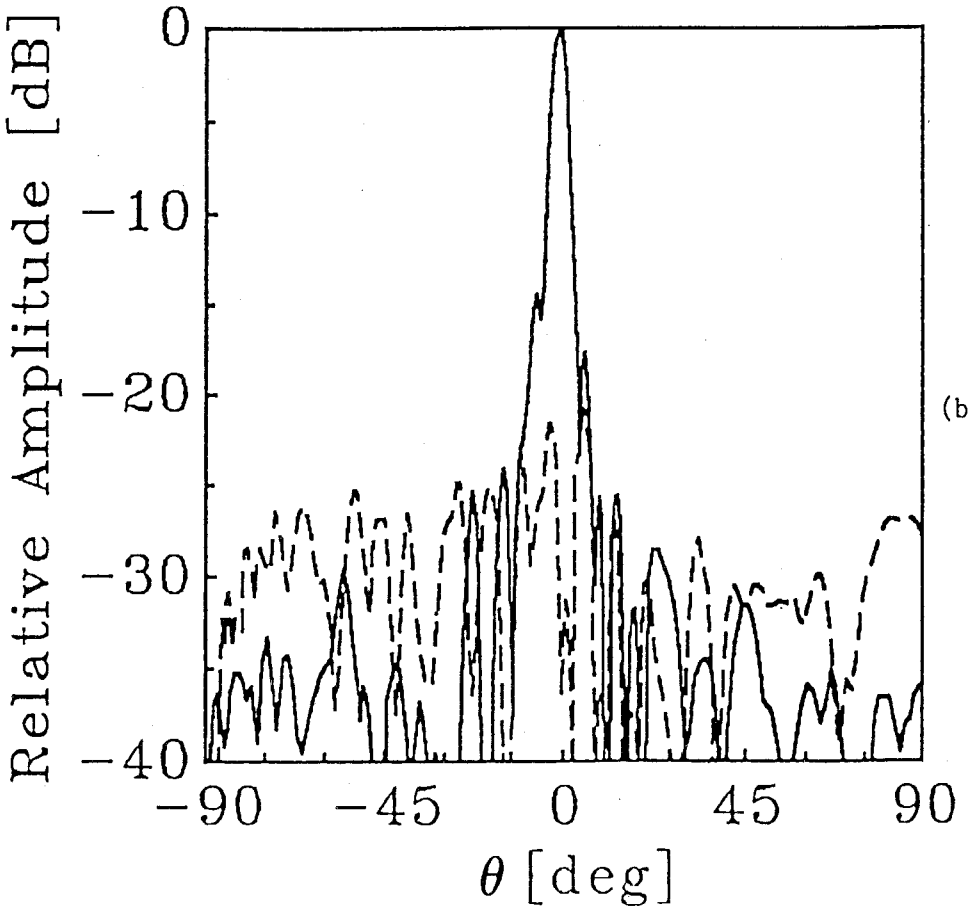

(b) ϕ=90° (H-plane).

Fig. 7-19. The Fresnel radiation patterns of antenna L6

(——:principal pol., - - :cross pol.).

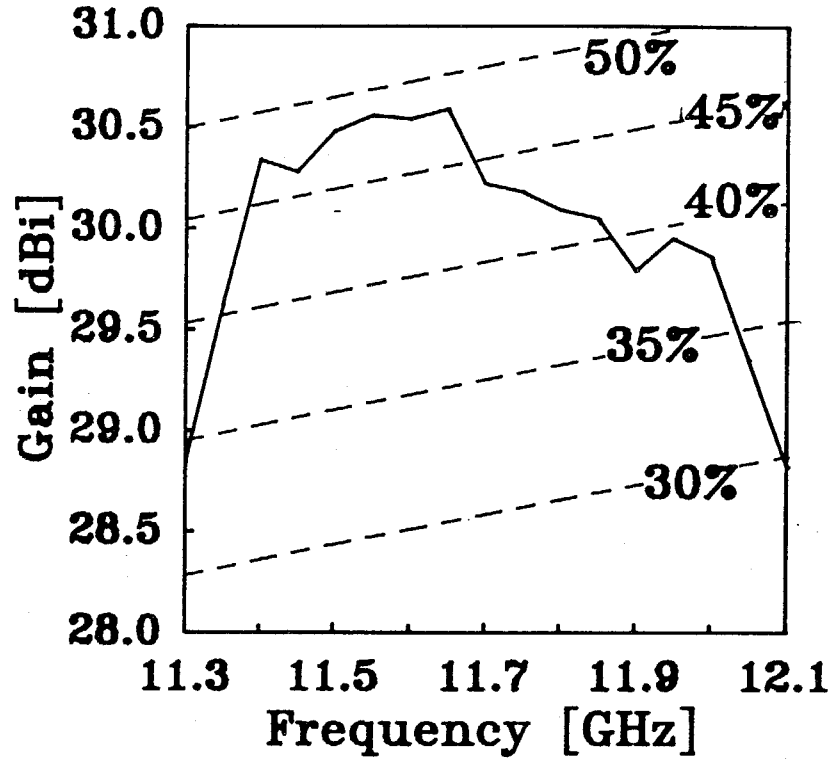

Fig. 7-20. The gain and the antenna efficiency of L6.

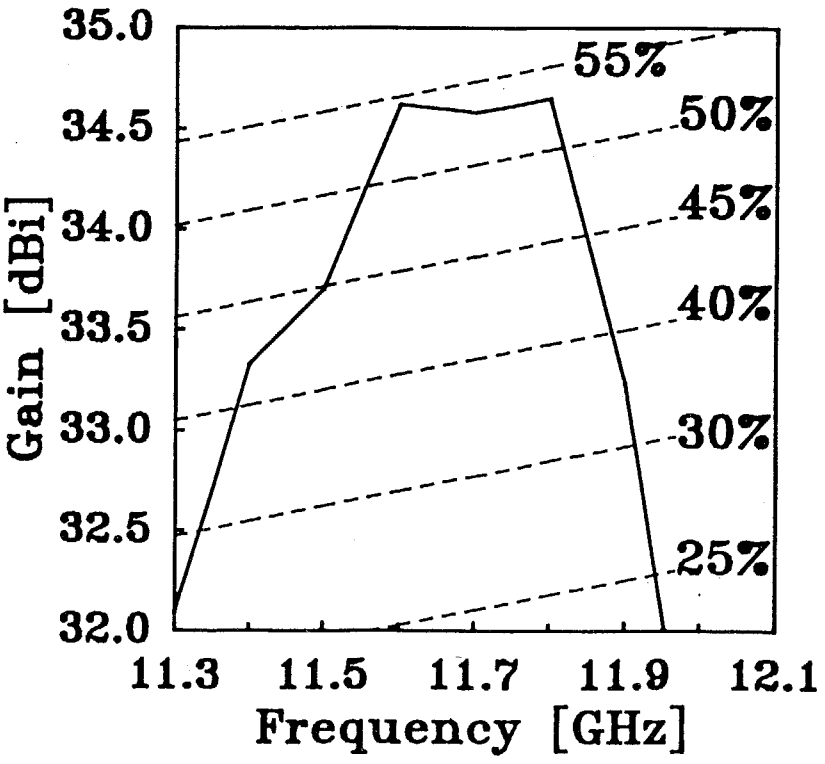

Fig. 7-21. The gain and the antenna efficiency of L7.

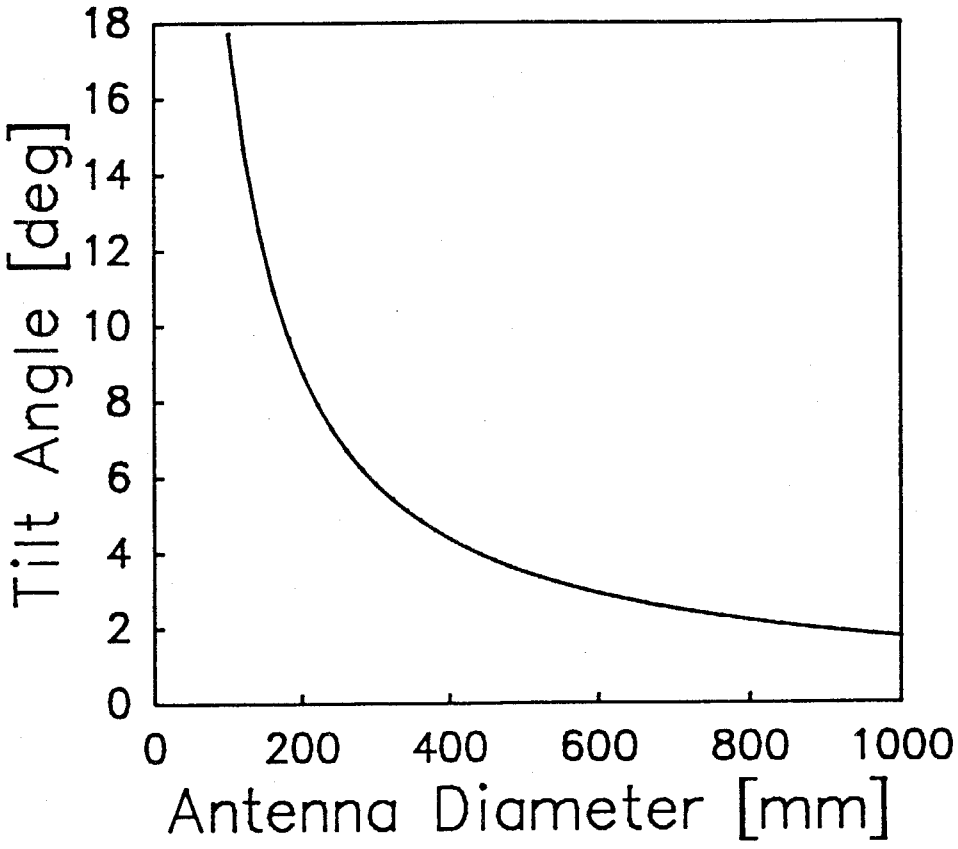

Fig. 7-22. The beam-tilt angle for normal null.

Table 7-4. The parameters of radomes.

Name of sample	R1	R2
Thickness t [mm]	1.0	4.0
Permittivity ε_r	3.5	2.14
Fresnel reflection coeff. Γ [dB]	-18	-12

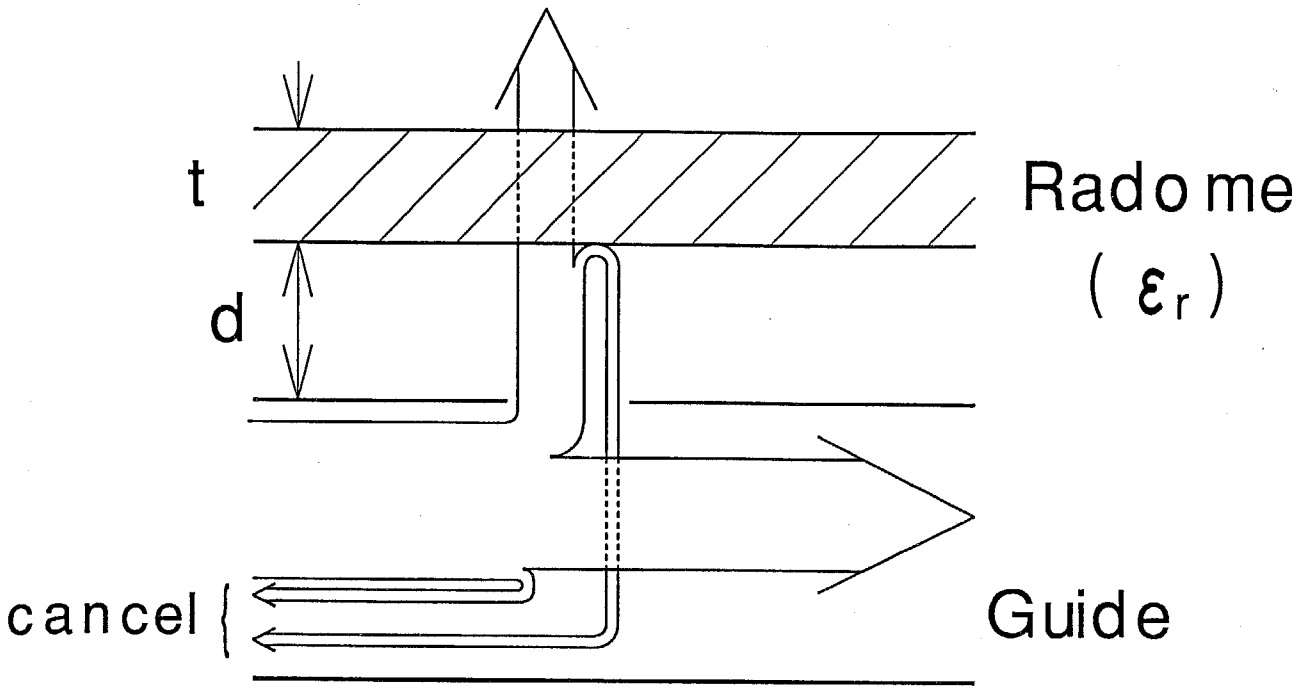

(a) Reflection model.

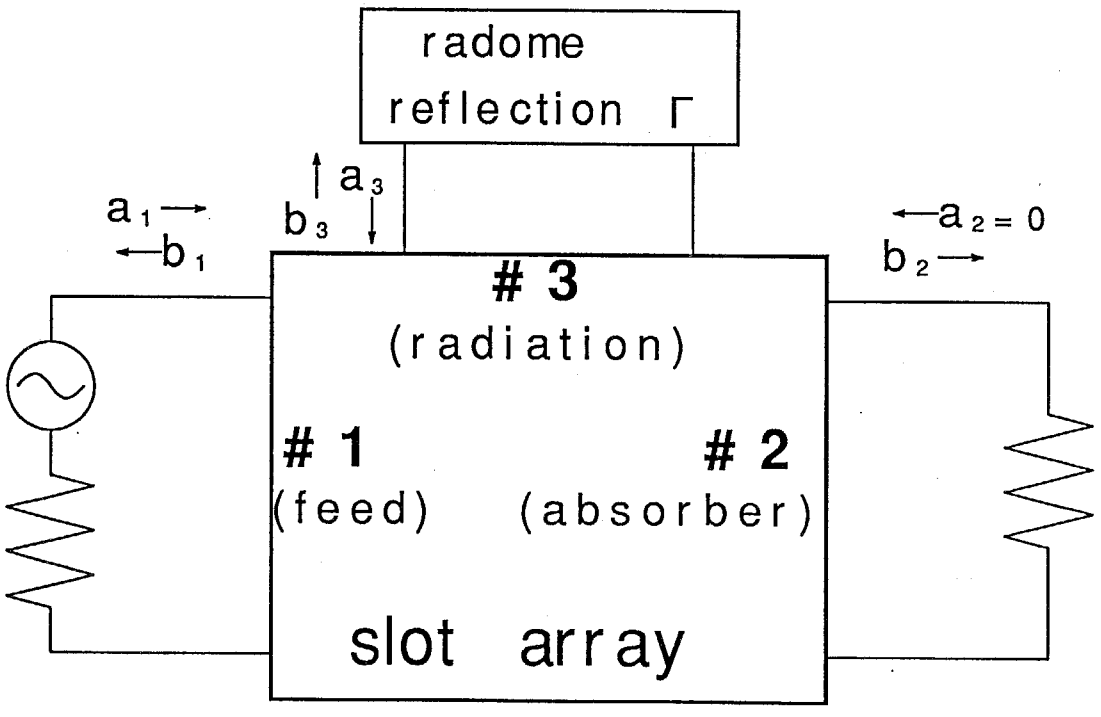

(b) S-matrix model.

Fig. 7-23. The reflection cancellation using the radome.

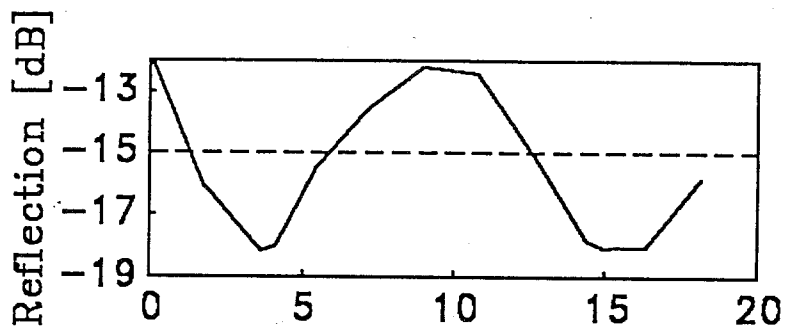

(a) Reflection from slot array.

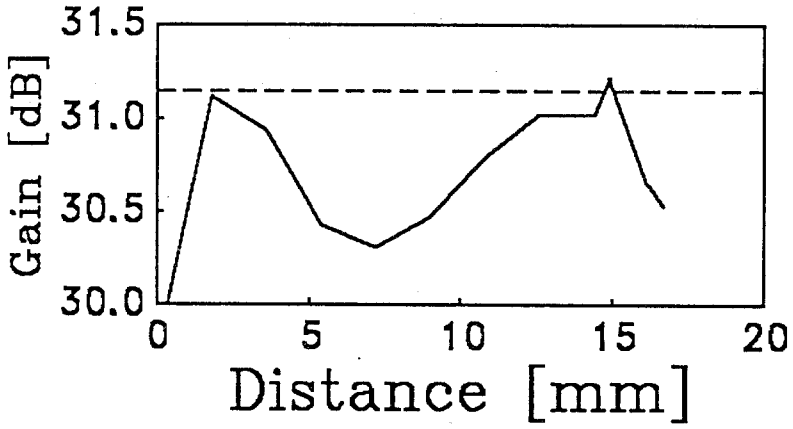

(b) Gain.

Fig. 7-24. The reflection and the gain of L6 with radome R1.

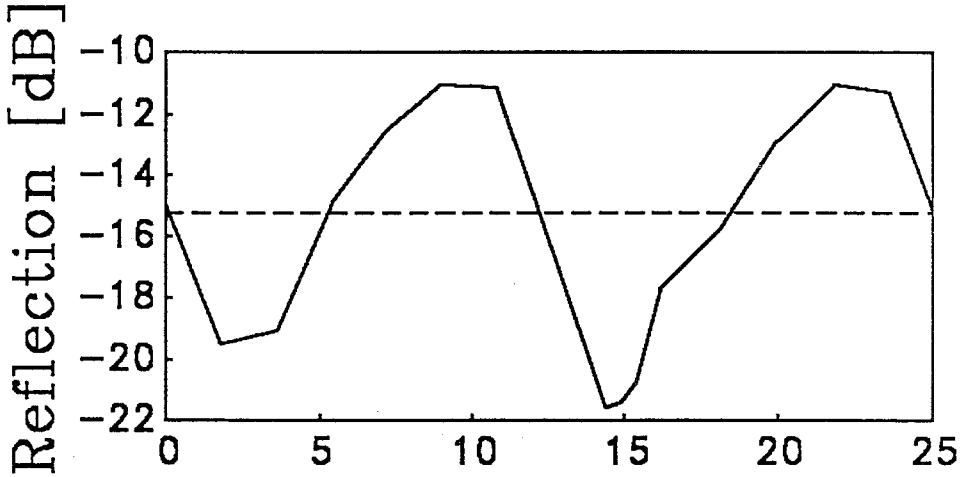

(a) Reflection from slot array.

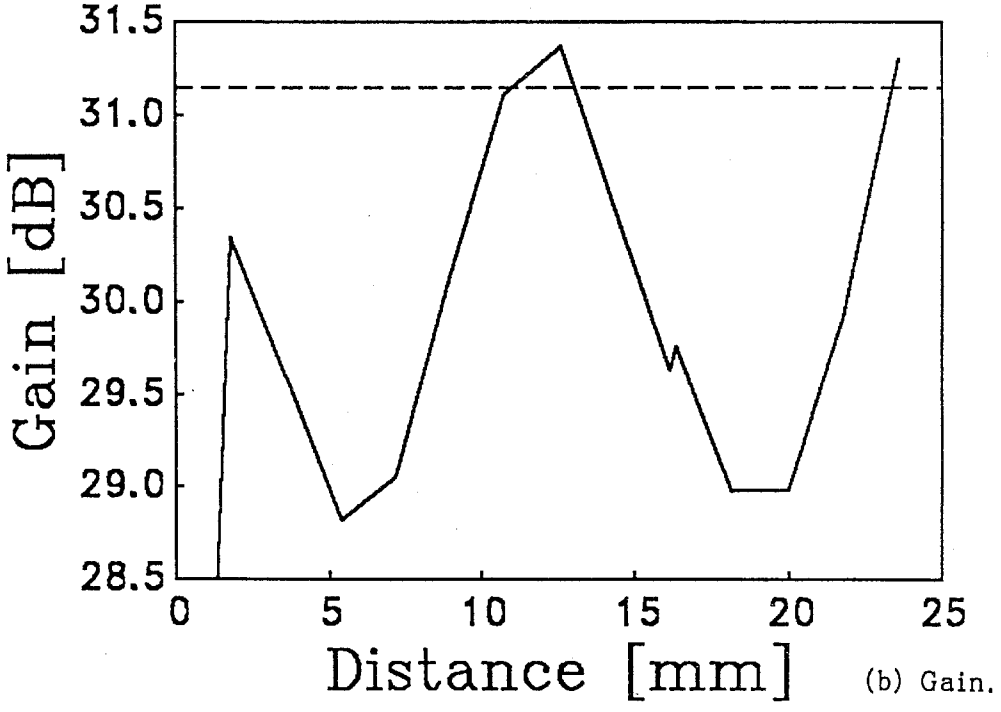

(b) Gain.

Fig. 7-25. The reflection and the gain of L6 with radome R2.

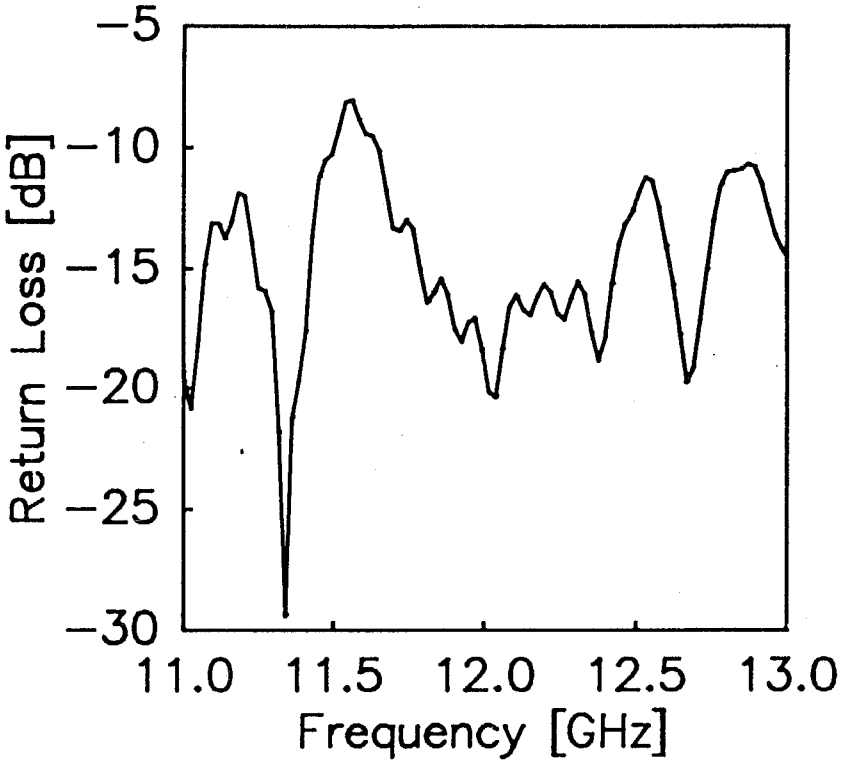

Fig. 7-26. The return loss of antenna L13.

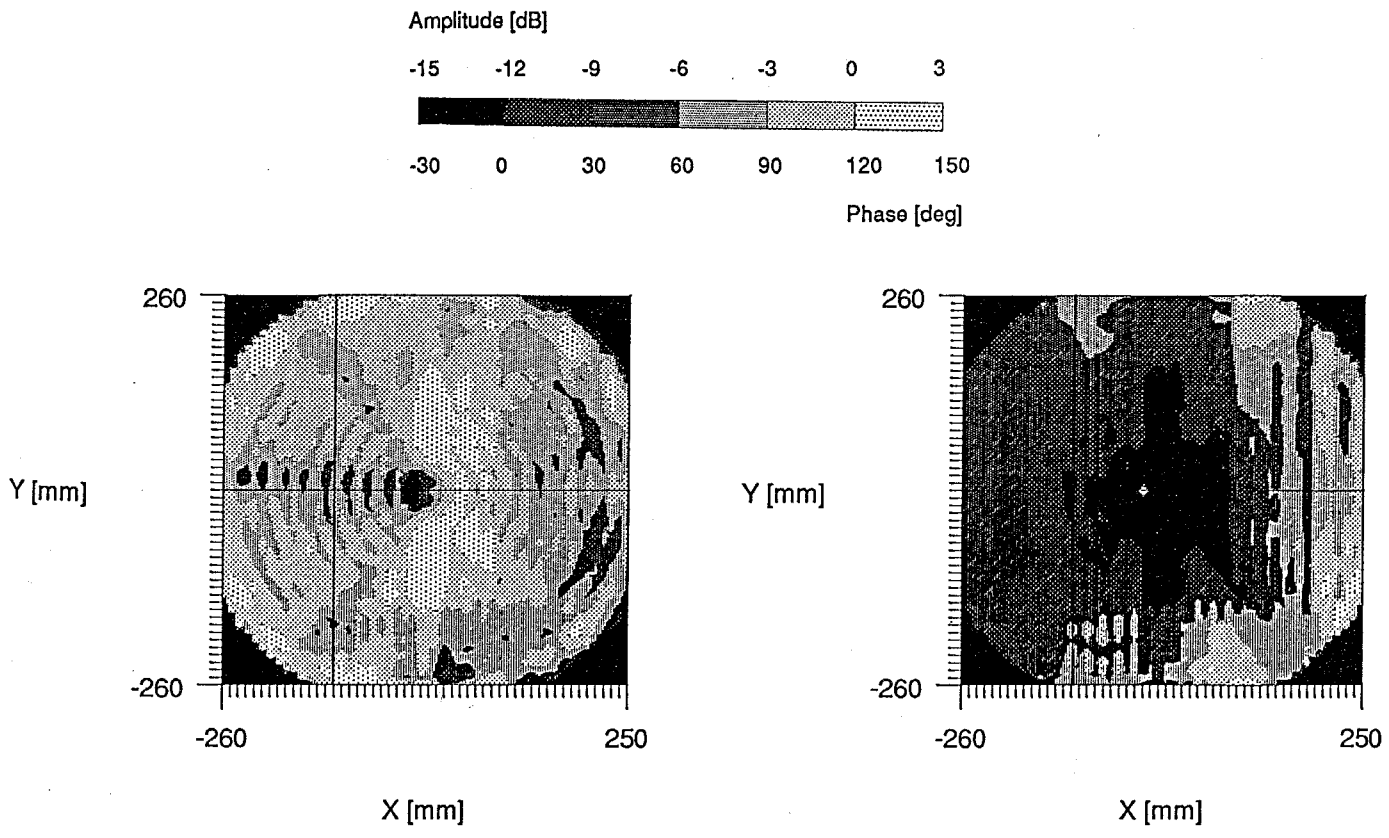

(a) Amplitude.

(b) Phase.

Fig. 7-27. The aperture field distribution of antenna L13 (f=11.7GHz).

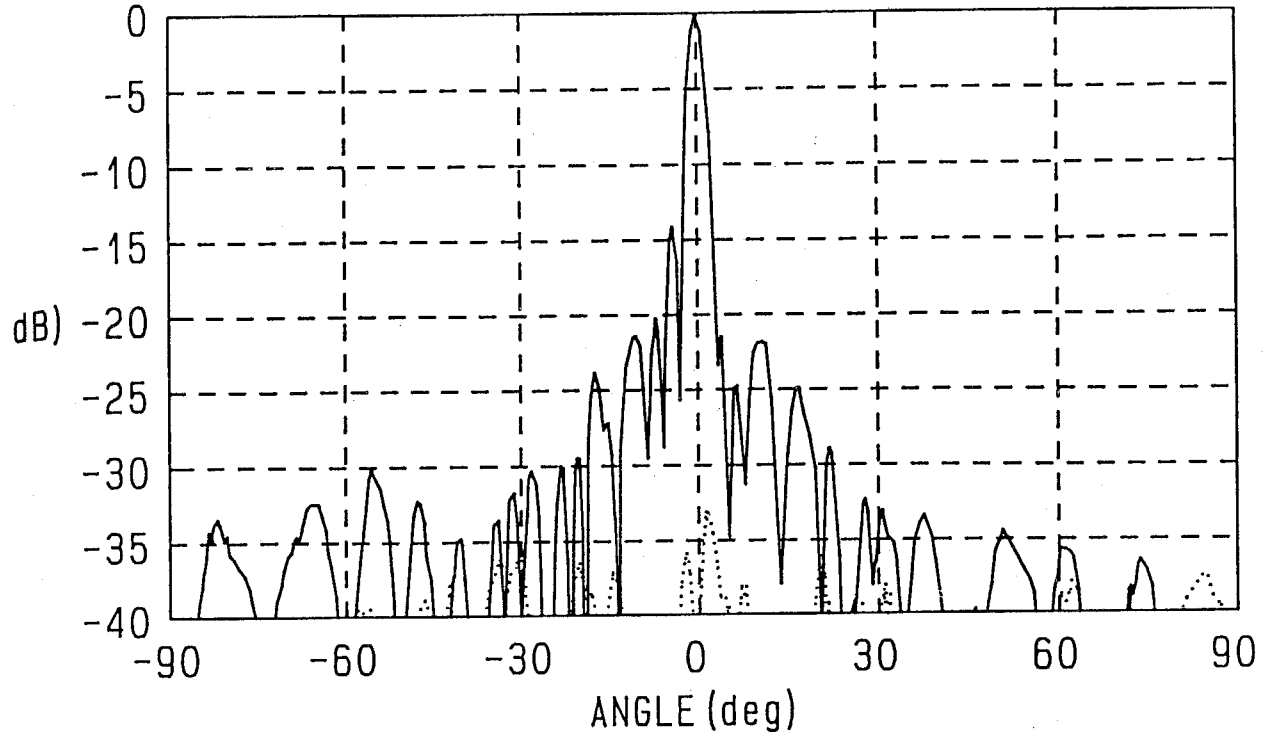

(a) ϕ=0° (E-plane).

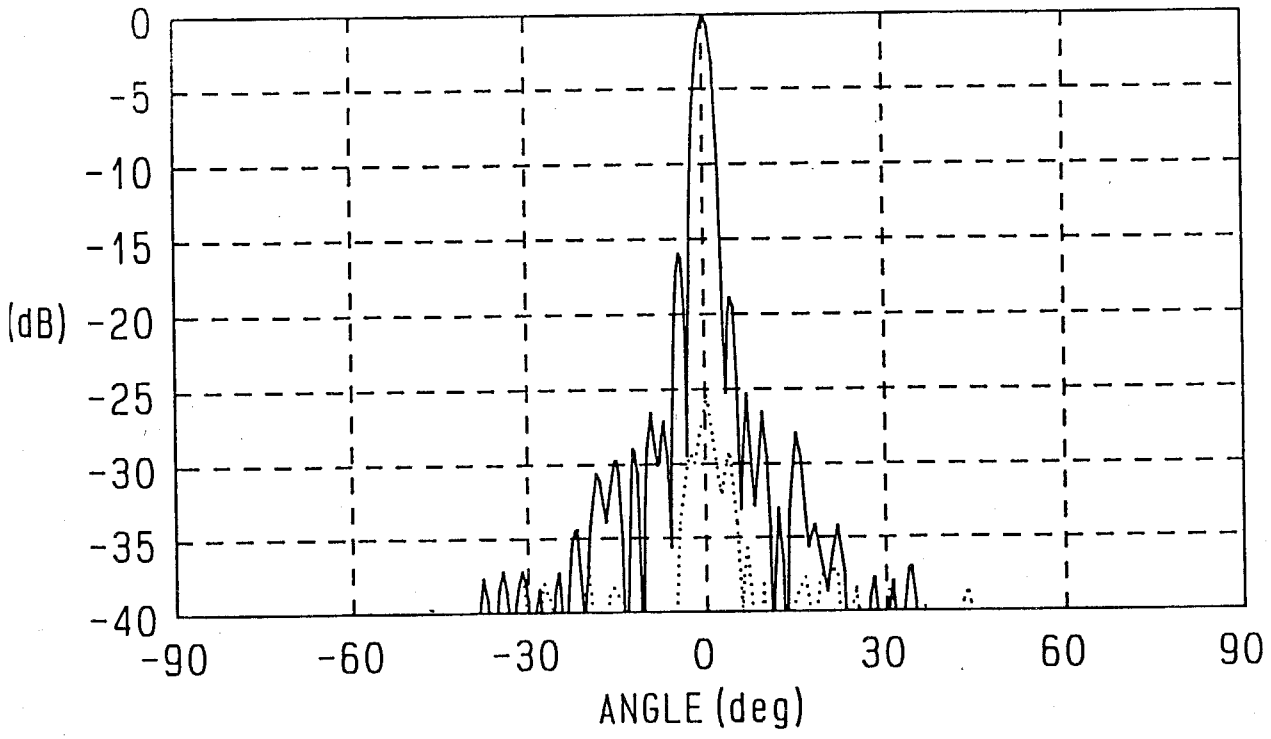

(b) ϕ=90° (H-plane).

Fig. 7-28. The Fresnel radiation patterns of antenna L13

(——:principal pol., - - :cross pol.).

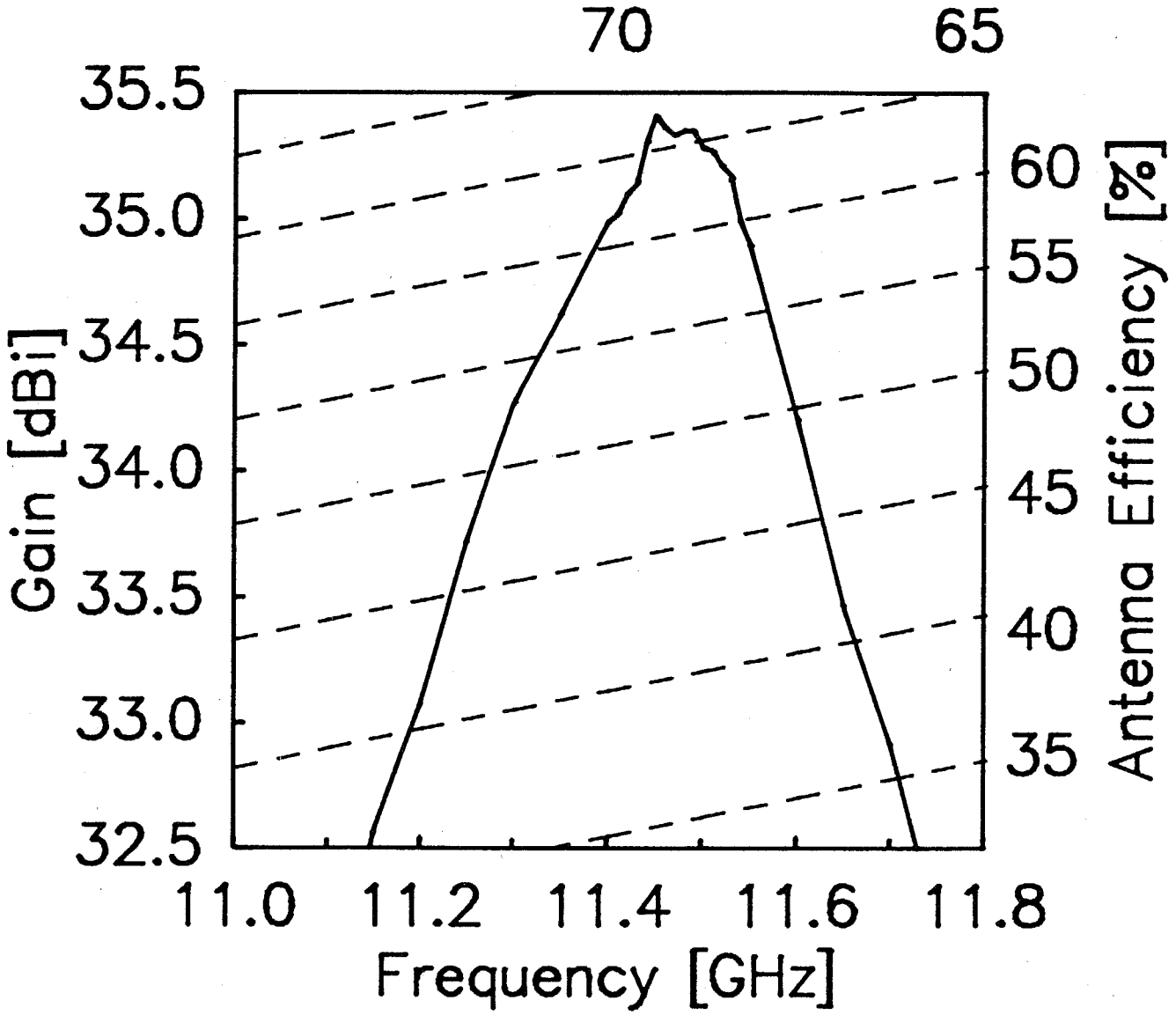

Fig. 7-29. The gain and the antenna efficiency of L13.

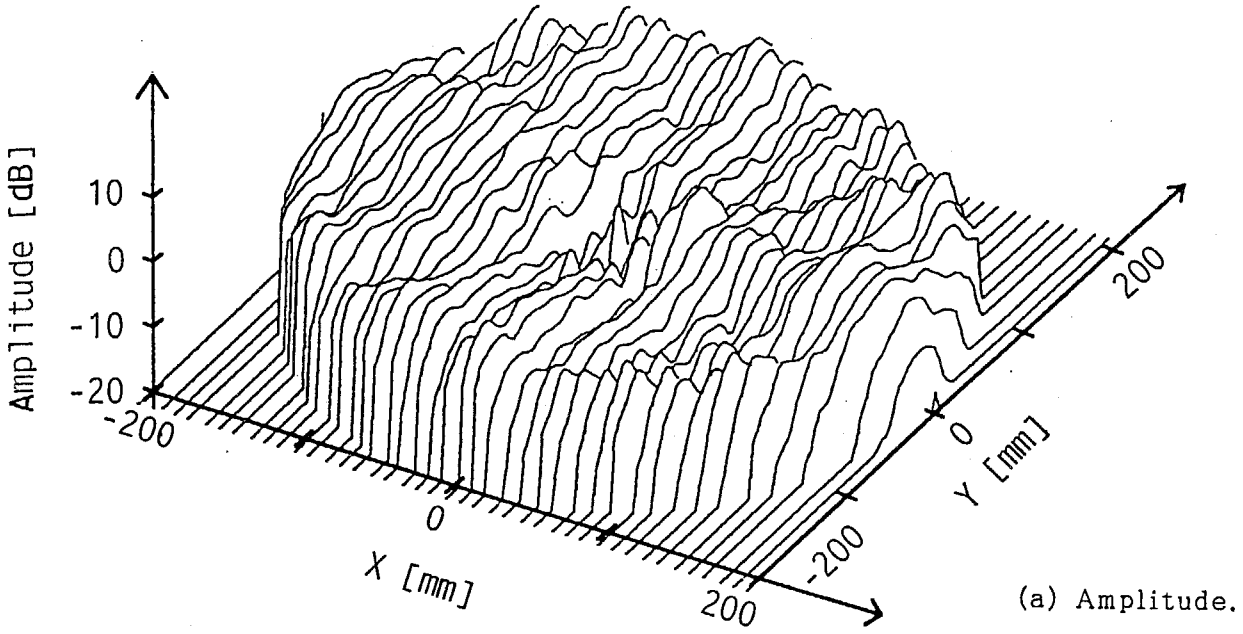

(a) Amplitude.

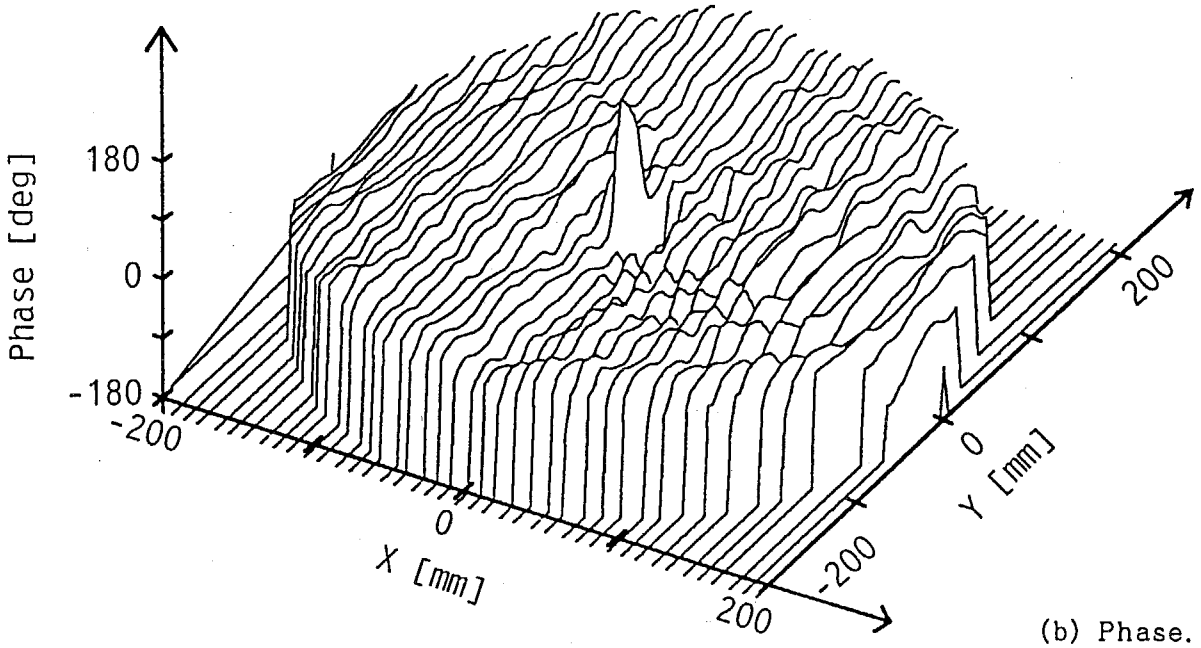

(b) Phase.

Fig. 7-30. The aperture field distribution of antenna L15 (f=11.7GHz).

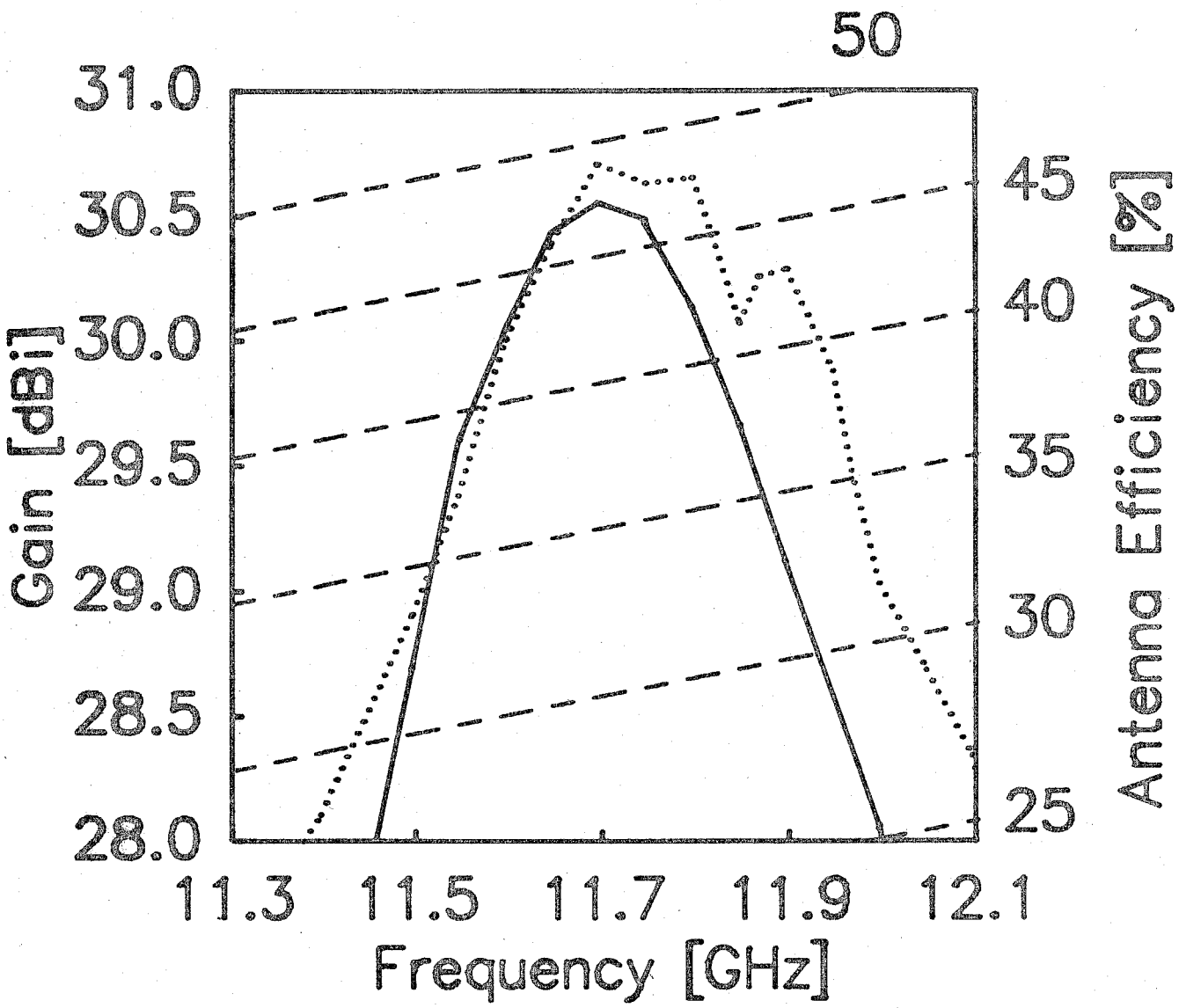

Fig. 7-31. The gain and the antenna efficiency of L15.

(——:L15, ····:L6)

CHAPTER 8. PARALLEL SLOT PAIR [SOLUTION #2]

8-1. Introductory Remarks

As mentioned in Sec. 7-6-1, the diffect of the slot set using additional reflection canceling slots is that the unwanted radiation from additional slots is not negligible, which results in the degradation of aperture illumination efficiency. An alternative slot set configuration is presented for LP-RLSA using a parallel slot pair in this chapter [1]. A parallel slot pair is a new radiation device consisted of two parallel slots. It radiates the pure desired polarization, while the reflection from it is negligibly small in the guide. The basic characteristics of parallel slot pair is discussed first. Using these pairs, an alternative configuration of a slot set is considered with small reflection. Numerical examples are given to select the optimum configuration. The experiments confirm the design.

8-2. Parallel Slot Pair

8-2-1. Concept

Figure 8-1 shows the configuration of a parallel slot pair. By analogy with the reflection mechanism of CP-RLSA slot pair, two slots are spacing $d \approx 1/4\lambda_g$ along the current flow to cancel the reflection. To determine the radiated polarization rigorously, the slots are parallel to each other. The parallel slot pair is, to say, a kind of matched element [2]. As an element, the radiation pattern of a pair is not broadside beam but rather similar to the endfire type. However, when the large number of the elements are arrayed, the element pattern is almost cancelled by array factor. The application of this configuration is not limited for LP-RLSA but for a variety of array antennas fed by the traveling wave.

However, the effects of reflection cancellation have not been observed by the experiments, since the design was not quantitative but only conceptual [3]. To cancel the reflection, the length L_1 and L_2 together with the spacing d should be numerically optimized taking the mutual coupling into account, since the mutual coupling is strong due to the parallel arrangement of slots.

8-2-2. Numerical Results

The design parameters are optimized to minimize the reflection by the moment method analysis (Sec. 2-2). The optimum L_2 and d are chosen for fixed L_1, which determines the coupling strength. The design parameters are listed in Table 8-1. Figure 8-2 shows the relation between L_1 and L_2 for various θ. When L_1 is approaching to the resonance, shorter L_2 can sufficiently suppress the reflection. This tendency is independent of θ. Figure 8-3 shows the relation between L_1 and d. The relation largely depends on θ. When L1 is small and the coupling is weak, d is about $1/4\lambda_g$ as the concept. The deviation of d cannot be neglected when the coupling becomes strong.

8-3. Configuration of a Slot Set for LP-RLSA using Parallel Slot Pairs.

8-3-1. Configuration of a Slot Set

As is stated in Chap. 7, the configuration of a slot set for LP-RLSA varies with the current flow direction ϕ. The simplest configuration is obtained by replacing each slot in a original slot pair (Fig. 8-4(a)) with a parallel slot pair (Fig. 8-4(b); 4-slot configuration). However, it is sometimes difficult to arrange, since the slots occupy so large space to avoid the overlap. As an alternative, only one of the slots in a LP-pair may be replaced by the parallel slot pair (Fig. 8-4(c); 3-slot configuration). In this case, the stronger-coupled slot is replaced, since the reflection is

stronger. It is another alternative that weakly coupled slot is removed and only one parallel pair radiates the desired polarization (Fig. 8-4(d); 2-slot configuration).

As for the former two, the coupling angle θ_1 and θ_2 are determined by Eqs. (7-3) and (7-4), while the lattermost one is determined as

$$\theta_3=\frac{\pi}{2}-\phi \qquad (8-1),$$

to radiate the X-polarization (co-ordinates are shown in Fig. 7-1).

In the practical design, the parameters for each parallel pair are those optimized in Sec. 8-2. The other independent parameters, e.g. L_1, L_3 and d_2 in 4-slot configuration, are selected so as to suppress the cross polarization.

To design the slot arrangement for the antenna, the combined use of these three configurations is necessary. Considering their advantages, the regions for sufficient configurations on the aperture are given as in Fig. 8-5. The boundary angles ϕ_1 and ϕ_2 ($0^\circ<\phi_1<\phi_2<90^\circ$) are determined as follows: ϕ_1 is mainly due to the limitation of 2-slot configuration, since the coupling strength decreases with the increase of ϕ. On the other hand, ϕ_2 is mainly determined from the reflection characteristics, as is mentioned in the next section.

8-3-2. Numerical Results

The same design parameters as Sec. 8-2-2 are used for the analysis. The design parameters are given as functions of coupling factor α.

Figure 8-6 shows an example of 4-slot configuration for $\phi=90^\circ$. In 4-slot configuration, the independent parameters are L_1, L_3 and d_2. In this example, the deviation of slot lengths are about 0.8mm for $\alpha>10$, which was neglected in the first design. As both parallel

pairs have the same coupling angle 45° ($sin\theta_1=sin\theta_2$), d_1 and d_3 seem to be constant. The 4-slot configuration is advantageous when the coupling angles of both parallel pairs are comparable, where the reflection from a single slot is considerably large.

Figure 8-7 shows an example of 3-slot configuration for ϕ=45°. In 3-slot configuration, the independent parameters are L_1, L_2 and d_2. In spite of the absence of the parallel slot, the weakly-coupled L_1 is almost equal to, or rather smaller than L_2 or L_3. The spacings d_1 and d_2 are much different from $1/4\lambda_g$.

Figure 8-8 shows an example of 2-slot configuration for ϕ=0°. The relation among L_1, L_2 and d are the same as given in Fig. 8-2 and 8-3. 2-slot configuration is advantageous for $\phi\approx0°$, where the radiation from weakly-coupled slots in 3- or 4-slot configuration are negligibly small.

The reflection coefficient of a slot set is given in Fig. 8-9. Under the condition of cross polarization suppression, the reflection is a little sacrificed, especially for $\phi\approx90°$.

In the same manner as explained in 7-4, the 1-dimensional array for specified ϕ is recalled to check the design sequence. Figure 8-10 shows the reflection coefficient of 1-dimensional array as a function of ϕ. The reflection is sufficiently suppressed to about -10dB except for $\phi\approx90°$, which is expected from Fig. 8-10.

8-4. Experiments

The model antenna, denoted by L17, is fabricated by using the numerical results. The design parameters are listed in Table 8-2. Figure 8-11 shows the slot arrangement, which is divided into eight regions.

The return loss is shown in Fig. 8-12. The maximum value of -12dB is rather smaller than the predicted one by the analysis.

The aperture field distribution is given in Fig. 8-13. The uniformity of amplitude is observed in ρ direction. However, the pattern seems to be split at the discontinuity of slot set configurations in ϕ direction. The phase distribution along Y-axis is different from other part, by which the return loss at the feed point seems to be improved. A considerably large cross polarization is radiated from 4-slot configuration regions.

The Fresnel radiation patterns are shown in Fig. 8-14. In H-plane, large lobes of cross polarization appear near the main lobe, which is theoretically predicted as shown in Fig. 8-15. In Fresnel region, the cross polarization is not cancelled. However, the cross polarization excited along Y-axis may affect the cross polarization pattern. On the other hand, the unwanted lobes are measured at around the endfire direction in E-plane, which is also predicted theoretically but higher than the theory. It is partly due to the element pattern of a parallel slot pair, while the ripple of the co-pol. aperture field may be the dominant reason.

The gain and the efficiency of the antenna are shown in Fig. 8-16. Owing to the degradation of aperture distribution, the peak gain is 33.0dBi where the antenna efficiency is 43%.

These results demonstrate the normal operation of the model antenna and the basic concept of the design is confirmed. The uniformity of the aperture illumination together with the suppression of cross polarization is required to improve the efficiency.

8-5. Concluding Remarks

This chapter presented a novel concept of parallel slot pair with small reflection. It is not only applicable to RLSA but other slot arrays fed by traveling wave [4][5]. For the application of LP-RLSA,

three types of slot sets using parallel slot pairs are proposed. They are numerically optimized to reduce the cross polarization with small reflection. The experiments with a model antenna demonstrate the design.

However, the appearance of the cross polarization is a problem to degrade the antenna performance. The discontinuity of slot arrangement between two regions may disturb the rotational symmetry of inner field, which is not taken into account in the slot coupling design. In the parallel plate waveguide, the phase discontinuity of inner field causes the shift of power flow direction [5]. One of the solution is to replace 4-slot config. by 3-slot one to reduce the unexpected effects of mutual coupling.

It is an advantage of this design over the additional slot set configuration presented in Chap. 7 that the aperture illumination loss is theoretically smaller (11% vs 15%) since the unwanted radiation to the endfire direction is suppressed. To this end, the suppression of the cross polarization is highly required.

References

[1] M. Ando, J. Takada and N. Goto, "A High Efficiency Radial Line Slot Antenna," IETJ Technical Report, RE88-30 (Sep. 1988).

[2] S. Silver (ed.), "Microwave Antenna Theory and Design," Sec. 9.23, McGraw-Hill, New York (1949).

[3] J. Takada, "A study of the slot arrangement for radial line slot antennas," Master's Thesis, Tokyo Institute of Technology (Feb. 1989).

[4] K. Sakakibara, J. Hirokawa, M. Ando and N. Goto, "A linearly-polarized slotted waveguide array with reflection canceling slot pairs," IEICE Technical Report (to be presented in Feb. 1992).

[5] J. Hirokawa, T. Miyagawa, M. Ando and N. Goto, "A Waveguide-fed

parallel plate slot array antenna for dual polarization use," Proc. 1992 IEICE Spring Conf. (to be presented in Mar. 1992).

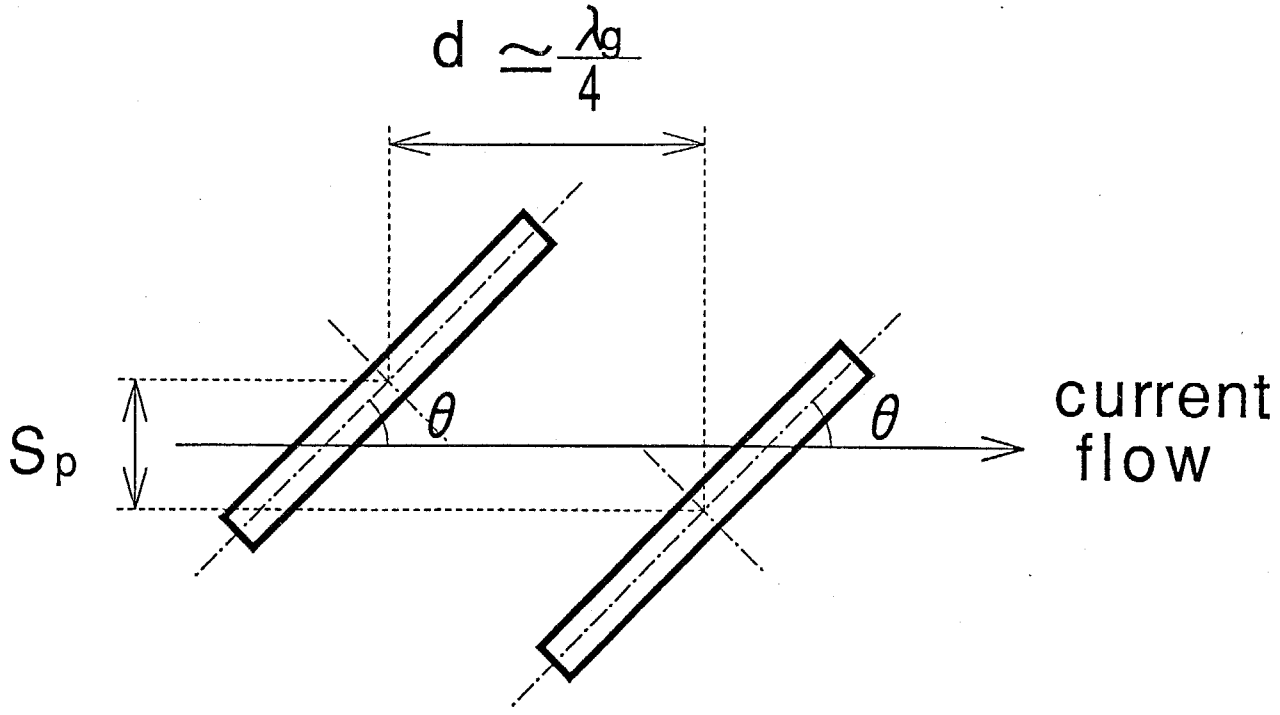

Fig. 8-1. Parallel slot pair.

Table 8-1. Design parameters in the analysis.

Frequency f[GHz]	12.0
Permittivity ε_r	1.48
Waveguide height du[mm]	7.5
Waveguide width S_w[mm]	16.25
Angular spacing in parallel pair S_p[mm]	0.0
Angular spacing between parallel pairs S_a[mm]*	8.13
Maximum coupling factor α_{max} [1/m]+	20.0
Antenna radius ρ [mm]+	200

*:for section 8-3,

+:for Fig. 8-10.

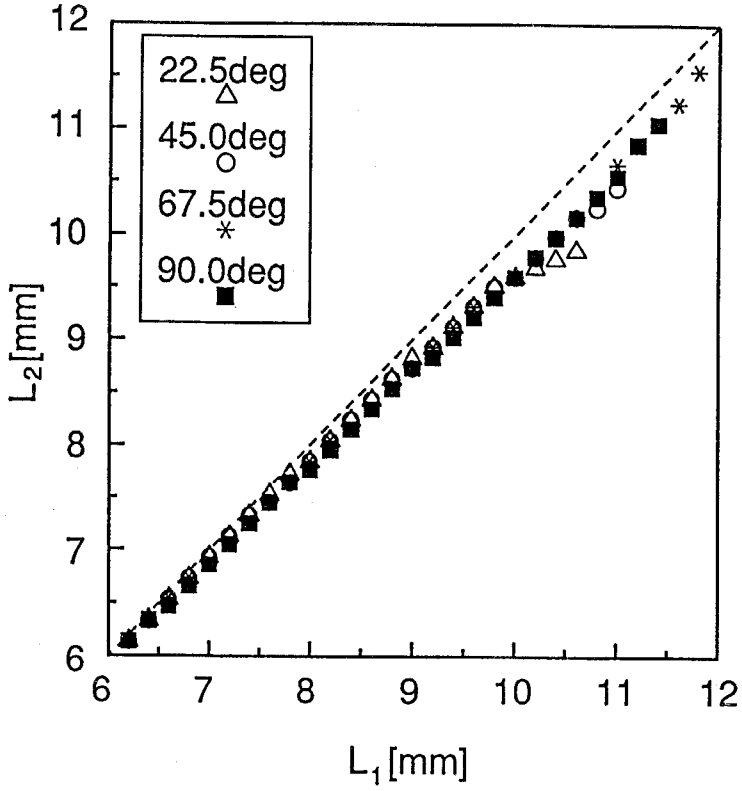

Fig. 8-2. L_1 vs L_2 for various θ.

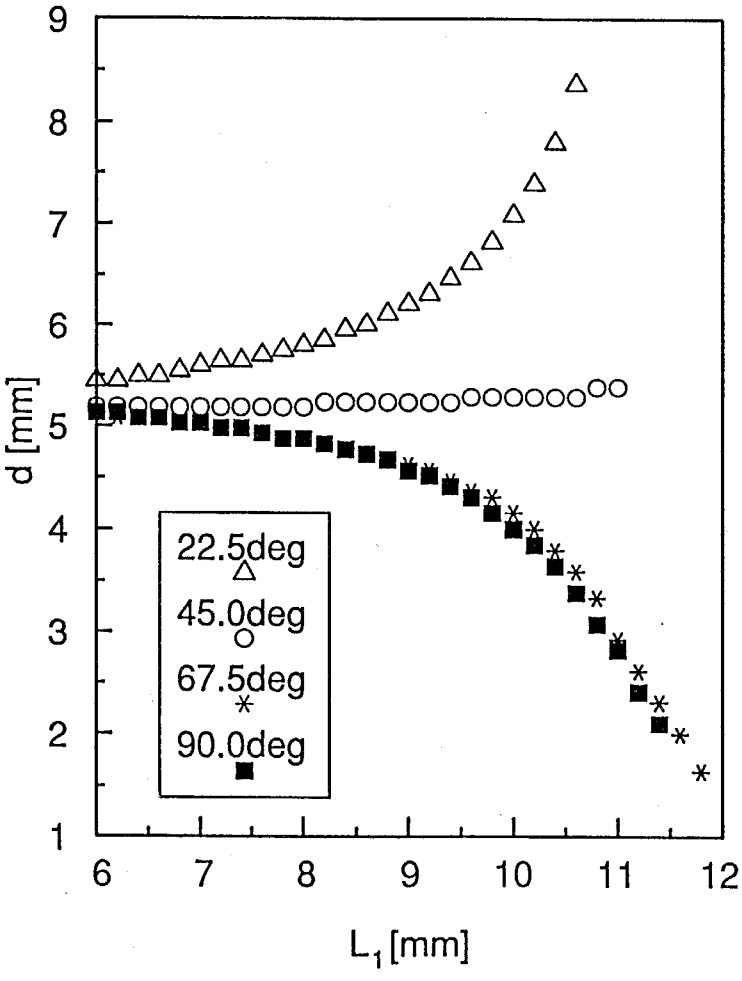

Fig. 8-3. L_1 vs d for various θ.

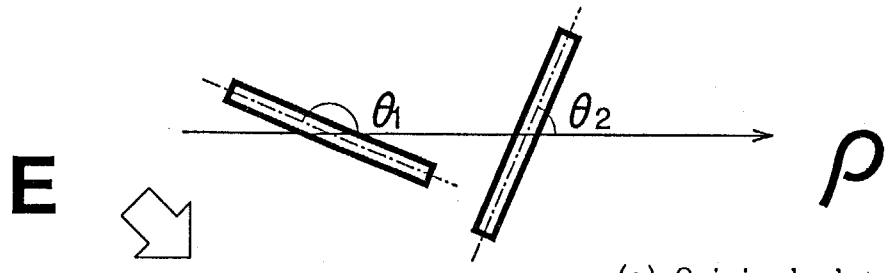

(a) Original slot pair.

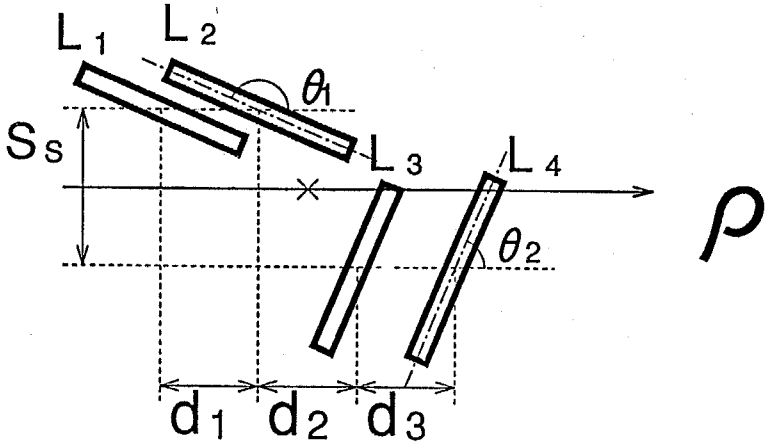

(b) 4-slot configuration.

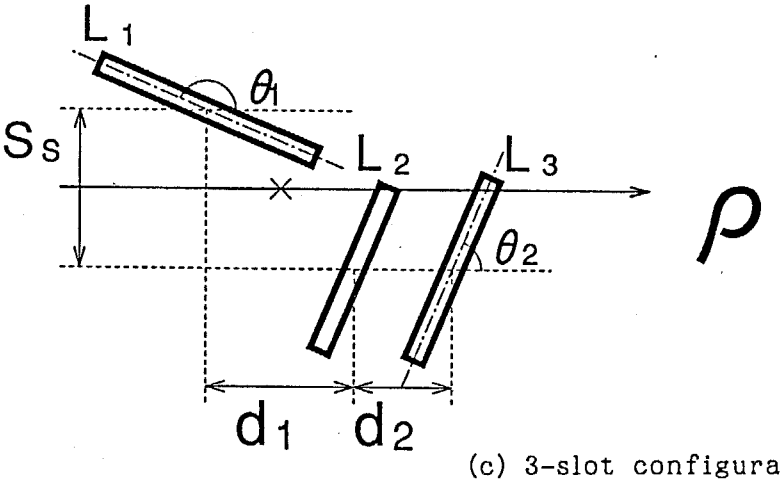

(c) 3-slot configuration.

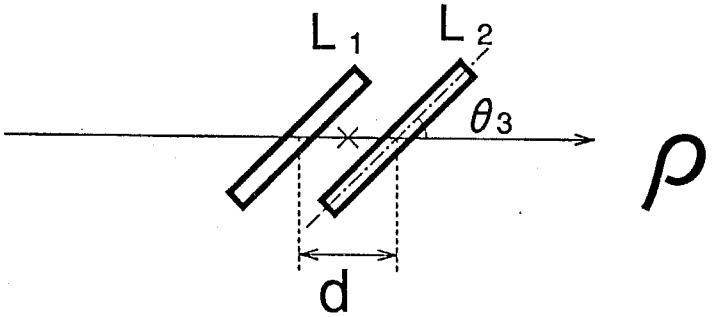

(d) 2-slot configuration.

Fig. 8-4. Configuration of a LP slot set using parallel slot pairs.

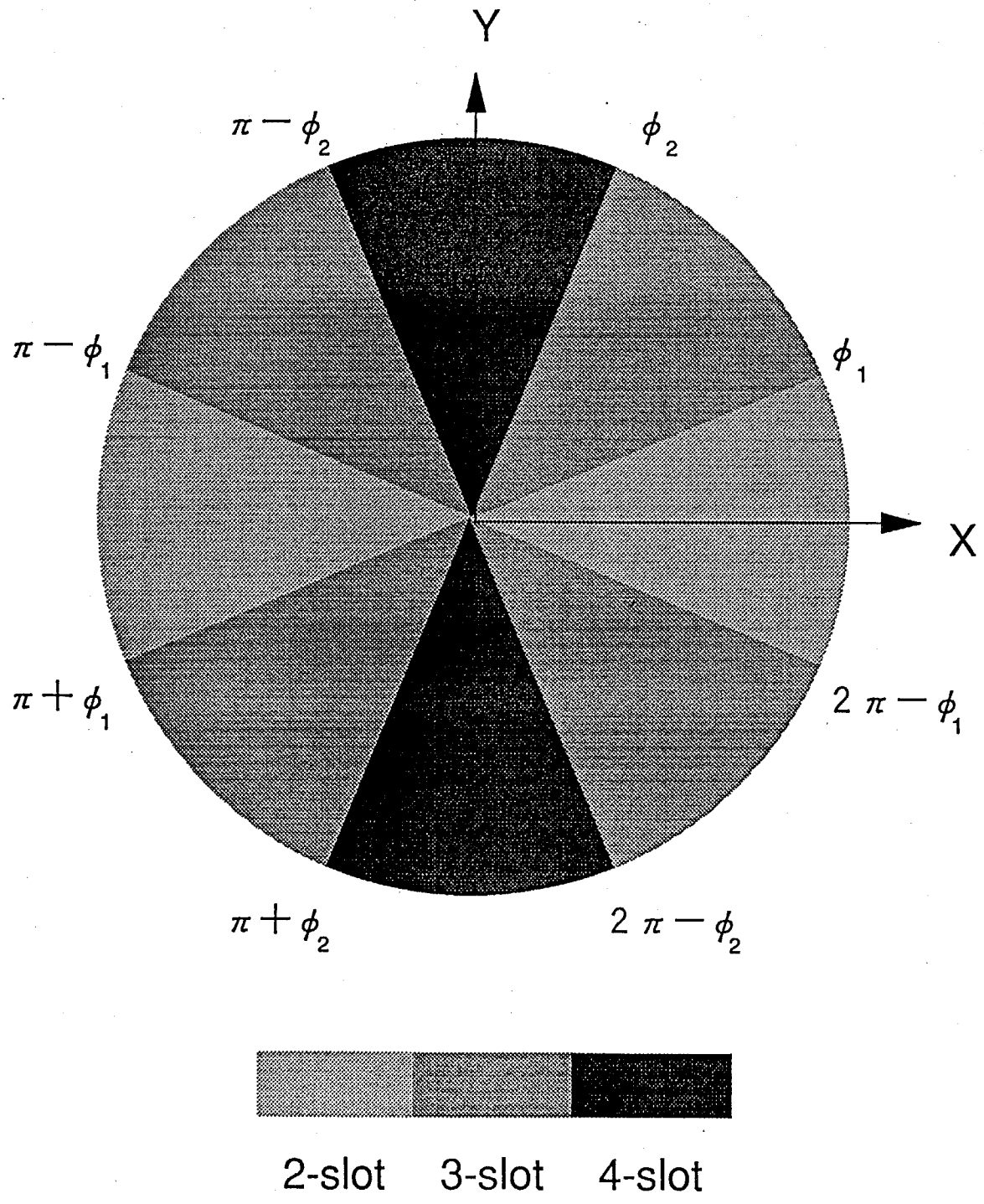

Fig. 8-5. The regeons for sufficient slot set configurations on the antenna aperture.

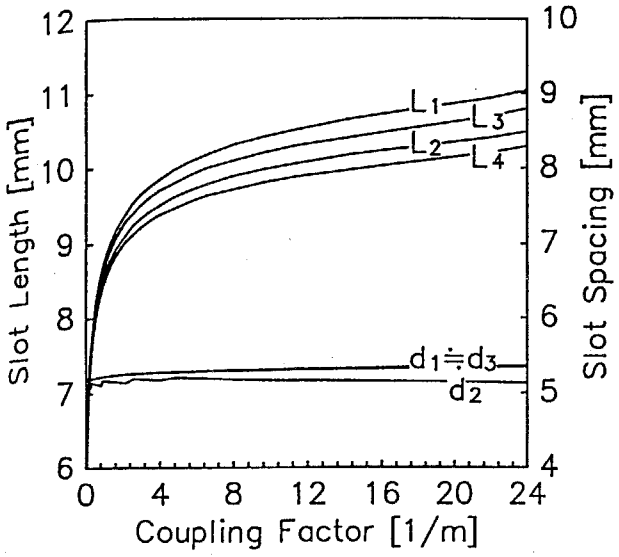

Fig. 8-6. Slot lengths and slot spacings for 4-slot configuration (ϕ=90°).

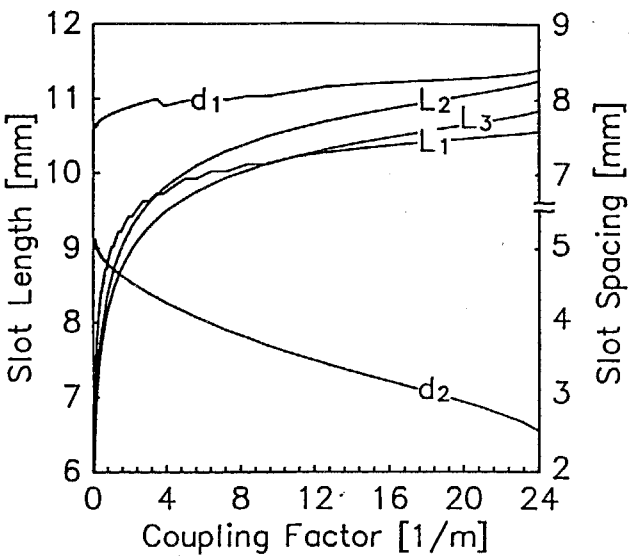

Fig. 8-7. Slot lengths and slot spacings for 3-slot configuration (ϕ=45°).

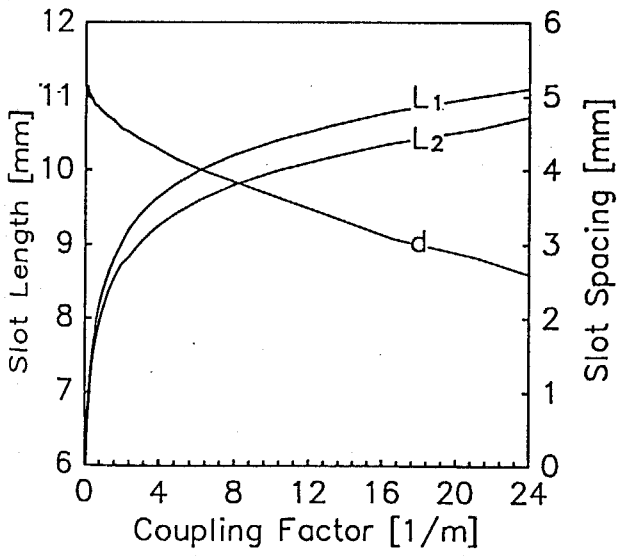

Fig. 8-8. Slot lengths and slot spacing for 2-slot configuration (ϕ=0°).

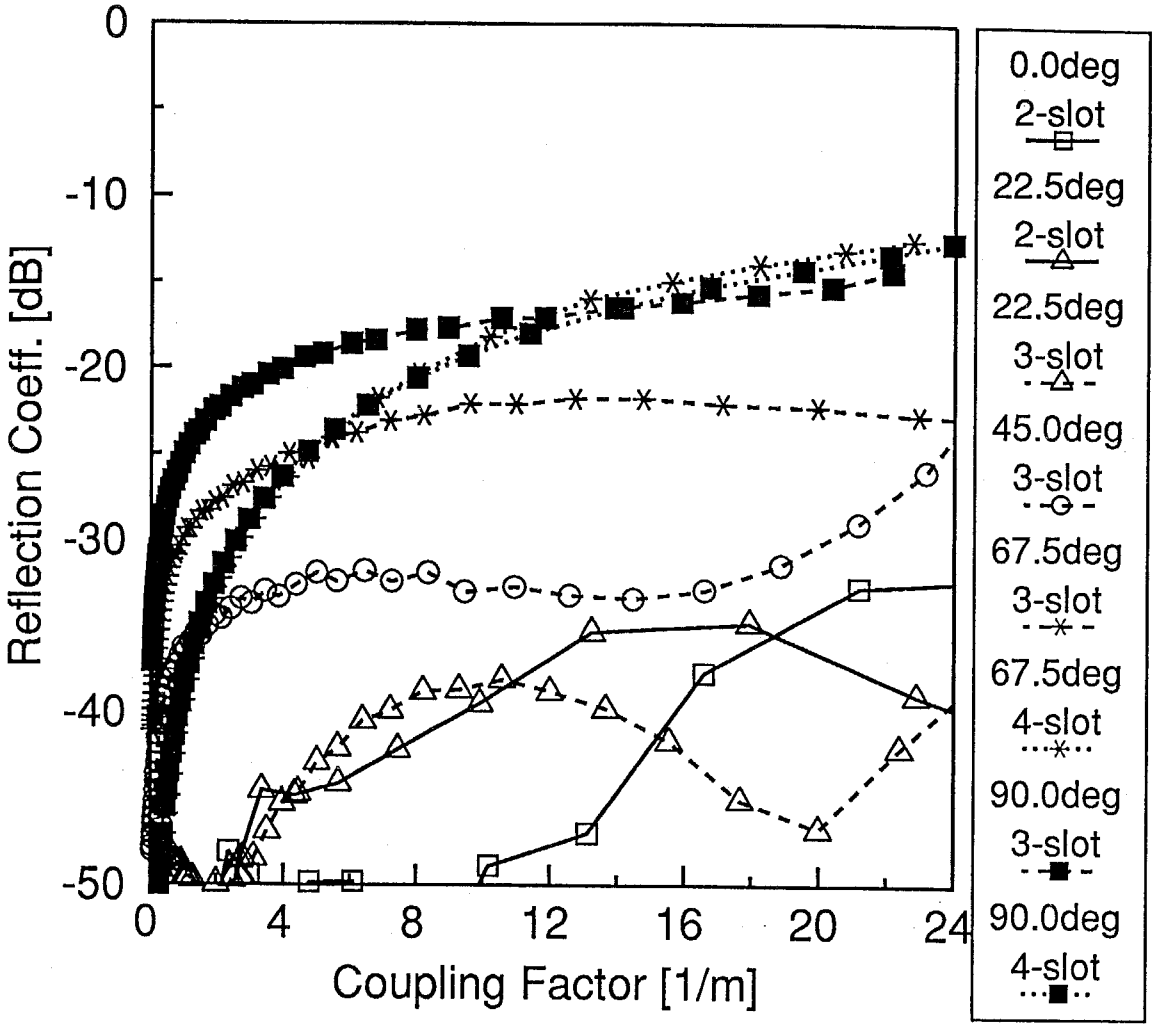

Fig. 8-9. Reflection coefficient of a slot set.

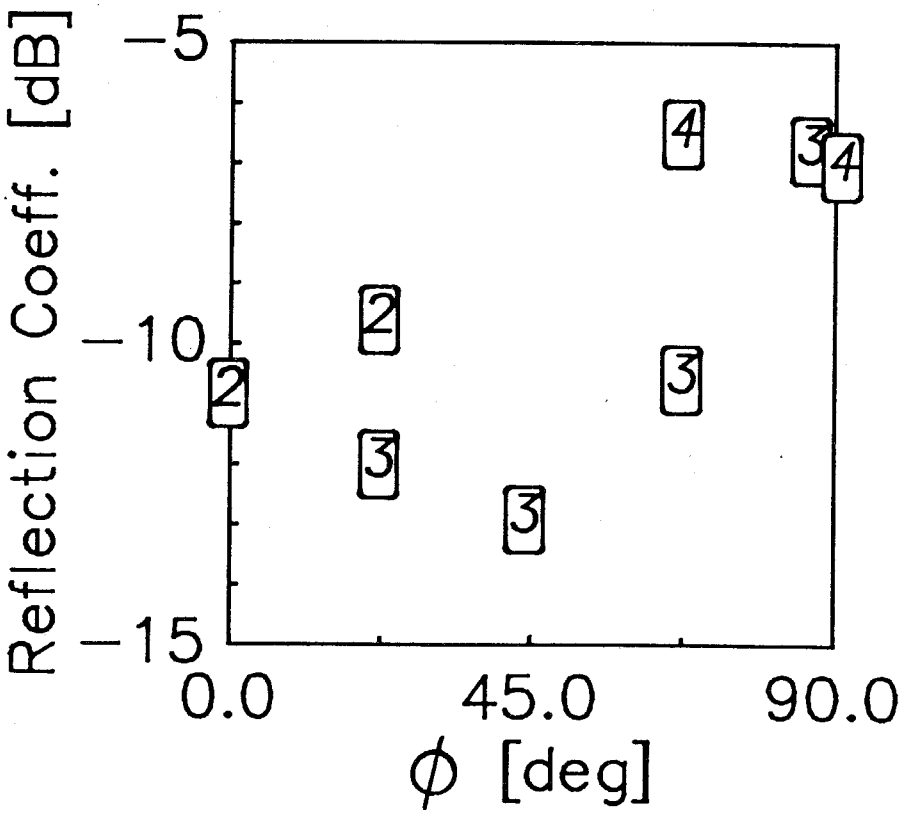

Fig. 8-10. Reflection coefficient of 1-dimensional array.

Table 8-2. Design parameters for a model antenna.

Name of model		L17
Frequency f[GHz]		12.0
Antenna diameter $2\rho_{max}$[mm]		600
Blocking diameter $2\rho_{min}$[mm]		60
Waveguide height du[mm]		7.5
Permittivity ε_r		1.48
Slot set angular spacing S_Φ[mm]		16.25
Boundary between 2-slot and 3-slot config. φ_1[deg]		22.5
Boundary between 3-slot and 4-slot config. φ_2[deg]		67.5
Maximum coupling factor α_{max} [1/m]		20.0
Slot length L[mm]	ϕ= 0deg	7.8~10.7
	ϕ=90deg	8.3~10.9
Number of slot N		2452

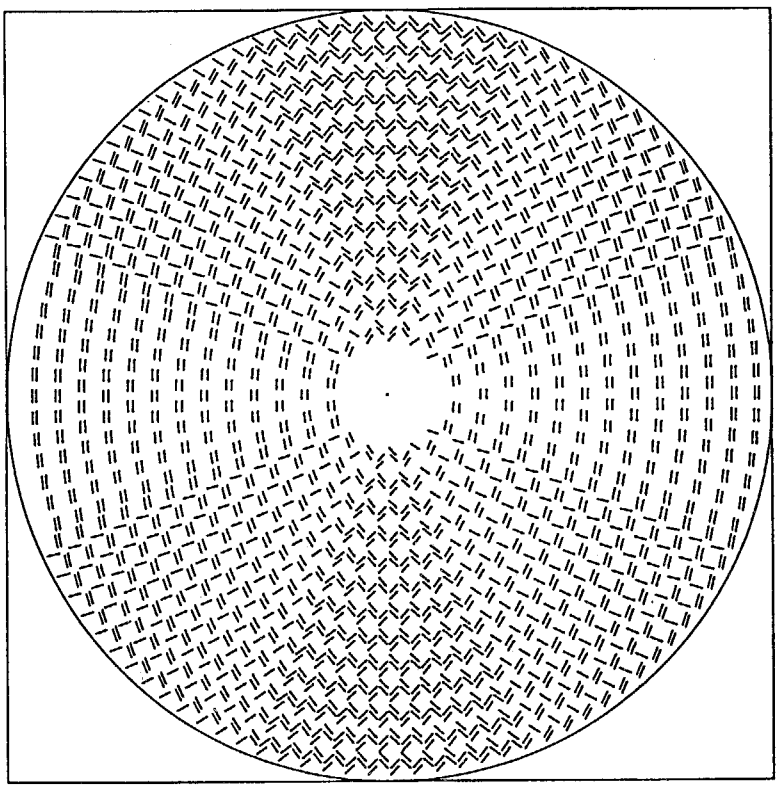

Fig. 8-11. Slot arrangement of model antenna L17.

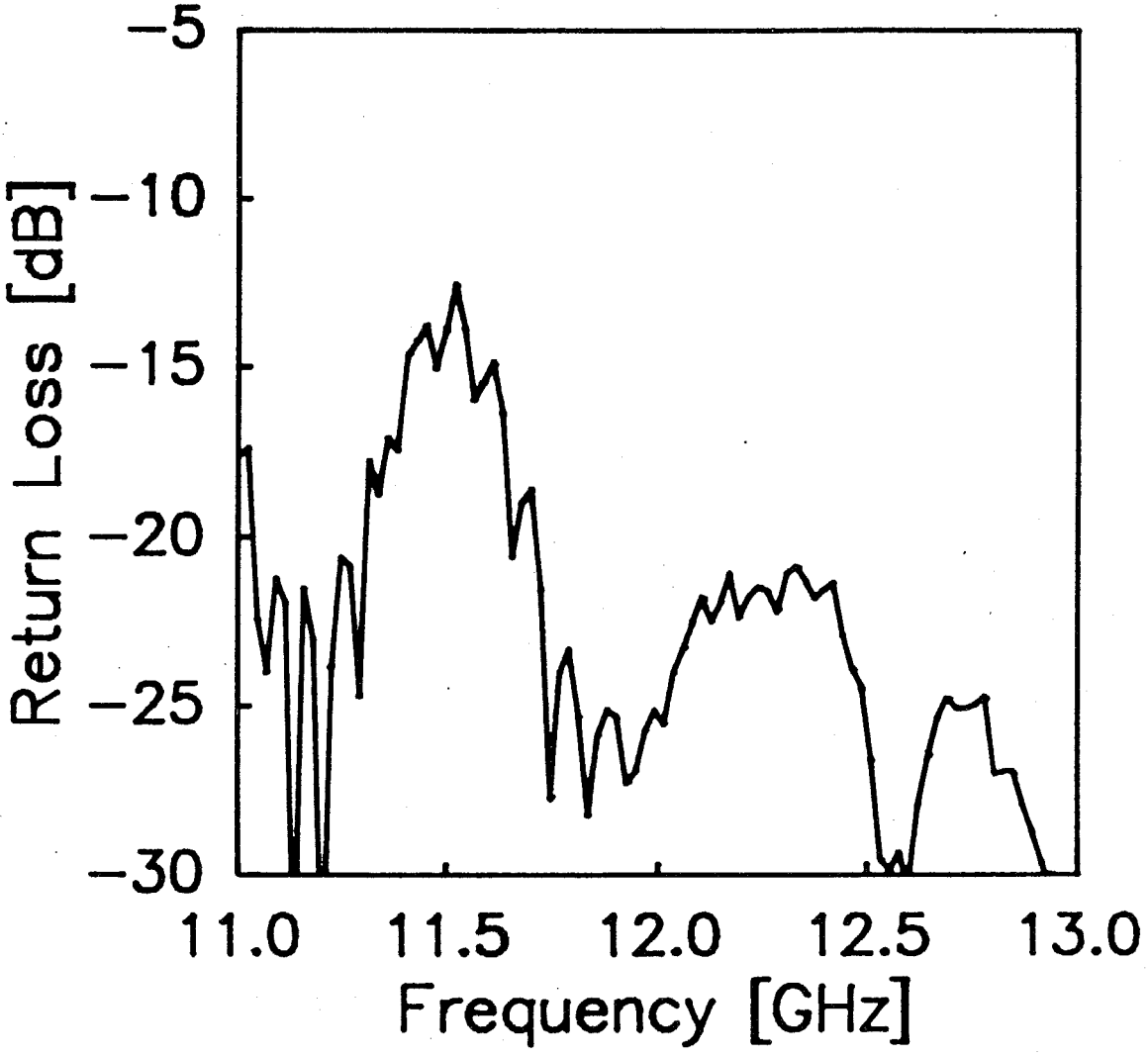

Fig. 8-12. Return loss characteristics for model antenna.

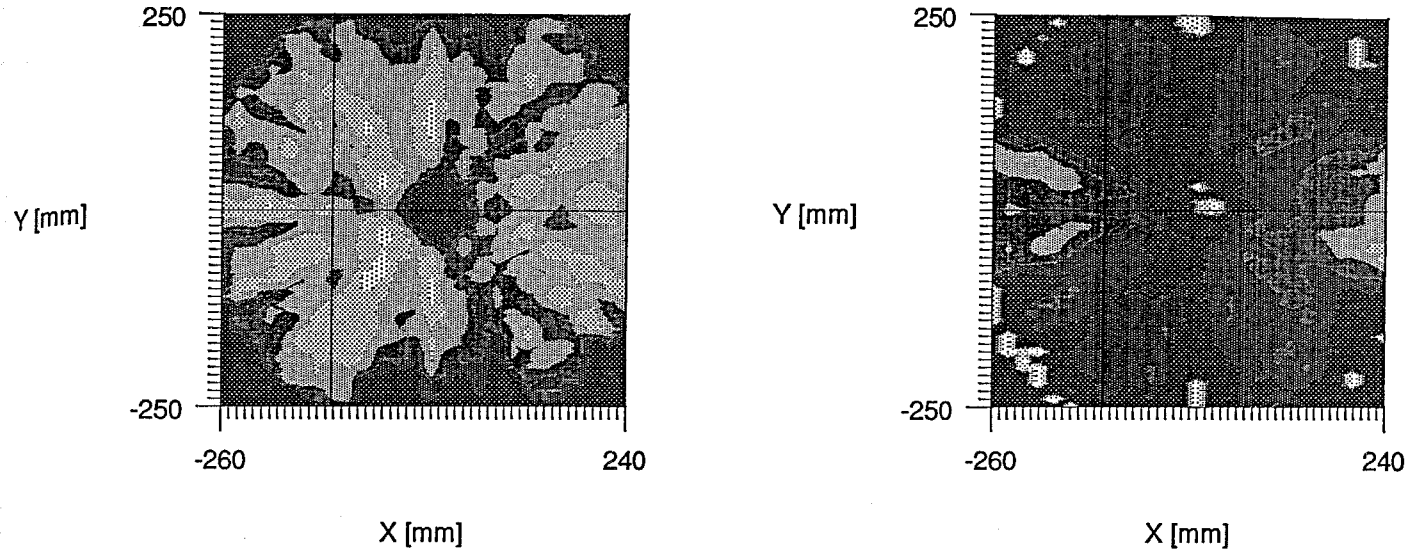

(a) Co-pol. amplitude.

(b) Co-pol. phase.

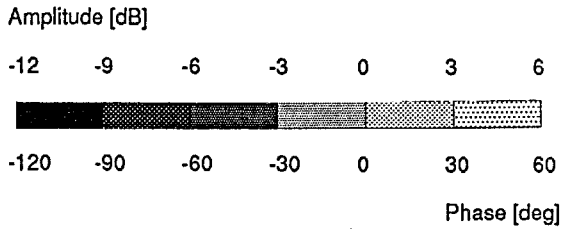

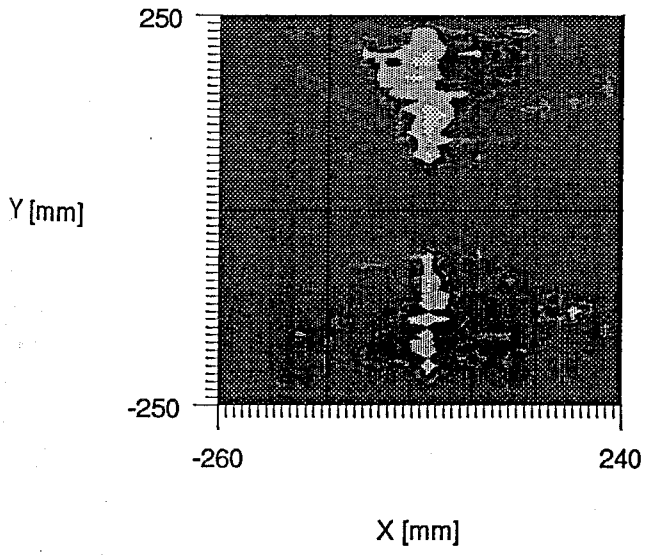

(c) Cross pol. amplitude.

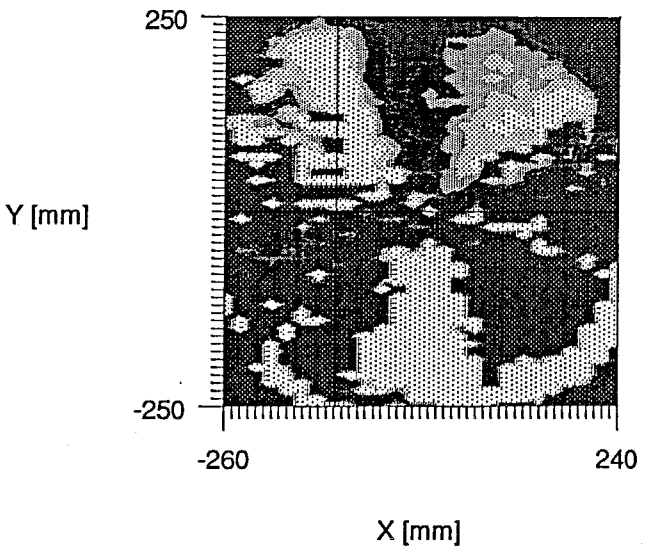

(d) Cross pol. phase.

Fig. 8-13. Aperture distribution for model antenna.

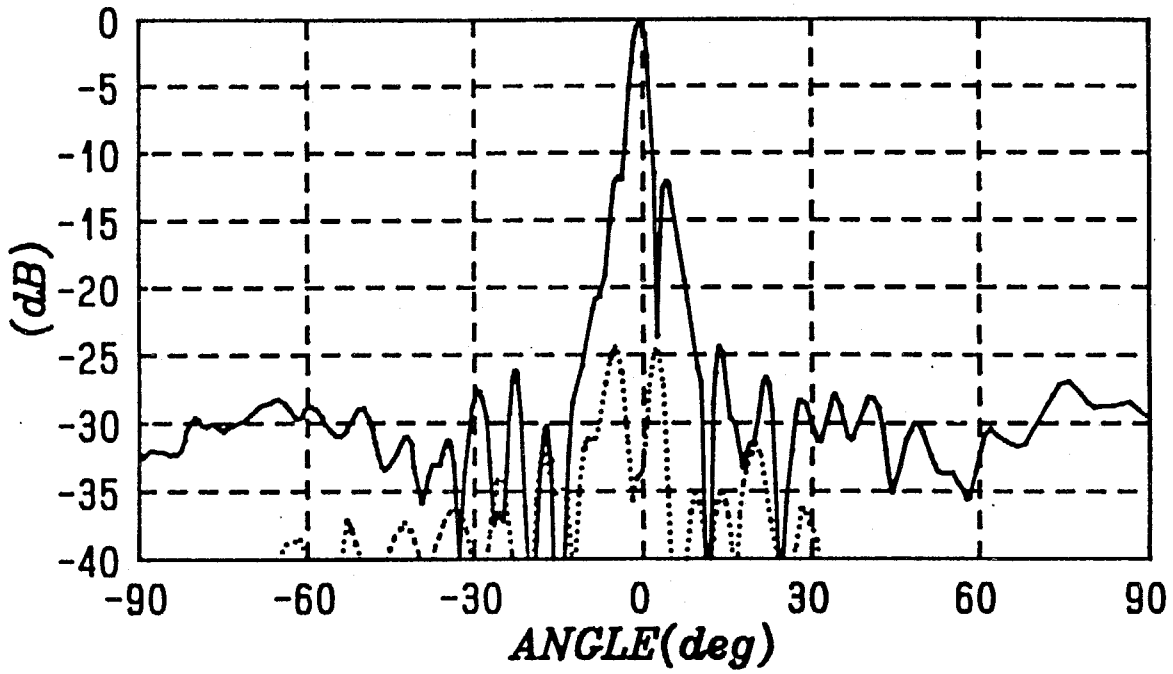

(a) E-plane (ϕ=0°).

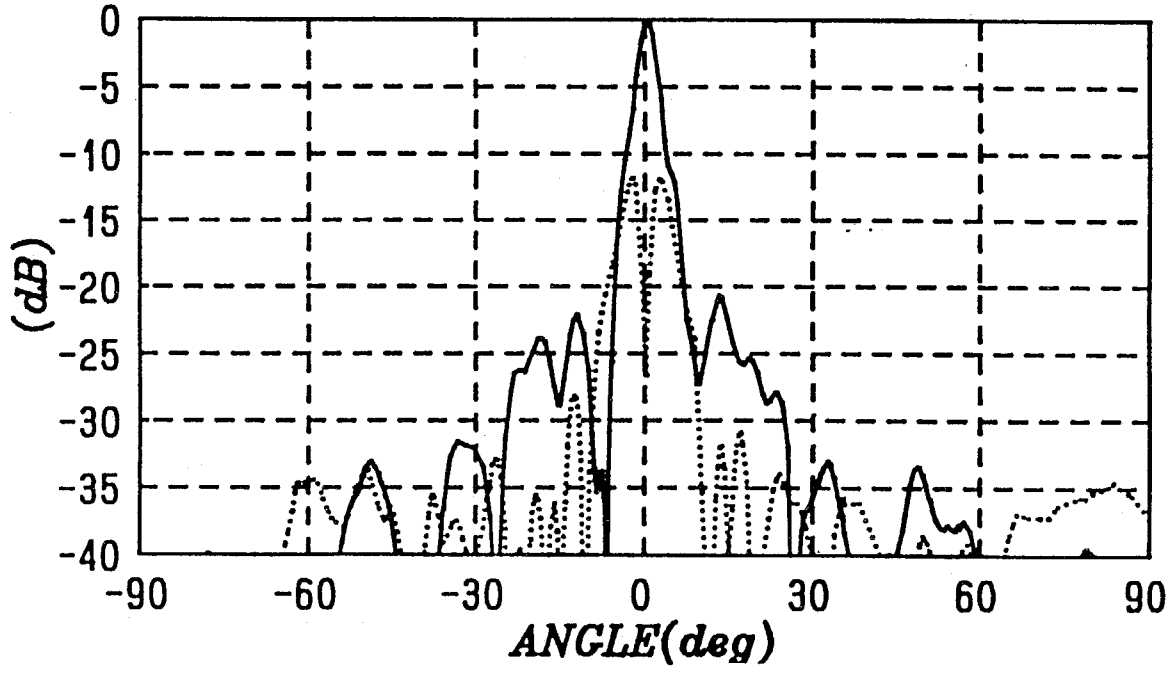

(b) H-plane (ϕ=90°).

Fig. 8-14. Radiation patterns for model antenna

(——: co-pol, ····: cross pol.).

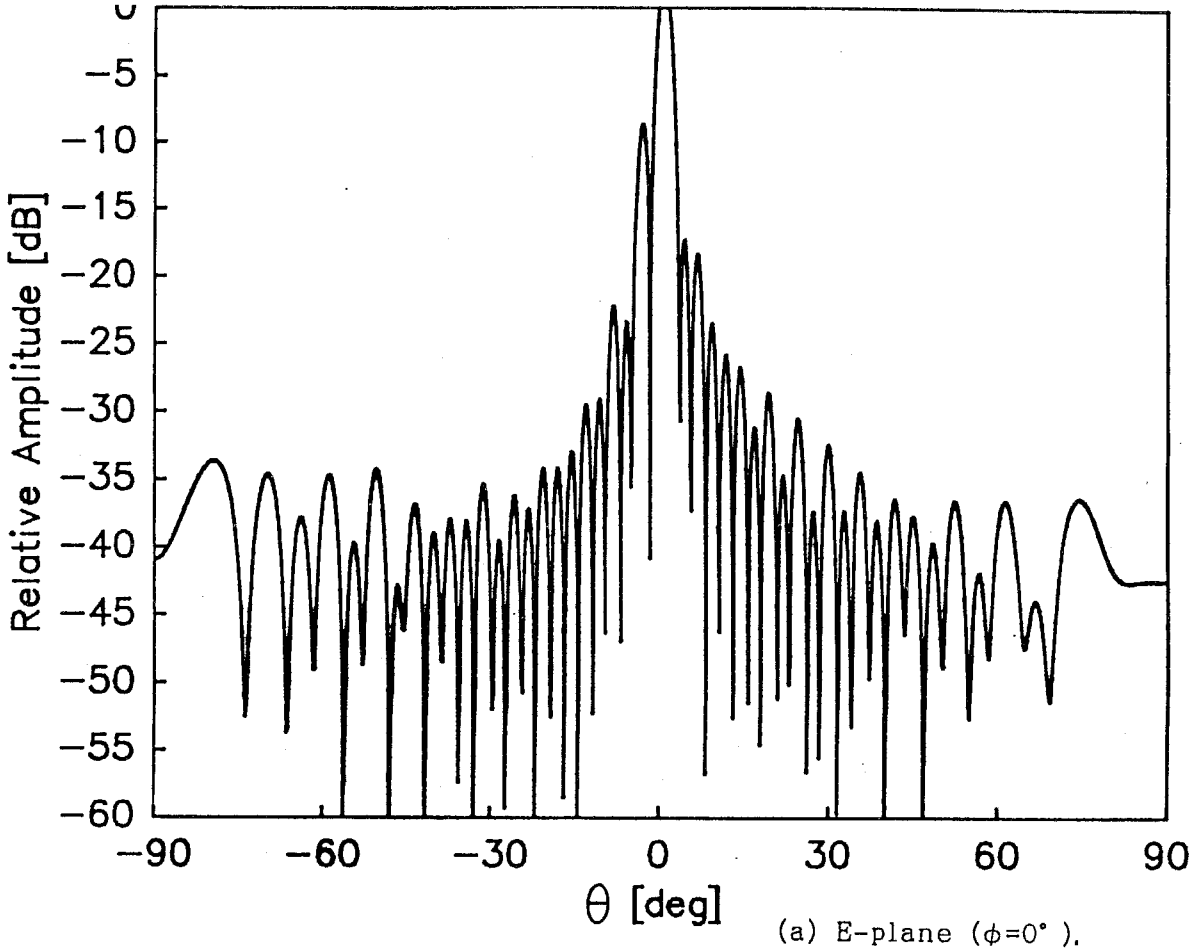

(a) E-plane (ϕ=0°).

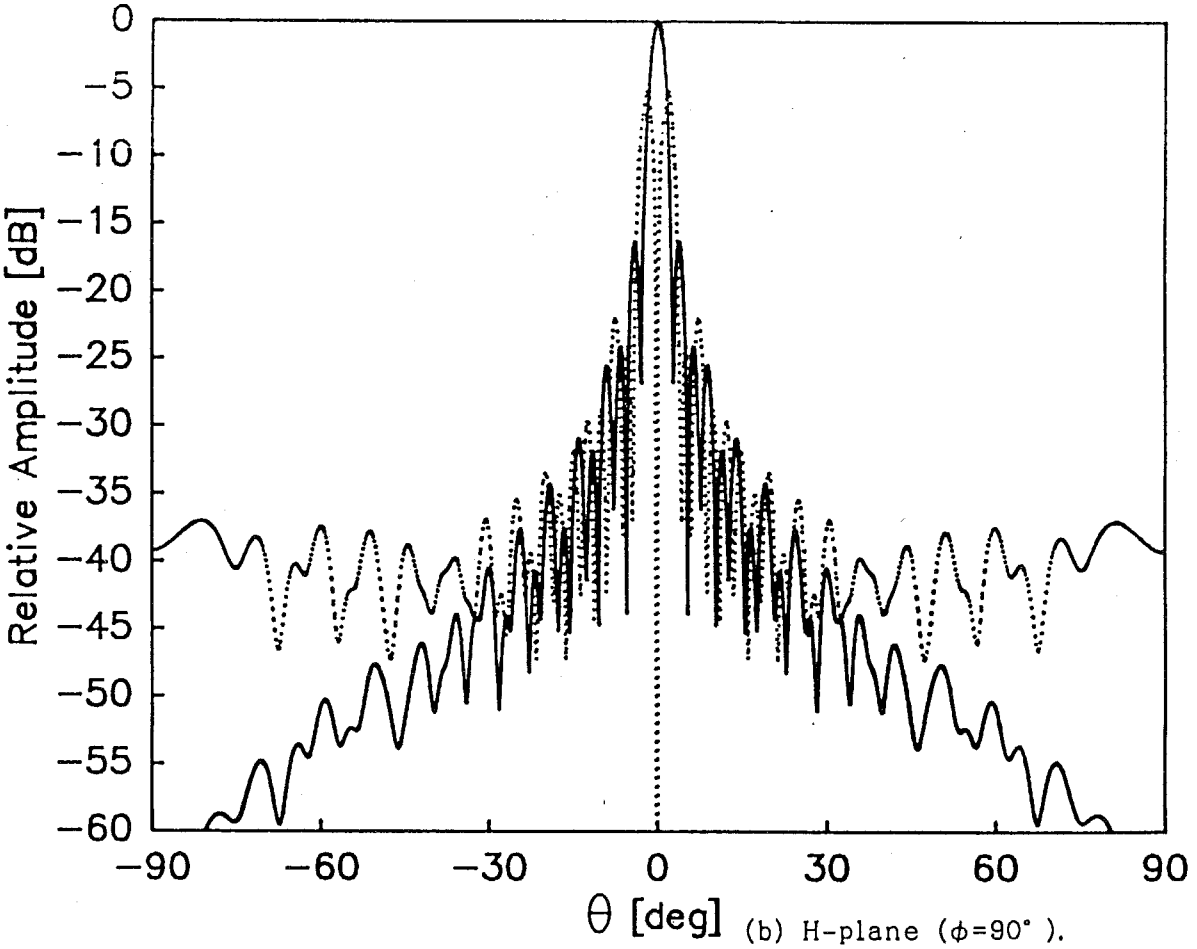

(b) H-plane (ϕ=90°).

Fig. 8-15. Theoretical radiation patterns in Fresnel region for ideally operating antenna

(——: co-pol, ····: cross pol.).

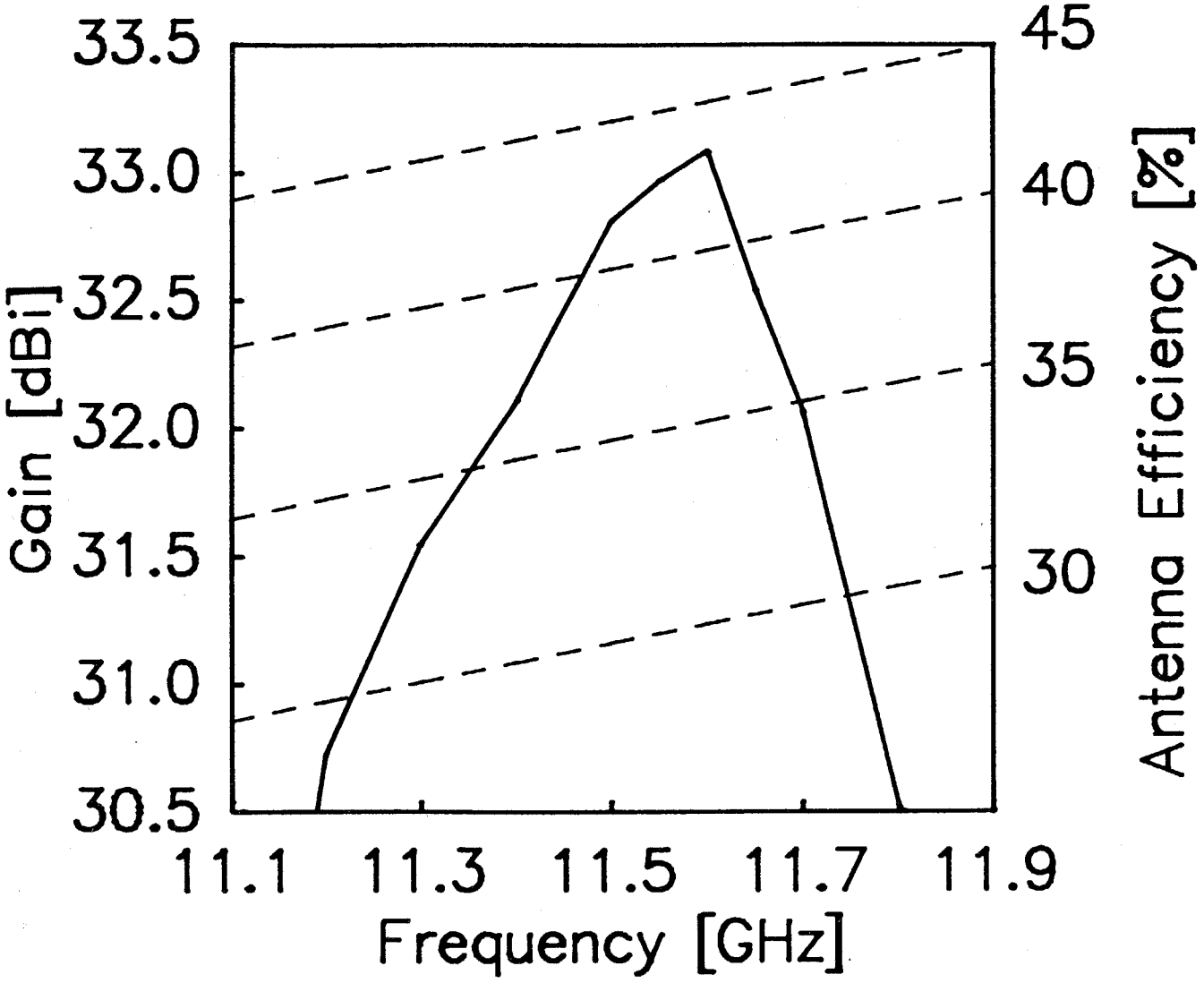

Fig. 8-16. Gain and efficiency of model antenna.

CHAPTER 9. CONCLUSION

9-1. Summary of Preceding Chapters

For the sake of the subscriber antennas in the DBS system, radial line slot antennas are investegated. The high efficiency can be realized by a simple configuration. The purpose of this study is to establish the general design technique of slot arrangement for radial line slot antennas.

The basic background for the slot design of RLSA was discussed in part 1.

The fundamental analytical techniques listed below are summarized in chapter 2;

(1) the slot coupling analysis by moment method, where the periodic boundary model is applied,

(2) the array gain calculation by induced electromotive force method, where a slot is replaced by a electrically small dipole.

For the preparation of slot arrangement design, coupling characteristics of one slot is discussed in chapter 3 by using the S-matrix equivalent circuit. The results are the following:

(1) A slot acts as a series impedance circuit.

(2) The dominant factor of slot coupling is the impedance matching, and the radiation is not always proportional to $sin\theta$, where θ is coupling angle of the slot.

Part 2 presented the aperture illumination design of RLSA in the traveling wave operation. Under the assumption of traveling wave operation, simplified design using the power relation is valid.

Chapter 4 gives an equivalent S-matrix circuit of a slot set, a unit radiator of polarization. It is necessary for the stable

operation to suppress the reflection from each slot set. The following procedure enables the slot design:

(1) The power relation design for the traveling wave operation is summarized.

(2) An expanded 3-port S-matrix is presented to express the radiated phase by assigning the radiation of principal polarization to the third port.

(3) The S-parameters are related to the design parameters.

Using the results obtained in chapter 5, chapter 6 discuss the effects of structural design parameters on the frequency bandwidth of double-layered RLSA. The results are the following:

(1) The bandwidth decreases for large diameter by the long line effect, and slot resonance also limit the bandwidth.

(2) The relative permittivity ε_r also change the effective waveguide length and higher ε_r results the narrower bandwidth.

(3) The waviguide height and the angular spacing of slot pairs do not affect on the bandwidth.

By controlling the slot coupling over the antenna aperture, the single-layered RLSA is able to be designed. Chapter 6 presented the design procedure of single-layered RLSA. The following results are obtained:

(1) The weakly coupled slots for the inner part and the strongly coupled slots for the outer part should be used to realize the unifrom aperture illumination.

(2) This design is confirmed by the model antennas, and the antenna efficiency of 84% is obtained by the 600mmϕ model.

The single-layered CP-RLSAs are now on the market (by Panasonic, NEC, Fujitsu General, Toshiba, Sharp etc.).

The difficulties in the design of LP-RLSA are the serious

reflection characteristics and the variation of the slot set configuration. Part 3 discussed the new design concepts for LP-RLSA with small reflection.

Chapter 7 presented a new configuration of slot set with the reflection canceling additional slots. The results presented are:

(1) The design parameters of a slot set are numerically optimized to suppress the reflection less than -40dB.

(2) The return loss of the model antenna is suppressed to -10dB and the antenna efficiency of 54% is obtained for 600mmϕ model.

(3) The techniques to improve the efficiency are listed up. By increase the slot coupling, the antenna efficiency of 67% is realized for 600mm model.

An alternative slot set using parallel slot pairs were presented in chapter 8. The parallel slot pair is a new radiation element for small reflection, which can be applied to various traveling wave antennas as well. The following results are obtained:

(1) A parallel slot pair is presented to cancel the reflection and its mechanism is explained.

(2) The slot sets for LP-RLSA are constructed by the use of parallel slot pairs. Three types of the configurations are appropriately arranged over the aperture.

(3) The experiments confirm the radiation of linear polarization with small reflection.

9-2. Remarks for Future Studies

Remarks for further investigations are listed below.

(1) The reuse of residual power for single-layered RLSA is required as mentioned in chapter 6. The matched elements vanish the termination loss, though the outermost conducting wall should be spirally shaped. An alternative non-uniform illumination is also

attractive, where the improvement of rotational symmetry is left for further study.

(2) The efficiency improvement of LP-RLSA presented in chapter 7. The uniformity of the illumination is not perfect at present. The return loss should also be improved by the use of radome or beam-tilt technique. The final criterion of the efficiency will be more than 80%.

(3) The use of parallel slot pair presented in chapter 8 is also an effective technique to obtain the uniform aperture illumination for efficiency improvement.

ACKNOWLEDGEMENT

I would like to express my gratitude to Professor Makoto Ando for his continuous guidance and encouragement. I also wish to express my gratitude to Professor Naohisa Goto for his supervision of the RLSA project and passionately discussion.

I am also grateful to Professors Y. Naito, Y. Shimizu, K. Furuya, T. Mizumoto, and the members of Microwave and Device Research Group of Tokyo Institute of Technology for their fruitful discussion. I am also indebted to Professor H. Arai of Yokohama National University for his useful suggestions.

Thanks are also due to Mr. K. Sakurai for his experimental helps, Ms. K. Kaneta for her businesslike support. I am also indebted to Mr. J. Hirokawa for his useful discussion.

I also express my appreciation to Mr. Y. Okazaki and Mr. M. Suzuki of Toppan Printing Co., Mr. S. Uchida of Anten Co., Mr. Y. Yamashita of Hi-Sheet Industries Ltd., Mr. T. Kimura of Hitachi Chemical Co., Mr. K. Hazeyama of Omnipack Electronics Co., Mr. Y. Nonaka of Toshiba Co., Mr. H. Matsuda of Inax Co., Mr. Y. Arai, Mr. T. Aoki and Mr. Yokokawa of Taisei Co. and Mr. H. Samura of Sanyo Chemical Co. for their help of antenna fabrication.

I would like to thank Mr. M. Takahashi, Mr. T. Ikeda, Mr. N. Yokoyama, Mr. T. Sumida, Mr. S. Hagiwara, Mr. S. Sumikawa, Mr. M. Saikawa, Mr. K. Yamamoto, Mr. H. Nagahama, Mr. N. Ueki, Mr. K. Nii, Mr. N. Yamaguchi, Mr. T. Kawakami and Mr. K. Ichikawa for their fruitful helps in this study. Thanks are also due to the members of Goto and Ando Laboratories.

This work is partly supported by the Scientific Research Grand-in Aid from the Ministry of Education, Science and Culture and by the Promoter of Science and Engineering.

Finally, I express the respects to my parents, sisters and fiancee for their mental support.

LIST OF PUBLICATIONS

1. WORKS CONCERNING THIS DISSERTATION

Papers

[1] J. Takada, M. Ando and N. Goto, "The bandwidth and the gain of radial line slot antenna with uniform slot density," Trans. IEICE, vol. E73, no. 8, pp. 1372-1377 (Aug. 1990).

[2] M. Takahashi, J. Takada, M. Ando and N. Goto, "A slot design for uniform aperture field distribution in single-layered radial line slot antennas," IEEE Trans. Antennas & Propag., vol. 39, no. 7, pp. 954-959 (July 1991).

[3] J. Takada, M. Ando and N. Goto, "An equivalent circuit of a slot in radial line slot antennas," Trans. IEICE, vol. E74, no. 9, pp. 2922-2928 (Sep. 1991).

[4] M. Takahashi, J. Takada, M. Ando and N. Goto, "Characteristics of small aperture single-layered radial line slot antennas," IEE Proc., vol. 139, pt. H (to be publeshed in 1992).

[5] J. Takada, M. Takahashi, M. Ando and N. Goto, "Radial line slot antennas," IEEE Tokyo Section Denshi Tokyo, no. 30 (to be published in Feb. 1992).

[6] J. Takada, M. Ando and N. Goto, "A reflection cenceling slot set in a linearly-polarized radial line slot antenna," to have been submitted in IEEE Trans. Antennas & Propag.

International conferences

(Site is only written for ones presented by the candidate)

[1] J. Takada, M. Ando and N. Goto, "Aperture diameter dependence of radial line slot antennas", 1989 International Symposium on Antennas and Propagation, Japan, 3C1-2, Nippon Toshi Center, Tokyo, Japan (Aug. 1989).

[2] M. Ando, M. Takahashi, J. Takada and N. Goto, "A slot design for

uniform aperture field distribution in single-layered radial line slot antennas," 1990 IEEE AP-S International Symposium, 46-5 (May 1990).

[3] J. Takada, M. Takahashi, T. Ikeda, M. Natori, M. Ando and N. Goto, "A single-layered circularly-polarized radial line slot antenna," Symposium on Antenna Technology and Applied Electromagnetics '90, pp.88-93, Canadian Institute of Industrial Technology, Winnipeg, Canada (Aug. 1990).

[4] M. Ando, M. Takahashi, J. Takada and N. Goto, "A single-layered radial line slot antenna for DBS reception," 20th European Microwave Conference, pp.1541-1546 (Sep. 1990).

[5] J. Takada, M. Takahashi, M. Ando and N. Goto, "An aperture synthesis of a single-layered radial line slot antenna," 3rd Asia-Pacific Microwave Conference, 5-1, Sun Shine City Prince Hotel, Tokyo, Japan (Sep. 1990).

[6] M. Takahashi, M. Natori, J. Takada, M. Ando and N. Goto, "A single-layered radial line slot antenna for DBS reception," 3rd Asia-Pacific Microwave Conference, 5-2 (Sep. 1990).

[5] J. Takada, M. Ando and N. Goto, "An equivalent circuit of a slot in radial line slot antennas," 3rd Japan-China Joint Meeting on Optical Fiber Science and Electromagnetic Theory, EMT-90-94, Shika-no-shima National Vacation Village, Fukuoka, Japan (Oct. 1990).

[6] M. Takahashi, J. Takada, M. Ando, N. Goto, M. Suzuki, Y. Okazaki and Y. Numano, "A small aperture single-layered radial line slot antenna for DBS reception," 7th International Conference on Antennas and Propagation, 15C-4 (Apr. 1991).

[7] M. Ando, M. Takahashi, J. Takada and N. Goto, "Characteristics of radial line slot antena for DBS reception," 1991 IEEE International Symposium, 53.2 (June 1991).

[8] J. Takada, M. Ando and N. Goto, "Suppression of reflection from slots in a linearly-polarized radial line slot antenna," 1991 IEEE AP-S International Symposium, 82.8, University of Western Ontario, London, Canada (June 1991).

[9] M. Takahashi, J. Takada, M. Ando and N. Goto, "High efficiency flat array antennas for DBS recepction," 21st European Microwave Conf., pp. 629-634 (Oct. 1991).

Papers of technical group on antennas and propagation IEICE Japan

(Site is only written for ones presented by the candidate)

[1] M. Takahashi, J. Takada, M. Ando and N. Goto, "A single-layered radial line slot antenna," AP89-54 (Oct. 1989).

[2] M. Takahashi, J. Takada, M. Ando and N. Goto, "A slot design of single-layered radial line slot antennas," AP89-103 (Jan. 1990).

[3] M. Takahashi, J. Takada, M. Ando and N. Goto, "Characteristics of single-layered radial line slot antenna," AP90-129 (Feb. 1991).

[4] J. Takada, M. Ando and N. Goto, "A design of a slot set with small reflection in a linearly-polarized radial line slot antenna," AP91-1, Kikai Shinko Kaikan, Tokyo (Apr. 1991).

National convention records of IEICE

(Site is only written for ones presented by the candidate)

[1] M. Ando, J. Takada and N. Goto, "Aperture-diameter dependence of efficiency of RLSA," SB-1-3 (Mar. 1989).

[2] J. Takada, M. Ando and N. Goto, "Frequency characteristics of radial line slot antenna with a uniform slot density," B-33, Kanagawa Univ., Kanagawa (Sep. 1989).

[3] M. Takahashi, J. Takada, M. Ando and N. Goto, "A design of a radial line slot antenna with uniform aperture distribution," B-

34 (Sep. 1989).

[4] T. Ikeda, J. Takada, M. Ando and N. Goto, "Slots reflection suppression of linearly-polarized radial line slot antennas," B-42 (Sep. 1989).

[5] M. Takahashi, J. Takada, M. Ando and N. Goto, "An aperture synthesis for single-layered radial line slot antennas," B-136 (Mar. 1990).

[6] J. Takada, M. Takahashi, M. Ando and N. Goto, "An equivalent circuit of slot pair for cricularly-polarized radial line slot antennas," B-137, Chuo Univ., Tokyo (Mar. 1990).

[7] J. Takada, M. Ando and N. Goto, "An Equivalent circuit of a slot for linearly-polarized radial line slot antennas," B-38, Hirosima Institute of Technology, Hiroshima (Oct. 1990).

[8] M. Takahashi, J. Takada, M. Ando and N. Goto, "Characeristics of small aperture radial line slot antennas," B-139 (Mar. 1991).

[9] J. Takada, M. Ando and N. Goto, "A design for suppression of reflection from slots in linearly-polarized radial line slot antennas," B-144, Tokushima Univ., Tokushima (Mar. 1991).

[10] J. Takada, M. Ando and N. Goto, "Suppression of reflection by parallel slot pairs in a linearly-polarized radial line slot antenna," B-48, Tamagawa Univ., Tokyo (Sep. 1991).

2. RELATED WORKS

Papers

[1] H. Moriyama, J. Takada, M. Ando and N. Goto, "A radial line slot antenna with an expanded slow wave structure," Trans. IEICE, vol. E71, no. 10, pp. 968-971 (Oct. 1988).

[2] J. Takada, M. Ando and N. Goto, "A beam-tilted linearly-polarized radial line slot antenna," Trans. IEICE, vol. J71-B, no. 11, pp. 1352-1357 (Nov. 1988) / Electronics and

Communications in Japan, pt. 1, vol. 72, no. 11, pp. 27-34 (translated into English, Nov. 1989).

[3] M. Ando, T. Numata, J. Takada and M. Ando, "A linearly polarized radial line slot antenna," IEEE Trans. Antennas & Propag., vol. AP-36, no. 12, pp. 1675-1680 (Dec. 1988).

[4] T. Kawakami, J. Takada, M. Ando and N. Goto, "A smaller radial line slot antenna," Trans. IEICE, vol. J73-BII, no. 12, pp. 942-944 (Dec. 1990).

[5] K. Ichikawa, J. Takada, M. Ando and N. Goto, "A radial line slot antenna without a slot wave structure," to have been submitted in Trans. IEICE.

International Conferences

(Site is only written for ones presented by the candidate)

[1] J. Takada, "A linearly-polarized radial line slot antenna," 16th International Symposium on Space Technology and Science, w-2-6, Hokkaido Univ., Hokkaido, Japan (May 1988).

[2] M. Ando, J. Takada, T. Numata and N. Goto, "A linearly-polarized radial line slot antenna," 1988 IEEE AP-S International Symp., 46-7 (June 1988).

[3] J. Takada, M. Ando and N. Goto, "A slot coupling control in circularly-polarized radial line slot antennas," 1989 IEEE AP-S International Symposium, 65-2, Red Lion Inn, San Jose, USA (June 1989).

Papers of technical group on antennas and propagation IEICE Japan

(Site is only written for ones presented by the candidate)

[1] J. Takada, T. Numata, M. Ando and N. Goto, "A beam-tilted linearly-polarized radial line slot antenna," AP87-132, Yamagata Univ., Yamagata (Feb. 1988).

[2] J. Takada, M. Ando and N. Goto, "A slot coupling control in circularly-polarized radial line slot antennas," AP88-77, Kanazawa Insitute of Technology, Ishikawa (Oct. 1988).

[3] Y. Numano, M. Suzuki, T. Kobayashi, M. Takahashi, J. Takada, M. Ando and N. Goto, "A small aperture single-layered radial line slot antenna with shroud," AP90-92 (Dec. 1990).

Papers of technical group on radio engineering ITE Japan

[1] M. Ando, J. Takada and N. Goto, "A high efficiency radial line slot antenna," RE88-30 (Sep. 1988).

National convention records of IEICE

(Site is only written for ones presented by the candidate)

[1] H. Moriyama, J. Takada, H. Sasazawa, K. Sakurai, M. Ando and N. Goto, "Characteristics of a forming-polyethylene slow wave structure in radial line slot antenna," B-104 (Mar. 1988).

[2] J. Takada, T. Numata, M. Ando and N. Goto, A beam-tilted linearly polarized radial line slot antenna," B-107, Waseda Univ., Tokyo (Mar. 1988).

[3] J. Takada, M. Ando and N. Goto, "Slot coupling controls in circularly-polarized radial line slot antennas," SB-1-4, Kinki Univ., Osaka (Mar. 1989).

[4] S. Hagiwara, J. Takada, M. Ando and N. Goto, "A matching slot in single-layered radial line slot antennas," B-40 (Oct. 1990).

[5] S. Sumikawa, M. Takahashi, J. Takada, M. Ando and N. Goto, "The effect of a matching spiral in a single-layered radial line slot antenna," B-41 (Oct. 1990).

[6] K. Ichikawa, J. Takada, M. Takahashi, M. Ando and N. Goto, "A radial line slot antenna without a slow wave structure," B-42 (Oct. 1990).

[7] M. Saikawa, K. Sakurai, J. Takada, M. Ando and N. Goto, "Two dimensional aperture distribution measurement system for planar antennas," B-74 (Mar. 1991).

[8] K. Ichikawa, J. Takada, M. Takahashi, M. Ando and N. Goto, "A radial line slot antenna with a small dielectric constant slot wave structure," B-137 (Mar. 1991).

[9] H. Nagahama, J. Takada, M. Takahashi, M. Ando and N. Goto, "A single-layered radial line slot antenna composed of dielectric substrate," B-138, Tokushima Univ., Tokushima (Mar. 1991).

[10] S. Sumikawa, M. Takahashi, J. Takada, M. Ando and N. Goto, "High efficiency single-layered radial line slot antennas," B-143 (Mar. 1991).

[11] K. Yamamoto, M. Takahashi, J. Takada, M. Ando and N. Goto, "The bandwidth of single-layered radial line slot antennas," B-145 (Mar. 1991).

[12] S. Hagiwara, J. Takada, M. Ando and N. Goto, "A power divider for wide band RLSAs," B-45 (Sep. 1991).

3. Other Works

Papers of technical group on antennas and propagation IECE Japan

[1] J. Takada, K. Sakurai, H. Arai, M. Ando and N. Goto, "Electrically small magnetic current loop antennas," AP86-76, Hokkaido Univ., Hokkaido (Oct. 1986).

National convention records of IECE

[1] J. Takada, K. Sakurai, H. Arai and N. Goto, "Efficiency measurements of electrically small magnetic current loop antenna," 41, Seikei Univ., Tokyo (Sep. 1986).

[2] J. Takada, K. Sakurai, H. Arai, M. Ando and N. Goto, "Electrically small magnetic current loop antennas on the buildings," 663, Keio Univ., Kanagawa (Mar. 1987).

APPENDIX A. DYADIC GREEN'S FUNCTIONS

A-1. Dyadic Green's Function for Free Space

A-1-1. Standalone Type

The free space dyadic function is given as [1]

$$\bar{G}_{out}(r|r_o)=-j\omega\varepsilon_o\left(\bar{I}+\frac{\nabla\nabla}{k_o^2}\right)\frac{\exp(-jk_o|r-r_o|)}{4\pi|r-r_o|} \qquad (A-1),$$

where ω is the angular frequency, ε_o is the permittivity of free space, k_o is the wavenumber in free space, r and r_o denote the observation point and the source point, respectively. $\bar{I}$ is the unit diadic. The oprator ∇ indicates differentiation with respect to r.

A-1-2. Periodic Type

The periodicity of S_ϕ along x-direction can be included in the diadic function as

$$\bar{G}_{out}(r|r_o)=-j\omega\varepsilon_o\left(\bar{I}+\frac{\nabla\nabla}{k_o^2}\right)\sum_{n=-\infty}^{+\infty}\frac{\exp(-jk_o|r-(r_o+nS_\phi\hat{x})|)}{4\pi|r-(r_o+nS_\phi\hat{x})|} \qquad (A-2).$$

For the practical point of view, the summation is done from -N to +N, and the value N is increased till the resultant field converges.

A-2. Dyadic Green's Function for Rectangular Waveguide with Periodic Boundary Condition

A-2-1. Ordinal Expression

The dyadic Green's function in the guide is expressed by the use of normal mode magnetic function H_ν as [2]

$$\bar{G}_{in}(r|r_o)=\begin{cases}\frac{1}{2}\sum_\nu H_\nu^{(-)}(r)H_\nu^{(+)}(r_o) & (z<z_o)\\ \frac{1}{2}\sum_\nu H_\nu^{(+)}(r)H_\nu^{(-)}(r_o) & (z>z_o)\end{cases} \qquad (A-3),$$

where z and z_o are the z coordinetes of r and r_o. $H_\nu^{(+)}$ and $H_\nu^{(-)}$

are the normal mode magnetic functions propagating +z and -z directions, respectively, defined as [1]

[TE mode (H mode)]

$$H_{h\nu}^{(\pm)}(r)=[\pm h_{h\nu}(\rho)+h_{hz\nu}(\rho)]\exp(\mp\gamma_\nu z) \tag{A-4},$$

[TM mode (E mode)]

$$H_{e\nu}^{(\pm)}(r)=\pm h_{e\nu}(\rho)\exp(\mp\gamma_\nu z) \tag{A-5},$$

where ρ is the transverse compontent of r, γ_ν is the wavenumber of ν-th defined later and h_ν are given by the Heltzian potentical as

[TE mode]

$$h_{h\nu}(\rho)=-\frac{1}{k_{c\nu}}\sqrt{Y_{h\nu}}\nabla_t\phi_{hu}(\rho) \tag{A-6},$$

$$h_{hz\nu}(\rho)=\hat{z}\frac{k_{c\nu}}{\gamma_\nu}\sqrt{Y_{h\nu}}\phi_{hu}(\rho) \tag{A-7},$$

[TM mode]

$$h_{e\nu}(\rho)=-\frac{1}{k_{c\nu}}\sqrt{Y_{e\nu}}\hat{z}\times\nabla_t\phi_{eu}(\rho) \tag{A-8}.$$

In Eqs. (A-6)~(A-8), ϕ is the Heltzian potential [1], which is determined by the boudary condition. For the periodic boudary on x-direction and electric wall y-direction [2],

[TE mode]

$$\phi_{hc\nu}=\frac{\sqrt{\varepsilon_{mn}}}{\sqrt{ab}}\cos\frac{2m\pi x}{a}\sin\frac{n\pi y}{b} \tag{A-9},$$

$$\phi_{hs\nu}=\frac{\sqrt{\varepsilon_{mn}}}{\sqrt{ab}}\sin\frac{2m\pi x}{a}\sin\frac{n\pi y}{b} \tag{A-10},$$

[TM mode]

$$\phi_{ecv}=\frac{\sqrt{\varepsilon_{mn}}}{\sqrt{ab}}\cos\frac{2m\pi x}{a}\cos\frac{n\pi y}{b} \tag{A-11},$$

$$\phi_{esv}=\frac{\sqrt{\varepsilon_{mn}}}{\sqrt{ab}}\sin\frac{2m\pi x}{a}\cos\frac{n\pi y}{b} \tag{A-12},$$

where

$$k_{c\nu}^2=\left(\frac{2m\pi}{a}\right)^2+\left(\frac{n\pi}{b}\right)^2 \quad : \text{cut-off wave number} \qquad (A-13),$$

$$\gamma_\nu^2=k_{c\nu}^2-\varepsilon_r k_o^2 \quad : \text{propagation constant} \qquad (A-14),$$

$$Z_{h\nu}=\frac{1}{Y_{h\nu}}=\frac{jk_oZ_o}{\gamma_\nu} \quad : \text{characteristic impedance of H mode} \qquad (A-15),$$

$$Y_{e\nu}=\frac{j\varepsilon_r k_oY_o}{\gamma_\nu} \quad : \text{characteristic admittance of E mode} \qquad (A-16),$$

where Z_o and Y_o are free space wave impedance and admittance, respectively.

A-2-2. Alternative Expression

The alternative expression of the dyadic Green's function in the guide is described. The representation presented in A-2-1 is not suitable when the relation between z and z_o changes in the integrals. The virtual cavity is composed of the virtual conducting walls separated by c [3]. The Green's function is given as

$$\begin{aligned}\bar{G}_{in}(r|r_o)=\bar{G}_{yc}(r|r_o)&+\frac{1}{4}\sum_\nu\frac{exp(+\gamma_\nu z_1)}{sinh(\gamma_\nu c)}\{H_\nu^{(+)}(r)exp(+\gamma_\nu z_2)\\&-H_\nu^{(-)}(r)exp(-\gamma_\nu z_2)\}H_\nu^{(+)}(r_o)\\&+\frac{1}{4}\sum_\nu\frac{exp(-\gamma_\nu z_2)}{sinh(\gamma_\nu c)}\{H_\nu^{(-)}(r)exp(-\gamma_\nu z_1)\\&-H_\nu^{(+)}(r)exp(+\gamma_\nu z_1)\}H_\nu^{(+)}(r_o)\end{aligned} \qquad (A-17),$$

where z_1 and z_2 ($z_1<z_2$) are the z cooridinates of the virtual walls and $c= z_2-z_1$. $\bar{G}_{yc}$ is the dyadic Green's function in the virtual cavity expanded in terms of the normal mode functions propagating in the $\pm y$ direction as

$$\bar{G}_{yo}(r|r_o)=$$

$$\begin{cases} \dfrac{1}{4}\sum_{\nu}\dfrac{1}{\sinh\gamma_{y\nu}b}[H_{y\nu}^{(-)}(r)-H_{y\nu}^{(+)}(r)] \\ \qquad\cdot[H_{y\nu}^{(+)}(r_o)\exp(+\gamma_{y\nu}b)-H_{y\nu}^{(-)}(r_o)\exp(-\gamma_{y\nu}b)] \\ \qquad\qquad\qquad\qquad\qquad\qquad\qquad\qquad (y<y_o) \\ \dfrac{1}{4}\sum_{\nu}\dfrac{1}{\sinh\gamma_{y\nu}b}[H_{y\nu}^{(-)}(r_o)-H_{y\nu}^{(+)}(r_o)] \\ \qquad\cdot[H_{y\nu}^{(+)}(r)\exp(+\gamma_{y\nu}b)-H_{y\nu}^{(-)}(r)\exp(-\gamma_{y\nu}b)] \\ \qquad\qquad\qquad\qquad\qquad\qquad\qquad\qquad (y>y_o) \end{cases}$$

(A-18).

In Eq. (A-17), the subscript y indicates the mode expansion in terms of y direction.

References

[1] H. Seki, "Moment and variational analysis of slotted waveguide antennas and its applicaitons," 1981 Doctoral Dissertation, Tokyo Institute of Technology (Dec, 1981).

[2] J. Hirokawa, M. Ando and N. Goto, "Analysis of slot coupling in a radial line slot antenna for DBS reception," IEE Proc., vol. 137, pt. H, no. 5, pp. 249-254 (Oct. 1990).

[3] H. Seki, "An alternative representation of electromagnetic fields in a rectangular waveguide with an aperture in its wall," 1984 IECEJ Natl. Conv. Rec., 16 (Sep. 1984).

APPENDIX B. MUTUAL RESISTANCE DERIVED BY ELECTROMOTIVE FORCE METHOD

Considering the coordinates of slots shown in Fig. 2-4, the electric field E_{21} induced at #2 by the current of #1 is given as

$$E_{21}=-\frac{jZ_0I_1d\ell_1}{2\pi k_0}\cos\alpha\left\{\frac{jk_0}{R^2}+\frac{1}{R^3}\right\}\exp(-jk_0R)R$$

$$+\frac{jZ_0I_1d\ell_1}{4\pi k_0}\sin\alpha\left\{-\frac{k_0^2}{R}+\frac{jk_0}{R^2}+\frac{1}{R^3}\right\}\exp(-jk_0R)\hat{\Phi} \quad (B\text{-}1).$$

The tangential component of E_{21} to #2 defined as E_{t21} is given as

$$E_{t21}=E_{21}\cdot(\cos\beta R+\sin\beta\hat{\Phi}) \quad (B\text{-}2).$$

The electromotive force method defines the impedance as [1]

$$P=\frac{1}{2}(-E_{t21}d\ell_2)I_2^*=\frac{1}{2}Z_{12}I_1I_2^* \quad (B\text{-}3).$$

Therefore the mutual resistance R_{12} is given as

$$R_{12}=Re(Z_{12})=-\frac{E_{t21}d\ell_2}{I_1} \quad (B\text{-}4).$$

Substituting Eq. (B-1) into Eq. (B-4), the expression of mutual resisutance given in Eq. (2-24), where the length of the current $d\ell_1$ and $d\ell_2$ are replaced by δ.

The self resistance R_{11} is derived by substituting $\alpha=\beta=\pi/2$ and taking the limitation of $R\to0$, as given by Eq. (2-25).

References

[1] N. Goto, "New antenna technology," Sec. 4.4, Ohm-sha, Japan (1986).

APPENDIX C. ELEMENTS OF EXPANDED S-MATRIX

From Eq.(3-9), following two relations are obtained;

$$|S_{11}|^2+|1-S_{11}|^2+|S_{13}|^2=1 \qquad (C-1),$$

$$S_{33}=\frac{S_{13}}{S_{13}^*}(1-2S_{11}^*) \qquad (C-2).$$

S_{13} denotes the radiation, the phase of which correspond to the excitation phase of slot relative to the incident wave. For the unit incidence from -z-direction, the slot is excited with v defined in Eq.(3-2). In this case, substitution of Eq.(3-1) into Eq.(3-3) results in

$$\angle v=\angle S_{11} \qquad (C-3),$$

and therefore,

$$\angle S_{13}=\angle S_{11} \qquad (C-4).$$

From Eq. (C-1) and Eq. (C-4), the resultant S_{13} is

$$S_{13}=\sqrt{1-|S_{11}|^2-|1-S_{11}|^2}\,exp(j\angle S_{11}) \qquad (C-5).$$

Substitution of Eq.(C-5) into Eq.(C-2) results in

$$S_{33}=(1-2S_{11}^*)exp(j2\angle S_{11}) \qquad (C-6).$$

APPENDIX D. IMPEDANCE MODEL AND RADIATED FIELD

If we assume

$$H_{in}=a_1 H_1^{(+)}+a_2 H_1^{(-)} \qquad (D-1)$$

for the general case of incident wave in Eq. (2-6), the excitation coefficient of slot v_o is given by v defined in Eq. (2-5) (n=1) as

$$v_o=(a_1-a_2)v \qquad (D-2),$$

which is obtained by applying the principle of superposition. From the circuit theory, the current I flowing through Z_s is given as

$$a_1-a_2=\frac{2Z_1+Z_s}{2\sqrt{Z_1}}I \qquad (D-3).$$

On the other hand, substituting Eq. (3-14) into Eq.(3-13),

$$v_o=\frac{2Z_o}{c_1^{(+)}}\cdot\frac{Z_s}{2Z_1+Z_s} \qquad (D-4).$$

Multiplying Eq. (D-3) and Eq. (D-4), the resultant equation is obtained;

$$v_o=\frac{Z_o}{c_1^{(+)}\sqrt{Z_1}}V \qquad (D-5).$$

APPENDIX E. POLARIZATION VECTOR

The unit vactor which is parallel to the desired polarization is summarized as follows:

[Right-hand circular polarization]

$$\hat{\beta}_R=\frac{1}{\sqrt{2}}(\hat{X}-j\hat{Y}) \qquad (E-1).$$

[Left-hand circular polarization]

$$\hat{\beta}_L=\frac{1}{\sqrt{2}}(\hat{X}+j\hat{Y}) \qquad (E-2).$$

[X linear polarization]

$$\hat{\beta}_X=\hat{X} \qquad (E-3).$$

[Y linear polarization]

$$\hat{\beta}_Y=\hat{Y} \qquad (E-4).$$

APPENDIX F. REFLECTION CANCELLATION USING RADOME

In the equivalent circuit shown in Fig. 7-21(b), the reflected wave at the input port b_1 is given as

$$b_1=S_{11}a_1+S_{12}a_2+s_{13}a_3 \qquad (F-1).$$

If S_{11} and S_{12} are know from the array analysis, the lossless condition of S-matrix results in

$$|S_{13}|^2=1-|S_{11}|^2-|S_{12}|^2 \qquad (F-2).$$

The reference plane of port #3 is selected so that S_{31} becomes real value.

On the other hand, the radome is also replaced by the reflection Γ, whose argument is controlled by the spacing between the slot plate and the radome. The reflection at the radome is expressed as

$$a_3=\Gamma b_3 \qquad (F-3),$$

while b_3 is also expressed from the definition of S-matrix as

$$b_3=S_{31}a_1+S_{32}a_2+S_{33}a_3 \qquad (F-4),$$

where $S_{31}=S_{13}$ is given by Eq. (F-2), while $S_{32}=S_{23}$ is obtained from the lossless condition at port #2 as

$$|S_{23}|^2=1-|S_{22}|^2-|S_{21}|^2 \qquad (F-5).$$

S33 is also given by substituting Eq. (F-5) into the following lossless condition at port 3 as

$$|S_{33}|^2=1-|S_{31}|^2-|S_{32}|^2 \qquad (F-6).$$

Substituting Eq. (F-4) into Eq. (F-3), a_3 is described by a_1 as

$$a_3=\frac{\Gamma S_{31}}{1-\Gamma S_{33}}a_1 \qquad (F-7).$$

Then Eq. (F-7) is substituted into Eq. (F-1), the relation between b_1 and a_1 is given as

$$b_1=\left\{S_{11}+\frac{\Gamma S_{31}^2}{1-\Gamma S_{33}}\right\}a_1 \triangleq S_{11}'a_1 \qquad (F-8).$$

If $|\Gamma S_{33}|<1$, S_{11} is given as

$$S_{11}' = S_{11} + \Gamma S_{s1}^2 \qquad \text{(F-9)},$$

where the minimum value is

$$S_{11}'_{min} = |S_{11}| - |\Gamma||S_{s1}|^2 \qquad \text{(F-10)}.$$